Influence of the seismic calculation method on a CLT constructed building

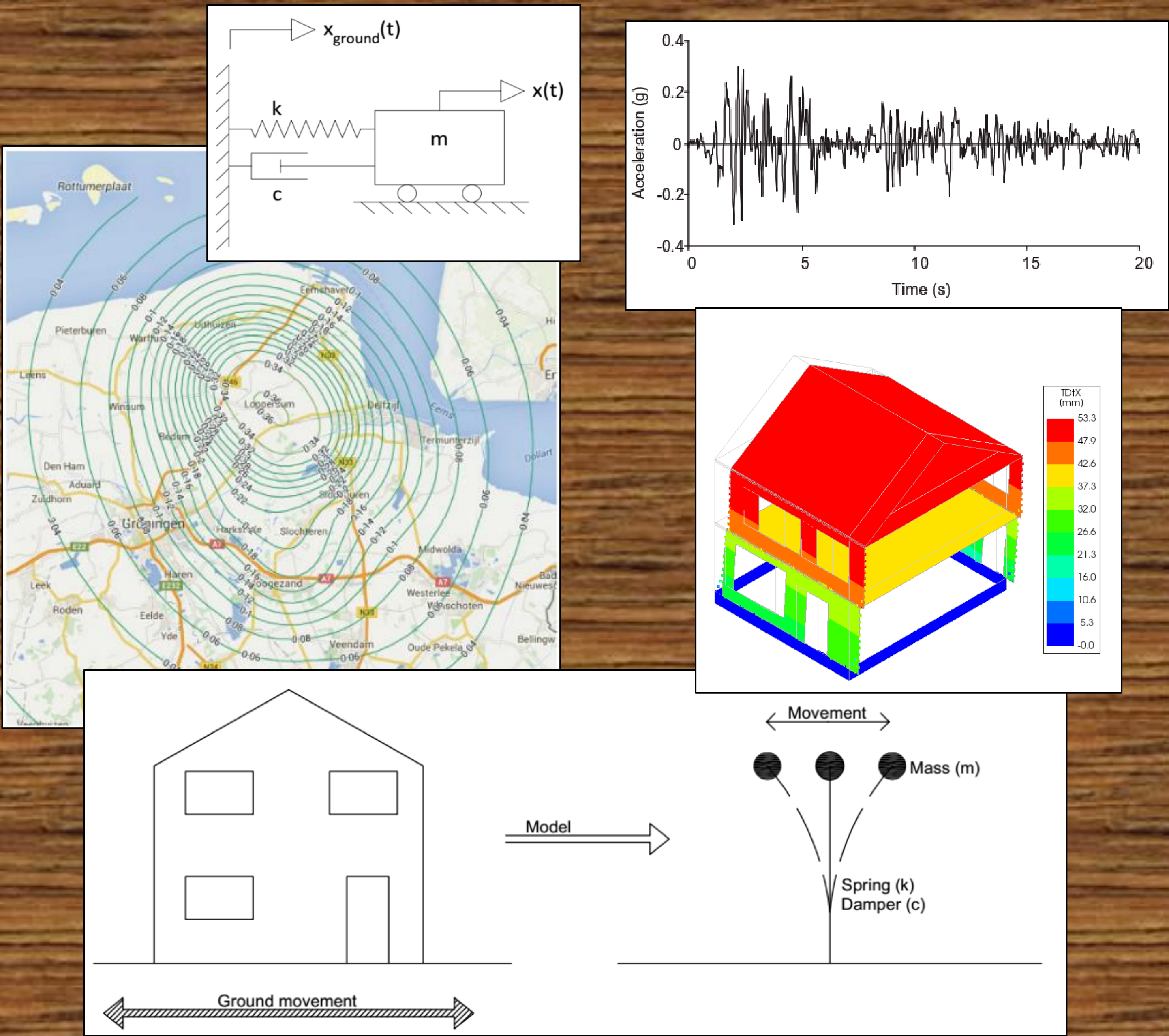

TU Delft

T.H.M.M. Arts

Influence of the seismic calculation method on a CLT constructed building

Subjected to human induced earthquakes

By

T.H.M.M. Arts

in partial fulfilment of the requirements for the degree of

Master of Science
in Civil Engineering

at the Delft University of Technology,

	Graduation coordinator		
Ir. L.J.M. Houben	Section	of	Road and railway engineering
	Graduation committee		
Prof. dr. ir. J.W.G. van de Kuilen	Section	of	Timber and timber structures
Dr. ir. G.P.J. Ravenshorst	Section	of	Timber and timber structures
Dr. ir. M.A.N. Hendriks	Section	of	Structural mechanics
Ir. R.H.G. Roijakkers			ABT

ABSTRACT

Due to gas extraction in the province of Groningen, the area is subjected to human induced earthquakes. The current building stock in the area is mostly constructed with masonry cavity walls and not designed taken this new phenomena into account. Therefore not all of the buildings are capable of resisting the earthquake forces in case of the heaviest predicted earthquake. For designing new buildings in this area the earthquakes have to be taken into account, this requests for a different way of thinking. A commonly used material in earthquake prone areas is the use of timber as construction material. Timber has the benefits that it is a light building material and is able to dissipate energy through its connections.

Besides the benefits of the traditional timber framed construction method there is a lot of new development in timber products. There is an increasing use and research in cross-laminated timber (CLT) from which stiff load bearing walls and rigid floor diagrams can be constructed. CLT can be made in prefabricated elements this leads to fast erection of a building. The benefit of using CLT is the self-centring capability and the repairability after an earthquake.

For the designing of buildings subjected to the human induced earthquakes there is a practical guideline applicable for the Dutch situation. This guideline is based on the Eurocode 8 and makes distinction between four calculation methods: Later force method (LF), modal response method (MR); non-linear static push-over (NLSP) and non-linear time history analysis (NLTH). This thesis is focussing on the first three methods. The lateral force method and modal response method allows the engineering to calculated the construction as an elastic structure. The reaction of the structure is translated into a response spectrum from which the elastic force is obtained. The response spectrum gives the resonance or damping of the structure, this is dependable on its natural period. However for constructing an economical feasible structure the non-linear reaction of the structure to the earthquake has to be taken into account. The main benefit of timber is the ability of dissipating energy through its connections by yielding of the nails. The connections react in a hysteretic manner to the cyclic loading, this is part of the non-linear behaviour. The non-linear behaviour of a structure is translated into a q-factor for which codes gives a value depending on the structural system. When applying this to the first two calculation methods an engineering can calculated as if the structure reacts elastic, while taken the non-linearity into account. This way of calculation is called force based calculation, since only the forces are regarded and not the displacement.

For applying a certain q-factor the structure has to be able to ensure a certain ductility demand, this is examined in this paper by performing a non-linear static push-over. The push-over is directed parallel to the front and back façade. By doing so a displacement based calculation is conducted. The building modelled is a single house from a block of six regular terraced build houses common for the area. The CLT house it is modelled in the FEM program DIANA, in which the CLT is modelled as 2D shells and the hysteretic behaviour of the connections is modelled as point interfaces using the tri-linear backbones of the cyclic test of the individual connections. This approach allows modification of distribution of the connections and geometry of the wall. Also it is possible to use different modelling programs.

The results of the push-over shows that it questionable on what is the yield force of the building for the elastic-plastic idealisation. This is directly related to the q_{μ}-factor of the building. The q_{μ}-factor is the force reduction factor due to the ductility. The q-factor is different because it also incorporates the over-strength of the building. The elastic-plastic idealisation makes it doubtful if the method which is described in the code is applicable for timber structures. Also the full mass of the building is used for the push-over method which represents only the fundamental mode shape. For representation of the fundamental mode shape two different load patterns are applied. So it is a force controlled push-over which is time independent. With these limitations the push-over is conservative for low-rise buildings. For high-rise buildings it can be beneficial especially when the model is used for optimisation of the structure.

The outcome of the first analysis of the building shows that the first lay-out of walls and connections is not sufficient. As mentioned benefit of the chosen modelling method is the ability of adjusting the design or the number of connections. In this way also the design can be optimised to obtain the maximum displacement for a certain load configuration. The first lay-out of the case study building failed at an angle bracket connecting the wall to the foundation. First an additional bracket was added however this was not sufficient to resist the heaviest earthquake which could occur in Groningen. Therefore an additional wall was added to the design and the requirements were met. However the expected q-factor of two, as given in the EC8 for CLT structures, was not achieved with the push-over. But the push-over stopped when failure occurred in one of the brackets. Meaning that the redundancy, the over-strength factors, are not incorporated in q_{μ}-factor determined with the push-over method.

When broaden the conclusion a low-rise building which is beneficial calculation with the elastic modelling methods and applying the q-factor which is in the Eurocode. When doing so ductility must be guaranteed and therefore capacity design must be taken into account. This is done by applying over-strength factors for structural elements with brittle failure. For high-rise buildings it can be beneficial to perform a non-linear static push-over. Especially if the connections on each floor are optimised to obtain maximum deformation. Regardless of the fact that the push-over method has its limitations. It still gives an indication of the ductility of the building and it can lead to a higher q-factor for the high-rise buildings. In the case of the seismic spectrum of Groningen it can even have enough ductility to fulfil the maximum displacement demand. But most of all it gives information about the behaviour of the building which is not obtained with a force based calculation.

PREFACE

This master thesis is written in order to obtain my master degree in structural engineering at Delft University of Technology. I started studying at the TU Delft after obtaining my Bachelor degree at the HAN university of applied science, during the bachelor I found out my interest for constructions. Therefore I chose to do a master study structural engineering at Delft University of Technology. After chosen the specialisation steel, timber and FRP and following the timber courses, the wide range of possibilities of timber caught my interest. For my master thesis I could combine the challenges of the new phenomena human induced earthquakes, which occur in the northern part of the Netherlands, and timber engineering. The master thesis is written between May 2016 and March 2017.

During this period I worked on my thesis at ABT in Delft. I would like to thank my college's for answering my questions and the advice they gave. I want to thank my graduation committee: Jan – Willem van de Kuilen, Geert Ravenshorst, Max Hendriks and Rudi Roijakkers for the guidance and advice they provided me during my master thesis. Finally I want to thank my family and friends for their support.

T.H.M.M. Arts
Delft, March 2017

List of symbols

CLT	Cross-laminated timber
D_y	Yield displacement
D_u	Ultimate displacement
D_t	Target displacement
EC	Eurocode
FEM	Finite element method
LF	Lateral force
LVL	Laminated veneer lumber
MDOF	Multi degree of freedom
MR	Modal response
NLSP	Non-linear static push-over
NLTH	Non-linear time history
NPR 9998	Dutch practical guideline (human induced earthquake)
OSB	Oriented strand board
PGA	Peak ground acceleration
SDOF	Single degree of freedom
TF	Timber framed
a	Acceleration
c	Viscous damping
E	Young's modulus
F	Force
F_b	Base shear force
G	Shear modulus
g	Gravitational acceleration
Hz	Hertz
k	Spring constant
k_{ag}	Dimensionless factor dependable on the consequence class of the structure
m	Mass
Prefab	prefabricated
q_{μ}	Reduction factor
q	Behaviour factor
S_{AE}	Elastic acceleration for SDOF
S_A	Inelastic acceleration for SDOF
S_{DE}	Elastic displacement for SDOF
S_D	Inelastic displacement for SDOF
q	Behaviour factor
T_e	Eigen period
T_n	Natural period

γ_{Rd}	Over-strength factor
λ	Reduction factor for buildings with three levels or less
μ	Ductility factor
ν	Poisson ratio
ξ	Damping ratio
ω_n	Natural frequency

CONTENT

1 INTRODUCTION

This chapter gives an introduction of the master thesis topic and explains the build-up of the report. First the problem definition and the scope of the subject is described. This is then translated into a main research question and sub-questions, which will be answered in the following chapters. Followed by a reading guide which gives an overview about what is explained in the main report and what can be found in the annexes.

1.1 Problem definition

In the Netherlands earthquakes were never considered as a problem. Although in the past several earthquakes, which has caused damage, were registered. The heaviest earthquake, a 5.8 on the scale of Richter, was registered in 1992 in Roermond (KNMI, 2016).

The earthquake was triggered by a natural cause. Namely due to sliding of the ground alongside normal fault lines (Peelrandbreuk), which is a fracture line in the earth crust. Along these fault lines ground movement is possible (fig. 1.1). The system of fault lines is a regional system in the earth crust. It is on the relative stable Euraziatic plate and leads to several minor earthquakes per year. Mostly with a magnitude between two and four on the scale of Richter.

Due to the strength of the newer constructed houses the damage from the earthquake from 1992 was limited to sliding of the landscape, damage due to falling objects and to old monumental buildings. There were no life threatening situations and therefore no adjustment to the building law taking seismic action into account was made.

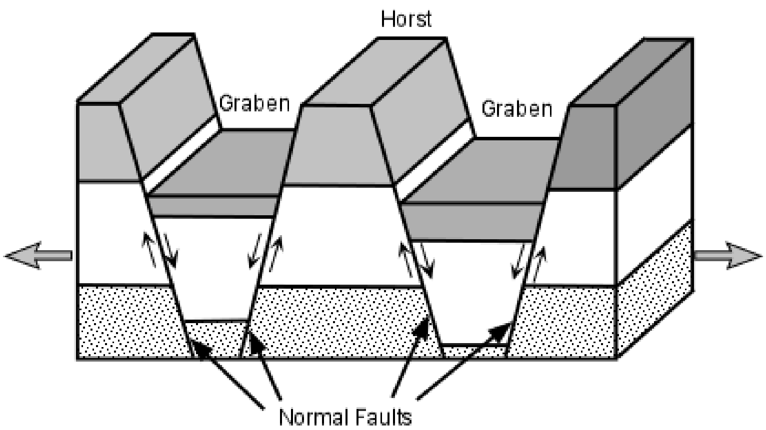

Fig. 1.1 System of horst and graben. The tension is coming from the movement of the larger plates resulting in uplifted blocks (horsts) and downward moving blocks (grabens). The sliding along the fault triggers the earthquakes (Nelson, 2016)

Recently this has changed due to gas extraction in Groningen and seismic calculation rules are developed. One of the largest gas fields of Europe was discovered in 1959, called the Slochteren gas field (fig. 1.2). The NAM (Dutch oil company) started extracting gas from these fields in 1963. At the time it was thought that the gas extraction would lead to ground inclination and create a bowl shape in the landscape of Groningen. This is a harmless effect, because the slope of the bowl is not steep enough to cause any local problems.

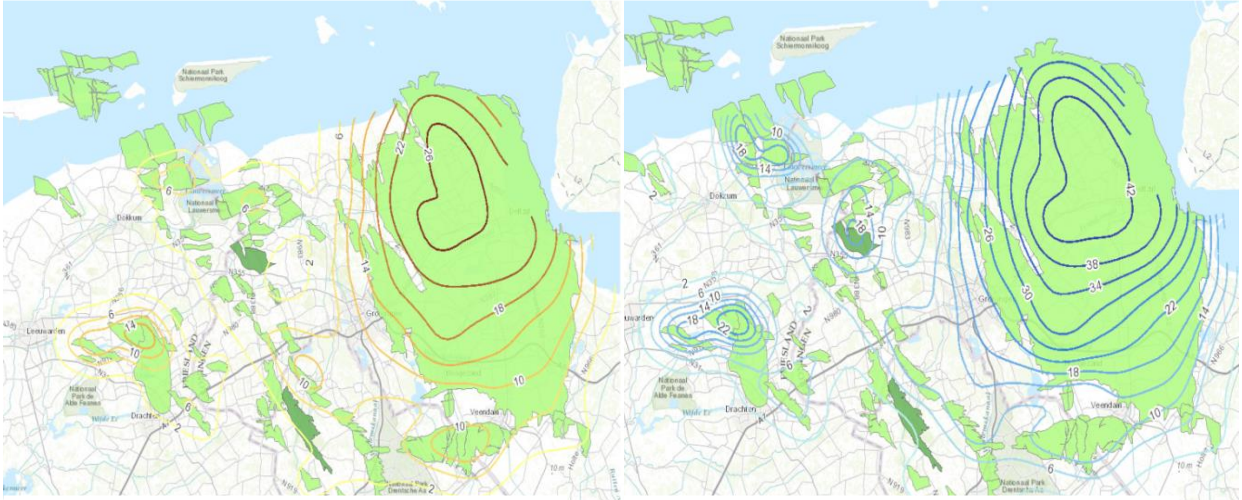

a) Inclination in 2008 in centimeter *b) Expected inclination 2080 in centimeter*

Fig. 1.2 Location of the Slochteren gasflield with the current and approximated future inclination. (NAM, 2016)

However besides the predicted ground inclination also earthquakes are occurring, starting from 1991 (fig. 1.3). These human induced earthquakes are caused by a sudden slide along gas reservoir boundaries, resulting in a sudden release of energy and therefore ground movement.

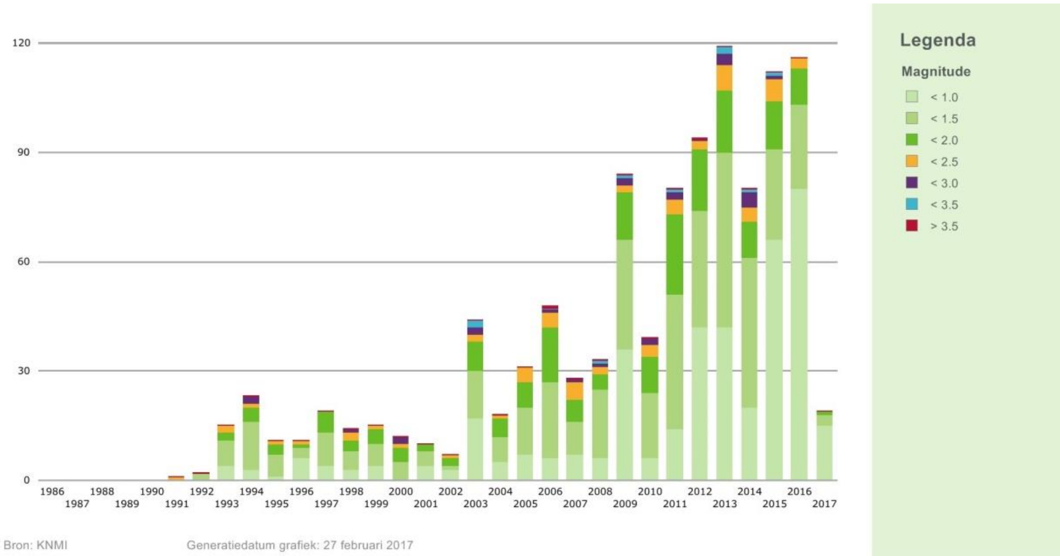

Fig. 1.3 Number of registered earthquakes in Groningen (NAM, 2016).

In this new seismic area most of the current building stock in the is not capable of resisting the forces from the ground movement, therefore some of the buildings are structural unsafe. This means that the current building stock has to be upgraded/redesigned and new buildings must be designed according to a new code taken the seismic actions on the buildings into account.

1.2 Scope

In this paragraph the challenges are listed that are following from the problem definition, most with regard to the use of timber. The thesis addresses the benefits when using timber, the background of human induced earthquakes and the influences of the different calculation methods.

Worldwide there is a lot of knowledge on seismic engineering mainly by countries which suffer from earthquakes triggered by natural causes namely due to movement of tectonic plates. The so called human induced earthquakes are a new phenomenon and has different characteristics then natural earthquakes , the differences will be discusses in chapter 2.

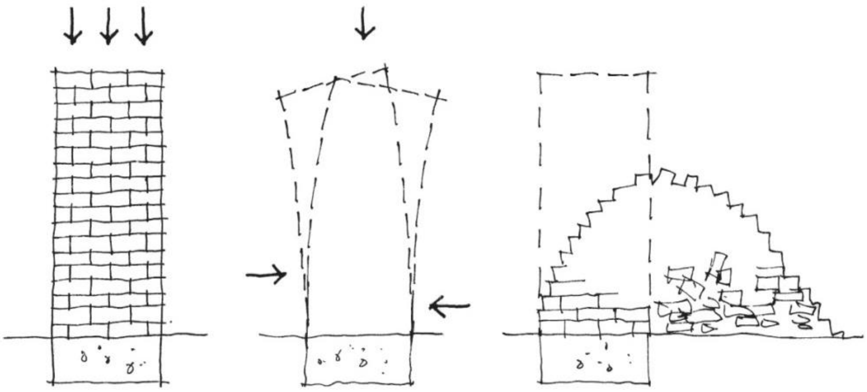

Fig. 1.4 Brick wall subjected to ground movement due to seismic forces (Branz, 2016).

As mentioned before part of current building stock is not capable of resisting the forces when the heaviest predicted earthquake occurs (fig. 1.4). This means that the current building stock needs be evaluated and where needed strengthened. This master thesis is not focussing on this aspect of the problem but on the design of new seismic resistant structures. This is done by searching for a solution in timber houses, without losing the identity of the Groningen area.

The thesis focusses on the influence of different calculation methods for timber structures. This is done by applying them to a case study building. The case study building is a traditional terraced house with masonry cavity walls which is redesigned to a timber structure. From the results of the calculation methods conclusions and discussions on how to calculate a timber structure are given.

1.2.1 Timber in seismic areas

Timber has specific benefits in seismic areas and is becoming even more interesting due to new development in the use and fabrication of timber based materials. In general timber structures in seismic areas have to following benefits.

1. Light weight of the structure
2. Redundancy due to different loading paths
3. Energy dissipative behaviour of the connections

These benefits will be further addressed in chapter 3.

There are several options for constructing in timber namely;

1. Prefabricated timber framed structures
2. Cross laminated timber (walls and floor) structures
3. Moment resisting frames
4. Pre-stressed timber construction, with dampers

This master thesis mainly focusses on CLT and timber framed structures.

1.3 Research questions

The problem definition and the scope has led to the following main research question.

1.3.1 Main question

"What is the influence of the seismic calculation method on a CLT structure? "

1.3.2 Sub-questions

Besides the main research question the following sub-questions are contributing to the research.

1. Can a terraced house with a timber structure withstand the seismic action in Groningen and keep their traditional appearance?

2. How does the seismic force influence the timber design and what are important factors to take into account?

3. What is the difference between the different seismic calculation methods?

4. What are the behaviour factors for timber structures and what is the background?

5. What are the options for modelling a timber structure in a finite-element package?

6. How to proof the q-factor for a structure using a non-linear static push-over?

7. Is possible to resist a heavier earthquake by optimisation of the design of the structure?

1.4 Reading guide

First an information about earthquakes and the differences between types of earthquakes is given. Followed by a short overview of the different calculation methods and the background of the dynamics used for seismic engineering. Then a first rough calculation is made of a structure with timber framed walls and CLT walls. The key results and steps are shown in the main report but a more detailed report is added in annex B. Then a short overview of finite element modelling options is given followed by explanation of the chosen option. A more detailed description and build-up of the model is added in annex C. The model is evaluated and results are discussed. Next this is translated and elaborated into a non-linear static push-over analysis. First general information about the push-over is given followed by application on the elaborated model. Concluded by recommendations and conclusions for the FEM modelling method, timber seismic engineering and calculation methods.

2 EARTHQUAKES

This chapter discusses the different types of earthquakes and how these earthquakes are triggered. The differences between the types of earthquakes are lined out followed by the consequences of these differences.

But first what is an earthquake? A definition of an earthquake given by the Collins English dictionary is as following:

> *" A sudden release of energy in the earth's crust or upper mantle, usually caused by movement along a fault plane or by volcanic activity and resulting in the generation of seismic waves which can be destructive"*

Citation 2.1 Definition of an earthquake (Collins English Dictionary, 2016).

As the definition states it is usually caused by movement along a fault or volcanic activity. For the Groningen situation this is not the case. The earthquakes are triggered due to human action, namely by the gas extraction and therefore called human induced earthquakes. Just like in the definition there is a sudden release of energy and the results can be destructive.

2.1 Types

As mentioned a coarse distinction can be between the following types of earthquakes:

1. Tectonic (volcanic)
2. Human induced

The main difference between the two types is the cause of the earthquake. The first type has a natural cause while the second is caused due to human interference.

2.1.1 Tectonic

Tectonic earthquakes are triggered due to movement of tectonic plates along fault lines. Fault lines are weak lines in a certain ground layer or plate. The movement is caused by volcanic activity in the inner earth crust. The movement can be categorized into three types due to the different boundaries:

- Convergent boundaries: Plates are moving apart and new crust is generated by the inflow of magma from below the crust. (Tension)
- Divergent boundaries: Plates are moving towards each other, where one of the plates slides beneath the other one and part of the crust is destroyed. (Compression)

- Transform boundaries: The plates slide alongside each other. (Shear)

When the pressure along the transform boundary increases to a certain level due to the movement a sudden release of energy will occur resulting in an earthquakes. The location where the energy is released is called the hypocentre or focus of the earthquake. The point perpendicular, where the seismic waves reach the surface, is called the epicentre. The hypocentre of tectonic earthquakes is generally more than ten kilometres below the epicentre.

The waves travelling from the hypocentre to the epicentre can be categorized into the following two types of waves.

- Primary waves (P-waves): Longitudinal waves (pressure wave) moving in the same direction as they are propagating with a speed around 6 km/h and therefore reaching the surface as first.

- Secondary waves (S-waves): Transverse waves (shear wave) moving perpendicular to their propagation with a speed around 3.5 km/h.

When reaching the surface the following surface waves occur, propagating over the surface from the epicentre outwards:

- Rayleigh waves: Acting from the epicentre over the surface and are generated by the primary and secondary waves causing the ground to move in an elliptical motion.

- Love waves: Propagating from the epicentre and causing a perpendicular motion.

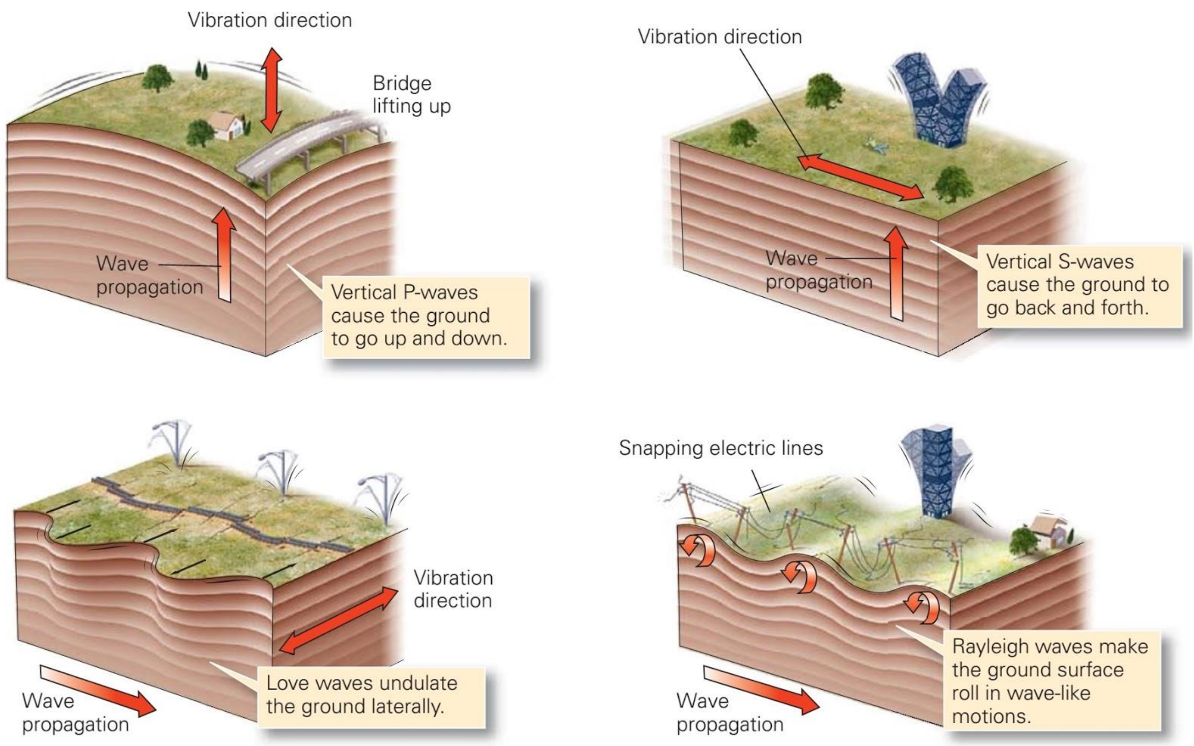

Fig. 2.1 The different wave propagations and the damage caused (Khattak, 2016)

When broaden the explanation of the tectonic earthquake it is the same as what happens with the horst and graben which led to the earthquake in Roermond. Due to movement and therefore tension on different 'blocks' of ground separated by a secondary fault line system the stresses are not in equilibrium causing an earthquake. The hypocentre of the earthquake was located at approximately seventeen kilometres below the epicentre (KNMI, 2016).

2.1.2 Human induced

As the name already mentions, they are triggered due to human interference. In the case of the Groningen situation the extraction of the gas has led to earthquakes.

The gas is extracted from a porous sandstone layer located approximately three kilometres below the surface. Due to the gas extraction the equilibrium in stresses between two ground blocks is disrupted. The blocks are separated by fault lines (fig. 2.2 a). With the pressure of the top layers acting on the sandstone layers and the difference in equilibrium this leads to a sudden slide of the block and release of energy, this is a so called human induced earthquake.

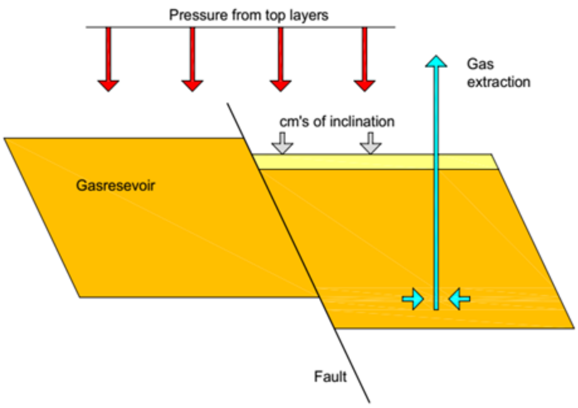

a) Mechanism triggering human induced earthquakes

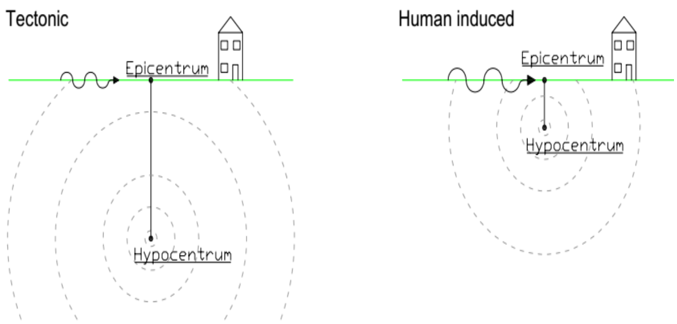

b) Distances of hypocentre

Fig. 2.2 Triggering and the difference between tectonic and human induced earthquakes

The fact that the sandstone layer is approximately three kilometres below surface also leads to a hypocentre close to the surface (fig. 2.3). Thus when the energy released at the hypocentre for both type of earthquakes is the same the damage at the surface caused by a human induced earthquake is more severe (fig. 2.2 b). The distance that the energy wave has to travel towards the surface is shorter for a human induced earthquake. Resulting in less damping and spreading of the wave but also a shorter duration of the earthquake.

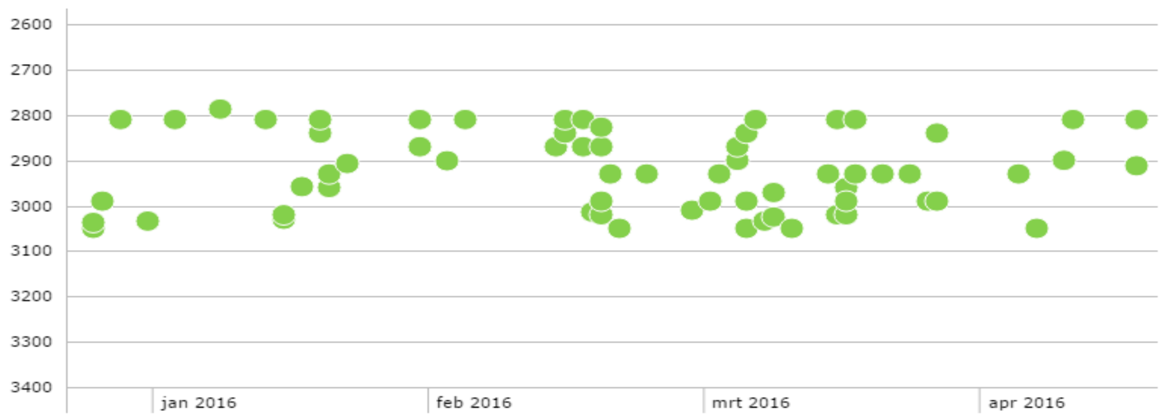

Fig. 2.3 Depth of the hypocentre of human induced earthquakes in Groningen (NAM, 2016).

2.2 Ground influence

Besides the distance of the hypocentre also the ground is of influence on the impact of the waves at the surface. Soft sentiments amplify the waves while hard rock sediments damp the waves.

Therefore the reaction caused by an earthquake is also related to the location of occurrence. In EC8 this is translated as following:

A. Rock $v_{s,30} > 800$ m/s
B. Dense sand, stiff clay $v_{s,30} = 360 - 800$ m/s
C. Dense or medium dense sand $v_{s,30} = 180 - 360$ m/s
D. Loose-to-medium cohesion less soil $v_{s,30} < 180$ m/s
E. Alluvium layer with stiff underlay

$v_{s,30}$ is the shear wave velocity at 30 meters below surface.

For the Groningen situation which is represented by the NPR 9998 a distinction between two ground conditions is made, namely normal and special conditions.

- Normal – no peat layers thicker than 1 metre starting 10 metres below surfaces and $v_{s,30} = 150 - 275$ m/s
- Special – peat layers thicker than 1 metre starting 10 metres below surfaces and $v_{s,30} = 150 - 275$ m/s

The NPR 9998 prescribes a location specific soil investigation where the shear wave velocity is measured. If the shear wave velocity is not known the first calculation can be made with a shear wave velocity estimated on the cone resistance of vertical pressure tests or mean values given in the code. However if the calculation is sensitive to small deviation of the shear wave velocity further investigation must be done.

When the specific location has normal ground conditions, the standard method for determining the response spectrum is advised. The response spectrum relates the earthquake characteristics to the behaviour of the structure this is further explained in the next chapter. Although it can be beneficial to apply the location specific method.

For locations with special ground conditions there are two options. First option is to apply the normal method for determining the response spectrum and multiply with a factor of 1.5. The second option is to use the location specific method for determining the response spectrum.

For the master thesis normal ground situation is assumed and therefore the normal method for determination of the response spectrum is applicable.

2.3 Impact measurement

Due to the differences between tectonic and human induced earthquakes, the characteristics are also different (table 2.1).

Table 2.1 General differences between tectonic and human induced earthquakes

Property	Tectonic	Human induced
Distance hypocentre	> 10 kilometre	3 kilometre
Duration	30-60 seconds	2-5 seconds
Frequency	1-2 Hz	2-10 Hz
PGA	< 0.5g	< 0.4g

These differences lead to a different approach for measuring the impact of the earthquakes. Normally earthquakes are measured with the Richter scale, however for comparison between the two types of earthquakes this does not gives a good overview. The Richter scale is a logarithmic scale which indicates the amount of energy released at the hypocentre, this does not give any indication about the impact of the earthquake at the surface.

Another measuring scale is the Mercalli scale. Instead of focussing on the energy released at the hypocentre, the Mercalli scale relates to the impact of the earthquake at the surface. The Mercalli scale (fig. 2.4) does not depend on the depth of the hypocentre and can be translated into a map which then shows the impact of the earthquake. Mostly the impact is highest at the epicentre and then gradually decreases.

EMS-98 Intensity	Felt	Impact	Magnitude (Approxi-mat Value)	Building Damage (Masonry)
I	Not felt	Not felt		
II-III	Weak	Felt indoors by a few people. People at rest feel a swaying or light trembling.	2 3	
IV	Light	Felt indoors by many people, outdoors by very few. A few people are awakened. Windows, doors and dishes rattle.		
V	Moderate	Felt indoors by most, outdoors by few. Many sleeping people wake up. A few are frightened. Buildings tremble throughout. Hanging objects swing considerably. Small objects are shifted. Doors and windows swing open or shut.	4	
VI	Strong	Many people are frightened and run outdoors. Some objects fall. Many houses suffer slight non-structural damage like hair-line cracks and falling of small pieces of plaster.		
VII	Very strong	Most people are frightened and run outdoors. Furniture is shifted and objects fall from shelves in large numbers. Many well-built ordinary buildings suffer moderate damage: small cracks in walls, fall of plaster, parts of chimneys fall down; older buildings may show large cracks in walls and failure of in-fill walls.	5	
VIII	Severe	Many people find it difficult to stand. Many houses have large cracks in walls. A few well built ordinary buildings show serious failure of walls, while weak older structures may collapse.		
IX	Violent	General panic. Many weak constructions collapse. Even well built ordinary buildings show very heavy damage: serious failure of walls and partial structural failure.	6	
X+	Extreme	Most ordinary well built buildings collapse, even some with good earthquake resistant design are destroyed.	7	

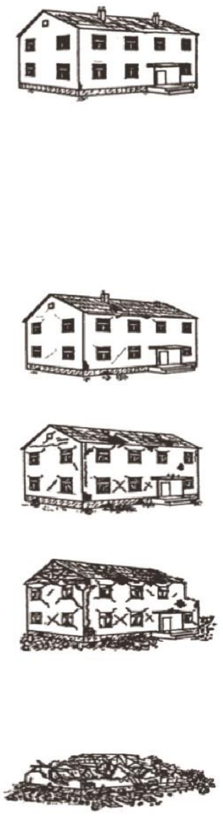

© Swiss Seismological Service

Fig. 2.4 Mercalli scale: European macro-seismic scale, introduced in 1998. For the Groningen situation the approximate magnitude value from the scale of Richter is not applicable (Swiss Seismological Service, 2016)

The earthquake at Roermond had a magnitude of 5.8 on the Richter scale and a VII on the Mercalli scale.

2.4 Peak ground acceleration

For calculation, the ground movement due to the earthquake is translated into a peak ground acceleration (PGA) map. For that reason ground motions, especially accelerations, caused by earthquakes are measured with seismometer. The data from these measurements is then translated to a PGA map, with a probability of occurring once in 475 years.

Fig. 2.5 Peak ground acceleration map of Groningen (Nederlandse praktijkrichtlijn (NPR 9998), 2015, December)

The peak ground acceleration (fig. 2.5) is given at a depth of 30 meters, this is due to the location specific soil conditions. Which influences the wave propagation as discussed in chapter 2.2.

3 SEISMIC ENGINEERING

Knowing the PGA and therefore the acceleration the forces can be calculated according to Newton's second law.

$$F = m \cdot a \qquad \text{(eq. 3.1)}$$

However this does not takes the reaction of the structure into account. Since the ground motion is a dynamic force the reaction of the structure is dependable on its mass and stiffness. There are multiple seismic calculation methods which takes this into account. This will be explained in this chapter.

From this it becomes clear that a response spectrum is needed. The response spectrum is made by linear elastic calculation from the dynamic input on a single degree of freedom system. However the structure will not always react linear elastic, therefore behaviour factors are introduced. To take the non-linear response into account. This is further elaborated in paragraph 3.3.

The previous chapters are very general and not specific for timber structures. From paragraph 3.4 the report focusses on the principles related to timber structures subjected to seismic forces.

3.1 Seismic force

The reaction from seismic force as well as from wind load is a lateral force acting on the structure. Difference between the lateral forces from wind and seismic, is that the wind force is dependable on the geometry of the structure whereas the seismic force is dependable on the stiffness and mass of the structure. The reaction of a building to the lateral forces(fig. 3.1) consists of shear walls and floors acting as diaphragms.

An earthquake also introduces vertical forces. In vertical direction the forces are generally neglected, according to the Eurocode 8. First of all the effects are covered by the partial factors for the permanent actions and the imposed loads. The partial factors are normally greater than 1.0, whereas for an earthquake which is an extreme load conditions these factors are 1.0. This is valid except when a structure has beams with a long span and significant mass along the span.

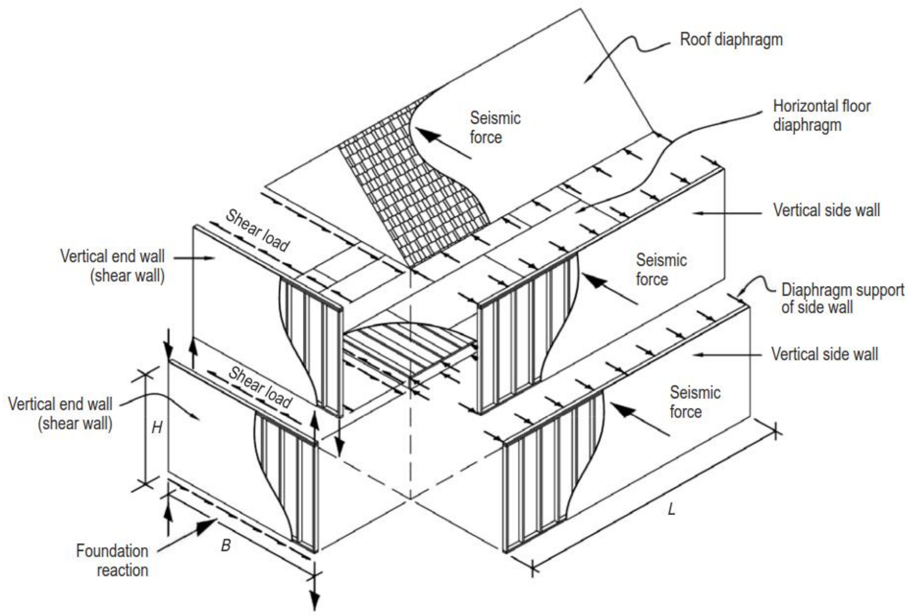

Fig. 3.1 Force distribution in a building with walls acting as shear walls and floors and the roof as horizontal diaphragm (NIST, 2014).

The calculation of the resistance of the building to wind loads is normally done elastic, due to the fact that it is not preferable to have permanent deformation due to plasticity. For seismic forces this is different. Since it is an extreme load condition a certain amount of damage and deformation is allowed. This is necessary to construct economically feasible structure.

The damage caused by the earthquake is divided into three limit states (Nederlandse praktijkrichtlijn (NPR 9998), 2015, December):

<u>Near Collapse (NC)</u>: the structure is heavily damaged; vertical elements still capable of transferring the vertical loads; non-load bearing parts of the structure may fail; large permanent deformation occur. The load bearing capacity of the structure prevents progressive collapse but when the structure is exposed to another earthquake or force, the structure will probably collapse. Therefore near collapse is an extraordinary design situation.

<u>Significant Damage (SD):</u> the damage is significantly; vertical elements still capable of transferring the vertical loads; non-load bearing parts are damaged; permanent deformation is less; economically non profitable to repair the structure.

<u>Damage Limitation (DL):</u> repair of the structure is not necessary; constructive elements are not significantly deformed and have obtained there stiffness and strength; non-load bearing elements are cracked but can easily be repaired; no significant permanent deformation.

The above damage levels are often translated into allowable deformation of the structure. For timber structures this is translated into a maximum of allowable uplift or inter-storey drift.

3.2 Calculation methods

The forces acting on the structure can be calculated with four different calculation methods according the EC8, namely:

- Lateral force analysis
- Modal response analysis
- Non-linear push-over analysis
- Non-linear time history analysis

The methods are listed from fast and simplistic to more elaborate and complex. This paragraph gives a short overview of the different methods which can be used. The first two methods will be applied in chapter 4 and the non-linear push-over analysis is further explained in chapter 6 and 7. The non-linear time history analysis is not used in this master thesis.

3.2.1 Lateral force analysis

This method assumes that the structure is vibrating in its first fundamental modal shape. This is because the building is schematised as a single degree of freedom system with a certain mass and stiffness (fig. 3.2).

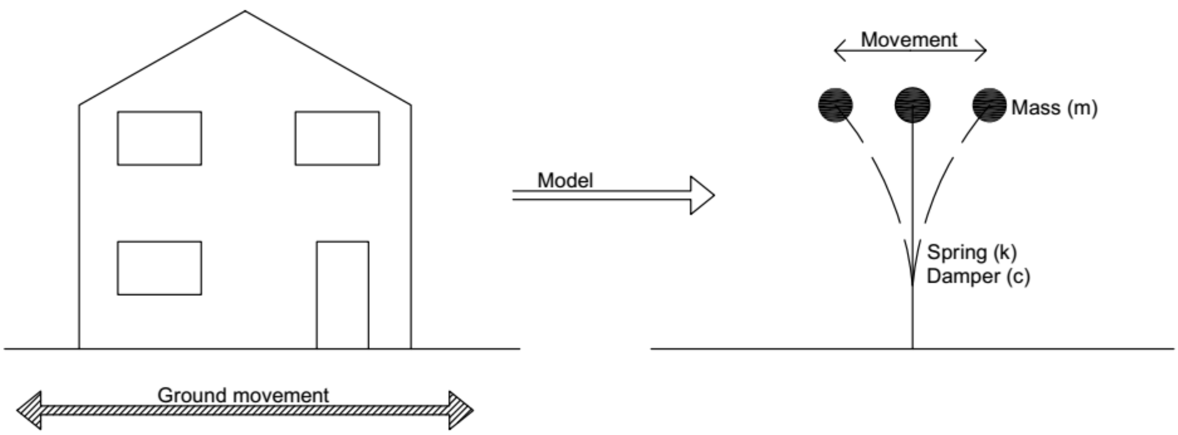

Fig. 3.2 Schematisation for the lateral force method

To account for the dynamic reaction of the structure to the earthquake a response spectrum is used. The response spectrum is explained in paragraph 3.3. The resonance or damping which is dependent on the natural period of the structure and the earthquake is translated into the response spectrum. From this the base shear force acting on the structure is obtained.

For calculation of the natural period different methods are proposed which will be addressed in chapter 4.The influence of the natural period is significant due to the fact that the reaction of the structure to the earthquake is dependable on this.

As mentioned the method assumes that the structure is vibrating in the first modal shape. However when the structure would be modelled as a structure with multiple masses there are also more modal shapes. This results in a different mass participation percentage for each modal shape. This is taken into account by introducing the λ factor which reduces the mass to 85% when the building has two or more storeys.

The nonlinear behaviour of the building is taken into account by using the q-factor this translates the elastic response spectrum to the design response spectrum. For this method the q-factor is given in the Eurocode 8. The q-factors are recommended values given for certain structural systems. By applying the q-factor the design shear force acting on the structure is calculated.

The main benefit of the method is that the calculation follows a normal elastic calculation and the effect of the non-linearity is taken into account by the q-factor. This makes it a fast and simple method which is applicable for simple and regular buildings. However the downside of the method is that it is force based and does not give any insight in the reaction and behaviour of the structure.

3.2.2 Modal response analysis

For a modal response analysis the building is schematised as a multi-degree of freedom system(fig. 3.3). This is done by translating the building into a discreet system with lumped masses and a certain stiffness for each storey.

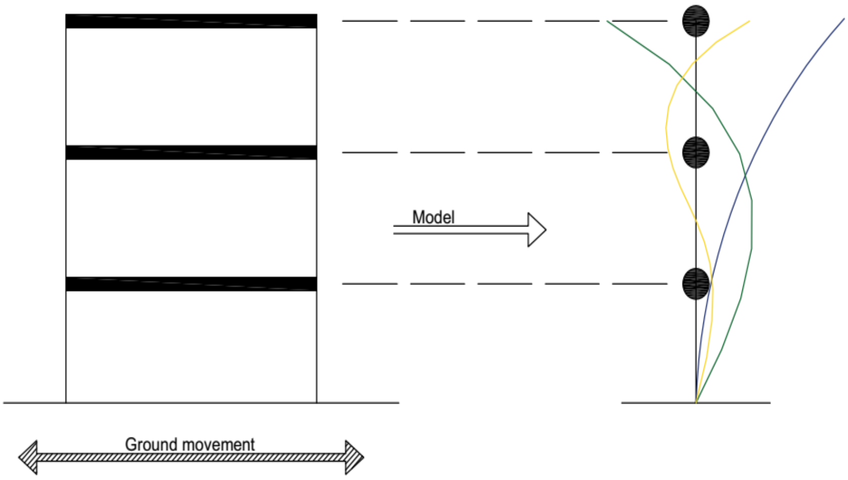

Fig. 3.3 Schematisation and modelling of a multi-storey building for a modal response analysis.

The number of the modal shapes is related to the number of masses. In other words if there are three lumped masses there are also three model shapes and therefore three base shear forces.

By making use of the dynamical method for the modal analysis, the natural period of each vibration mode is calculated. This is done by setting the determinant of the system to zero. Resulting in the eigenvalues which are then translated into the natural period. Then with the use of the response spectrum this is then translated into the base shear for each natural period. The load distribution in this case is dependable on the vibration mode. The shape of the modal response is determined by the eigenvectors of the system.

Since multiple vibration modes are considered not all of the mass is participating in each vibration mode. Resulting in the following requirement. A total of 90% or more of the total mass of the building and each individual mode with a mass participation of 5% more must be taken into account.

The modal responses may be taken independent of each other if the following condition is fulfilled.

$$T_j \leq 0.9 \cdot T_i \qquad \text{(eq. 3.2)}$$

Where T_i and T_j are the natural periods of the different modal responses. When the modal responses can be taken independent of each other the SRSS-method (square root of sum of squares) may be applied for combining the seismic effects from each vibration mode.

$$E_E = \sqrt{\sum E_{E,i}^2} \qquad \text{(eq. 3.3)}$$

Where E_E is the total seismic effect and $E_{E,I}$ is the effect of each individual mode. The seismic effect can either be the forces or the displacement.

If the modal responses cannot be taken independently they need to be combined using the CQC-method (Complete Quadratic Combination). Because using the SRSS-method would give an unconservative result if the two natural periods of the mode shapes are close to each other. The CQC-method is described in section 4.2.1.3 of EC8-2.

Also for the modal response method the non-linearity of the structural system is taken into account by the q-factor. With the use of the q-factor the elastic response spectrum is translated to the design response spectrum taking the damping or resonance of the structure into account.

The benefit of using the modal response spectrum analysis is that it takes multiple modal shapes into account. This is important when the building has irregularity and the first modal shape is not governing. Meaning that one of the other vibration modes have a high mass participation percentage. The method is more elaborate but gives a better insight in the dynamics of the structure. Downside is that it is force based and does not give any information about the behaviour of the structure.

3.2.3 Non-linear static push-over analysis

The previous two methods are force based, with the q-factor dependable on the structural system of the building. A non-linear static push-over analysis gives a view of the behaviour of the building and its displacement in its first fundamental mode shape. The principle of the method is to combine the push-over of a MDOF system with the response spectrum analysis of an equivalent SDOF system. For visualisation the spectrum is translated into an acceleration-displacement diagram. How this is done is further explained in the next paragraph. For the visualisation also the elastic spectrum is translated to the inelastic spectrum.

The analysis is carried out with constant vertical gravity loads and an increasing monotonically horizontal loading pattern. This means that the push-over is force controlled and does not give information about the behaviour of the structure after reaching the ultimate force. There are two loading patterns which need to be taken into account. The first is related to the mass and height of the building. The second is related to the displacement as can be calculated from the Rayleigh method. From these two push-overs the most unfavourable result has to be used for further analysis. Consequently this means that the analysis is most accurate for buildings oscillating in the first mode.

The benefits of the method is that it gives information about the strength and ductility of the structure. This is not obtained by the previous two methods, which are based on elastic calculation with a q-factor. A limitation of the method is that it is time-independent. Meaning that it does not takes the effect of higher modes into account. As a result it is inaccurate for buildings which oscillates in higher modes and does not gives an insight in the dynamic behaviour of the structure after reaching its maximum force.

3.2.4 Non-linear time history analysis

This method does not make use of the response spectrum to relate the response of a structure to an earthquake. It makes use of a recorded earthquake signal and therefore this method is time dependent. To take into account heavier earthquakes then registered the earthquake signal can be magnified by a certain factor. For a good overview the building has to be subjected to multiple earthquake signals. Since every earthquake signal is different it has different frequencies to which the structure can resonate.

The benefit of the method is that it gives information about the dynamical behaviour of the structure and is not limited to a single oscillation mode. It also gives an insight in the strength and force distribution, this is all related to the proper detailing of the structure. Downside is that it is a very elaborate and time consuming method especially since more time signals have to be applied, but the method is accurate. Due to the long calculation time the method is not often used as design method but it is used for determination of the capacity of existing buildings.

3.3 Response spectrum

In the previous paragraph the response spectrum is often mentioned. This will now be further explained in this paragraph.

When designing a structure in a seismic area, the building can be subjected to ground motions caused by an earthquake. The movement of the ground introduces dynamical forces on a structure, which are related to the stiffness and damping of the structure. To take this into account the structure is modelled as an linear elastic single degree of freedom (SDOF) system (fig. 3.4 a).

From earlier earthquakes the ground movement and also the acceleration is registered (fig. 3.4 b). Using the registered accelerations of the measured earthquakes and the SDOF system the reaction from a building to an earthquake is translated to a force acting on the structure. By calculating this for structures with different natural periods[1] a linear elastic response spectrum is produced. When the natural period is close to one of the periods of the earthquake this leads to resonance resulting in an amplified response. From this diagram the magnification factor of the force acting on the structure, due to the earthquake, can be obtained. By doing this for several categorised earthquakes and then envelope and smooth them a linear elastic spectrum is obtained (fig. 3.6). The categorisation is dependable on the ground conditions, this affects the propagation of the waves from earthquakes. The following explanation is derived from *Seismic design of buildings to Eurocode 8,* edited by Ahmed Y. Elghazouli.

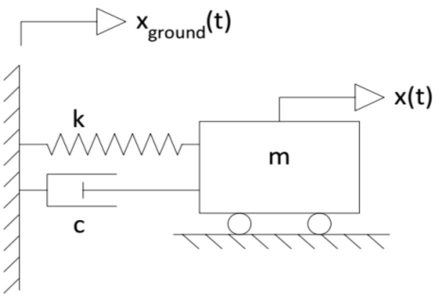

a) Single degree of freedom system

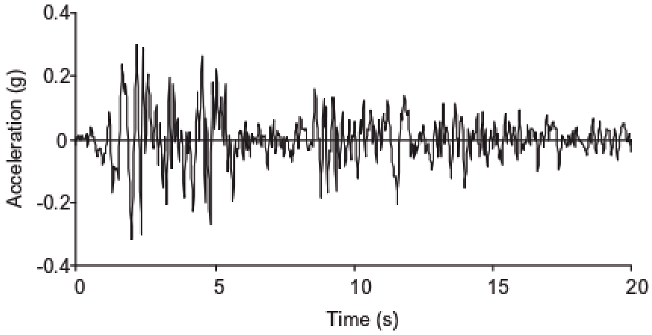

b) Acceleration diagram measured by a accelerometers.

Fig. 3.4 The acceleration is the input on the single degree of freedom system to calculate the elastic response spectrum.

The reaction of the SDOF system to the earthquake can be described by its equation of motion.

$$m\ddot{x} + c\dot{x} + kx = kx_{ground} + c\dot{x}_{ground} \qquad \text{(eq. 3.4)}$$

Where *m* is the mass of the system, *c* the viscous damping and *k* the spring stiffness. Furthermore $\ddot{x}$, $\dot{x}$, x are respectively the acceleration, velocity and displacement of the SDOF system. Finally x_{ground} is the ground displacement and $\dot{x}_{ground}$ is the ground velocity.

The previous equation can be rewritten in the following form.

$$m\ddot{x} + c\left(\dot{x} - \dot{x}_{ground}\right) + k\left(x - x_{ground}\right) = 0 \qquad \text{(eq. 3.5)}$$

By introducing $y = x - x_{ground}$ which is the relative displacement the equation becomes.

$$m\ddot{y} + c\dot{y} + ky = -m\ddot{x}_{ground} \qquad \text{(eq. 3.6)}$$

To find the natural periods the homogeneous part of the differential equation (eq. 3.4) is solved. First equation is rewritten in the following way.

$$\ddot{x} + 2\xi\omega_n\dot{x} + \omega_n^2 x = 0 \qquad \text{(eq. 3.7)}$$

[1] Further explained in chapter 4.1.1.1

With $\xi = c/2\sqrt{km}$ and $\omega_n = \sqrt{k/m}$, solving this differential equation leads to.

$$x(t) = e^{-\xi\omega_n t}\left(A\cos(\omega_1 t) + B\sin(\omega_1 t)\right) \qquad \text{(eq. 3.8)}$$

With $\omega_1 = \omega_n\sqrt{1-\xi^2}$ and A, B can be determined with the initial conditions.

The damping ratio ξ for the systems is taken at 5 %, this is due to the energy dissipation capabilities of a structure. As can be seen it is related to the linear viscous damping but this is hard to calculate therefore the assumption of a damping ratio of 0.05 is usually applied in earthquake calculations.

From (eq. 3.8) the Eigen period of a system becomes.

$$T_e = \frac{2\pi}{\omega_1} \qquad \text{(eq. 3.9)}$$

Since the part of the damping ration is almost equal to unity $\sqrt{1-\xi^2} = \sqrt{1-0.05^2} \approx 1$, the natural period is used for response diagram is.

$$T_n = \frac{2\pi}{\omega_n} \qquad \text{(eq. 3.10)}$$

When the frequency of the building is close to one of the frequencies of the ground movement this amplifies the acceleration of the structure. This is also dependable on the damping ratio of the structure, which is normally set to 5%, equals 0.05.

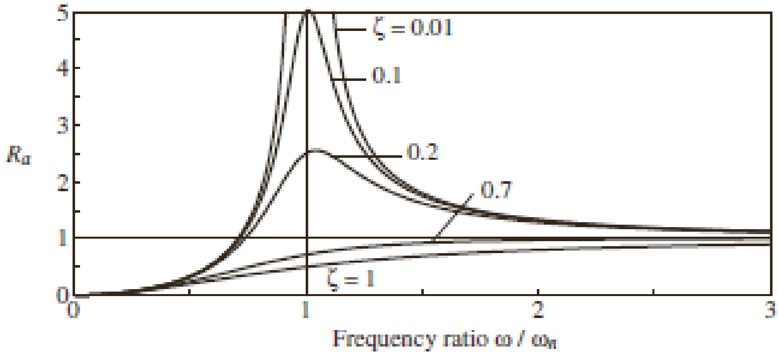

Fig. 3.5 Principle of the amplitude magnification factor for a SDOF. Earthquakes consists of multiple harmonic forces therefore there are more crucial ratio's. (Chopra, 2012)

By calculation and solving the differential equation (eq. 3.4) for various natural periods and earthquake signals the response spectra are made. The solution to (eq. 3.4) can be found with use of the Duhamel integral or Fourier analysis (not elaborated in this report). The reactions have lots of irregularities at the maxima and minima, therefore this is converted into response spectra using the envelopes (fig. 3.6). For the transformation statistics and engineering judgement is used. The response diagram consist of a part with constant acceleration (T_B - T_C), constant velocity (T_c - T_D)and constant displacement from the point T_D. However for the Groningen situation which is described in the NPR 9998 the spectrum consist of a branch with constant acceleration and displacement. this is possibly due to curve fitting.

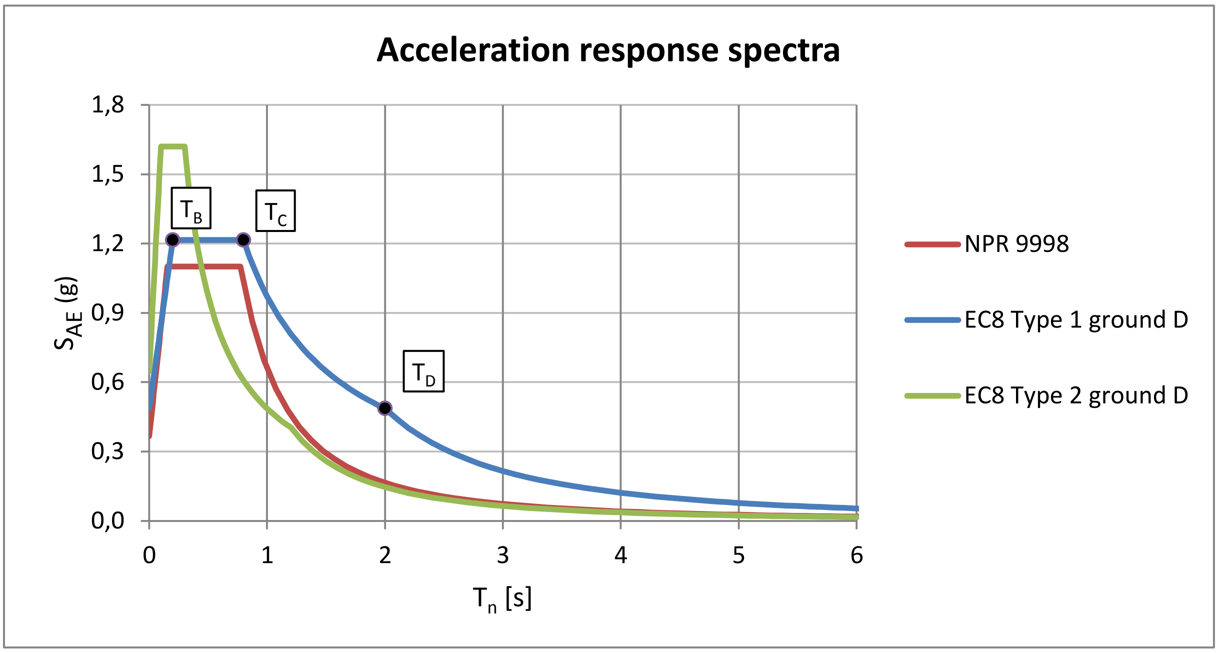

Fig. 3.6 Spectra from the NPR and EC8, where in the EC8 a distinction is made between types of earthquakes. From the graph it becomes clear that the characteristics of the earthquake has an influence on the reaction of the structure, translated into the response spectrum. The background of these differences is explained in chapter 2. A description and calculation of the linear elastic response spectrum can be found in appendix B. The NPR consequence factor (k_{ag}) = 1.4 and PGA = 0.36g. For EC8 type 1 and 2, distinction is made between magnitude of the surface waves.

From the response spectrum diagram the horizontal force, the base shear, can be determined.

$$F_b = m \cdot S_{AE}(T) \qquad \text{(eq. 3.11)}$$

Where F_b is the base shear force, m the mass and $S_{AE}(T)$ the magnified ground acceleration from the response spectra, the value from the figure has to be multiplied by g the gravity constant (9.81 m/s²). As mentioned the magnification of the PGA is related to the stiffness of the building which is expressed in its natural period. If the natural period of the structure is close to one of the dominant periods of the earthquake the structure attracts more force from the earthquake, due to resonance, which is translated into a higher acceleration magnification factor (fig. 3.7).

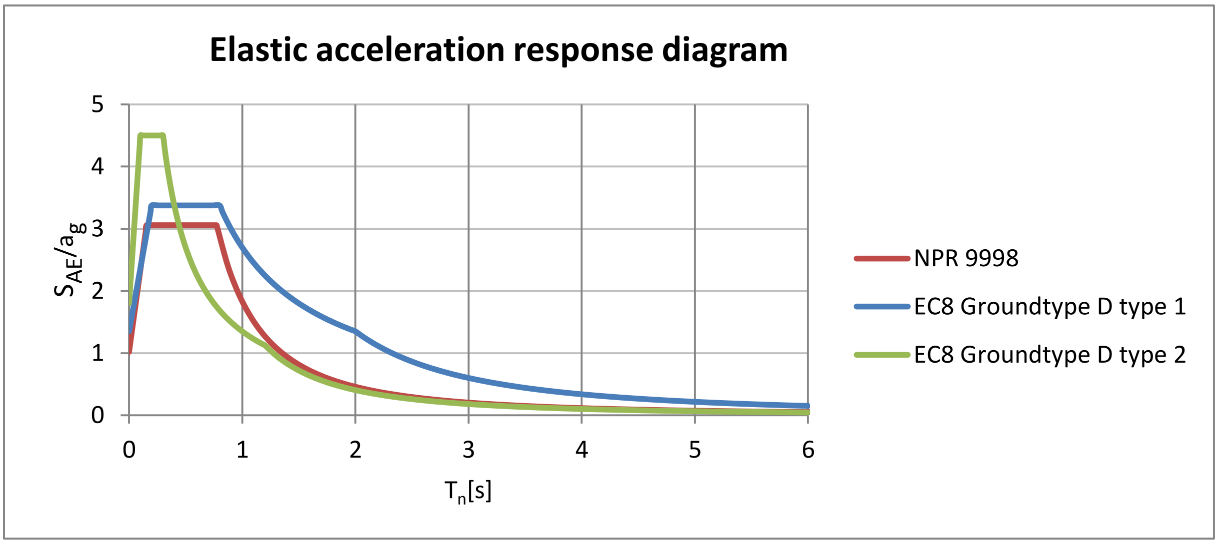

Fig. 3.7 Visualisation of the magnification of the peak ground acceleration, with the same input as in fig. 3.6. The figure is obtained by dividing magnified ground acceleration by the initial PGA, giving the normalised values.

The response spectra in fig. 3.6 is the elastic response and does not take ductility and energy dissipation into account. Therefore a certain behaviour factor (q-factor) is introduced, from which the design response spectrum can be obtained.

$$F = m \cdot \frac{S_{AE}(T)}{q} \qquad \text{(eq. 3.12)}$$

The influence of the q-factor is further addressed in paragraph 3.4 and shown in fig. 3.11.

3.3.1.1 Influences of the mass

From the dynamical background the influence of the mass of the structure becomes clear. It is directly influencing the lateral force as can be seen from equations 3.11 and 3.12. Besides this the mass can also be found in the calculation of the natural period which is linked to the reaction of the structure. When equation 3.7 is rewritten the natural period can be calculated as following.

$$T_n = 2\pi\sqrt{\frac{m}{k}} \qquad \text{(eq. 3.13)}$$

From this the negative part of the mass becomes clear. When the stiffness remains the same and the mass is lowered this leads to a shorter natural period. Resulting in a higher magnification factor, except when remaining on the plateau of the spectrum. There will be no negative effect if $T_n < T_C$. A lower mass can have a negative effect resulting in a shorter natural period, but it is the square root of the mass which contributes to the natural period. Therefore a lower mass is still favourable since its contribution is linear in the calculation of the base shear force (eq. 3.11).

3.3.2 Displacement spectrum

Besides the acceleration also the displacement spectrum is determined with dynamics. The maximal acceleration is reached when the relative displacement (y) is at its maximum and the relative velocity ($\dot{y}$) is zero, which implies that the damping is zero ($c \cdot \dot{y} = c \cdot 0 = 0$). This is only at the point of maximal acceleration. At this point the spectral displacement is linked to the acceleration in the following way, both are forces (first mass times acceleration and spring stiffness times displacement):

$$mS_{AE} = kS_{DE} \qquad \text{(eq. 3.14)}$$

Where S_{AE} is the elastic acceleration factor and S_{DE} is the elastic displacement.

Note: It is the absolute acceleration of the mass ($\ddot{x} + \ddot{x}_{ground}$) and the relative displacement (y) of the mass to the ground. Meaning that the force in the spring is determined by the relative displacement while the acceleration on the mass is dependable on the SDOF system and the ground acceleration.

When rewriting the stiffness using the natural period of the system the following relation is obtained.

$$T_n = \frac{2\pi}{\omega_n} = \frac{2\pi}{\sqrt{k/m}} \qquad \text{(a)}$$

$$k = \frac{4\pi^2}{T_n^2} m \qquad \text{(b)} \qquad \text{(eq. 3.15)}$$

$$S_{DE} = S_{AE} \cdot \frac{T_n^2}{4\pi^2} \qquad \text{(c)}$$

From this the displacement spectrum can be obtained from the elastic acceleration spectrum fig. 3.8. The q-factor is not applicable on the displacement, but only on the forces.

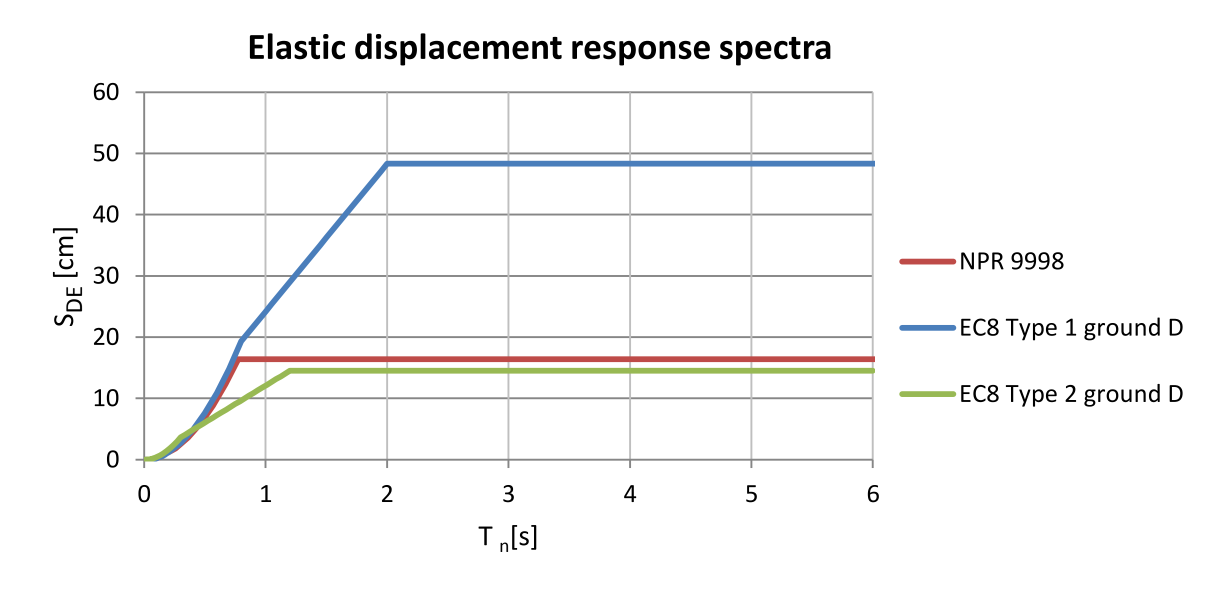

Fig. 3.8 The displacement spectrum for the different earthquakes, related to the natural period of the building. This leads to a limited displacement coming forward from the earthquake characteristic for type 2 and NPR 9998.

Visible in the graph are the different parts of the acceleration response spectrum can be distinguished. Namely the acceleration branch at the start followed by the velocity and finally the constant displacement. Since the NPR 9998 does not have a branch with constant velocity only two branches are obtained.

3.3.3 Acceleration displacement diagram

The acceleration displacement diagram (AD diagram) is made by combining the acceleration (fig. 3.6) and displacement diagram (fig. 3.8). The difference in the graphs is due to the fact that the NPR 9998 does not have a branch with constant velocity.

The AD diagram is used for visualisation between the earthquake (demand) and the building (capacity), this is further addressed in chapter 6.

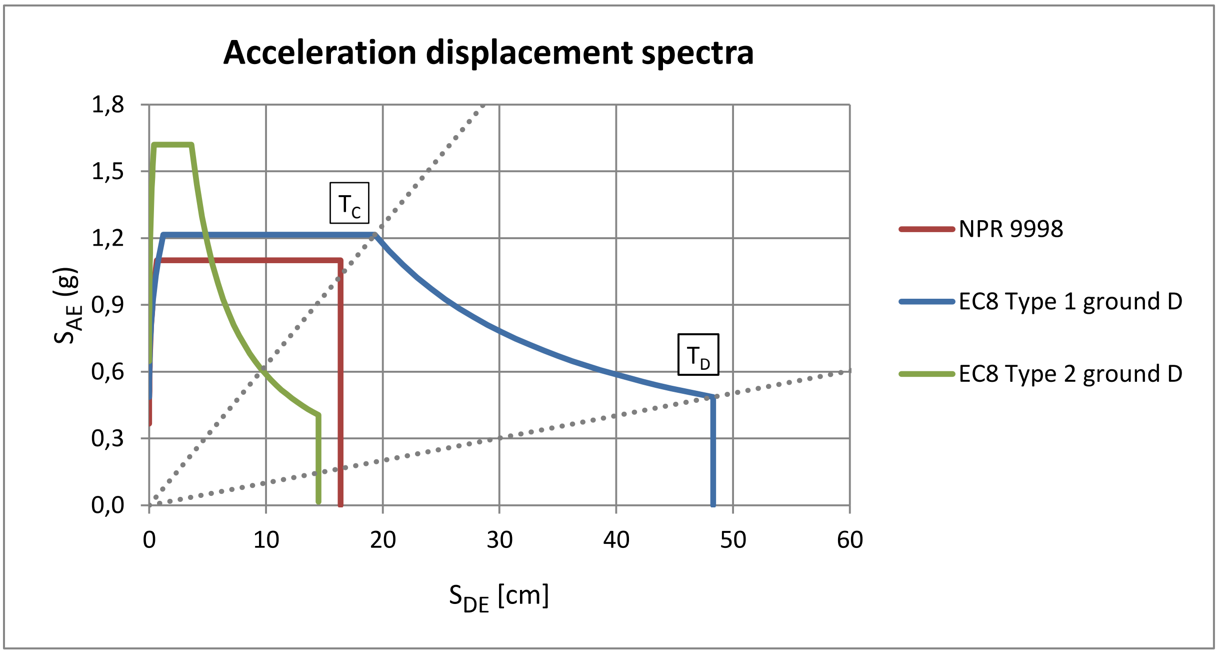

Fig. 3.9 The acceleration displacement diagram for the elastic situation. The dotted lines show the corresponding natural period of a building for EC8 type 1 ground D.

The maximum elastic ductility demand in the AD-diagram for the NPR 9998 and EC8 type 2 is different from the EC8 type 1. This leads to the fact that the it is possible for a building to fulfil the maximum demanded displacement of the NPR 9998 and EC8 type 1. Also because the derivation of the spectra showed that the displacement and acceleration spectra are not directly related to the mass. The mass is related to the force and the natural period of the building which is linked to the reaction of the building and therefore its location in the spectrum. This shows the influence of the earthquake signal and the ground influences leads to a different AD – diagram.

3.4 Behaviour factors for timber constructions

The response spectrum derived with the principles from the dynamic background is calculated with an elastic spring in the SDOF. However structures will not react linear elastic but non-linear, to account for this a behaviour factor called the q-factor is introduced.

The q-factor gives an indication of the ability of a structure to dissipate energy and withstand large deformations without failure (Ceccotti & Sandhaas, 2010). Attention must be paid to the fact that the q-factor is not mainly dependable on the material but on the structural system as a whole.

Design concept and ductility class	*q*	Examples of structures
Low capacity to dissipate energy - DCL	1,5	Cantilevers; Beams; Arches with two or three pinned joints; Trusses joined with connectors.
Medium capacity to dissipate energy - DCM	2	Glued wall panels with glued diaphragms, connected with nails and bolts; Trusses with doweled and bolted joints; Mixed structures consisting of timber framing (resisting the horizontal forces) and non-load bearing infill.
	2,5	Hyperstatic portal frames with doweled and bolted joints (see **8.1.3(3)**P).
High capacity to dissipate energy - DCH	3	Nailed wall panels with glued diaphragms, connected with nails and bolts; Trusses with nailed joints.
	4	Hyperstatic portal frames with doweled and bolted joints (see **8.1.3(3)**P).
	5	Nailed wall panels with nailed diaphragms, connected with nails and bolts.

Fig. 3.10 Examples for the ductility classes according to EC8 for timber structures

When applying the q-factor the elastic response diagram is transformed into a design response spectrum. The codes give a certain value for the q-factor, depending on the structural systems (fig. 3.10), which can be applied for calculation. This allows the engineer to calculated with an reduced elastic force.

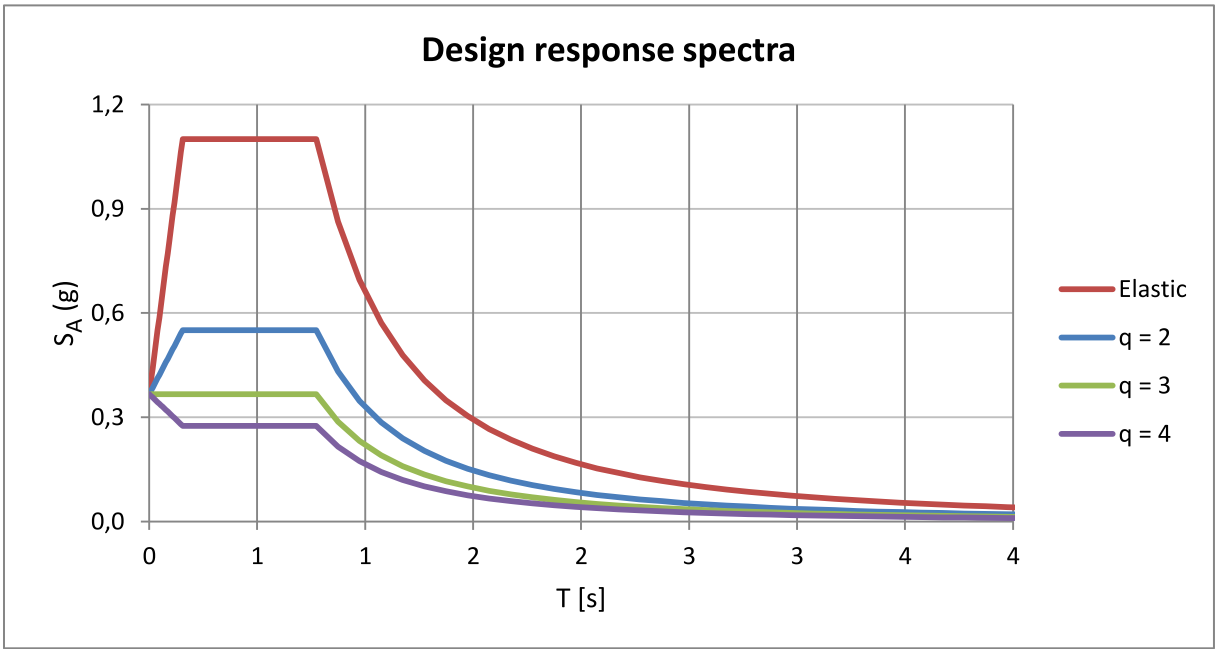

Fig. 3.11 The response spectrum with the q-factors taken into account. The design response spectrum is made for the NPR 9998 with the same input as in fig. 3.6.

3.4.1 Energy dissipation of timber structures

For timber construction the q-factor is mainly dependable on the hysteretic behaviour of the connections which allow energy dissipation. During loading plasticization of the steel connectors occurs which allows the connection to deform (fig 3.12). To be sure that ductile deformation occurs first and no brittle failure takes place, over-strength factors are applied. This principle is explained in paragraph 3.4.

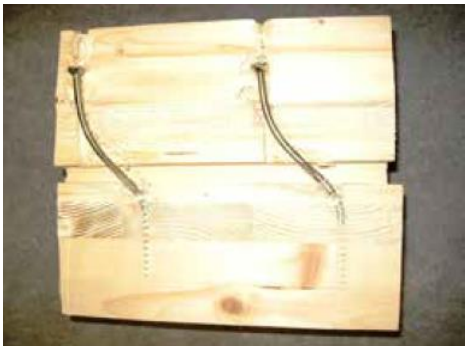

Fig 3.12 Ductile failure mode of metal connectors. (FPinnovations, 2013)

3.4.2 Connections

For the energy dissipative behaviour the connections are of crucial importance. There is a difference between the connections for timber framed walls (TF) and for CLT walls. For TF walls the panels are connected to the timber frames by a large number of nails which can all deform, whereas this is not the case for CLT structures. This has as consequence that CLT is less energy dissipative, resulting in a lower q-factor. Apart from the connection of the sheeting for TF walls they both have connections in common (fig 3.13).

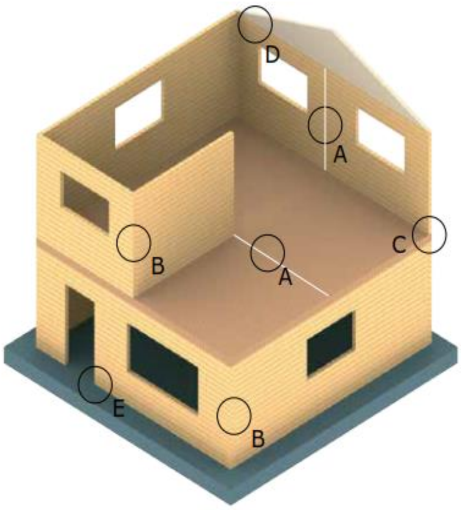

Fig 3.13 Definition of joints in a CLT structure (FPinnovations, 2013)

The following connection are used for the construction of a CLT house.

A. Panel – panel connection
B. Wall – wall connection
C. Wall – floor connection
D. Wall – roof connection
E. Wall – foundation connection

3.4.2.1 Timber framed panels vs. CLT panels

Before going into a more detailed description of the connections for the two most common wall types will be addressed.

Timber framed wall

For timber framed construction a frame work is made consisting of post and beams onto which the sheeting is attached. There are different sheeting materials for instance OSB, particleboard or LVL. The sheeting material is most of the time nailed to the framework. Next the elements are connected to the foundation or floor by hold-downs and angle brackets.

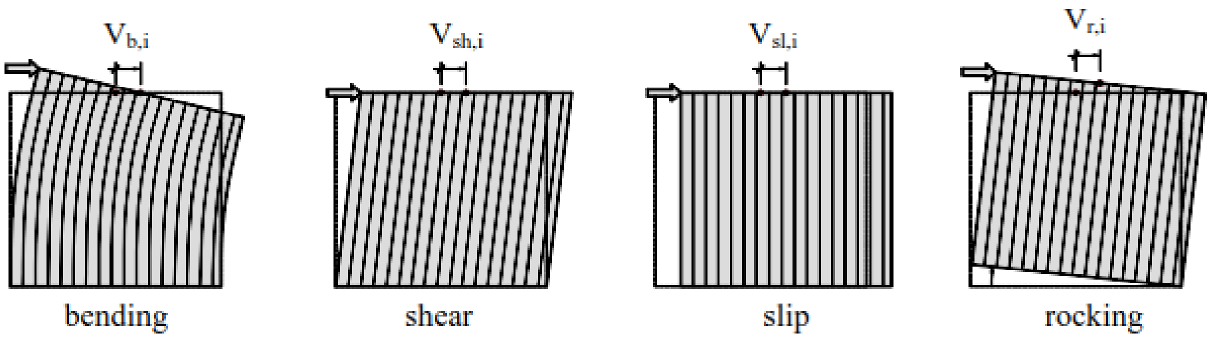

Fig. 3.14 Deflection of a horizontally in plane loaded wall (Piazza, 2013).

When a TF wall is subject to a cyclic horizontal load it deforms and the connections can start to yield and dissipate energy. The total deformation capacity of a TF wall is determined by the following aspects.

- Bending deformation of the wall (bending)
- Shear deformation of the wall (shear)
- Sliding of the connections (slip)
- Uplift from the overturning moment (rocking)

The sliding is due to the reaction forces in the angle brackets which connect the wall to the floor or foundation. Also the nails between the sheeting and the frame contribute to the sliding. Hold-downs are mainly used for restricting the uplift due to the overturning moment.

The bending and shear deformation of the wall are a brittle failure mode. While the slip and rocking deformation are ductile failure modes, if the connection are designed properly. When correctly designed TF has high potential energy dissipation due to the yielding of the large number of nails between the frame and sheeting. Besides the energy dissipation this also ensures redundancy due to the large number of loading paths. However it must be ensured that yielding starts at these connections, therefore capacity design is important and the over strength factors must be taken into account.

Cross-laminated timber wall

CLT is build up out of cross wise connected timber boards (fig. 3.15), creating a solid timber element which can be used as loadbearing element. CLT is suitable for walls loaded in plane as well as for floors which are loaded out of plane.

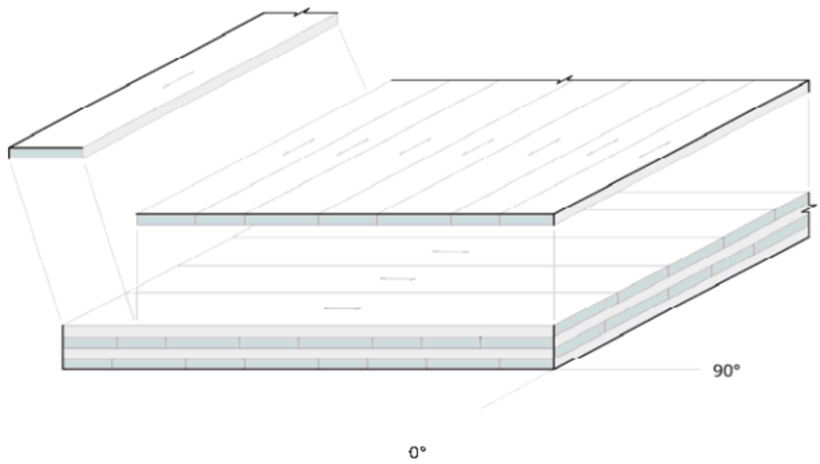

Fig. 3.15 Cross-laminated timber build-up (ProHolz Austria, 2014)

CLT walls are normally made of softwood boards, mostly spruce of strength class C24 is used. The boards are bounded together at the sides of the boards and optionally at their narrow faces (fig. 3.16). CLT generally consist of 3, 5 or 7 layers, with thicknesses ranging from 12 to 45 millimetre. The single boards commonly have a width of 150 millimetre and the entire CLT panel can be until lengths of 16 meter and widths up to 3 meter. Research has shown that these dimensions are extended to 30 by 4.8 meter (ProHolz Austria, 2014).

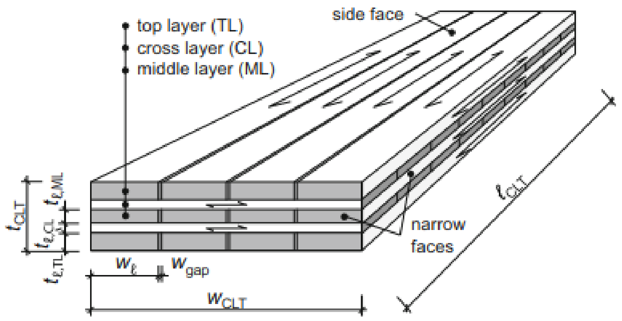

Fig. 3.16 Drawing of CLT with specific terms (Brandner, Flatscher, Ringhofer, Schikhofer, & Thiel, 2015).

In contrary to TF construction the CLT construction the wall itself is stiff and has less contribution to the horizontal displacement .Therefore research suggests that the contribution of deformation for CLT is mainly focused on the connections (Piazza, 2013).

The contributions of the total deflection for a CLT wall connected to the foundation with four angle brackets is as following:

- CLT (bending and shear): 5-10%

- Slip 20-25%
- Rocking 65-75%

With different configuration of connecters the contribution of the elements to the total deflection changes, however the CLT deformation remains relatively small (<11%). The percentages given are for a wall with a height and length of 2.5 metres. If the height over length ratio is lowered there will be more slip and les rocking of the wall. Also the wall had no openings. When openings are added, for example for windows or doors, the contribution of the CLT to the total horizontal deflection increases.

The disadvantage of using CLT is that there is less deformation in a CLT panel wall then a TF wall leading to a lower ductility factor due to the lower capability of dissipating energy.

The advantage on the contrary is that there will be less permanent damage after an earthquake. Due to the stiffer structure and the self-centring capabilities of the CLT wall. The self-centering capability is due the fact that most of the rocking deformation can be restored. Another advantage is the reparability. The connections can be repaired by making use of remaining nail locations in the connection or by relocation of the connection.

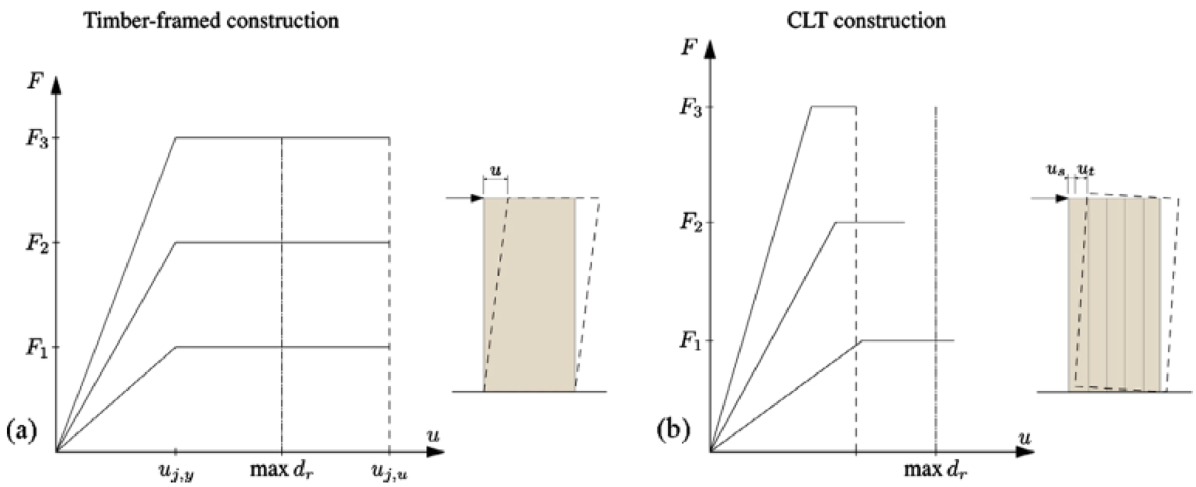

Fig. 3.17 Simplified bilinear load-deflection graphs for TF and CLT walls. The difference in deformation in clearly visible. (Werner, Hummel, & Vogt, 2014)

Both types react different to the applied lateral force. The above figure shows the force distribution of three walls with each different lengths. For the TF walls the stiffness of the wall is dependable on the length of the wall. CLT walls in contrary are fully depended on the stiffness of the connection. The difference is stiffness between the CLT walls is related to the number of shear connectors used, the number of hold-downs is the same since these are only applied at the corners of the walls.

3.4.2.2 Angle bracket

The angle brackets (fig. 3.22) are used along the length of the wall on specific centre to centre distances. It is best to apply symmetrical. Besides the resistance against sliding due to the shear forces the angle brackets also restrict the wall against the uplift coming from the overturning moment. From research it is shown that the contribution of the vertical resistance of the shear brackets is approximate 50% of the total vertical resistance (Gavric, Fragiacomo, & Ceccotti, 2013).

3.4.2.3 Hold-down

Hold-downs are used at the corners of wall section mainly to prevent uplift and are very strong and stiff in axial direction. However loaded in shear the stiffness and strength is negligible in comparison to the angle brackets. This is mainly due to buckling of the steel part of the hold-down.

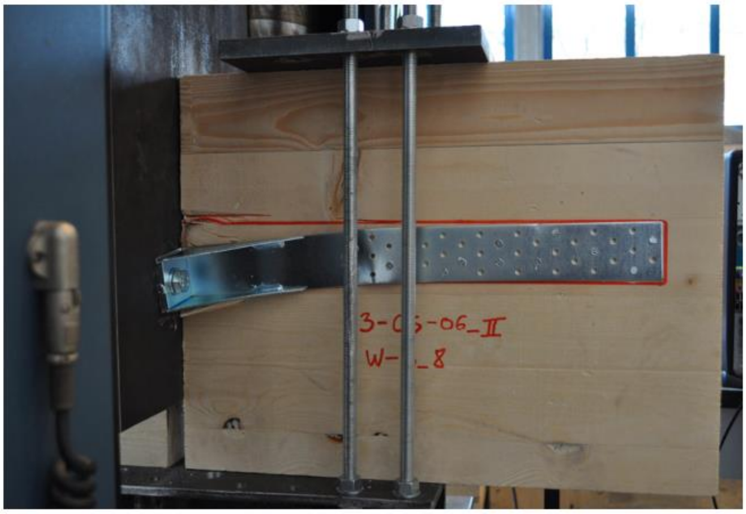

Fig. 3.18 Hold-down connector tested in shear (Gavric, Fragiacomo, & Ceccotti, 2013).

3.4.3 Single wall

As seen from figure 3.1 an earthquake eventually results into a horizontal force acting on the shear walls of the building. The wall resists the horizontal forces from the earthquake as well as the vertical forces from the dead load of the building.

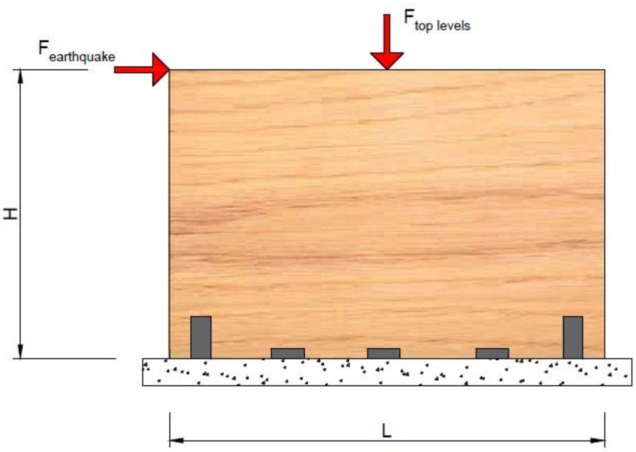

Fig. 3.19 Forces acting on a timber shear wall. The wall is connected to the foundation of floorby hold-downs at the corners and angle brackets in between.

For transferring the forces the walls are connected to the foundation or floor. Resulting in the following reaction forces (fig. 3.20). From the figure it can be seen that there are two models used for the assumption of the reaction forces. The left option is a simplified conservative option whereas the right model is more realistic. The left option assumes that all tensile forces are restrained by the hold-downs and shear forces by the angle bracket. The right figure shows that also the angle brackets restrain the vertical forces as mentioned before.

Fig. 3.20 Two different models of the reaction forces. The left has been used often, it assumes that the angle brackets only restrain shear forces. While the right option also takes the vertical strength of the angle brackets into account.

The moment is simply calculated by multiplying the horizontal force by the height and dividing by the length of the wall.

3.5 Capacity design principal

Important for seismic design is the capacity design principle. It ensures that the structure is designed such that a certain favourable failure mode will occur first. This is applicable on the entire structure also on its foundation. In case of the timber building the ductility of the connections has to be obtained before brittle failure occurs in one of the other elements of the structure.

The principle referred to is schematized by Professor Paulay's ductile chain (fig. 3.21). The chain illustrates that to ensure ductile and dissipative behaviour no brittle failure modes must occur before the ductile mode starts to deform. Otherwise the chain will break before it had the change to elongate.

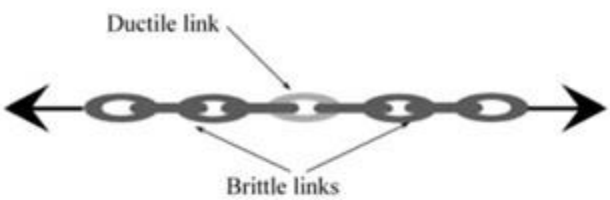

Fig. 3.21 Professor Paulay's 'ductile chain' (Elghazouli, 2009).

To account for this the brittle links, failure modes, are calculated with an over-strength factor (γ_{Rd}) of 1.3. and 1.6 for respectively brackets/hold-downs and screwed joints (Gavric, Fragiacomo, & Ceccotti, 2013).

$$F_{Rd,ductile}\gamma_{Rd} \leq F_{Rd,brittle} \qquad \text{(eq. 3.16)}$$

For instance when using CLT several brittle failure mechanism can occur (fig. 3.22). As the figure shows different kinds of failure can occur in the connection itself.

Fig. 3.22 Brittle failure modes of CLT connections: failure of steel hold-down, pull through of the bolt in the steel part of the angle bracket and yielding of the steel part of angle bracket with nails withdrawal. (Gavric, Fragiacomo, & Ceccotti, 2013)

The connection must be the ductile link and not the timber frame, because the frame has a higher change of brittle failure. However also the connection can fail in a brittle manner, to account for this the principle has to be applied up until connector level. The connector must be able to develop plastic hinges in the nails(Fig 3.12).

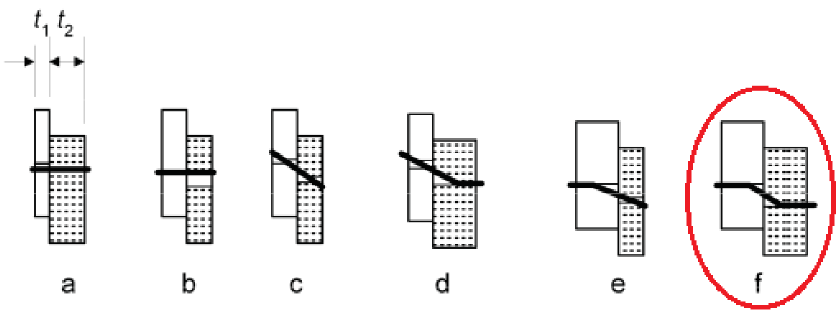

Fig. 3.23 Ductile failure of a nailed timber-timber connection (EC5)

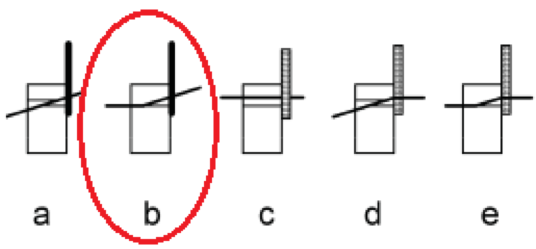

Fig. 3.24 Ductile failure mechanism for timber-steel connections with thin steel plates (EC5)

As mentioned the connector itself is of importance, the length of the connector influence the ductility (fig. 3.25). According to research the nails must have a length of 60 millimetre or more to ensure ductile behaviour (Dujic, Klobcar, & Zarnic, 2007).

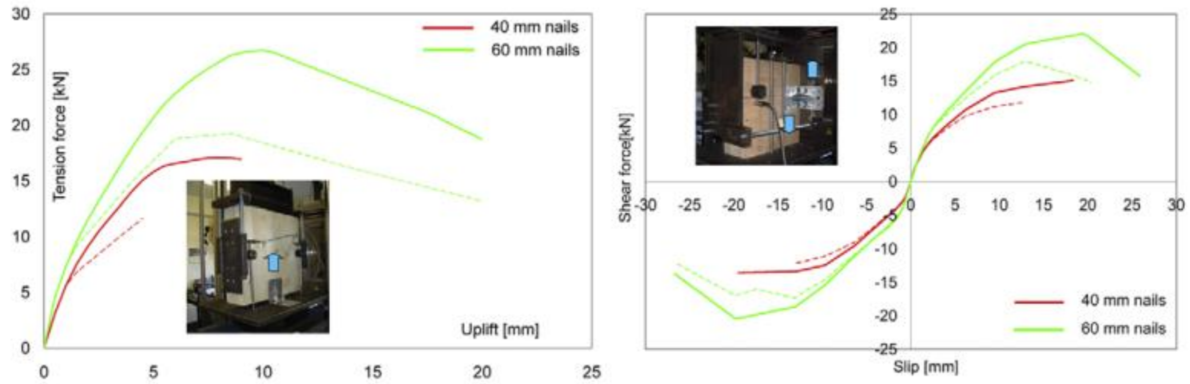

Fig. 3.25 Test results for different nail lengths. Left; axial strength, right; shear strength. (Dujic, Klobcar, & Zarnic, 2007)

4 LATERAL FORCE AND MODAL RESPONSE ANALYSIS

To start the seismic calculation on timber buildings a case study building (fig. 4.1) is introduced. It is a typical building of the Groningen area and is not designed on resisting the lateral forces from the induced earthquake. This chapter describes the building which is redesigned in timber instead of the original building constructed with brick cavity walls. Followed by a lateral force and modal response analysis.

4.1 Timber house

The building is an existing common terraced house, located in Groningen. Instead of performing the analysis for the entire block, one house is extracted (fig. 4.1). The front and back façade are remaining as originally drawn when the building was constructed. On the sides there are no windows due to the fact that when considering the entire block these walls are the house dividing walls.

Fig. 4.1 Front (left) and back (middle) facade of a terraced build house in Groningen. Followed by a picture of a common terraced house.

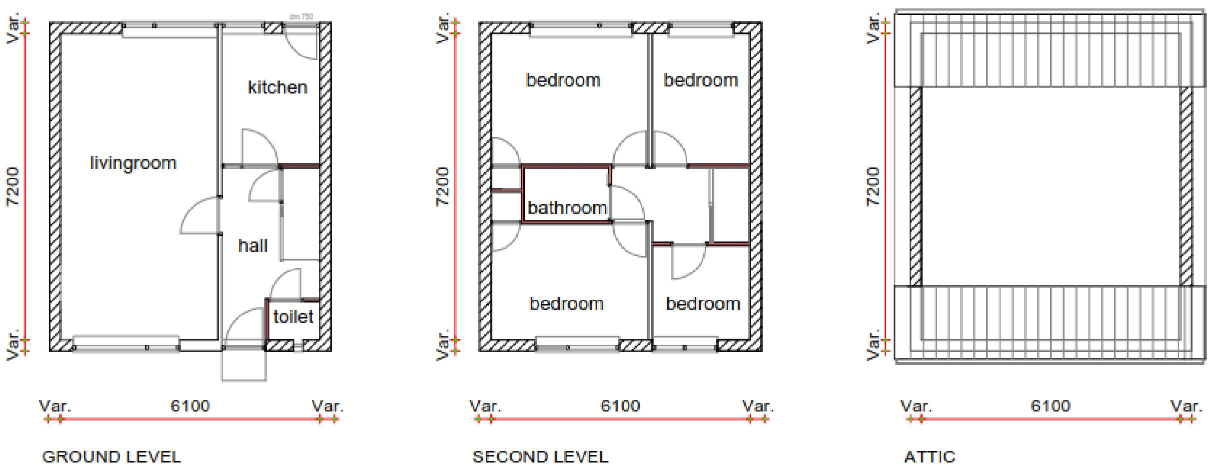

Fig. 4.2 Plan overview of a terraced build house.

For the building multiple calculation methods can be used as mentioned in paragraph 3.2:

- Lateral Force (LF)
- Modal Response (MR)
- Non-Linear Static Push-over (NLSP)
- Non-Linear Time History analysis (NLTH)

In this chapter a lateral force and modal response analysis is made for timber framed walls and a more detailed description of the calculation is provided in annex B. These methods allow the engineer to calculated the structure elastically whit the non-linearity taken into account by the q-factor. In chapter 6 a non-linear static push-over is performed for the building in CLT.

4.1.1 Timber framed walls

The timber framed wall is build-up from studs, beams and sheeting (fig. 4.3 a). The frame is made of timber C24 and the sheeting is a 15 millimetre OSB plate applied on both sides. The timber framed walls can be prefabricated to ensure fast erection on the building site. The finish on the outside of the panels consist of brick sleeves, to be able to reduce the mass of the building as much as possible. Brick sleeves are thin bricks glued to a sheeting material (fig. 4.3 b).

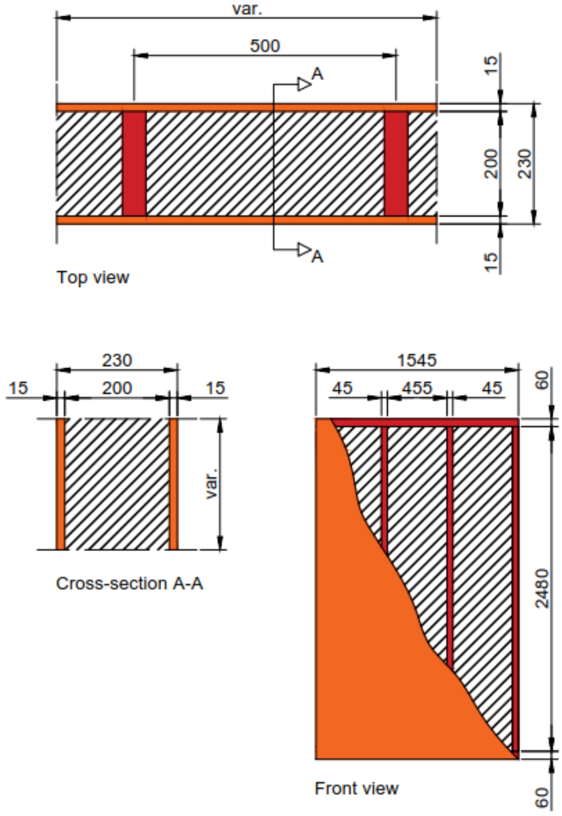

a) Overview of the timber-framed wall panels

b) Facade element of timber framed wall with brick sleeves (Hedach AG, 2017)

Fig. 4.3 Overview of a possible timber framed construction element

The erection time of the building is minimized by making the panels prefab in a factory, besides fast erection this has the benefit that part of the assembling is done in a controlled environment. At the building site the prefab panels can be hoisted in easily due to the light weight and be mounted on to the foundation.

4.1.2 Mass calculation

The mass calculation is made in the calculation report in annex B resulting in the following table.

Table 4.1 Overview of the masses per level of the building.

Level	Σ m [ton]
Attic	15.6
First floor	12.9
Ground floor	28.9
Foundation	22.9
Total	**80.3**

The low mass of the timber building is one of the benefits as mentioned in chapter 3. The mass in table 4.1 consist of the self-weight and the imposed loads on the floors.

4.1.3 Stiffness

First the stiffness of the building is calculated in a simplistic manner. For this the stiffness of the OSB panels is used, this provides a decent estimation for calculation of the forces acting on the building. Only the load-bearing walls are taken into account and it is assumed that the plan of the building is adjusted for the walls to have the height of the entire building.

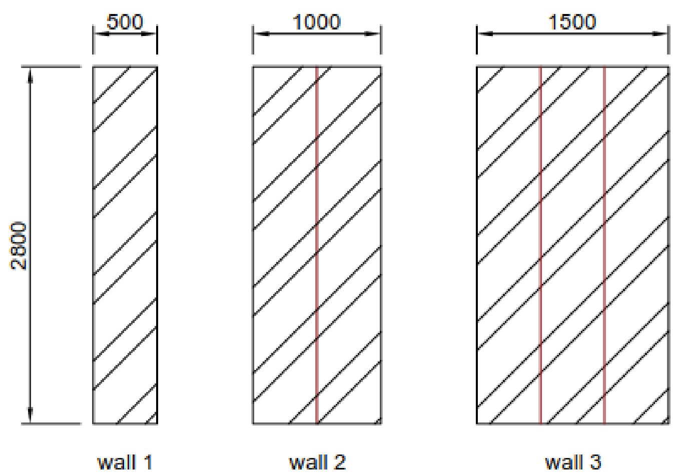

Fig. 4.4 Walls used for calculation, it is assumed that these walls are located at both sides of the building.

Due to the short loading time the timber panels will react stiffer and therefore the modulus of elasticity is multiplied by 1.1, according to the NPR 9998, chapter 8.0.

$$E_{OSB} = 1.1 \cdot 4000 = 4400\ N/mm^2 \qquad \text{(eq. 4.1)}$$

4.2 Lateral force analysis

The principle of the lateral force method is that the building itself is translated into a SDOF system (fig. 4.5), with a certain natural period for determining the reaction of the building.

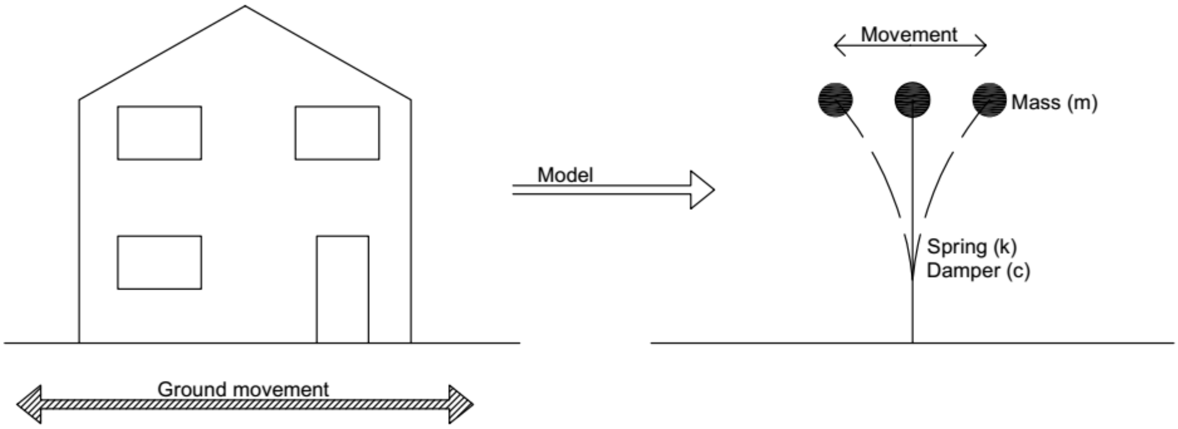

Fig. 4.5 Modelling of the structure into a SDOF system.

The basic formula for the lateral force method.

$$F_b = S_{AE(T_1)} \cdot m \cdot \lambda \qquad \text{(eq. 4.2)}$$

Where λ is a correction factor which is 0.85 when the natural period is lower than $2T_c$ and the building has more than two building levels, g is the gravity constant, m is the mass and $S_{AE(T_1)}$ is the acceleration factor depending on the natural period of the building.

4.2.1 Natural period

The natural period, needed to determine the reaction of the building to the seismic forces, is calculated using the following four options (Hummel 2016).

$T_1 = C_t \cdot H^{3/4}$ From EC 8 (eq. 4.3)

$T_1 = 0.09 \cdot H \cdot \sqrt{L}$ From Pauley and Priestley (eq. 4.4)

$T_1 = 02 \cdot \sqrt{d}$ From EC 8 (eq. 4.5)

$T_1 = 2\pi\sqrt{\sum_{i=1}^{n} m_i \cdot u_i^2 \Big/ \sum_{i=1}^{n} F_i \cdot u_i}$ Rayleigh method (eq. 4.6)

(eq. 4.3) An approximation which is only related to the height of the building, this equation is applicable for buildings up to 40 m. The value C_t is 0.085 for moment resistant space steel frames, 0.075 for moment resistant space concrete frames and for eccentrically steel frames and 0.05 for all other structures. This shows that timber is not specifically specified and therefore it has a C_t factor of 0.05. This makes it a really rough lower bound calculation.

(eq. 4.4) Also includes the length of the building and does not account for the stiffness.

(eq. 4.5) Where *d* is the horizontal displacement at the top of the building when the vertical load is applied in horizontal direction on the building. This method takes the bending and shear stiffness of the building into account, but is more time consuming. For this method the structure is modelled as a cantilever and the displacement only due to bending is calculated using general mechanic equations.

(eq. 4.6) For the Rayleigh method the storey drifts are calculated for equivalent lateral forces, increasing linear of the height of the building. As well as for the previous method the schematisation of the building is according to fig. 4.6

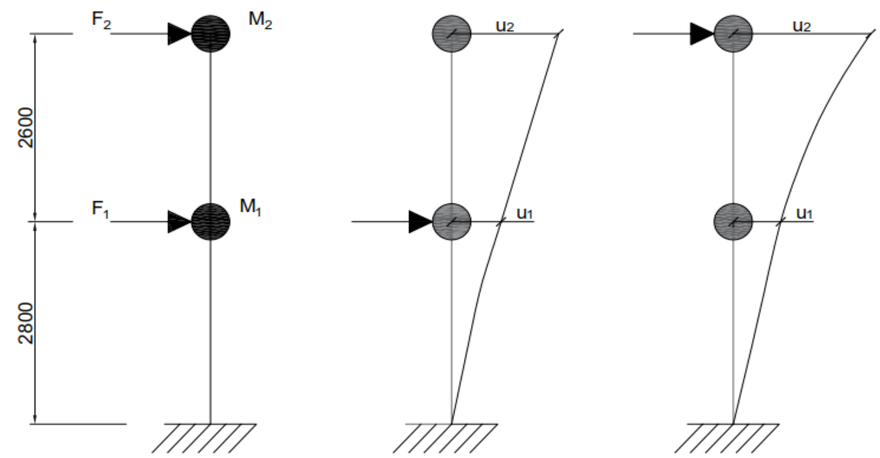

Fig. 4.6 Overview of schematization used for calcution of the natural period.

The above schematization is used for calculating the displacement for the EC8 (2) and Rayleigh method, using mechanical engineering formula's. The ground is assumed as a rigid constrained as in fig. 4.6 and the moment of inertia is calculated taken the OSB plates of the wall into account.

table 4.2 Outcome of the different calculation methods for the natural period.

Method	symbol	unit	natural period
EC8 (1)	T	s	0.25
Pauley and Priestley	T	s	0.28
EC8 (2)	T	s	0.65
Rayleigh method	T	s	0.60

A more detailed of the natural period calculation can be found in annex B.

This rough calculation is made for the OSB wall, to give an indication of the natural period. The first two methods (eq. 4.2 and eq. 4.3) both are dependent on the geometry of the building which is not very accurate therefore these two methods are lower bound solution. The other methods are dependable on the stiffness of the structure and therefore more accurate.

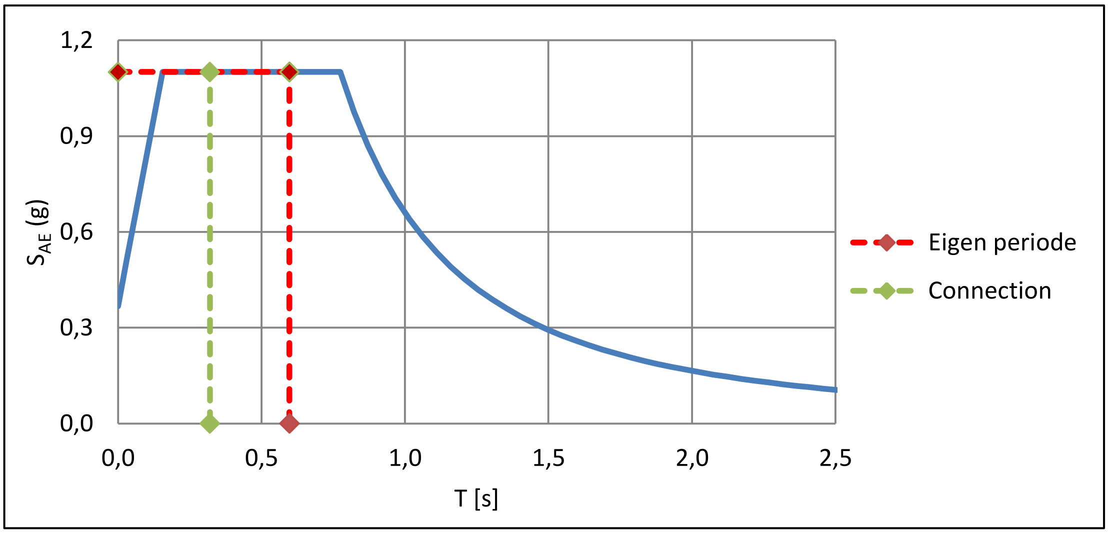

Fig. 4.7 Elastic response spectrum with both natural periods shown, both leading to the plateau.

The above response spectrum is determined in Appendix A. The PGA which is used is 0.36g meaning the building is located in the most unfavourable seismic location in Groningen(fig. 2.5). Also the outcome of the calculation made by taken the connections into account is shown in the elastic response diagram. Both lead to an acceleration factor at the plateau of the diagram, the stiffness need to be reduced to have the benefit of lowering the acceleration factor. Therefore it is unlikely that buildings with less than three levels have a natural period outside the plateau. For fast calculation one can use the plateau value due to the width of the plateau almost every low-rise building will fall into this category. The two different calculations also show the importance of the calculation of the stiffness of the building.

4.2.1.1 Stiffness in the connection

The calculation with assuming all the displacement in the connection is already more accurate and realistic than the previous calculation. The calculation is made according to 'voorbeeldberekeningen NEN'.

From research the horizontal displacement can be addressed to the following components (Hoekstra, 2012):

- Sliding in the connection, sheet material connected to the framework
- Sliding of the hold-downs
- Compression perpendicular to the grain
- Shearing of the sheet
- Tension in the posts
- Displacement of the lower beam

It is assumed that the first two components leading to 65% of the total displacement. First the slip in all connections is calculated for a wall of 1500 millimetre and an OSB plate with a thickness of 15 millimetre. Assuming ductile failure by yielding of the connectors (fig. 4.8).

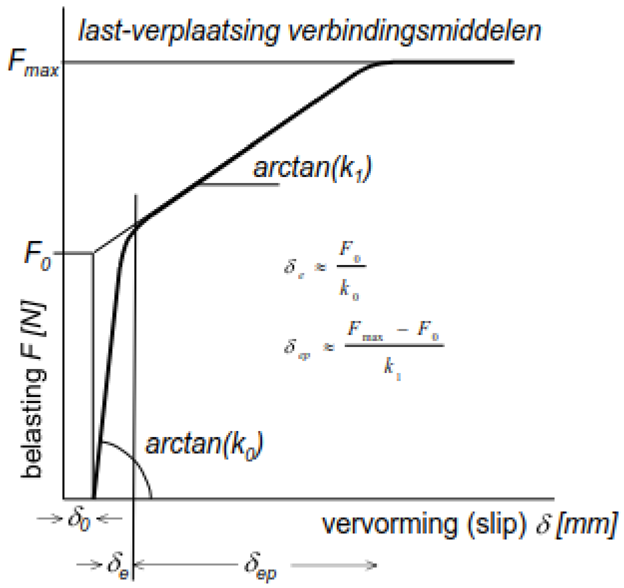

Fig. 4.8 Load-displacement curve for slender connectors (NEN voorbeeldberekeningen, 2015).

The figure shows the load-displacement curve used for calculation of the slip of the connectors. For the calculation the sliding of the hold-down is calculated as well as for the nails, this is then translated to the total displacement of each floor.

Further calculation is made and the resulted in the following displacements;

First floor: 13.9 mm

Second floor 30.4 mm

When applying the Rayleigh method the natural period of the building is calculated.

Natural period: 0.32 sec

Adjust number of connectors: q = 4 assumption and F_{nail} = 735N, $F_{b,shear}$ = 261 kN

$$\text{Number of nails} = \frac{(261/4)}{735} \cdot 10^3 = 89 \qquad \text{(eq. 4.7)}$$

The number of nails is calculated from the force according to the plateau of the response spectrum. This ensures that most of the connectors will yield and that the deformation as assumed is reached.

However the conclusion of the calculation is that the stiffness and the mass of the building leads to a natural period belonging to the plateau of the response spectrum.

4.3 Base shear force

The base shear force is calculated with the following formula (eq. 4.2) according to the NPR9998.

$$F_b = S_{AE(T_1)} \cdot m \cdot \lambda \tag{eq. 4.8}$$

This leads to the following elastic base shear force.

$$F_{b,elastic} = 1.1 \cdot 9.81 \cdot (15.6 + 12.9) \cdot 0.85 = 261 \text{ kN} \tag{eq. 4.9}$$

4.3.1 Force distribution

The EC8 prescribes two options for the force distribution, namely based on height (eq. 4.10) or displacement (eq. 4.11). With this the fundamental first vibration mode of the system is approximated. The most unfavourable distribution of the two has to be used in further calculation.

The force distribution according to the ratio of the mass (m_i) and height(z_i);

$$F_i = F_b \cdot \frac{z_i \cdot m_i}{\sum_{j=1}^{n} z_j \cdot m_j} \tag{eq. 4.10}$$

Option two is force distribution according to the ratio of the mass and displacement (s_i). The displacement of the mode shape are calculated in annex B;

$$F_i = F_b \cdot \frac{s_i \cdot m_i}{\sum_{j=1}^{n} s_j \cdot m_j} \tag{eq. 4.11}$$

Table 4.3 Overview of the force distribution.

Level	Attic [kN]	First floor [kN]	Total [kN]
eq 4.10	183	78	261
eq 4.11	204	57	261

With these forces and the q-factor the number of nails connecting the sheeting to the frame can be calculated as well as the dimensions of the posts and beams of the frame. Especially the lower beam is of interest due to the fact that this is loaded in compression perpendicular to the grain.

4.3.2 Wind load

For comparison the wind load on the building is calculated. The building is located in wind area II according to the Dutch national annex. The calculation is made for the weaker axis namely the axis in the length of the terraced build houses.

Area on which the wind acts is equal to 49.13 m^2 resulting in a design force of 94.0 kN. When adding the force due to the friction the total lateral force is equal to 125.4 kN for a block of six houses. The total moment due to the wind force for the entire block is equal to 450 kNm.

4.4 Modal analysis

For preforming the modal analysis the theory from 'Dynamics of structures – theory and applications to earthquake engineering (Chopra, 2012), chapter 18 is used.

The modal analysis makes use of the following element matrices.

$$\underline{\underline{M}}\ddot{u} + \underline{\underline{k}}u = 0 \qquad \text{(eq. 4.12)}$$

The element stiffness matrix of the schematized building is obtained by making use of unit displacements. The mass matrix is obtained by using the modal masses as in fig. 4.6.

The model used is a two degree of freedom system shown in (fig. 4.6). By setting the determinant of the homogeneous equation (eq. 4.12) to zero the eigenvalues can be calculated. From the eigenvalues the natural frequencies can be obtained by taking the root of the eigenvalues. The next step is to search for the eigenvectors of the system which indicate the modal shapes of the system.

With the calculated natural frequencies the eigen periods of the different modes can be calculated. This can then be transferred to the base shear force for each mode, taking the participating mass into account. Finally the force distribution over the height of the building is according to the eigenvectors of the system.

4.4.1 Input parameters

For the stiffness the OSB plates are taken into account which are translated into a spring stiffness for the stiffness matrix. The mass distribution remains the same from the lateral force method.

4.4.2 Results

The results below are given for the two modal shapes of the building. It is clear that there is not much deviation from the lateral force method which is logical due to the fact that the governing mode shape is the first mode.

Table 4.4 Overview natural period and mass participation of the modes.

Mode	Natural period [s]	Mass* [ton]	Mass participation (%)
1	0.60	23.4	82.1
2	0.08	5.1	17.9

For the calculation of the total shear force per level the SRSS (square root of the sums of squares)is used. This is applicable since natural periods of the modes are fulfilling the requirements for calculating them as independent modes (eq. 3.2).

$$E_E = \sqrt{\Sigma\, E_{E;i}{}^2} \qquad \text{(eq. 4.13)}$$

Table 4.5 Overview of the shear forces per level of the building.

Level	Mode 1 [kN]	Mode 2 [kN]	Total [kN] (SRSS)
Attic	197.1	-18.8	198.0
First floor	252.5	38.1	255.4

Also of interest is the mass participation percentage of the building for each mode. The mass participation factor is directly linked to the λ in the lateral force analysis. The λ is a reduction factor for the mass participation when there are multiple mode shapes. Table 4.4 shows that the reduction of the mass participation of the first mode is indeed more than 15%, this justifies the use of the λ factor .

4.4.2.1 Y – direction

The Y – direction consists of two walls with a length of 7.2 metre. Therefore this wall is very stiff leading to a magnification factor equal to that of the plateau, resulting in the same forces as for the smaller walls in X – direction. Due to the fact that the wall is larger and has more shear capacity then in X – direction no further verification is made.

4.5 Lateral force method for CLT

The principle which has been used for the calculation of the timber framed house is now applied for the calculation of the CLT building. For the build-up of the CLT building see chapter 5 where this is discussed together with the modelling of the building.

Since the CLT wall is stiffer, because there are less connections to deform. Consequently it is assumed that the building is in the plateau of the response spectrum. Therefore only the mass of the building is needed for the calculation of the base shear force.

Table 4.6 Weight distribution of the CLT building

Level	Σ m_i [ton]
Attic	17.4
First floor	20.0
Total	**37.4**

The base shear can be calculated (eq. 4.8).

$$F_{b,elastic} = 1.1 \cdot 9.81 \cdot (17.4 + 20.0) \cdot 0.85 = 343 \text{ kN} \quad \text{(eq. 4.14)}$$

This is needed for the non-linear static push-over in chapter 6.

4.6 Conclusion

The outcome of the calculations in this chapter are still the elastic base shear forces. To construct an economically feasible building the forces must be reduced by taken ductility into account. By doing so remaining damage after an earthquake is accepted for the near collapse criteria.

For CLT the Eurocode 8 gives a q-factor of two. Since it is beneficial to calculated with a q-factor as high as possible the building is modelled and a non-linear static push-over will be executed to investigated the ductility. However when the q-factor is overestimated this leads to ductility demand which cannot be obtained from the building. This then leads to a underestimation of the forces acting on the structure which can result in a collapse of the building. The outcome and conclusion of the push-over will not be limited to the case study building. Also a prediction or conclusion will be made for high-rise buildings.

CLT is chosen due it more simplistic manner of modelling which is addressed in the next chapter. But also for its benefits in recoverability and reduced damage after a seismic event compared to timber framed structures.

5 MODELLING

This chapter contains the build-up of the model which is used for the non-linear static push-over in chapter 6. Also an overview is given about previous modelling methods found in literature, finalised by arguments for the current modelling approach adapted in this report.

To check the modelling method, a comparison between a single CLT wall system modelled in FEM package of DIANA and the outcome of cyclic experiments is made.

Next the lay-out of the building and details of the walls, floors, roof and connections are shown. The details are described followed by a method of modelling and the assumptions and simplifications which are made.

After this the walls of the case study building are modelled and analysed, followed by the total first floor, second floor and finally the total building. A more detailed overview of the modelling input can be found in annex C.

5.1 Modelling methods

In research different models are described for predicting seismic behaviour of timber buildings (Ceccotti & Sandhaas, 2010). Distinction is made between a modelling approach for timber framed and CLT structures.

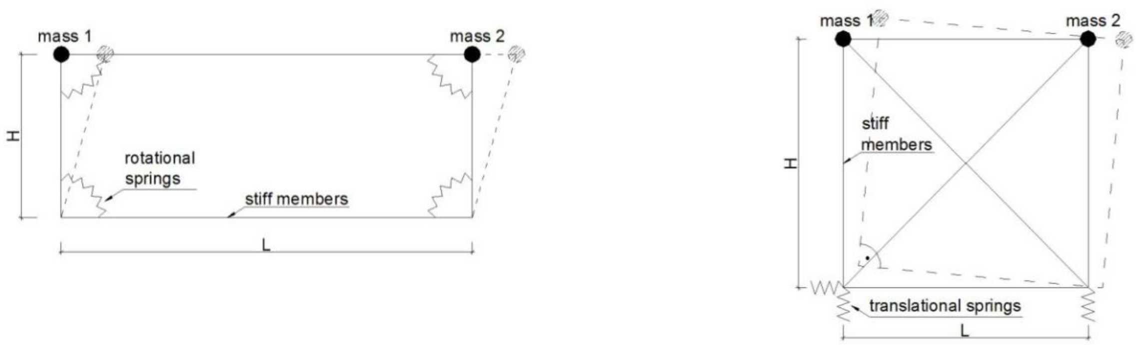

Fig. 5.1 Deformation of timber shear walls. Left: timber framed wall. Right: CLT wall. Both from Drain 3DX model (Ceccotti & Sandhaas, 2010).

For timber framed walls a model is suggested which uses lumped masses and stiff members. The deformation is simplified in the rotational springs at the corners of the frame (fig. 5.1). These springs are representing the displacement of the structural frame. A drawback is that this method assumes that the behaviour of the full timber framed element is known and calculated back to the four rotational springs as in the model.

For the CLT walls the frame consists of stiff truss members and the deformation is assigned to the translation springs. Where the horizontal springs are representing the angle brackets and the vertical the hold-downs. Also this method makes use of backward calculating the stiffness of the springs for representing the entire elements. This is a drawback when there are no test results for calibration of the elements, for instance when the openings or location of the connections changes. Another drawback is the fact that there is no information about the stresses in the material only the displacement is known.

A second method is by start modelling on connection level. The model is 2D and consists of the entire CLT wall, angle brackets, hold-downs and screws. By also adding the floors and roof a full building can be modelled. An additional benefit is the capability of modelling the connection between the perpendicular walls. Creating a model including the boxed behaviour of the building. This increases the strength and stiffness of the building due to the walls perpendicular to the loading direction.

For this thesis the second method is chosen, because this gives the freedom of adjusting the lay-out of the connectors for the specific building.

The material properties of the CLT are known, however for the connections the input has to come from experiments. From these experiments it is possible to apply hysteretic behaviour of the connections in the model, this is done by calibration to cyclic tests of single connections. Modelling hysteretic behaviour is very complex. A more simplistic approach is modelling the backbone curves from the cyclic tests. Modelling the connections separately allows one to take bi-axial action of the connections and strength degradation into account.

5.2 Experimental wall

The first model made is of a CLT wall which is used in experiments, this allows verification of the used modelling method.

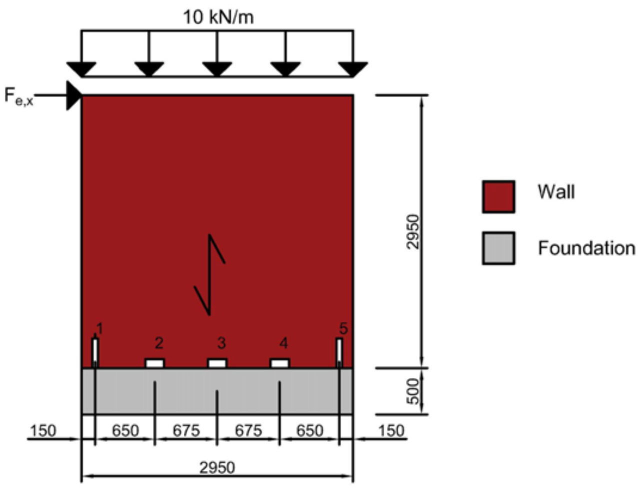

Fig. 5.2 Overview of the used experimental wall with a thickness of 85 millimeter and the grain direction of the most outer layer of the CLT. There is an additional vertical force of 10 kN/m and the connection to the foundation consists of two hold-downs at the corners and three angle brackets in between.

The input for the hold-downs and angle brackets is obtained from experimental tests (Gavric, Fragiacomo, & Ceccotti, 2013), described in the following paper:

- (Gavric, Fragiacomo, & Ceccotti, Cyclic behaviour of typical metal connectors for cross-laminated (CLT) structures, 2013)

The experimental cyclic push-over test is from 'Non-linear simulation of shaking-table tests on 3- and 7- storey X-lam timber buildings' (Rinaldin & Fragiacomo, 2016) and the results are shown in fig 5.5.

5.2.1 Model

For the model the orthotropic material properties depend on the local axis of the elements shown in fig. 5.3.

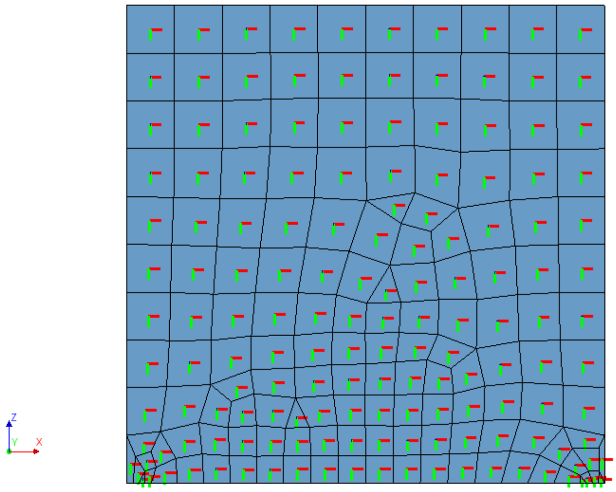

Fig. 5.3 Local axis of the elements

For the walls the local axis of the elements is the same in all the direction namely the x-axis is along the width of the element (shear), y-axis is along the height (axial) and z-axis is out of plane.

The input parameters listed in the table below, are obtained from research (Bogensperger, Moosbrugger, & Silly, 2010) and (Blass & Fellmoser, 2004) . The values for the young's and shear modulus are calculated for a wall with a thickness of 85 millimetres and layer thickness of seventeen millimetres, same as used for the experiment.

Table 5.1 Input parameters for the experimental wall.

Input wall	symbol	value	unit
Thickness	t_{wall}	85	mm
Young's modulus	E_x	4622	MPa
	E_y	6748	MPa
	E_z	11000	MPa
Poisson ratio	ν	0.30	-
Shear modulus	G	582	MPa

The foundation is modelled as an isotropic material, resembling a stiff, compared to the timber walls, concrete foundation.

Table 5.2 Input of the foundation.

Input foundation	symbol	value	unit
Thickness	t_{wall}	600	mm
Young's modulus	$E_{foundation}$	30000	MPa
Poisson ratio	ν	0.30	-

The elements used, for the walls and foundation, are 2D curved shell elements. The geometry and location of the connections is shown in fig. 5.3 as well as the vertical load.

5.2.1.1 Connections

The applied connections are modelled using non-linear point interface. The input is obtained from tests results (Gavric, Fragiacomo, & Ceccotti, 2013). As starting point the mean values of the test results are used, for constructing the backbone diagrams of the connections.

Table 5.3 Input for the diagrams in DIANA.

Force	Hold-down		Angle bracket	
	Force [kN]	Displacement [mm]	Force [kN]	Displacement [mm]
Shear force	0.0	0.0	0.0	0.0
	3.1	1.1	19.5	11.7
	8.5	36.8	22.8	28.5
			18.3	31.9
Axial force	0.0	0.0	0.0	0.0
	34.4	8.8	16.3	7.3
	41.1	20.3	20.0	17.7
	33.0	23.8	15.9	23.2

The above table is visualised in the graphs in fig. 5.4. In the graph an additional branch is added for the compression in axial direction. This is a stiff branch since the connection itself is not reacting in compression. The compression is transferred to the underlying floor or foundation.

The failure mechanisms of the connections are described in the research from which the input of the connections is obtained. The hold-down in tension was failing due to the vertical displacement of the wall. This led to pull out of the nails. In shear local buckling occurred in the steel parts of the hold-downs or bending of the steel and withdrawal of the nails. This however happened at large displacement, more than 100 millimetre. The angle bracket showed a ductile failure mode in shear direction which is the main load bearing direction of these connections. The failure mode is yielding, by two plastic hinges, of the nails in the wall. The angle brackets also have a significant load bearing capacity in axial direction. However when loaded in tension a brittle failure mode occurred namely pull-through of the bolt. This can be resolved with the use of the capacity design principle, to ensure a ductile failure mode. Concluding that the input of the connections is not fully utilised.

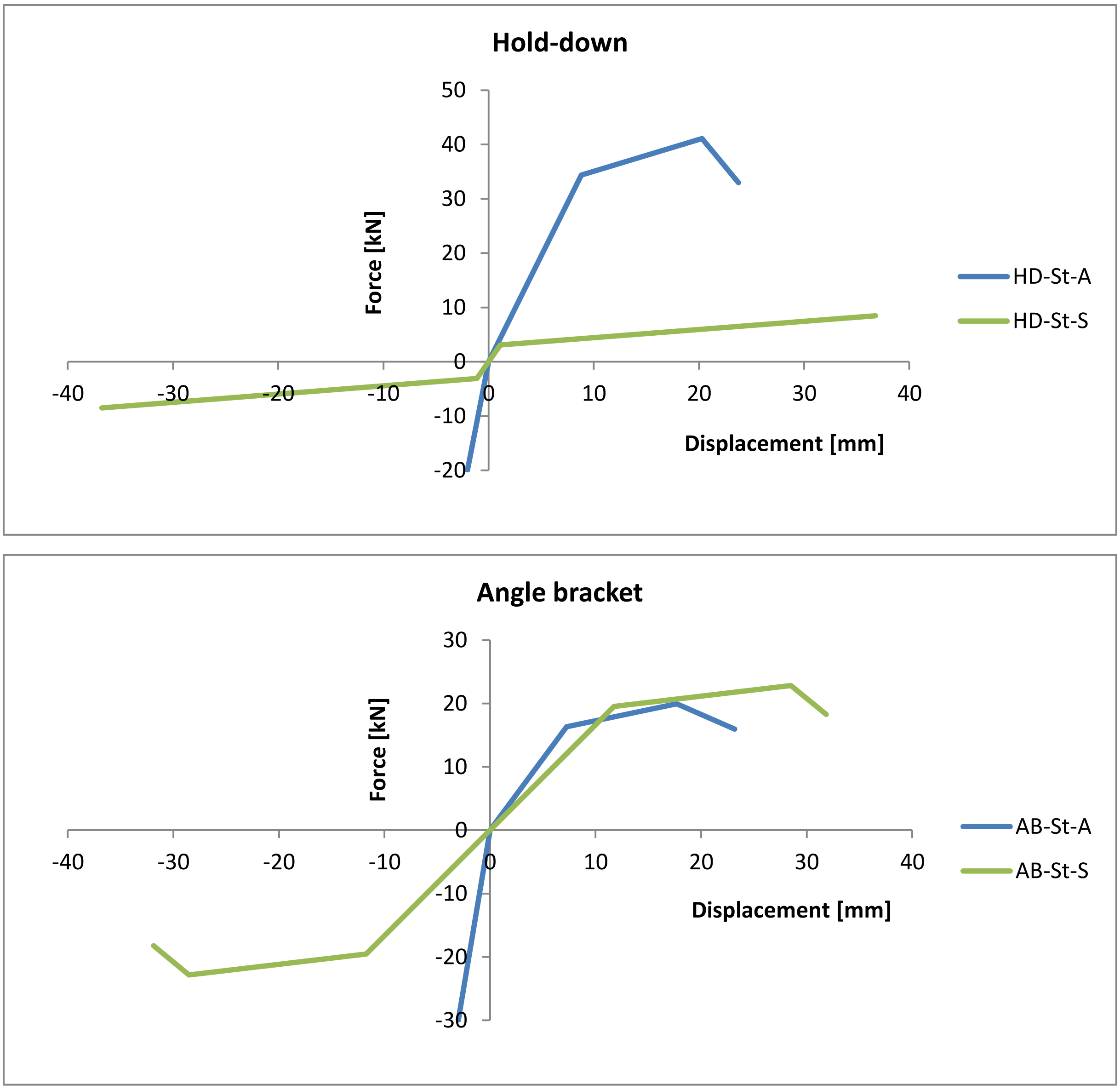

HD = hold-down   St-A = steel|timber Axial

AB = angle bracket   St-S = steel|timber Shear

Fig. 5.4 Input of the connectors.

The shear and hold-downs are modelled as bi-axial springs/interfaces. This is important for the force distribution of the wall as explained in 3.4.3. Due to the interaction in the two directions there is also an overall force reduction. Since this option is not directly available in DIANA a reduction of 15% will be taken into account due to the bi-axial interaction (Hummel & Seim, 2016). This is a conservative option.

5.2.1.2 Line interfaces

Besides point interfaces also line interfaces are applied to model the interaction between the foundation and the CLT wall. The line interface is a nonlinear elastic line interface assuring the vertical contact stiffness in compression and allowing free deformation in shear and tension.

5.2.2 Results

The results from the experiment is shown in fig 5.5, with the configuration as in fig. 5.2. This result is used as comparison for the output of the DIANA model. It shows that the maximum force is approximately 85 kN and a displacement of 50 millimetre of the outer envelope. From the results given in fig 5.5 for the comparison/ indication of the outcome the top right area of the figure is used.

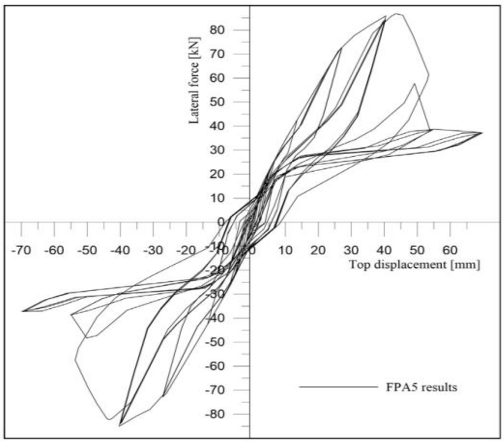

Fig 5.5 Results of a cyclic push-over of the wall shown in fig. 5.2. (Rinaldin & Fragiacomo, 2016)

The output from the FEM analysis is obtained from the reaction force at the point corner where the prescribed displacement is applied and resulted in the figure below.

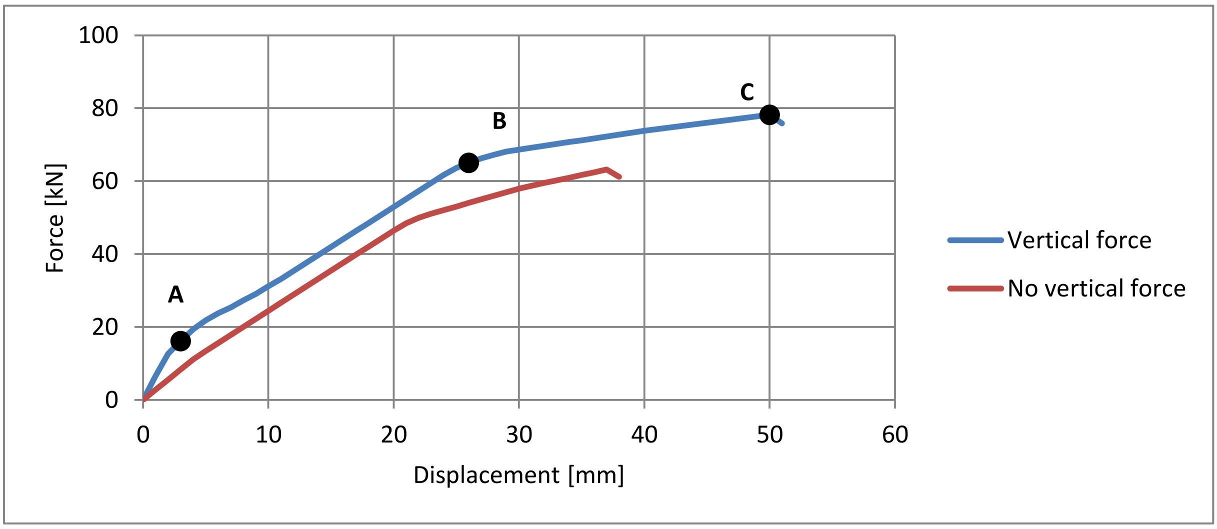

Fig. 5.6 Result from the push-over of the numerical wall.

Comparing the results from the above figure to the results from (fig 5.5) it is visible that the maximum force for the numerical method is slightly lower. This can be due to the fact that the values used from the experiments of the individual connectors are mean values and also due to the fact that the bi-axial strength of the shear connectors is under estimated. Concluding the numerical results are in the same range of order and are not overestimating the experimental results regarding the maximum force. For the maximum displacement the same holds as for the strength.

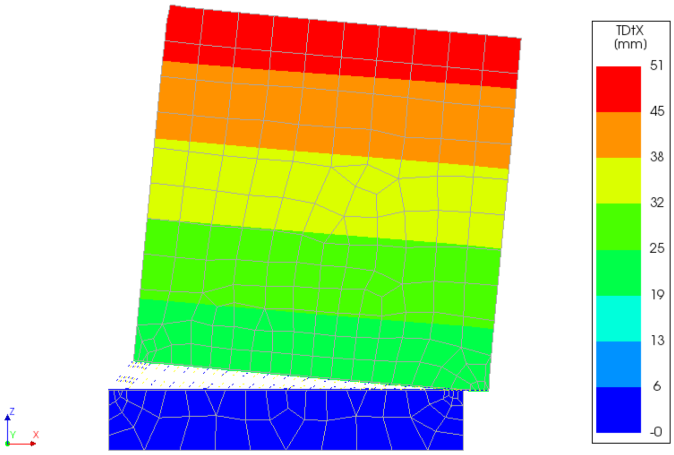

Fig. 5.7 Overview of the final horizontal displacement due to sliding and rocking deformation.

The results also show a combination of displacement due to rocking of the wall and sliding. The maximum horizontal displacement of the angle brackets is 32 millimetre the additional horizontal displacement at the top is then due to rocking of the wall.

5.2.3 Analysis of the experimental wall

The analysis of the wall is divided into three parts where there is a change in stiffness. The following three branches are analysed. From the origin to point A, from A to B and finally from B to C.

Table 5.4 Points of interest from the force-displacement curve.

Point	Displacement [mm]	Force [kN]
A	3	16.2
B	26	65.0
C	50	78.2

The deformation of the walls at these point is shown below (from A to C).

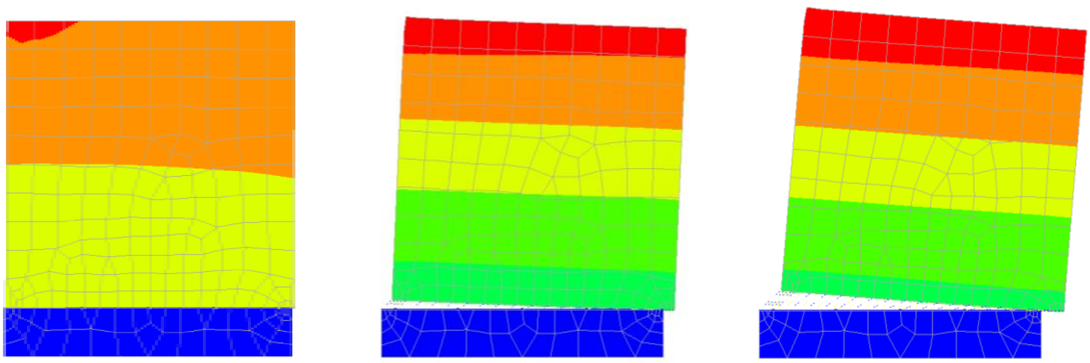

Fig. 5.8 Deformation of the wall at different steps.

To explain the differences between the branches the forces and displacement at the point nodes is further examined around the previous listed points.

Table 5.5 Force and displacement table of the load steps around point A. The node number corresponds with the connections from the left to the right of the wall.

Displacement	Node	X - direction		Z - direction	
Horizontal		Force [kN]	Displacement [mm]	Force [kN]	Displacement [mm]
3 mm at the top	1 HD	3.2	1.9	0.5	0.1
	2 AB	3.2	1.9	0.0	0.0
	3 AB	3.3	2.0	0.0	0.0
	4 AB	3.3	2.0	0.0	0.0
	5 HD	3.2	2.0	0.0	0.0
4 mm at the top	1 HD	3.3	2.5	1.2	0.3
	2 AB	4.2	2.5	0.2	0.1
	3 AB	4.3	2.6	0.0	0.0
	4 AB	4.3	2.6	0.0	0.0
	5 HD	3.3	2.6	0.0	0.0

The first branch, from the origin to point A, of the load displacement graph is very stiff. This is due to the fact the besides the angle brackets also the hold-downs are restraining the sliding of the wall. There is also no rocking of the wall because the uplift is restrained by the top pressure. This also explains the difference between the graph where no vertical pressure is added.

Table 5.6 Forces and displacement in the connections at point B of the load-displacement curve.

Displacement	Node	X - direction		Z - direction	
Horizontal		Force [kN]	Displacement [mm]	Force [kN]	Displacement [mm]
24 mm at the top	1 HD	4.6	10.9	34.5	9.0
	2 AB	18.0	10.8	14.9	6.6
	3 AB	18.1	10.9	9.3	4.1
	4 AB	18.3	11.0	4.0	1.8
	5 HD	4.6	11.4	0.0	0
25 mm at the top	1 HD	4.6	11.2	34.9	9.6
	2 AB	18.4	11.1	15.9	7.1
	3 AB	18.6	11.2	9.9	4.4
	4 AB	18.8	11.3	4.3	1.9
	5 HD	4.7	11.7	0.0	0.0
26 mm at the top	1 HD	4.6	11.4	35.2	10.2
	2 AB	18.8	11.3	16.4	7.5
	3 AB	18.9	11.4	10.6	4.7
	4 AB	19.2	11.5	4.6	2.1
	5 HD	4.7	11.9	0.0	0.0

The second branch, from point A to B, has a decreased stiffness compared to the first branch. The additional horizontal force has to be restrained fully by the angle brackets. Therefore there is less force needed for the sliding of the wall. Besides the decrease in stiffness for the sliding mechanism there is also additional rotation due to the rocking mechanism. This is visible in table 5.6 where the vertical force in the hold-down and angle brackets has increased.

Table 5.7 Final steps in the push-over analysis.

Displacement	Node	X - direction		Z - direction	
Horizontal		Force [kN]	Displacement [mm]	Force [kN]	Displacement [mm]
51 mm at the top	1 HD	6.4	23.1	40.8	19.9
	2 AB	21.7	23.0	18.9	14.8
	3 AB	21.8	23.1	17.1	9.5
	4 AB	21.8	23.2	9.9	4.4
	5 HD	6.5	23.7	0.5	0.1
52 mm at the top	1 HD	6.0	20.5	34.0	23.3
	2 AB	21.2	20.4	19.8	17.4
	3 AB	21.3	20.5	17.7	11.2
	4 AB	21.3	20.6	11.9	5.3
	5 HD	6.1	21.2	0.9	0.2

The third branch starts at point B and ends at point C. This branch has an even more reduced stiffness as the previous branch. This can be addressed to the lower stiffness from the reactions of the angle brackets. At point C the wall has reached its ultimate load. This is due to the tension in the hold-down at location 1 (fig. 5.2). After reaching the ultimate load the force in the hold-down reduces and the displacement increases whereas the forces in the angle brackets are still increasing. Finally no equilibrium can be found and failure of the wall occurs due to the rocking mechanism.

5.2.3.1 Verification of the forces

Since this is the experimental wall which is tested in a laboratory the verification of the strength of the wall is assumed to be fulfilled.

5.3 Model of the timber house

Now that the modelling method is verified the method is applied on the case study building addressed in chapter 4. For the walls as well as for the floors 5-layerd CLT will be used. shown in the table below. The dimensions are determined with tables used for predesigning the components (W. u. J. Derix GmbH & Co. | Poppensieker & Derix GmbH & Co. KG, 2016). The timber used for fabrication of the elements is spruce with strength class C24.

Table 5.8 Build-up of the timber elements.

Element	thickness [mm]	build-up [mm]	density [kN/m^2]
Wall	100	20 |20 |20 |20 |20	0.45
Floor	130	|30| 20 |30| 20 |30|	0.59

The details used for the building can be roughly divided into wall-wall, wall-floor and wall-roof details. These details make use of the following connections; hold-downs, angle brackets and screws.

A build-up for the wall is proposed is following:

- Outside finish possibly with OSB and brick sheeting

- Isolation with mineral wool, additionally with a sub-structure
- CLT wall element
- Room for installation
- Gypsum plaster plate

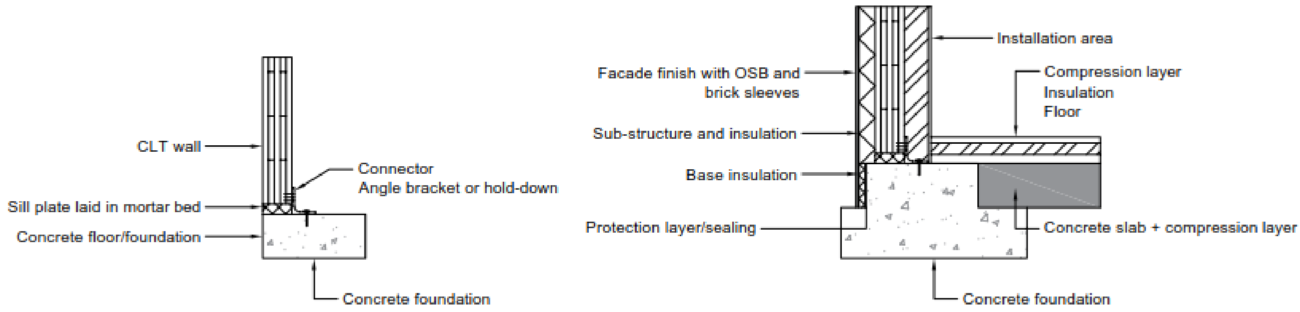

Fig. 5.9 Detail of the wall-foundation connection.

The build-up of the connection with the concrete foundation will be as following;

- A film which protects the CLT against rising moisture from the concrete
- Timber sill fully rested on the base below and the sill is placed in a low shrinkage mortar bed.
- And the brackets connecting the CLT to the concrete foundation.

Example of brackets which can be used for the connections are shown below in fig. 5.10 a and b. The hold-downs at the foundation the hold-downs are connected to the wall with 12 ring nails 4 x 60 mm and to the foundation with a 16 mm diameter bolt. The angle brackets are connected to the wall using 11 ring nails 4 x 60 mm and anchored to the foundation with a 12 mm diameter bolt.

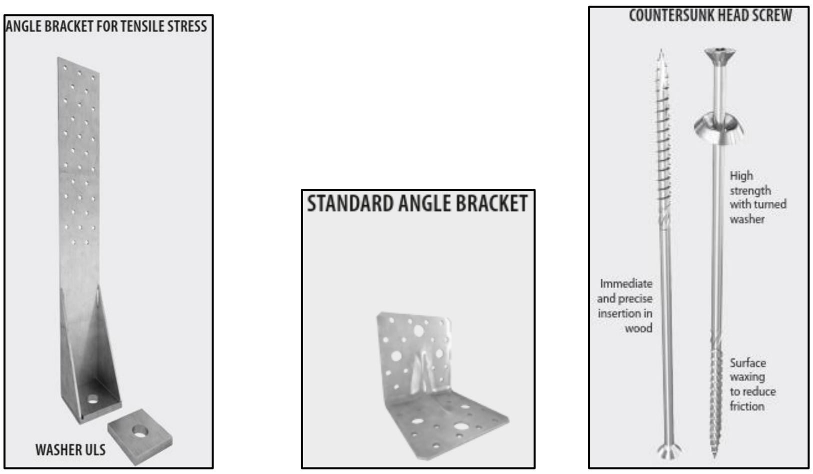

A) Hold-down (WHT) *B) Angle bracket (WBR)* *C) Screws (HBS)*

Fig. 5.10 Overview of connections and connectors used for the details of the building. (Rothoblaas, 2016)

Next step is the connection of the walls perpendicular to each other. This is done with screws. The same holds for the connection between wall and floor.

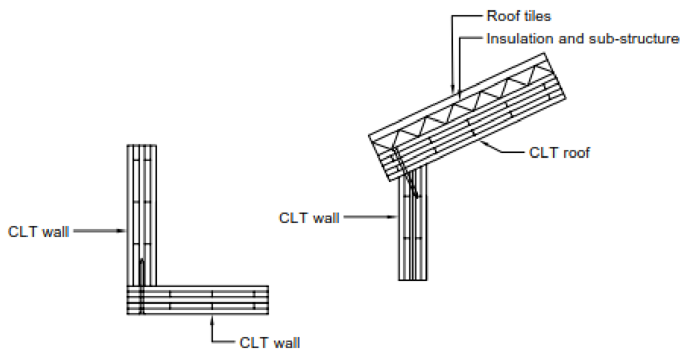

Fig. 5.11 The wall to wall connection and roof detail. The walls in have the same build-up as in fig. 5.9.

The screws (fig. 5.10 C) for the wall – wall connection are placed at varying centre to centre distances. The impact of the centre to centre distance can be related to the stiffness and strength of the entire structure, this will be explained in 5.3.4.

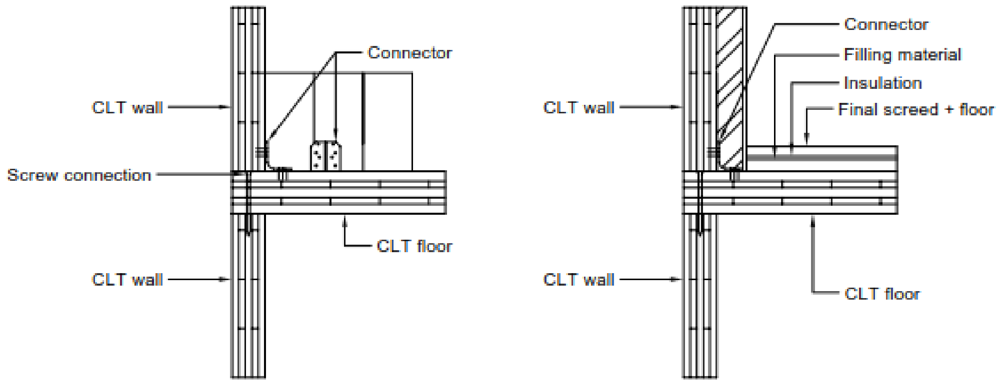

Fig. 5.12 Detail of the wall - floor connection

The floor, as well as the roof is first connected to the lower walls with screws. Next the walls on the first and second floor are connected to the floor below with angle brackets and hold-downs. The number and centre to centre distance of the screws which attach the floor to the walls is kept constant.

Table 5.9 Number of screws modelled.

Wall – floor	length [mm]	no. of screws	C.T.C.
X – direction	6400	24	256
Y – direction	7500	29	250

Drawback of the detail shown in fig. 5.12 is the compression perpendicular on the grain which occurs on the floor, due to the upper wall. However since the limited height of the building the floor is capable of resisting the forces.

The model is built by regarding the above details. It is assumed that the roof is connect rigidly by adding sufficient number of screws.

Beneficial of this method is the possibility to inspect and if needed repair the connections, due to the installation area.

5.3.1 Mass

For the analysis of the building the mass is of importance, it is directly linked to the base shear force. The mass is calculated according to the structural details given in previous paragraph. An overview of the mass is given in the table below. The given mass is including the imposed loads on the floors.

Table 5.10 Mass of the CLT elements.

Element	thickness [mm]	weight [kN/m^2]	mass input [ton/m^3]
Roof	130	0.88	0.69
Floor	130	1.54	1.20
Wall	100	0.95	0.97

5.3.1.1 Imposed load

Besides the self-weight also the imposed loads are taken into account.

$$q_{imposed} = 1.75 \cdot 0.18 = 0.315 \text{ kN/m}^2 \qquad \text{(eq. 5.1)}$$

These values are according to the Dutch code and further specified in the calculation in annex B.

The total vertical force on the building. with additional forces on the first and second floor is equal to 37.4 tons (367 kN). The first load step of the push-over analysis is the application of the vertical pressure. the total vertical reaction force is equal to 360 kN which is in the range of the assumed reaction force. The difference can be explained due to the estimation of the openings in the front and back façade and by using centrelines of the walls for the modelling.

5.3.2 Ground floor

The ground floor consists of prefabricated concrete hollow-core slabs (fig. 5.9) with a thickness of 200 millimetre and finished with a 50 millimetre cement screed. The concrete floor is not modelled, because of its height from ground level it is unlikely to contribute to the vibration modes.

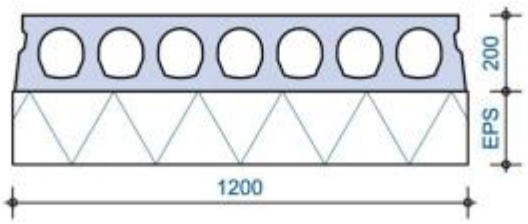

Fig. 5.13 Cross-section of a concrete hollow-core slab, with isolation (EPS) (VBI, 2016).

The foundation needs to be adjusted to support the prefab concrete slabs. The foundation will be wider and supporting the concrete hollow-core slab.

5.3.3 Walls

The walls from the case study building addressed in chapter 4 are first analysed separately (fig. 5.14 & fig. 5.15). This allows to check the difference of the full building and the separate walls.

- Wall A front wall without openings to check influence of the openings.
- Wall B front wall with openings
- Wall C back wall with openings

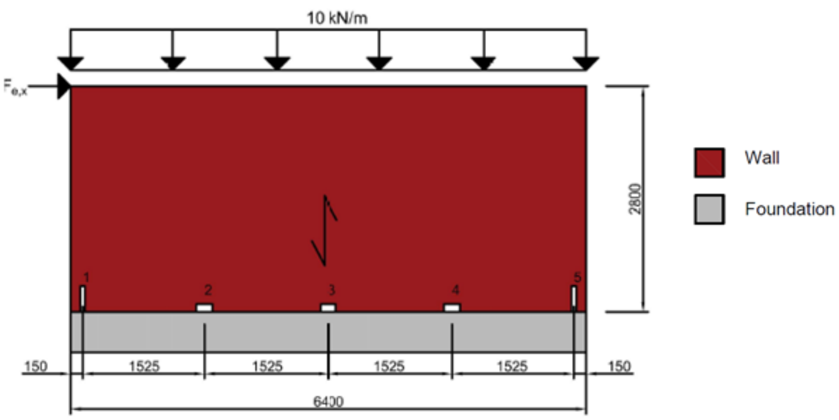

Fig. 5.14 Dimensions and location of angle brackets and hold-downs for wall A.

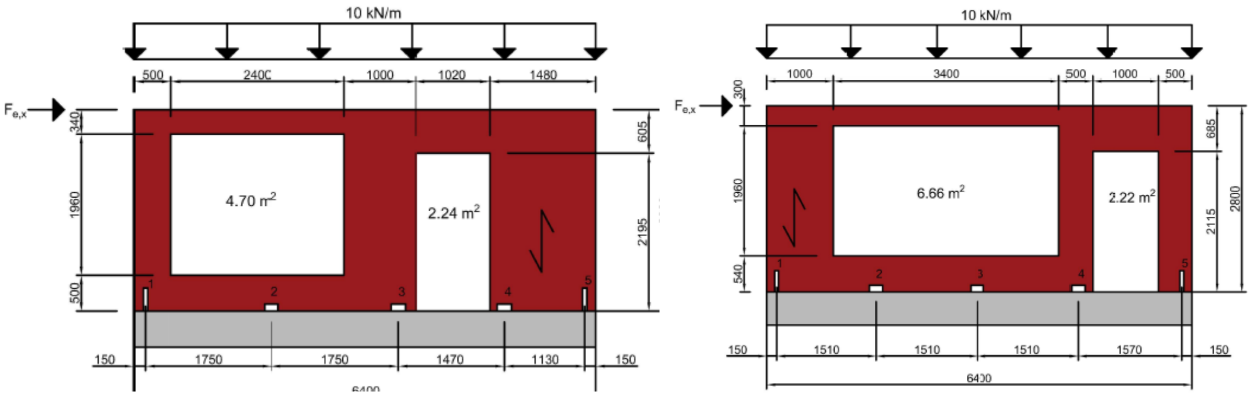

a) Wall B *b) Wall C*

Fig. 5.15 Dimensions and location of angle brackets and hold-downs for wall B and C, where the window and door openings are added.

Due to the differences in thickness of the layers also the properties for the orthotropic shells are changed.

Table 5.11 Input for the orthotropic shells.

Input wall	symbol	value	unit
Thickness	t_{wall}	100	mm
Young's modulus	E_x	6748	MPa
	E_y	4622	MPa
	E_z	11000	MPa
Poisson ratio	ν	0.30	-
Shear modulus	G	563	MPa

5.3.3.1 Number of connections

A simply calculation/ prediction is made for determining the number of connectors needed for each wall. From the lateral force calculation made for the CLT in chapter 4.5 the following elastic force distribution over the height is used for determining the number of connectors.

$F_{attic} = 236 \text{ kN} \text{ . } h_{attic} = 5.4 \text{ m}$

$F_{floor} = 107 \text{ kN} \text{ . } h_{floor} = 2.8 \text{ m}$

For calculation of the number of hold-downs the 5% percentile of the maximum tensile force in a hold-down is equal to $F_{0.05} = 42.40$ kN. According to the NPR 9998 the material factor $\gamma_m = 1.0$ and according to the EC5 the modification factor $k_{mod} = 1.1$. Furthermore it is assumed that all the vertical forces is restraint by the hold-downs, assuming that the angle brackets do not corporate in the vertical restriction.

$$\begin{aligned} &5.4 \cdot 236 + 2.8 \cdot 107 - n_{hold-down} \cdot 42.4 \cdot 6.4 = 0 \\ &n_{hold-down} = \frac{5.4 \cdot 236 + 2.8 \cdot 107}{1.1 \cdot 42.4 \cdot 6.4} = 5.3 \end{aligned} \qquad \text{(eq. 5.2)}$$

The vertical weight is not taken into account due to the fact that in the calculation this is compression and works favourable for the number of connecters. A q-factor of 2 is applied conform EC8 for the estimation of the number of hold-downs. This resulted in the following number of hold-downs 2.7. The first calculations will be made with hold-downs at the corners of each wall. This leads to a total of two hold-downs restraining the uplift when loading from one side.

However it can be assumed that the hold-down in y-direction restrained the uplift when the building is loaded from x-direction. due to the connection between the perpendicular walls. Besides this there is also the beneficial axial capacity of the angle brackets and pressure from the above floors resulting in less uplift of the building. Therefore the first estimation on the number of hold-downs is equal to two.

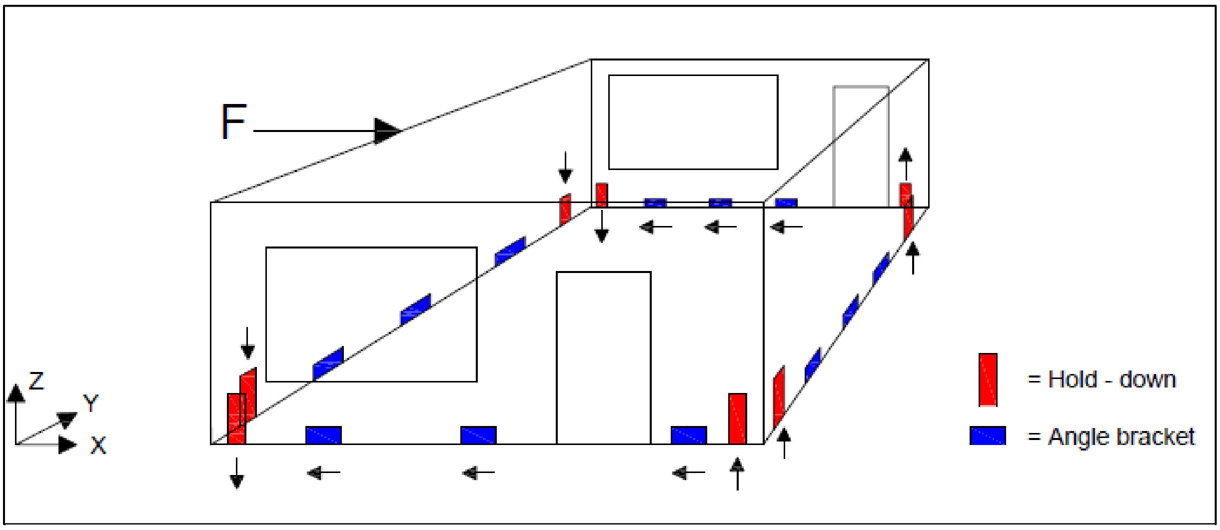

Fig. 5.16 Overview with the connectors taken into account for the estimation of the number of connectors.

The same rough approximation is made for the shear connectors. The 5th percentile of the ultimate force $F_{0.05} = 24.89$ kN.

$$n_{angle\ brackets} = \frac{343}{1.1 \cdot 24.89} = 12.5 \qquad \text{(eq. 5.3)}$$

When applying the q-factor and dividing the number of angle brackets over the walls the total number of angle brackets per wall is 3.1. The number of angle brackets used will be set to three as first approximation.

Table 5.12 Overview of the number of connections per wall.

Connector	X-direction	Y-direction
Hold-down	2	2
Angle brackets	3	3

The floor on the second floor has the same number of connections since the horizontal force and uplifting force is lower this is sufficient.

5.3.3.2 Openings

By first performing a test with a wall without any openings the influence of these openings can be analysed. Research has resulted in analytical formula's (Dujic, Klobcar, & Zarnic, 2007).

The research stated that the reduction on the shear strength for CLT walls can be approximated by the following :

$$F_{opening} = F_{full} \cdot r(2-r) \qquad \text{(eq. 5.4)}$$

Where r is the panel area ration which is calculated by the following formula.

$$r = \frac{1}{1+\frac{\alpha}{\beta}} = \frac{H\sum L_i}{H\sum L_i + \sum A_i} \qquad \text{(eq. 5.5)}$$

With,

H	Height of the wall element
L	Length of the wall element
ΣL_i	Length of full height wall segments
ΣA_i	Sum area of openings
$\alpha = \frac{\Sigma A_i}{HL}$	Ratio of openings in wall element
$\beta = \frac{\Sigma L_i}{L}$	Ratio of full wall segments

For wall B this leads to a panel ratio of 0.55 and therefore the reduction of the shear strength 0.79 of the full wall. The formula (eq. 5.5) uses 0.5% inter storey drift as a guideline for determining the lateral force capacity. The 0.5% inter storey drift equals 14 millimetre displacement.

For wall C this leads to a panel ratio of 0.39 and therefore the reduction of the shear strength 0.63 of the full wall.

5.3.4 1st and 2nd floor

Now everything is combined. The walls in the two directions are connected (fig. 5.11) and the first floor is fully modelled. The input for the floor is calculated with a reference board thickness of 130 millimetre and equal layers. The floor is modelled as an orthotropic CLT slab, loaded out of plane by self-weight and the imposed load from paragraph 5.3.1.1.

Table 5.13 Input of the orthotropic floor.

Input floor	symbol	value	unit
Thickness	t_{floor}	130	mm
Young's modulus	E_x	9471	MPa
	E_y	1899	MPa
	E_z	11000	MPa
Poisson ratio	ν	0.30	-
Shear modulus	G	505	MPa

Between the screws there is a line interface representing the allowing withdrawal of the screws and supporting compression.

5.3.4.1 Input of the connections

The connection between the floor and the lower walls is made with self-tapping screws as well as the wall to wall connection. A detail can be found in fig. 5.12. As input for the model the backbone curves of test results are used (fig. 5.17) from the following research.

- (Gavric, Fragiacomo, & Ceccotti, Cyclic behavior of typical screwed connections for cross-laminated (CLT) structures, 2014)

Since the results for the shear directions (WW-L-P and WF-L-P) is almost the same for the different layer set-up the most unfavourable is used for modelling. The difference of layer set-up referrers to the number of layers of timber perpendicular or parallel to the shear direction.

The red graph which shows the withdrawal resistance of a single screw but it also has a compression branch. This branch is very stiff and represents the compression of the two timber elements. For instance the floor is compressed on to the wall below. In this case the screw is not doing anything and the reaction is of the timber floor onto the timber wall. In tension the rope effect limits the withdrawal of the screw which is visible in the graph. There is a high tensile force and limit displacement.

For the floor to wall connection HBS Ø10 x 260 screws were used in the experiments and for the wall to wall connection HBS Ø10 x 180.

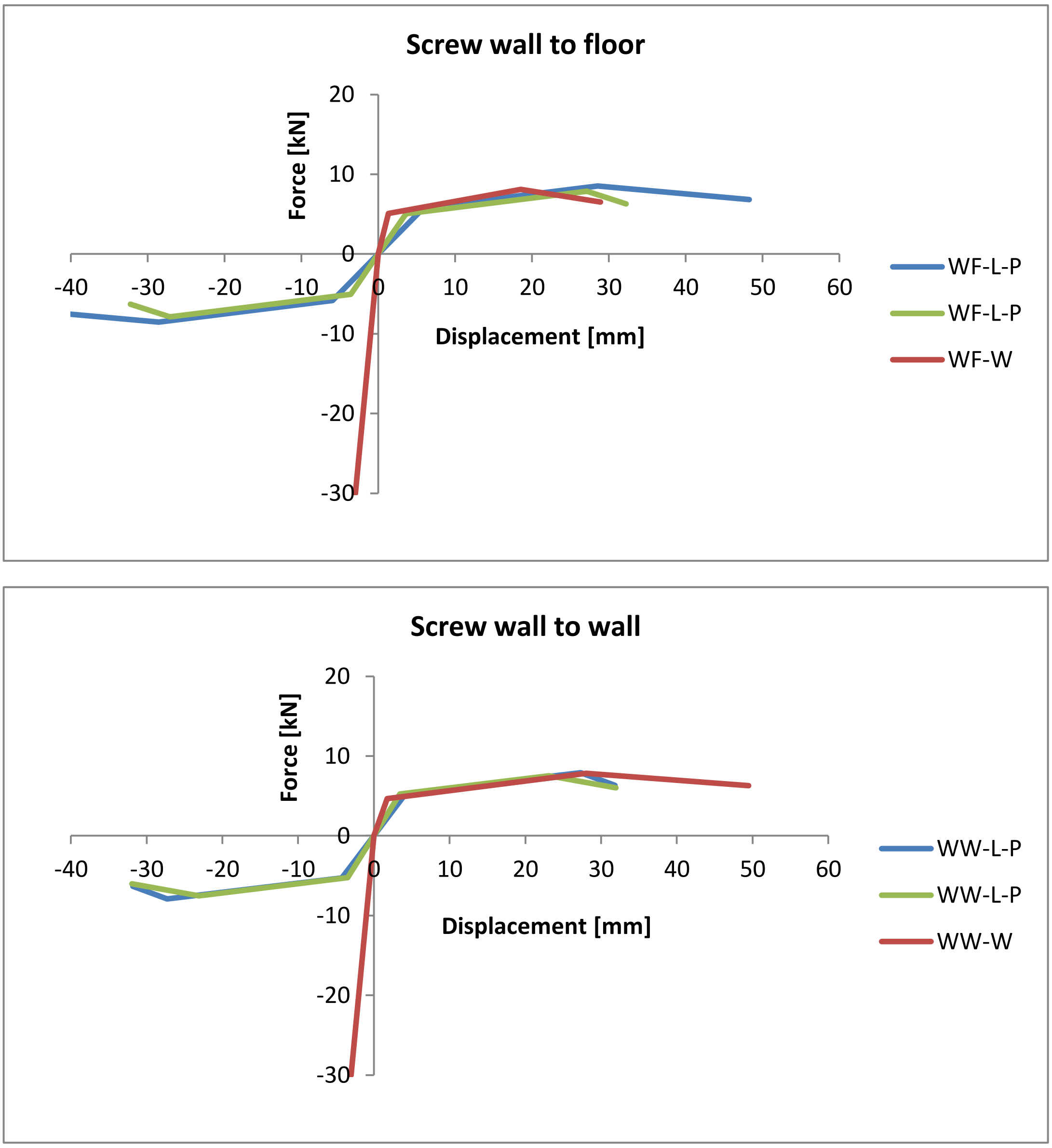

WF-L-P	=	Wall – Floor Lateral	WW-L-P	=	Wall – Wall Lateral
WF-W	=	Wall – Floor Withdrawal	WW-W	=	Wall – Wall Withdrawal

Fig. 5.17 Input for the screw. The graphs are for a single screw.

The minimum distance for screws and nails in CLT is 10*d*. (Brandner, Flatscher, Ringhofer, Schikhofer, & Thiel, 2015)

Minimum spacing screws = $10 \cdot 10 = 100$ mm

Minimum spacing nails = $10 \cdot 4 = 40$ mm

5.4 Results

The described model is analysed in steps and the results are discussed in this paragraph. The results will be discussed in the following order:

- Walls
- Walls combined with the first floor
- Building up to the second floor
- Total building

The results shown are the load-displacement diagrams from a displacement based push-over. Followed by the forces and displacement in the connections.

5.4.1 Walls

First results of the three different walls are shown. The walls are all loaded by a prescribed displacement from the upper left corner pushed to the right (fig. 5.18) and secondly from the right upper corner pushed to the left (fig. 5.19). The results are obtained from the reaction force at the point of the described displacement.

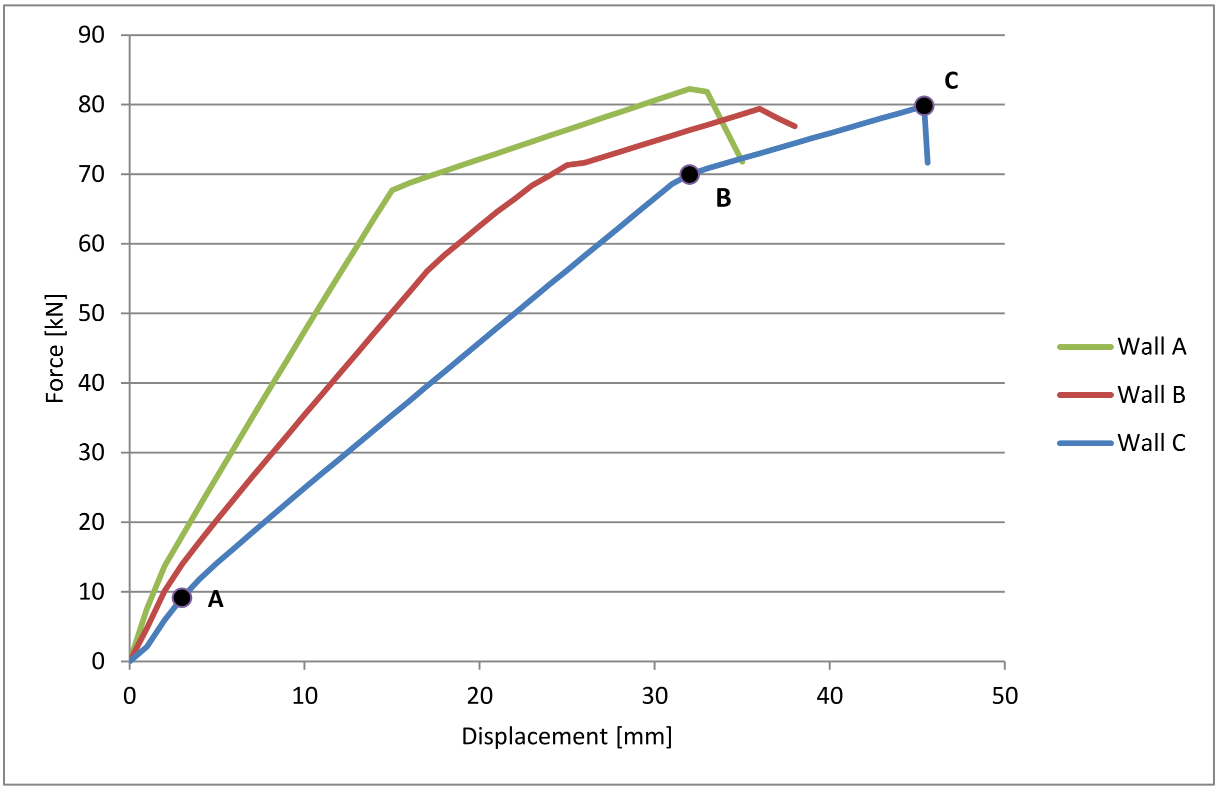

Fig. 5.18 Force displacement diagrams of the walls. The additional displacement of wall B and C can be explained due to the decrease in stiffness of the total CLT wall.

For wall C the points in the graph are further analysed in the same way as for the experimental wall.

Table 5.14 Points of interest for wall C.

Point	Displacement [mm]	Force [kN]
A	3	9.13
B	32	69.94
C	45.4	79.80

One of the major differences between the experimental wall and wall C is the geometry. Wall C has a different height-length ratio, wall C is longer than the experimental wall. This results in less rocking deformation and more sliding of the wall. Furthermore the openings of the wall results in a higher deformation of the wall itself, also visible in the table with the figures below.

Table 5.15 Forces and displacement of the connection at a horizontal displacement of three millimetre.

Step	Node	X - direction		Z - direction	
		Force [kN]	Displacement [mm]	Force [kN]	Displacement [mm]
4	1 HD	1.94	0.72	0.80	0.20
	2 AB	1.38	0.83	0.00	0.00
	3 AB	1.42	0.85	0.20	0.09
	4 AB	1.37	0.82	0.00	0.00
	5 HD	3.01	1.11	0.03	0.00

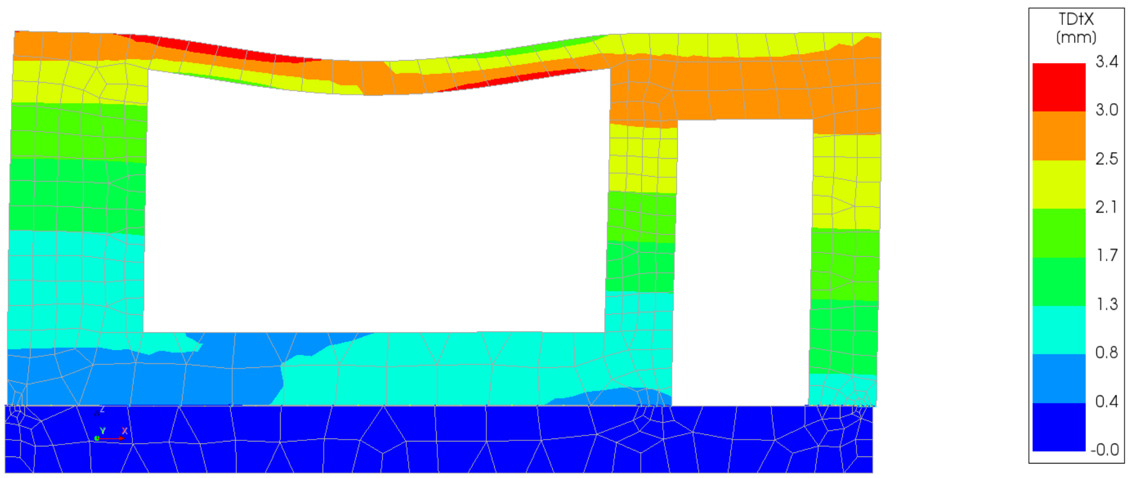

Next point B is evaluated. Table 5.16 shows that at the bottom left corner the hold-down is restraining the uplift. The sliding of the wall is restrained by the angle brackets which from this point have reached the more ductile branch of the tri-linear backbone. The transition point from the backbone curve is at a displacement of 11.74 and a force of 19.53 kN. Furthermore it can be seen that the horizontal deformation in the hold-down is increasing due to the fact that it is in the more ductile branch of the backbone.

Table 5.16 Forces and displacement of the connection at a horizontal displacement of 32 millimetre.

Step	Node	X - direction		Z - direction	
		Force [kN]	Displacement [mm]	Force [kN]	Displacement [mm]
33	1 HD	4.59	11.15	18.45	4.73
	2 AB	19.63	12.24	0.00	0.00
	3 AB	19.69	12.55	3.40	1.51
	4 AB	19.32	11.61	1.33	0.59
	5 HD	6.70	25.06	0.00	0.00

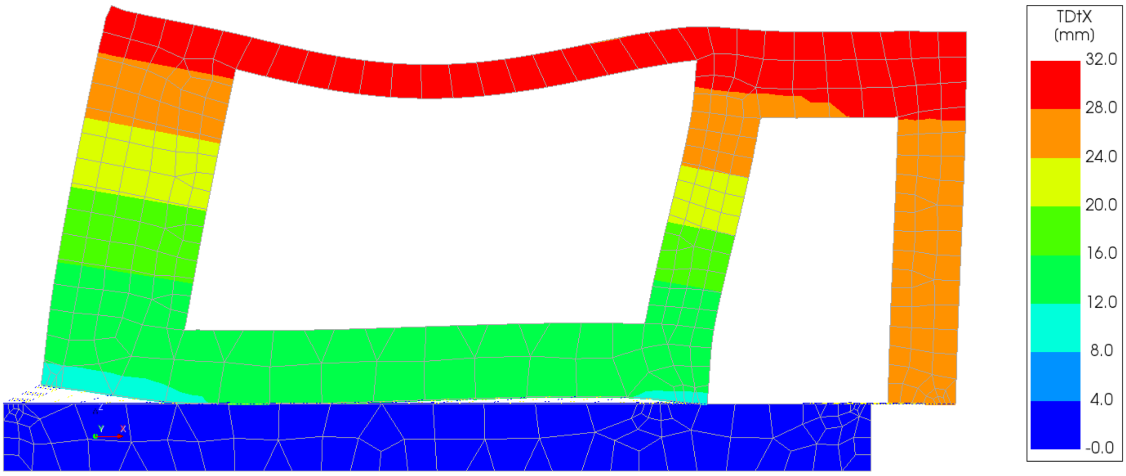

At the final step it is visible that the wall is failing due to sliding. The final deformation in the hold-down is reached and therefore not capable of restraining any forces. These forces have to be restrained mostly by the three angle brackets which will then reach their final capacity.

Table 5.17 Forces and displacement of the connection at a horizontal displacement of 47 millimetres.

Step	Node	X - direction		Z - direction	
		Force [kN]	Displacement [mm]	Force [kN]	Displacement [mm]
48	1 HD	6.20	21.72	21.38	5.78
	2 AB	21.74	22.98	0.00	0.00
	3 AB	21.81	23.35	3.92	1.74
	4 AB	21.60	22.64	1.63	0.72
	5 HD	8.46	36.64	0.00	0.00

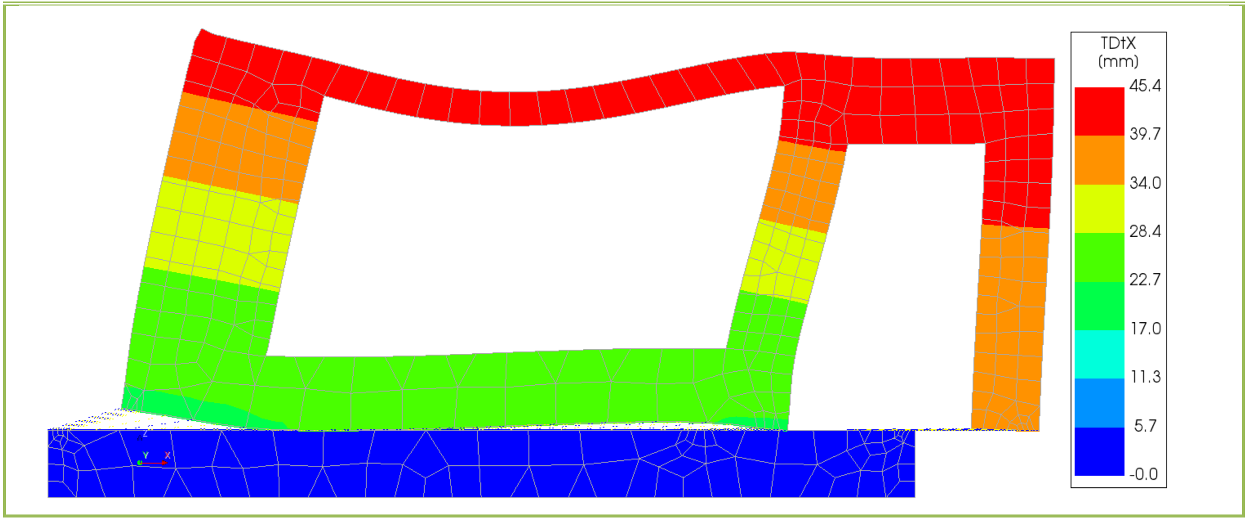

5.4.1.1 Influence of the openings.

The influence of the openings is compared to the suggested reduction value. The force reduction is in the same order for the model as calculated with the formula (table 5.18). The difference can be assigned to the different distribution of the connections and the geometry of the openings.

Table 5.18 Overview of the differences between the values from the modelled walls and the analytical formula by Dujic. The table gives the reduction due to the openings in the walls compared to wall A.

Wall	Force		Stiffness	
	Model	Dujic	Model	Dujic
Wall B	0.74	0.79	0.67	0.27
Wall C	0.52	0.63	0.48	0.19

However there is a difference in reduction of the stiffness. this can be due to the difference in lay-out of the walls. There a various differences between the walls modelled by Dujic and the walls in this report. Most significant differences are the length-height ratio. lay-out of connectors and the input of the connections. The walls modelled in this paper will mainly fail due to shear resistance. because of the length-height ratio.

5.4.1.2 Load direction

Now the walls are loaded from the upper right corner and pushed to the left. Due to the location of the openings of the walls and the and the distribution of the connections.

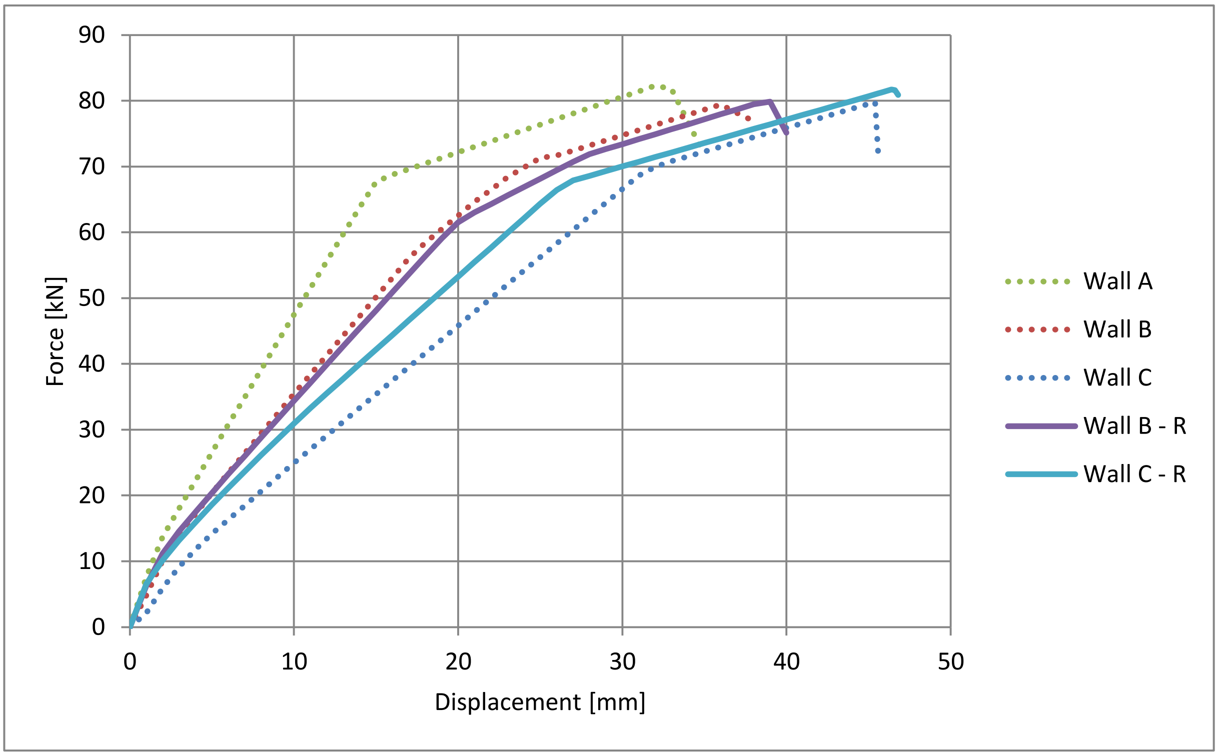

Fig. 5.19 Load - displacement graph of the walls loaded from the right upper corner. The dotted lines are representing the walls loaded for the upper left corner pushed to the right. While the continuous lines are representing the walls which are loaded from the upper right corner and pushed to the left. For wall A there is no difference since the wall and the location of the connections is symmetrical.

The most difference can be found in wall C. This is due to the fact that the part of the wall resisting the uplift is reduced. When the load is applied on the right upper corner only the hold-down next to the door opening will restrain the vertical uplift. Resulting in more rotation and displacement.

5.4.2 First floor

Next the walls are connected with screws in such way that a boxed structure is created. In the model three different connections are analysed to determine the influence of the connection.

- Fully connected – stiff connection.
- Connection with screws - a certain stiffness depending on the amount of screws.
- No connection.

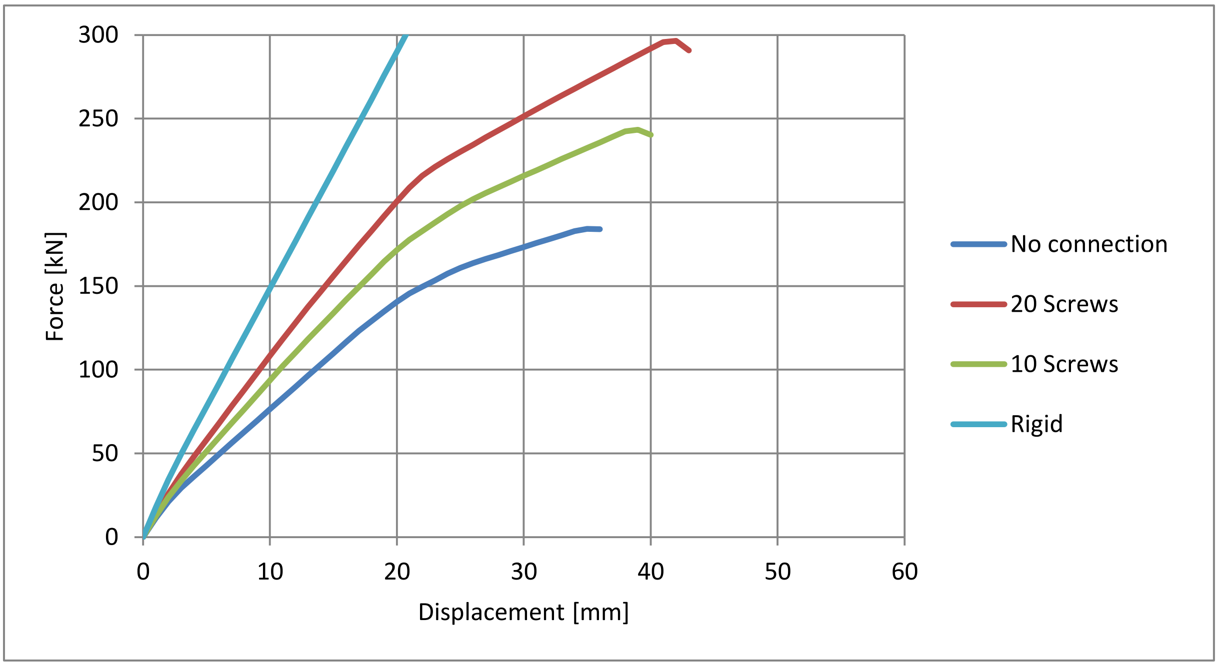

Fig. 5.20 Results for the connection of the perpendicular walls. Number of screws in the legend is per corner of the building.

Fig. 5.20 shows the results of the four different options. If the wall is fully connected to the wall perpendicular the structure becomes very stiff and strong due to the box action. On the other hand if the walls are not connected all the forces are transmitted through the walls parallel to the forces. By adding screws the connection between the walls have a certain stiffness and the resistance of the total structure increases. It shows the importance of modelling the entire structure. For the model the connection between the walls will be made with ten screws, this ensures the increased forces and additional stiffness and limits the number of screws.

5.4.3 Second floor

With the same method the second floor is added to the model. However there is a slight difference in the backbones of the connections. Where the previous connection were attached to the foundation the connections of the 2nd floor are attached to the CLT floor. Secondly the location of the connections is adjusted due to the fact that there are no openings at the lower side of the wall. Finally the connectors also differs since they are not attached to a rigid concrete foundation but screwed or bolted to a more elastic CLT floor.

The angle bracket used is a BMF 100 x 100 90 x 3 mm connected to the wall with eight 4 x 60 mm ring nails and with 4 x 60 mm annular ring nails with two additional HBS screws 4 x 60 mm to the floor. The hold-down used at the first floor are 100 mm shorter than those on the ground floor. The hold-downs used are the WHT440 attached to the timber wall with nine nails ring nails and through the first floor with a sixteen millimetre bolt.

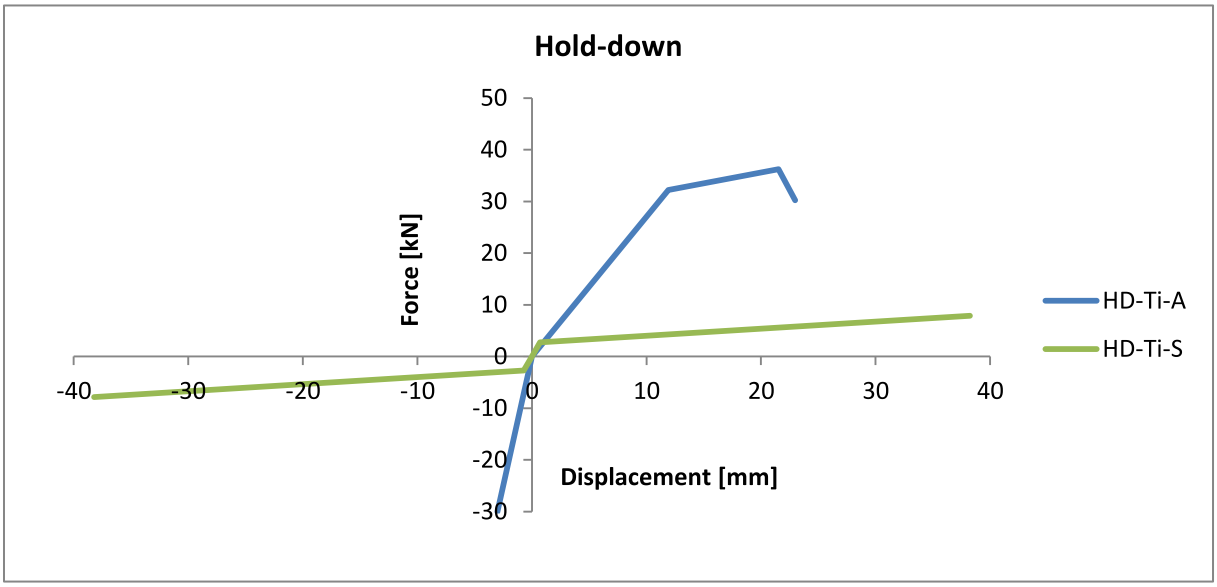

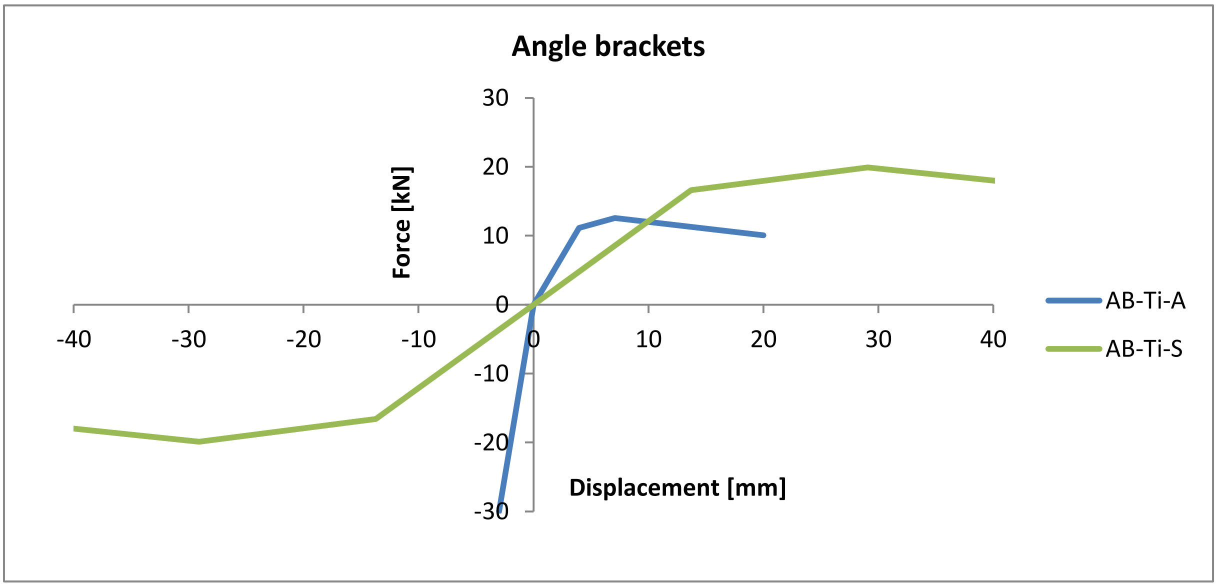

HD = hold-down Ti-A = timber|timber Axial

AB = angle bracket Ti-S = timber|timber Shear

Fig. 5.21 Input of the connectors at the first floor.

The distribution of the connection on the second floor is done with equal distances. The hold-downs are located at 150 millimetres from the edges and the angle brackets are located with a centre to centre distance of 1525 millimetres.

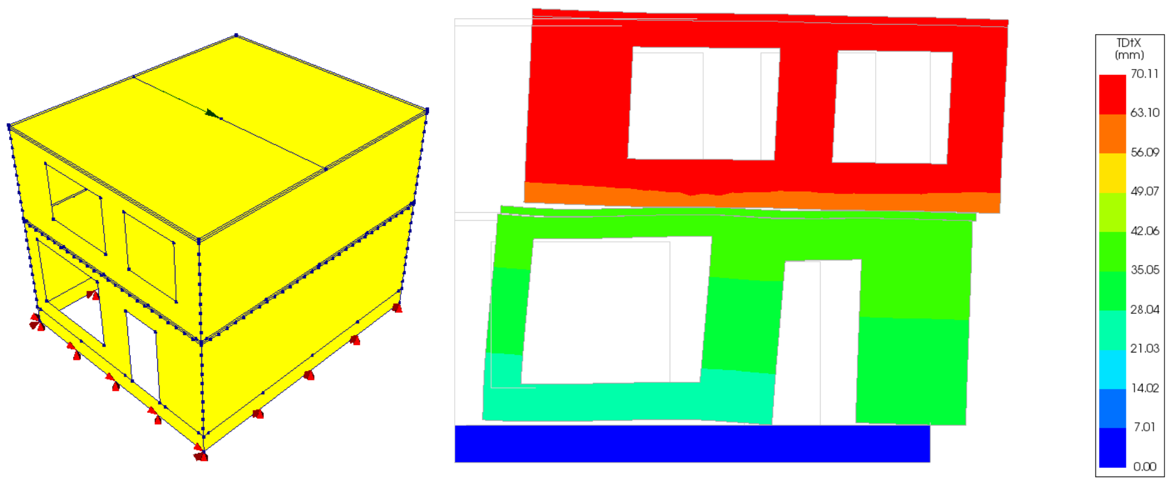

Fig. 5.22 Model of the building up to the second floor and the displacement from the results.

A prescribed deformation is applied in x-direction at the top of the second floor. The result of the deformation controlled push-over is shown compared to the push-over of only an one storey building. Fig. 5.23 shows the inter-storey drifts of the two push-overs. The maximum force for the two storey building is 211 kN while the maximum force for one storey building is higher at a value of 240 kN.

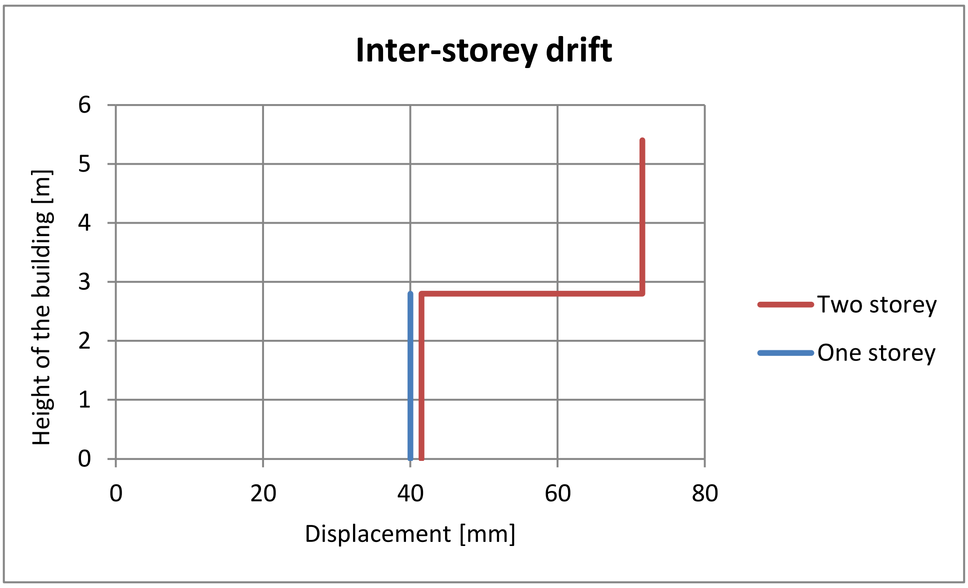

Fig. 5.23 Inter-storey drift for the push-over of the one and two storey model.

The difference in the above graph can be explained by the fact that the push-over is displacement based. The larger displacement is reached due to the fact that there is also displacement at the second floor. The displacement is a combination of sliding and rocking of the first and second floor. However the maximum force of the system is reduced due to the fact that the angle bracket in the part next to the door opening on the first floor has an increased load, due to the deformation of the second floor. Also less rocking deformation of the first floor is possible due to the increased mass of the building. This effect is minimal since the governing mechanism is sliding due to the length height ratio of the building.

5.4.4 Total building

An overview of the model with all the interfaces is shown in fig. 5.24.

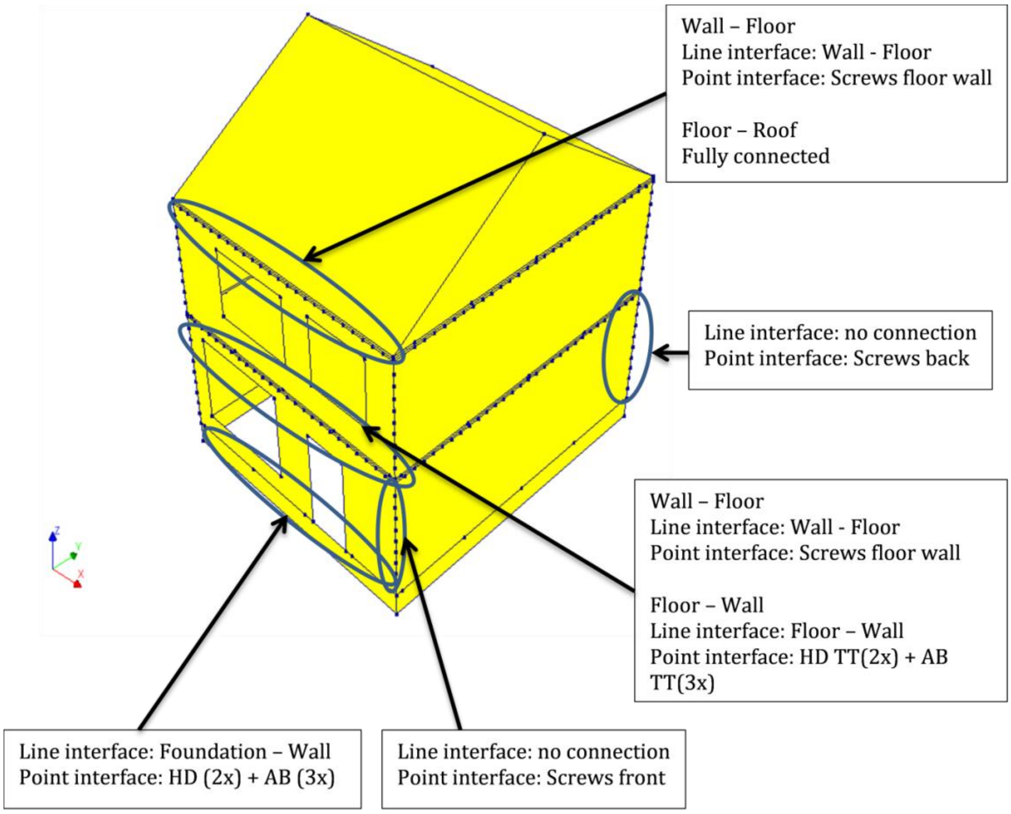

Fig. 5.24 Overview of the model with all the interfaces applied.

The roof is connected to the front and back wall by screws (fig. 5.11) and not additionally connected to the side wall. The stiff direction of the orthogonal input is towards the front and back wall. The input for the roof is the same build-up of CLT as the floor. The weight is shown in table 5.10.

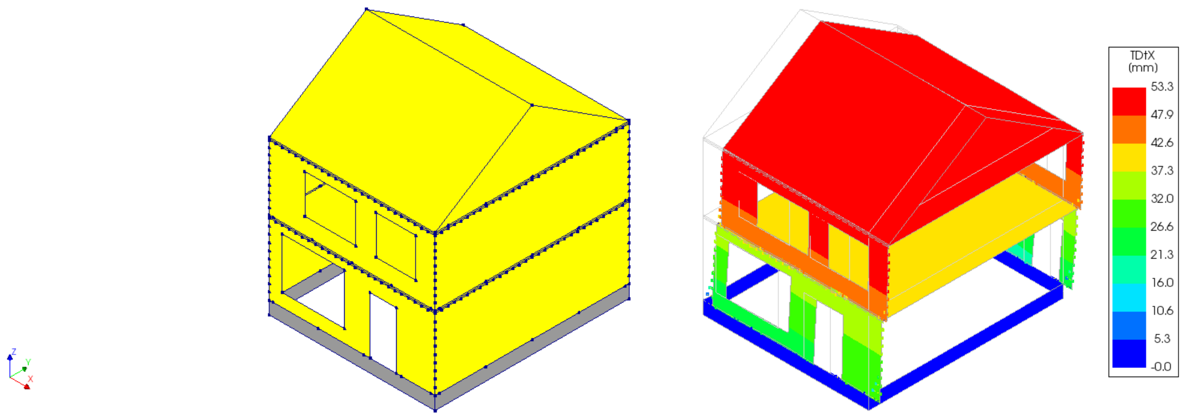

a) Overview of the modelled building. *b) Example of the results of the displacement for the front and back walls.*

Fig. 5.25 Total model which will be used in chapter 6 and an example of the outcome.

6 PUSH-OVER ANALYSIS

First the lateral load applied to the modelled building is determined conform NPR 9998, which refers to EC8. With this input the analysis in DIANA can be performed and the push-over curve of the building can be produced. Another important aspect when preforming a non-linear static push-over is the translation from a MDOF system back to a SDOF system. This makes it possible to relate the push-over to the demand curve of the earthquake. Due to the transformation both curves are plotted in the AD-diagram and results of the non-linear static push-over are analysed.

6.1 Lateral load

The push-over analysis is described in Eurocode 8 chapter 4.3.3.4.2 Non-linear static (pushover) analysis. It is a non-linear static analysis with monotonically increasing horizontal loads. The purpose of performing a push-over analysis is to obtain the ‘capacity curve’ of the building and determine the q_μ-factor which is needed.

According to EC8 4.3.3.4.2.2 two lateral load distribution must be applied on the structure:

- Uniform pattern with lateral forces proportional to the mass (eq. 6.1).
- Modal pattern, lateral forces are proportional to the lateral forces calculated with the elastic analysis (eq. 6.2).

$$F_i = \frac{m_i}{\sum_j m_i} F_b \qquad \text{(eq. 6.1)}$$

$$F_i = \frac{m_i s_i}{\sum_j m_j s_j} F_b \qquad \text{(eq. 6.2)}$$

Where S_j and S_i are the displacement of the different storeys of the building. This is calculated with the Rayleigh method in chapter 4. With the above distribution it is assumed that the force remains constant over time. This would not be the case in a cyclic loading or an earthquake, therefore this is an assumption.

Table 6.1 Load distribution ratios according to mass and to displacement.

Level	Σ m_i [ton]	Ratio 1*	S_i	Ratio 2
Attic	20.0	0.53 (1.00)	3.36	0.78 (1.00)
1st floor	17.4	0.47 (0.825)	1.10	0.22 (0.28)
Total	**37.4**			

* in an earlier stage the weight calculation was differently the ratio was 1:0.825. this is kept in the results.

In between the brackets of the third column the ratio of forces is given. Meaning if 1kN is applied on the attic floor the force acting on the first floor is equal to 0.825kN.

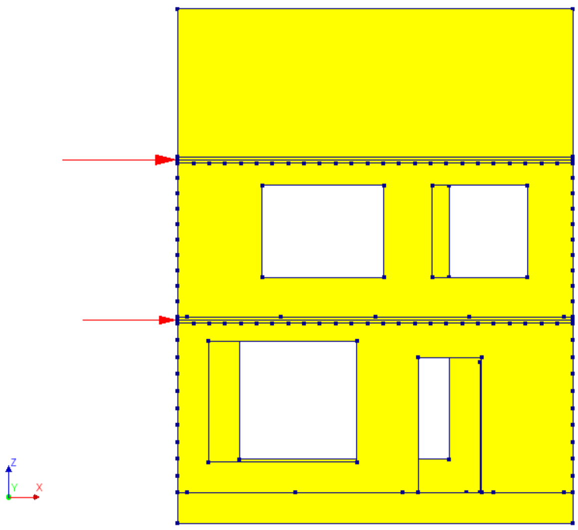

Fig. 6.1 Front view of the model with the applied forces.

The above forces are applied at the centre of the left side of the floors, consequently the building was also loaded from the right side but this was not governing. The monotonic increasing lateral force is increased until failure in one of the brackets occurs.

6.1.1 Push-over results

Both force distributions are applied on the building and led to the following results.

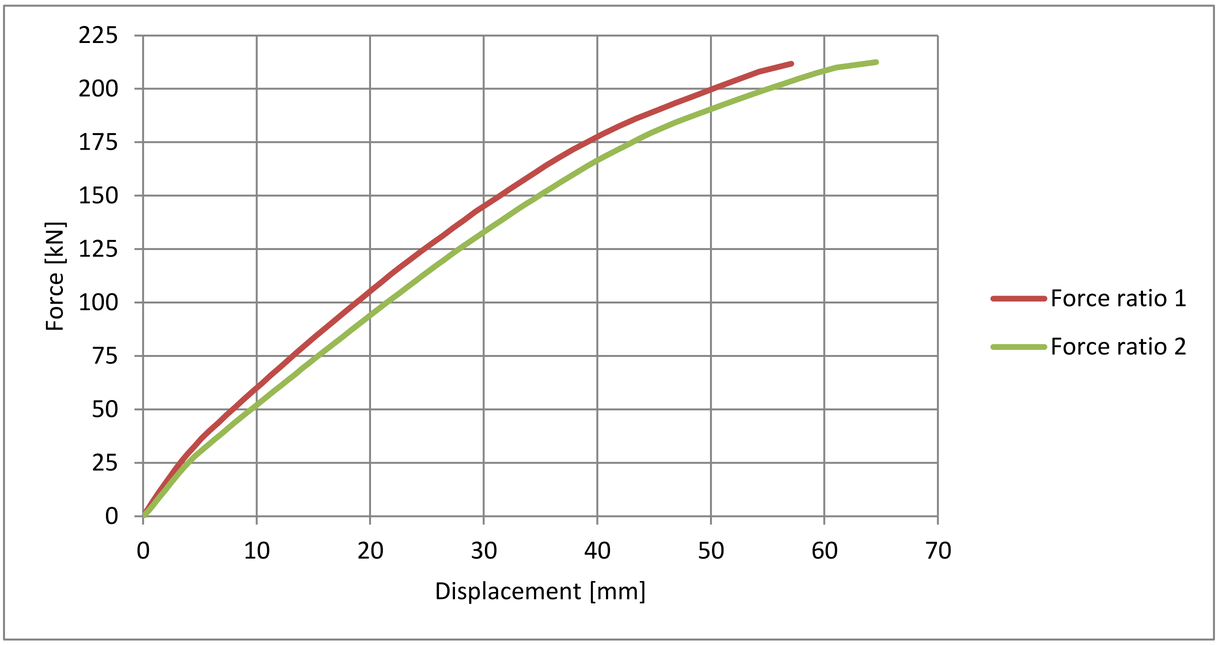

Fig. 6.2 Results of the push-over.

The maximum force for both the ratios is equal however the displacement is not and therefore the most unfavourable push-over is obtained from force ratio 1. This is due to the fact that the second level has not displaced as much compared to ratio 2.

Fig. 6.2 shows a smooth curve this in contrary to the push-over of the single walls. This is due to the fact that not all connections are loaded until the same point in the tri-linear backbone curve. For force ratio 1 the connections at the first floor remain in the first elastic branch. Besides the loading pattern also the connection between the perpendicular walls are contributing to the smoothness of the curve. Table 6.2 shows that the brackets connected to the first floor are not reaching there more ductile branch (fig. 5.21). Since there is a different stiffness at each connection this explains the smoothness of the curves.

Table 6.2 Force and displacement in the connections at different load steps.

		Step 10		Step 50		Step 62	
Location	no.	Force [kN]	Displacement [mm]	Force [kN]	Displacement [mm]	Force [kN]	Displacement [mm]
Foundation	1	2.2	0.8	4.7	12.0	6.6	24.6
	2	1.5	0.9	19.7	12.4	22.2	25.2
	3	1.5	0.9	19.4	11.7	22.0	24.2
	4	1.8	1.1	20.2	15.1	22.5	28.8
	5	2.9	1.1	5.2	15.4	7.3	29.1
First floor	1	1.3	0.4	3.6	6.9	3.9	9.3
	2	0.6	0.5	8.9	7.4	12.0	9.9
	3	0.6	0.5	8.5	7.0	11.4	9.4
	4	0.7	0.5	8.7	7.2	11.7	9.7
	5	1.8	0.5	3.6	6.9	3.9	9.3

The first part of the curves, until 25 kN base shear force, are stiffer this is due to the fact that the hold-downs are also resisting part of the horizontal force.

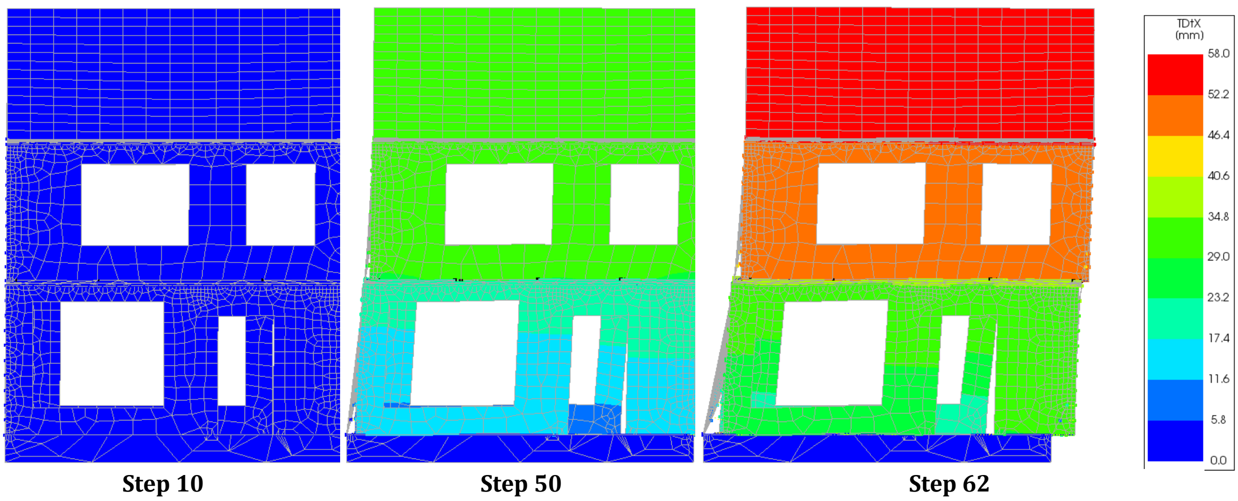

Fig. 6.3 Horizontal deformation at the different load steps.

The figure shows the deformation of the building and it can be seen that the maximum deformation capacity of the second floor is not reached. Therefore the design of the connections should be modified to obtain maximum displacement by using less nails. This lowers the force needed at the connections for the nails to deform. When there are less nails in the connection the force in a single nail increases.

6.2 MDOF to SDOF

For the visualisation and to be able to use the response spectrum the push-over curve has to be translated to a SDOF capacity curve. The derivation and explanation of this translation is based on EC8 annex B and 'A nonlinear analysis method for performance based seismic design'. (Fajfar, 2000).

The Eurocode 8 assumes the following relation:

$$\bar{F}_i = m_i \phi_i \qquad \text{(eq. 6.3)}$$

Where F_i is the normalized lateral force, ϕ_i is the normalized displacement, m_i is het mass of the i^{th} floor. To translate the MODF system, which is modelled, to a SDOF system the transformation factor must be calculated. To be able to this the following formulas are applied.

$$m^* = \sum m_i \phi_i = \sum \bar{F}_i \qquad \text{(eq. 6.4)}$$

Where m^* is the equivalent mass of the one degree of freedom system. Next the transformation factor is determined:

$$\Gamma = \frac{m^*}{\sum m_i \Phi_i^2} = \frac{\sum \bar{F}_i}{\sum \left(\frac{\bar{F}_i^2}{m_i} \right)} \qquad \text{(eq. 6.5)}$$

The use of the transformation factor is shown in fig. 6.4. It translates a MDOF system to a SDOF system. The figure shows a two degree of freedom system but this can also be done to a system with more degrees of freedom.

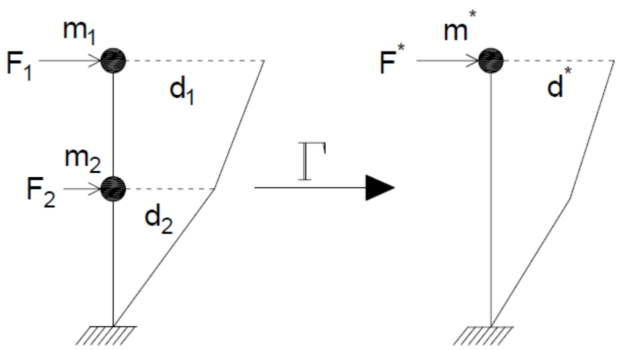

Fig. 6.4 Visualisation from a MDOF to a SDOF system.

With this factor the force and displacement of the MDOF system can be translated to an equivalent SDOF.

$$F^* = \frac{F_b}{\Gamma}$$
$$d^* = \frac{d}{\Gamma} \quad \text{(eq. 6.6)}$$

d and F_b are respectively the displacement of the control node and the base shear from the push-over analysis.

When this is done the push-over analysis is converted into a capacity curve. The capacity curve is then transformed to a linear elastic-plastic idealised curve. The EC8 uses method principle of equal energy for the linear plastic-elastic idealisation.

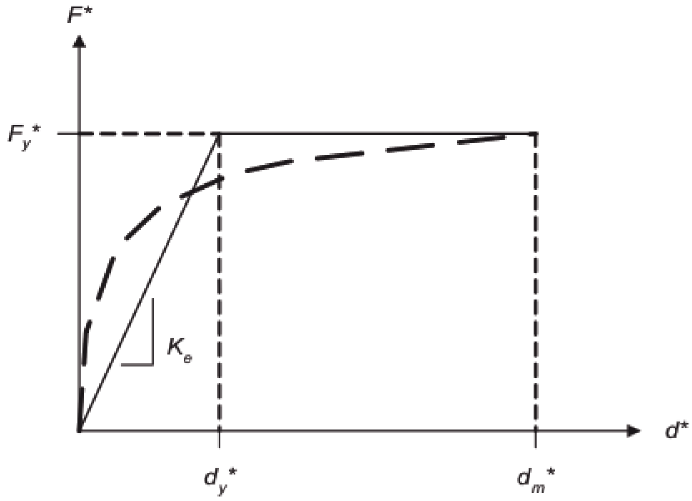

Fig. 6.5 Idealisation method based on equal energy used in Eurocode 8 (Elghazouli, 2009).

Then the natural period of the idealized equivalent SDOF of freedom system is calculated in the following way.

$$T^* = 2\pi\sqrt{\frac{m^* d_y^*}{F_y^*}} \quad \text{(eq. 6.7)}$$

Where d_y is the displacement at the formation of the first plastic hinge and F_y is the corresponding yield force. When the natural period is known also the elastic acceleration is known and the elastic displacement of the equivalent SDOF system can be calculated.

$$S_{DE}^* = S_{AE}\left(T^*\right)\left[\frac{T^*}{2\pi}\right]^2 \quad \text{(eq. 6.8)}$$

The elastic displacement can be translated to the target displacement. The target displacement is the displacement which is need to obtain a certain force reduction. This is related to the natural period of the equivalent SDOF system.

$$d_t^* = \frac{d_{et}^*}{q_\mu}\left(1+\left(q_\mu - 1\right)\frac{T_C}{T^*}\right) \geq d_{et}^* \quad T^* < T_C \quad \text{(eq. 6.9)}$$

$$d_t^* = d_{et}^* \quad T^* \geq T_C \tag{eq. 6.10}$$

Where the factor q_u stands for the needed reduction for fulfilling the strength requirements. This is the differences between the elastic force in the demand curve and the maximum force from the capacity curve (eq. 6.11). The q_u is not the same as the q-factor. The q-factor is also influenced by for instance the over-strength of the structure.

$$q_\mu = \frac{S_e\left(T^*\right)}{\left(F_y^*/m^*\right)} \tag{eq. 6.11}$$

The principle of the target displacement is visualised in the graphs below.

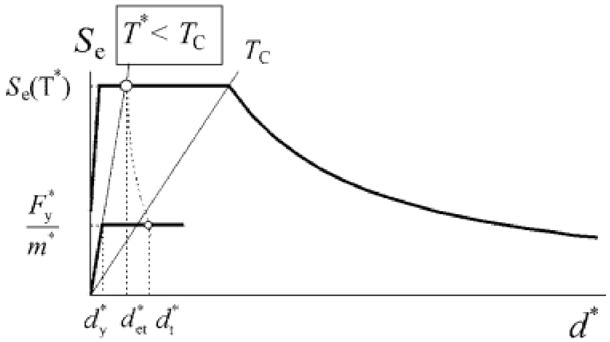

Short range period

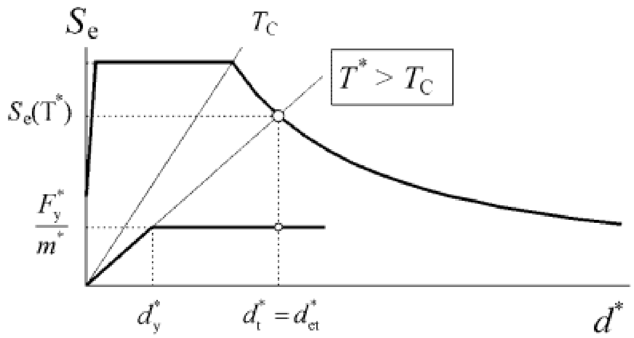

Medium and long period range

Fig. 6.6 Graphs from EC8 annex B, for determining the target displacement

There is a difference in between short period ($T^* < T_C$) and medium to long periods ($T^* > T_C$), this is due to experimental results addressed in research (Miranda & Bertero, 1994). For the medium and long periods the system uses equal displacement between the elastic and inelastic demand curve. For short periods the principle of equal energy is used. This means that the inelastic displacement demand is not equal to the elastic displacement demand. So for short-period structures the inelastic displacement demand (μ) is larger than the elastic displacement demands ($d_t^* < d_{et}^*$, see fig. 6.6).

A fact is that this will always be the case for the NPR 9998 since there is no branch for the constant velocity. This leads to a maximum displacement at the transition point *Tc* (fig. 6.8). However research states that this leads to conservative results for short-period structures in case of low ductility demand (μ < 4) (Fajfar, 2000).

From this the ductility demand can be calculated with the following equation, which is related to the needed reduction factor.

$$\mu = 1 + \left(q_\mu - 1\right)\frac{T_C}{T^*} \quad T^* < T_C \tag{eq. 6.12}$$

$$\mu = q_\mu \quad T^* \geq T_C \tag{eq. 6.13}$$

But also the q_μ - factor can be calculated for constant ductility factors.

$$q_\mu = \left(\mu - 1\right)\frac{T}{T_C} + 1 \quad T < T_C \tag{eq. 6.14}$$

$$q_\mu = \mu \quad T \geq T_C \tag{eq. 6.15}$$

This results in the following graph which shows the relation between the ductility demand and the reduction factor at different natural periods. It is clearly visible that the transition point is at T_C. From this the inelastic demand spectrum can be obtained (fig. 6.8).

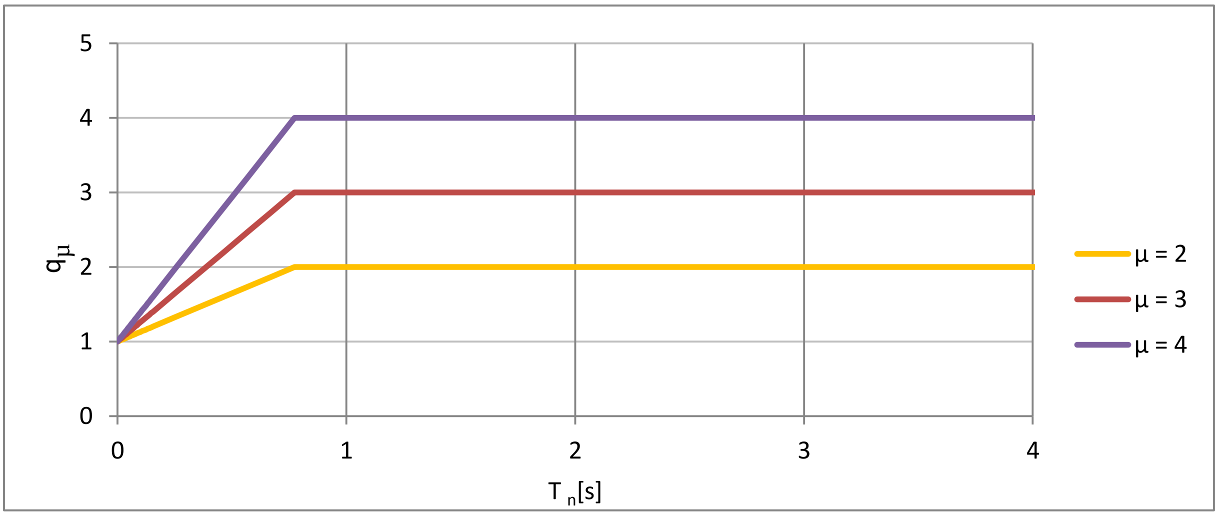

Fig. 6.7 The relation between the reduction factor for the inelastic demand curve and the ductility factor.

Also the ductility factor can be used in the formula for calculation of the target displacement.

$$d_t^* = d_{et}^* \frac{\mu}{q_\mu} \quad \text{or} \quad d_t^* = d_y^* \cdot \mu \quad T < T_C \tag{eq. 6.16}$$

$$d_t^* = d_{et}^* \quad \text{or} \quad d_t^* = d_y^* \cdot \mu \quad T \geq T_C \tag{eq. 6.17}$$

The target displacement of the SDOF system can be translated to the target displacement of the MDOF system with the translation factor.

$$d_t = \Gamma d_t^* \qquad \text{(eq. 6.18)}$$

6.3 Demand and capacity curve

Interpretation of the push-over analysis is done by using demand and capacity curves. This enables visualisation of the results and gives a better understanding of the influence of different parameters. This paragraph summarises the demand and capacity curves which can be obtained from the translation described in the previous paragraph.

6.3.1 Capacity curve

The capacity curve only depends on the structural characteristics. Via the push-over analysis the characteristics result in a force-displacement diagram of the structure. which relates the base-shear to the top displacement of the structure. This is the force-displacement diagram of a MDOF system. however with the translation factor as explained in chapter 6.2 the results can be translated to a SDOF. Next the translated force-displacement diagram is schematized to a linear elastic-plastic diagram and the capacity curve is made.

However there are multiple options for the schematization to a linear elastic-plastic diagram. which all results in different stiffness and therefore a different natural period.

6.3.2 Demand curve

The demand curve is related to the acceleration-displacement diagram. With addition of the ductility factor the inelastic demand curve is obtained (fig. 6.8). Whereas the capacity curve is solely related to structural characteristics, the demand curve is depended on the earthquake characteristics which are applied for calculating the response diagram. The derivation of the A-D diagram is explained in chapter 3.3.1.

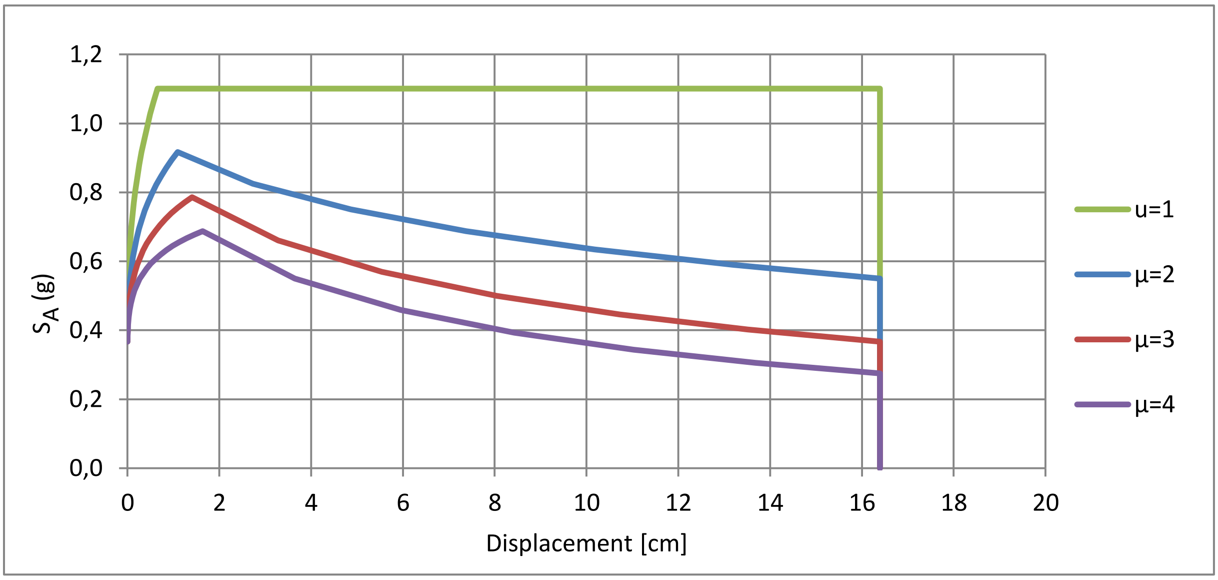

Fig. 6.8 A-D diagram for different ductility factors.

The inelastic demand lines are obtained as following. With a certain ductility demand the corresponding reduction factor for different natural periods of the building is calculated. The relation between ductility factor and the inelastic demand from fig. 6.7 is also visible. It can be seen that the reduction factor is increasing until reaching the transition point T_C between short and medium-large range period structures.

6.4 Push-over

The above description is applied on the push-over results from the model in the first paragraph. The outcome of the translation of the push-over analysis shows the governing natural period of the equivalent SDOF system is 0.45 seconds ($T^* < T_C$). Leading to an acceleration of 1.1g which corresponds with the plateau of the response spectrum. The needed reduction factor $\left(q_\mu\right)$ is equal to 2.33 and the ductility factor (μ) is 3.30.

First the transformation factor for the transformation of a MDOF to a SDOF system is calculated.

$$\Gamma = \frac{m^*}{\sum m_i \Phi_i^2} = \frac{32.59}{20 \cdot 1^2 + 17.4 \cdot 0.72^2} = 1.12 \qquad \text{(eq. 6.19)}$$

With this factor the output of the push-over analysis is translated to an equivalent SDOF in order to visualise the push-over in the acceleration displacement diagram.

Table 6.3 Overview of the output from MDOF to SDOF in brackets the normalised displacement is added for calculation of m*.

Description	Symbol	Value	Symbol		Unit
Mass	m	37.40	m*	32.59	Ton
Displacement	$D_{1st.}$	38.54 (0.72)	$D_{1st.}$ *	34.42	mm
	D_{attic}	53.28 (1.00)	D_{attic} *	47.59	mm
Force	F_y	169	F_y*	151	kN
Natural period			T*	0.45	s

With these values the push-over results are shown in the figure below, for the equivalent SDOF system (the green dotted line). From these results an elastic-plastic idealisation is made with the principle of equal energy and an assumed yield force of 80% F_{max}. The point for the yield force is assumed since it is not clearly visible when the first plastic mechanism occurs.

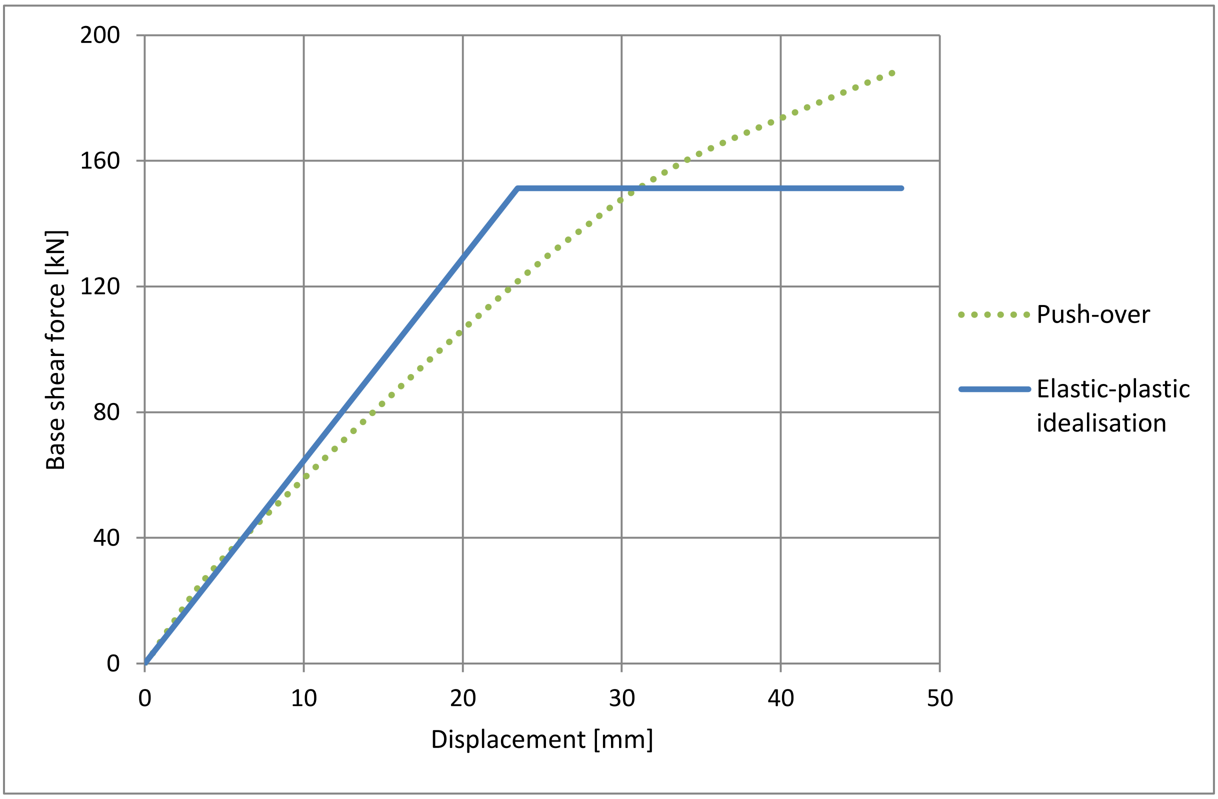

Fig. 6.9 Idealisation of the translated push-over results, with the principle of equal energy.

To be able to visualise the result from the push-over curve the force is transformed by dividing it with its mass and the gravitational acceleration.

$$S_{ay(g)} = \frac{F^*}{m^* \cdot g} = \frac{151}{32.59 \cdot 9.81} = 0.47 \qquad \text{(eq. 6.20)}$$

Also the representative natural period of the on degree of freedom system is calculated.

$$T^{*} = 2\pi\sqrt{\frac{m^{*} d_{y}^{*}}{F_{y}^{*}}} = 2\pi\sqrt{\frac{32.59 \cdot 23.44 \cdot 10^{-3}}{151}} = 0.45 \text{ s} \qquad \text{(eq. 6.21)}$$

The results are visualized below in the acceleration displacement diagram.

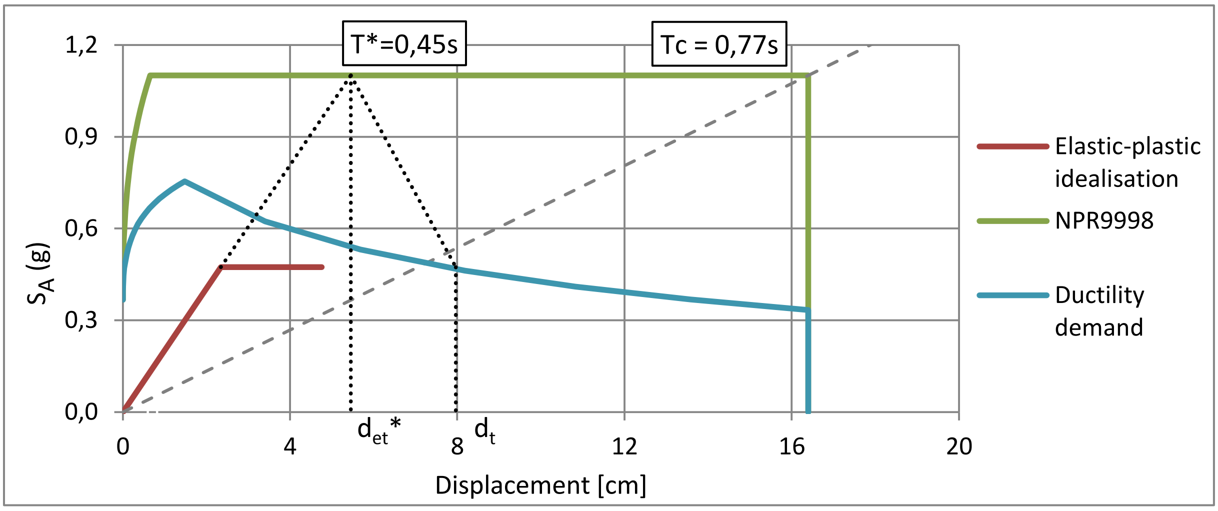

Fig. 6.10 Visualised overview of the push-over analysis.

As can be seen the period of the SDOF from system is lower than T_C from the AD diagram. First the reduction factor is calculated (eq. 6.16) after this the ductility factor μ is determined.

$$q_{\mu} = \frac{S_{AE}}{S_{ay}} = \frac{1.10}{0.47} = 2.33 \qquad \text{(eq. 6.22)}$$

From this the demanded ductility factor is calculated for $T^{*} < T_{C}$.

$$\mu = \left(q_{\mu} - 1\right)\frac{T_{C}}{T^{*}} + 1 = \left(2.68 - 1\right)\frac{0.77}{0.45} + 1 = 3.30 \qquad \text{(eq. 6.23)}$$

The target displacement of the wall is as following.

$$S_{D} = \mu \cdot D_{y}^{*} = 3.30 \cdot 23.44 = 77.34 \text{ mm} \qquad \text{(eq. 6.24)}$$

Finally this is translated into a target displacement for the MDOF system.

$$D_{t} = 1.12 \cdot 79.34 = 89.59 \text{ mm} \qquad \text{(eq. 6.25)}$$

The target displacement is not reached in this case. Since the maximum displacement of the MDOF system is 53.28 mm. Visual this can be seen by the capacity curve of the building not intersecting the ductility demand curve in fig. 6.10.

6.4.1 q-factor

A different method which is sometimes used for calculation of the reduction factor is based on the energy expression.

$$q_\mu = \sqrt{2\mu - 1} \quad \text{(eq. 6.26)}$$

This equation gives an indication of the reduction factor and is not dependent on the natural period of the building as in fig. 6.7. The μ-factor is the ratio between the ultimate and elastic displacement. For the push-over result from fig. 6.9 this results in the following calculation.

$$\mu = \frac{d_u}{d_{et}} = \frac{47.59}{23.44} = 2.03 \quad \text{(eq. 6.27)}$$

Resulting in a reduction factor of 1.75.

$$q_\mu = \sqrt{2 \cdot 2.03 - 1} = 1.75 \quad \text{(eq. 6.28)}$$

This however does not incorporates the over-strength and redundancy of the structure. Also the push-over was aborted at the first failure of a bracket. Resulting that the q-factor will be higher than the determined q_μ-factor.

6.5 Significant damage

For the limit state, significant damage a different response spectrum is applicable. This is obtained by adjusting the consequence factor (k_{ag}) from 1.4 to 0.7. This also changes the inelastic demand curve of the building. While the capacity curve of the building remains the same.

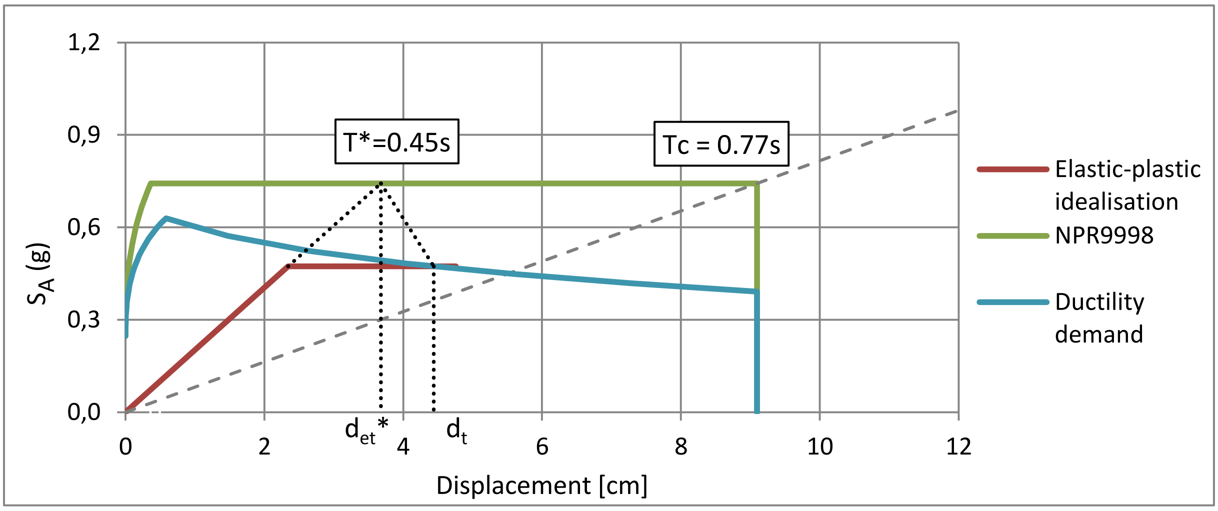

Fig. 6.11 AD-diagram for significant damage (k_{ag} =0.7) with the idealisation of the push-over result of the building.

It is visible that the needed reduction factor changes from 2.33 to 1.57, this is due to the fact that the acceleration factor at the plateau of the elastic response spectrum (S_{AE})changes from 1.10 to 0.74. Resulting in a ductility demand of 1.89.

6.6 Damage limitation

In case of damage limitation the consequence factor changes from 0.7 to 0.3 and the acceleration factor at the plateau from 0.74 to 0.42. This results in a linear reaction of the building when schematised as is done until now .

$$q_{\mu} = \frac{S_A}{S_{AE}} = \frac{0.42}{0.47} = 0.89 \leq 1 \qquad \text{(eq. 6.29)}$$

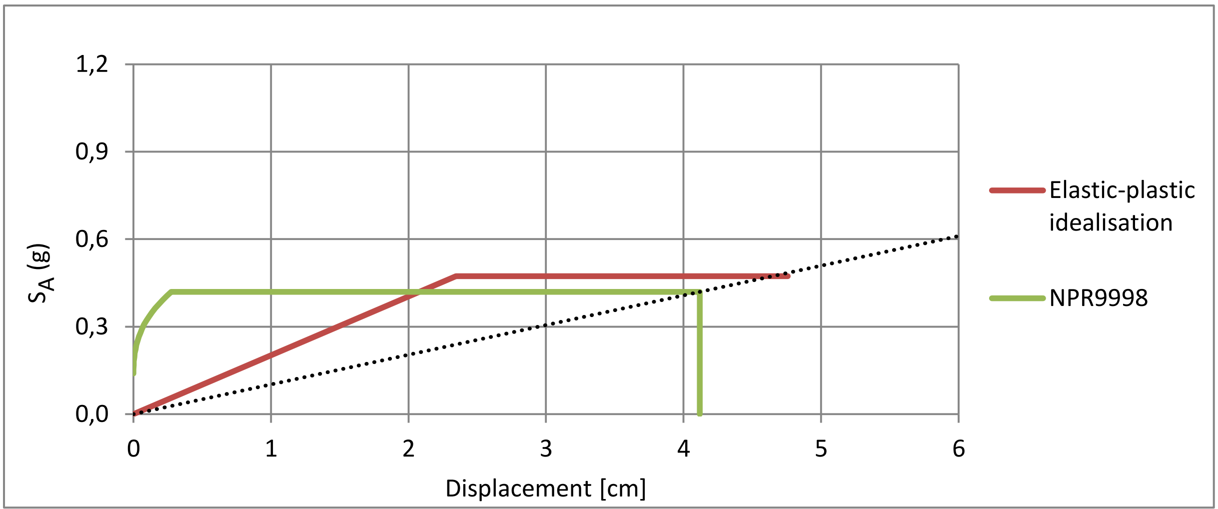

Fig. 6.12 Outcome for the damage limitation.

This leads to the fulfilment of the requirements for damage limitation also according to the allowable inter-storey drift. The building will react linear according to the specific elastic-plastic idealisation. Therefore the CLT is beneficial since there will be almost no remaining damage to the building.

6.6.1 Inter-storey drift

The inter-storey drift limit, according to EC8 4.4.3.2, is set to:

$$d_r v \leq 0.005h \qquad \text{(eq. 6.30)}$$

This is the limit for the worst case scenario where the non-structural elements are brittle. The *v* is a reduction factor according to 4.4.3.2 (2) and depends on the importance class.

According to the Eurocode 8, a normal house is of importance class 2 corresponding with a *v* of 0.5 and therefore the limit of the inter-storey drift is the following:

$$d_r \leq 0.01h \qquad \text{(eq. 6.31)}$$

This leads to a maximum inter-storey drift of $0.01 \cdot 2700 = 27$ millimetre meaning that the top displacement is allowed to be approximate 54 millimetres to fulfil the criteria for damage limitation.

d_r is the difference between the top and bottom displacements of the floors and for this method a different response spectrum must be used.

Table 6.4 Overview of floor displacement and inter-storey drift.

Floor	Displacement [mm]	Inter-storey drift [mm]
First floor	37.3	16.0 < 27.0
Second floor	53.3	

6.7 Verification of forces

Besides the force –displacement diagram also the forces acting on the structure will be verified.

This is checked with the k-method (Blass & Fellmoser, 2004) for CLT (d_t = 100 mm). The method takes into account the ratio between the thickness of the layers in the two directions. It uses the layers in one direction and adds the influence of the layers in the other direction. This is furhter elaborated in annex C. For calculation of the design values the material factor (γ_m) is 1.25 and modificiation factor (k_{mod}) is 1.1 because of the short load duration.

$$k_3 = 0,61 \rightarrow f_{m,0,\text{ef}} = 0,61 \cdot 24 = 14,72 \text{ N/mm}^2$$
$$k_4 = 0,42 \rightarrow f_{m,90,\text{ef}} = 0,42 \cdot 24 = 10,08 \text{ N/mm}^2$$

Resulting in the following maximum bending force:

$$N_{xx} = \frac{d_t \cdot f_{m,0,ef} \cdot k_{\text{mod}}}{\gamma_m} = \frac{100 \cdot 10,08 \cdot 1.1}{1.25} = 887 \text{ N/mm}$$

Now for compression and tension for loads parallel to the wall.

Compression

$$N_{yy} = \frac{k_3 \cdot f_{c,0,eff} \cdot d_t \cdot k_{\text{mod}}}{\gamma_{\text{m}}} = \frac{0,61 \cdot 21 \cdot 100 \cdot 1.1}{1.25} = 1127 \text{ N/mm}$$
$$N_{xx} = \frac{k_4 \cdot f_{c,0,eff} \cdot d_t \cdot k_{\text{mod}}}{\gamma_{\text{m}}} = \frac{0,42 \cdot 21 \cdot 100 \cdot 1.1}{1.25} = 776 \text{ N/mm}$$

Tension

$$N_{yy} = \frac{k_3 \cdot f_{t,0} \cdot d_t \cdot k_{\text{mod}}}{\gamma_{\text{m}}} = \frac{0,61 \cdot 14 \cdot 100 \cdot 1.1}{1.25} = 751 \text{ N/mm}$$
$$N_{xx} = \frac{k_4 \cdot f_{t,0} \cdot d_t \cdot k_{\text{mod}}}{\gamma_{\text{m}}} = \frac{0,42 \cdot 14 \cdot 100 \cdot 1.1}{1.25} = 517 \text{ N/mm}$$

Shear capacity: This is checked with the program CLT designer and the maximum shear force is equal to 200 N/mm, also checked with other research (Bogensperger, Moosbrugger, & Silly, 2010).

The forces on the figures are given for the local axis of the wall element

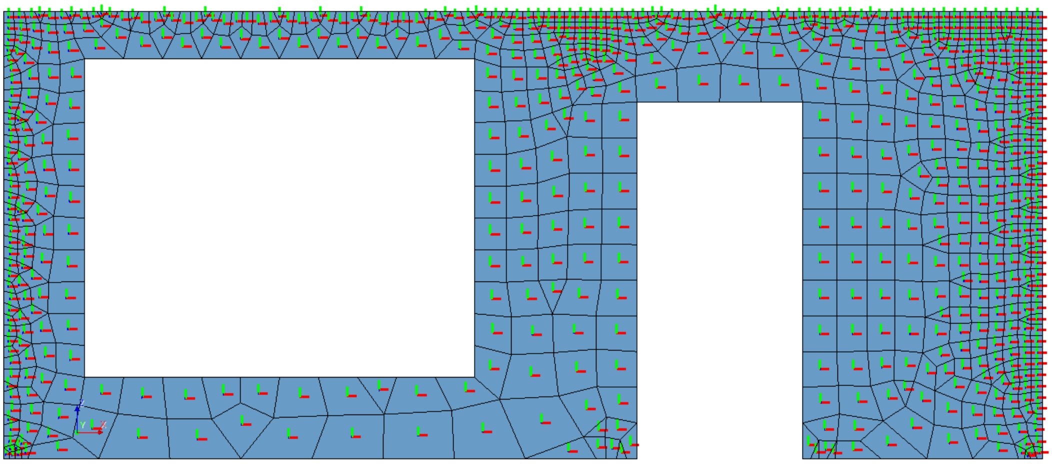

Fig. 6.13 Overview of the local axis of the wall element.

The x-axis is in the shear direction along the wall, y-direction is the height of wall and z-direction is perpendicular to the wall.

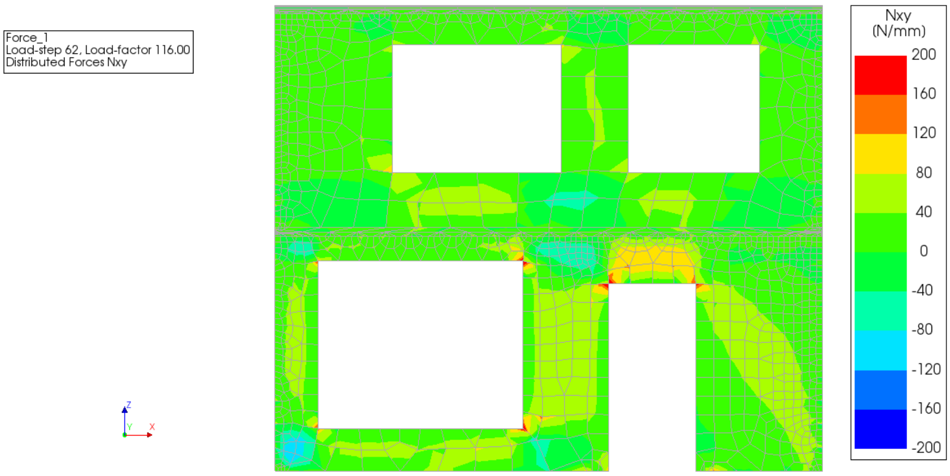

Fig. 6.14 Shear force (Nxy) on the front walls at the final load step.

The only locations where the shear force is critical is at the corners of the openings on the first floor. These peak force can also be caused by extrapolation between the integration points from the FEM analysis.

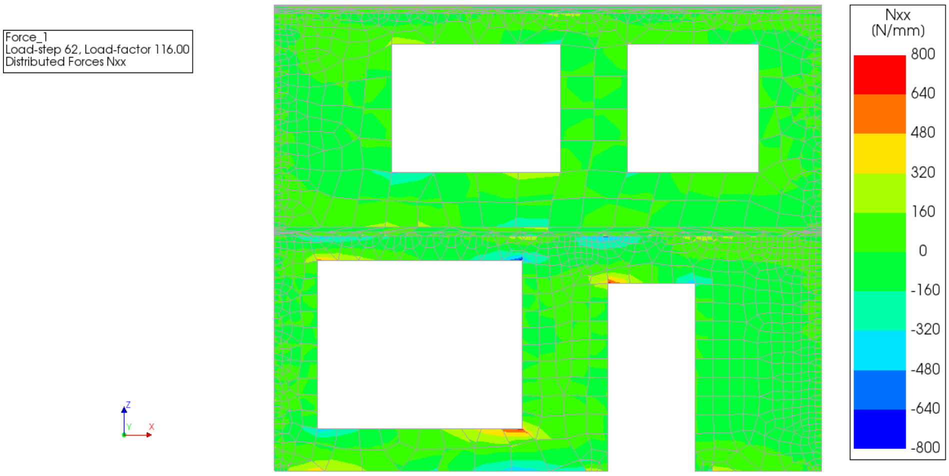

Fig. 6.15 Horizontal force (Nxx) on the front walls at the final load step.

There is a peak compression force above the door opening, for which the same holds as stated at fig. 6.14. Also at the corners of the window opening there are peak values this is mainly due to the bending of the wall. Finally there are higher forces at the shear connectors.

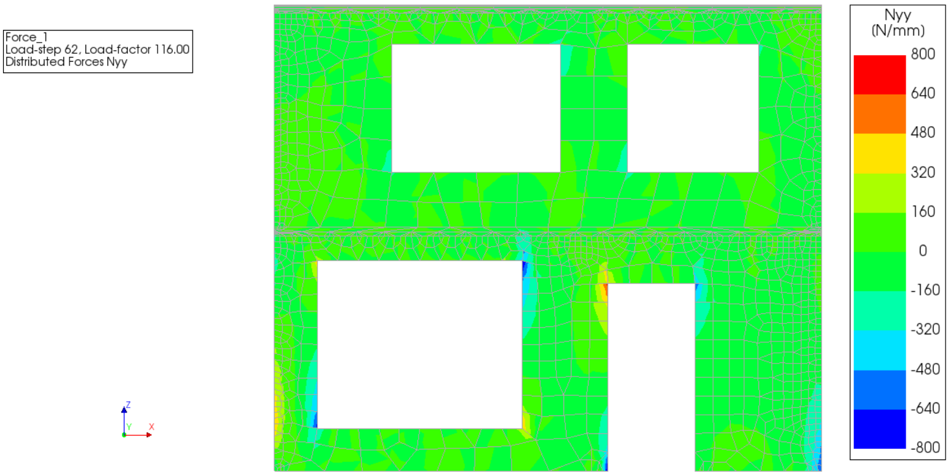

Fig. 6.16 Vertical force (Nyy) on the front walls at the final load step.

There are peak forces at the corners of the openings, where there is tension at the left side and compression at the right side due to the bending. Next there is a compression at the location of the hold-down at the right corner. The peaks shown are mostly due to the bending of the CLT and so the maximum membrane force of the CLT is higher than the value from the legend.

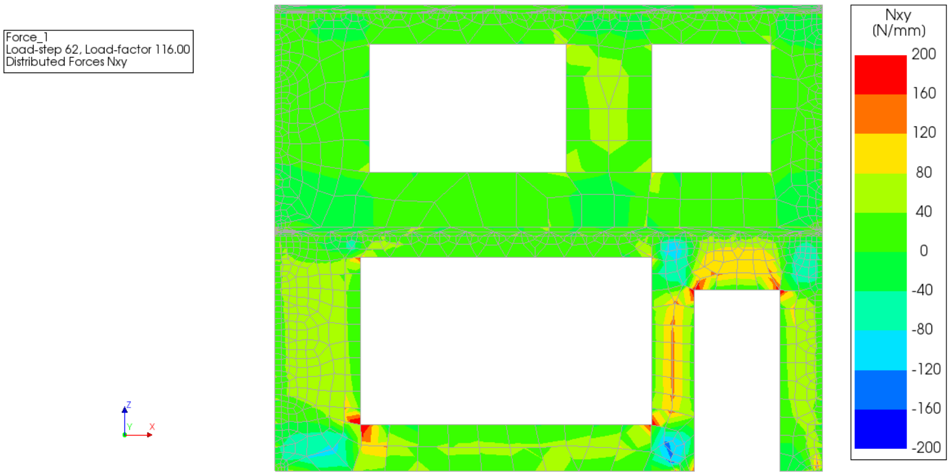

Fig. 6.17 Shear force (Nxy) on the back walls at the final load step.

The shear forces at the back side of the building are more critical. Besides the peaks at the corners there is also a peak in shear force in between the window and the door opening. Therefore it is suggested to decrease the width of the window opening.

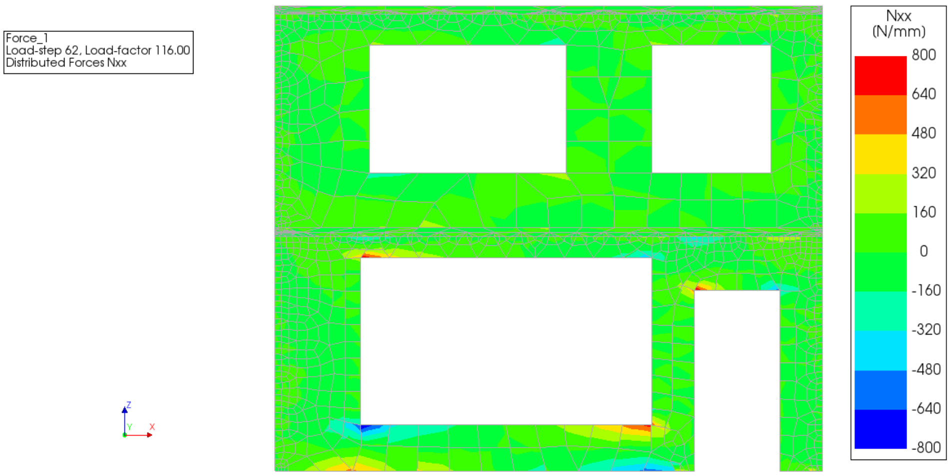

Fig. 6.18 Horizontal force (Nxx) on the back walls at the final load step.

For the horizontal forces the same holds as for the horizontal forces at the front walls.

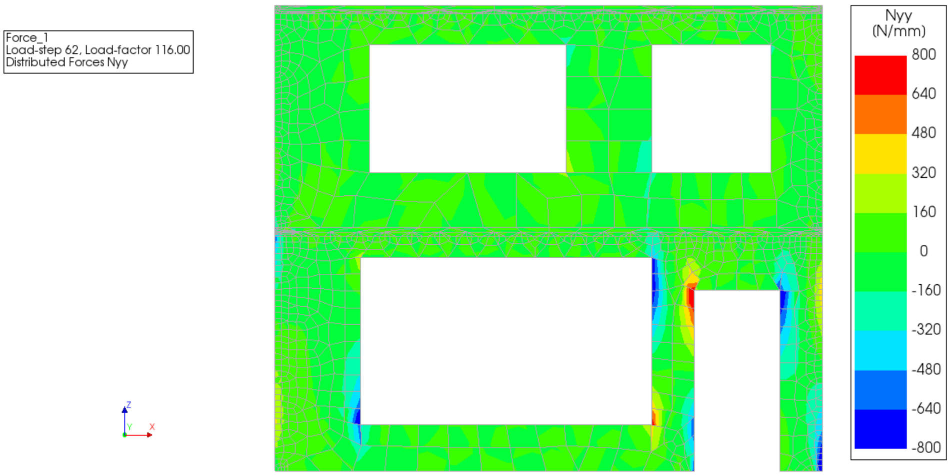

Fig. 6.19 Vertical force (Nyy) on the back walls at the final load step.

The vertical forces on the wall are increased this is due to the large opening area compared to the front wall. However since the outer layer of the CLT elements is in vertical direction, the load bearing capacity in y-direction is higher. Also most of the forces are due to the bending of CLT.

7 PARAMETERS AND OPTIMIZATION

This chapter gives an overview of the parameters which are of influence on the analysis of the push-over results. The following parameters will be addressed:

- PGA
- Elastic-plastic idealisation
- Application of the force distribution

The influences of the parameters is not limited to the case study only. Also a discussion is added in case different building lay-outs were tested. This results in a more general overview of the applicability and limitation of the non-linear static pushover as a calculation method.

The building has not met the requirements as shown in chapter 6. The building has either not enough deformation capacity to fulfil the requirements for the needed q_μ-factor. Or the elastic strength of the building is sufficient to lower the needed q_μ -factor. The last part of this chapter gives solutions for this and new analysis are performed. The following solutions will be discussed:

- Adding an additional angle bracket
- Adding an additional shear wall

The solutions are followed by a conclusion on the effectiveness and the applicability of the purposed method.

7.1 Peak ground acceleration

The PGA is dependent on the location of the building and influences the total seismic force. The case study building did not fulfil the requirements. Now it is hypothetical located at a different location with a lower PGA. By changing the PGA the demand curve changes while the capacity curve obtained from the push-over remains the same.

The fact that the capacity remains the same results in the same natural period. For the case study building the natural period will remain below the transition point T_C. Since the demand curve changes this results in a reduction of the force and therefore the needed q_μ -factor (fig. 7.2). But the natural period of the building is below the transition point T_C so the ductility factor is determined with the energy principle. This results in a different inelastic demand curve when the PGA value is changed, this is visible in the equation below.

$$\mu = 1 + \left(q_\mu - 1\right)\frac{T_C}{T^*} \quad T^* < T_C \qquad \text{(eq. 7.1)}$$

When the ductility factor is kept the same for different PGA's this would lead to fig. 7.1. The figure shows the different inelastic lines for all the PGA's. It does not shows the elastic demand curve for the different PGA's. This is shown in fig. 7.2.

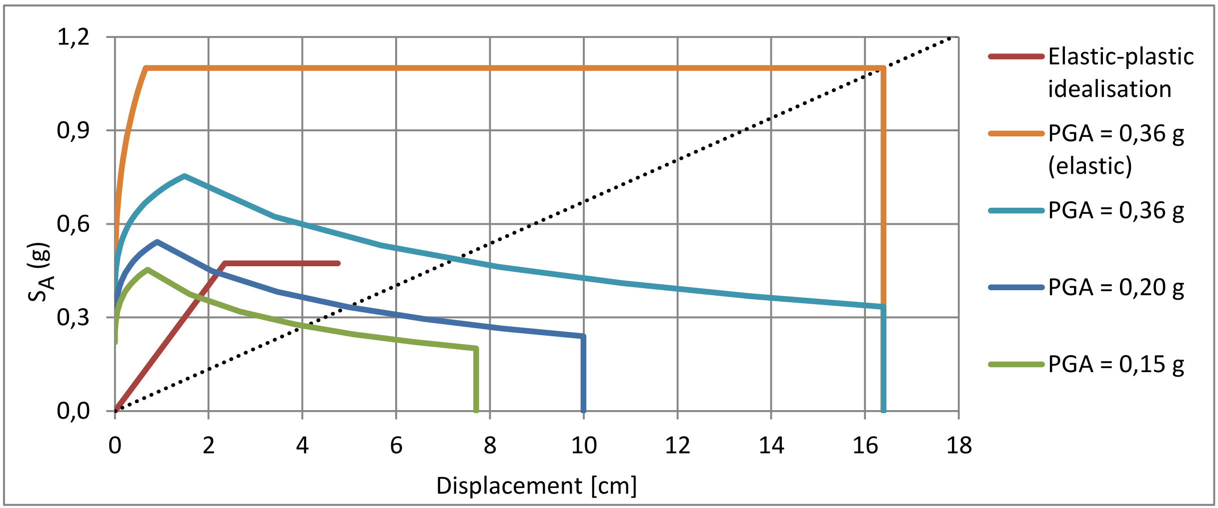

Fig. 7.1 AD diagram when the q_μ-factor and the ductility are not linked.

From the elastic demand curves it is visible that also the q_μ -factor and therefore the ductility factor changes (eq. 7.1).

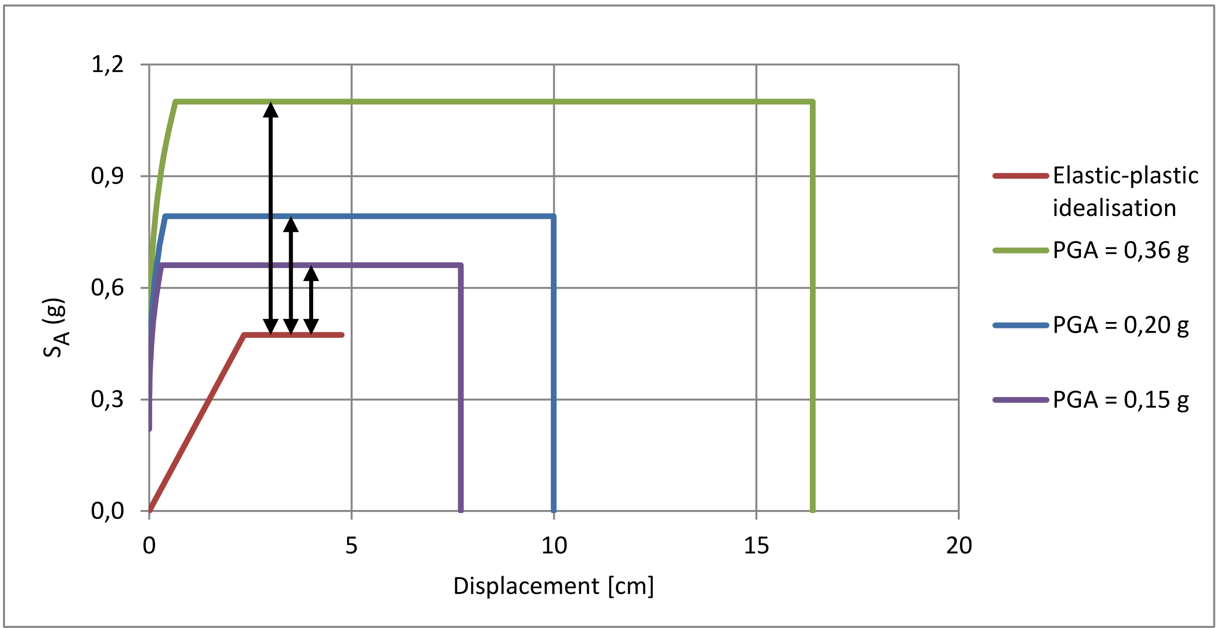

Fig. 7.2 Difference in q_μ-factor which needs to be obtained.

The values which belong to fig. 7.2 are shown table 7.1 and the influences of changing the PGA is translated into fig. 7.3

Table 7.1 Overview of output for different PGA's.

PGA (g)	Behaviour factor [q_μ]	ductility factor [μ]	Natural period [T*]
0.36	2.33	3.30	0.45 sec
0.20	1.67	2.08	0.45 sec
0.15	1.40	1.61	0.45 sec

When visualising the output from table 7.1 the structure is only capable of fulfil the requirement at a PGA of 0.15g. Whereas if the ductility demand is not linked to the q_{μ} -factor the building would resist a PGA of 0.20g.

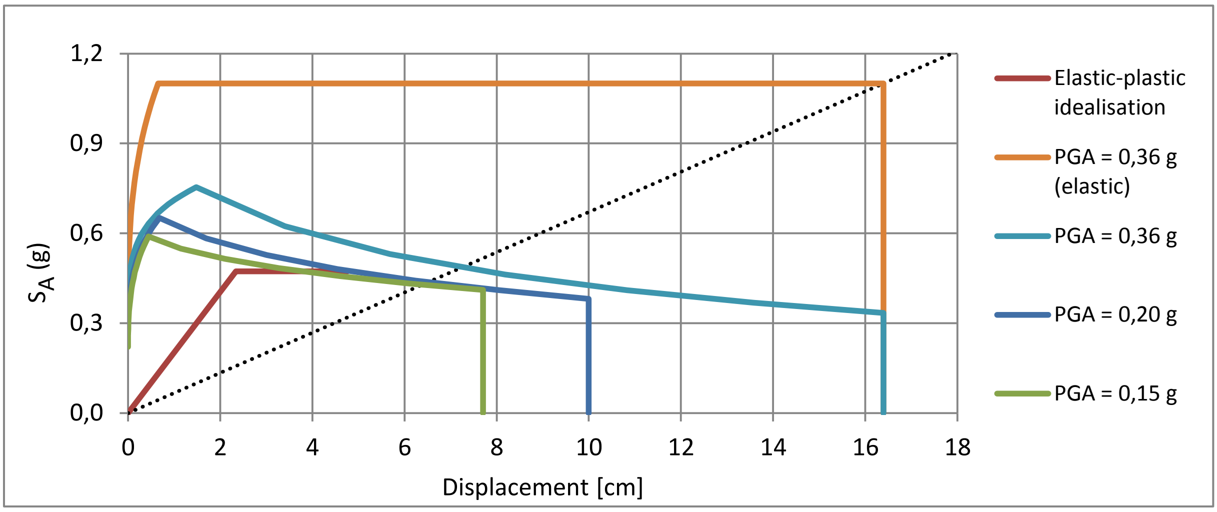

Fig. 7.3 AD diagram with the adjusted ductility demand curves.

But the ductility demand is linked to the q_{μ} -factor resulting in a maximum PGA of 0.19g, shown in the figure below.

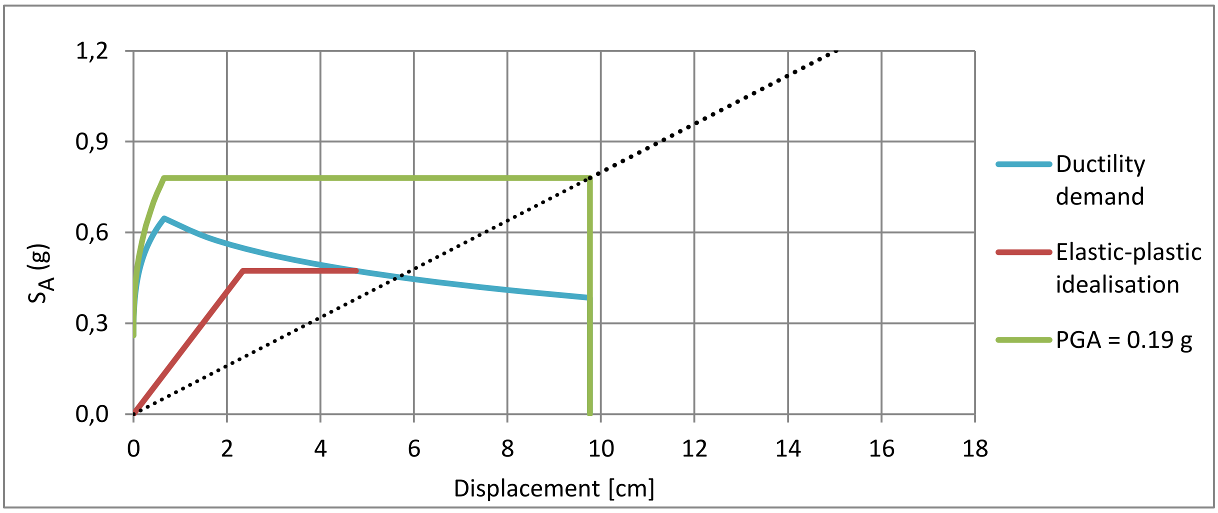

Fig. 7.4 Maximum PGA conform the push-over method.

The needed reduction factor is equal to 1.65 and the ductility factor is 2.03.

<u>Displacement</u>

Besides that a lower PGA leads to a lower seismic force it also reduces the displacement in the demand curve. This is due to the fact that the acceleration and displacement spectra are dependable on the acceleration and not on the mass. This leads to the possibility that if a structure can undergo a large displacement it can easily fulfil the maximum target displacement from the earthquake.

7.1.1 Discussion

When changing the PGA this has a direct influence on the earthquake force on the building and therefore the needed q_μ-factor. If the q_μ -factor is reduced this also has influences on the ductility demand of the structure. When the structures natural period is below the transition point *Tc* the relationship with q_μ -factor and ductility is not linear. For the NPR 9998 there is no constant velocity branch after the transition point *Tc*. Resulting in the fact that the energy principle for ductility demand is always valued or the maximum demanded ductility is reached. This is visualised in fig. 7.5. Where two different capacity curves are drawn in the an elastic response diagram. The figure shows that after reaching a higher natural period then T_C (blue line), the maximum target displacement of the demand curve remains constant. In other words $d_{et} = d_t$, where the elastic displacement remains the same and therefore also the target displacement.

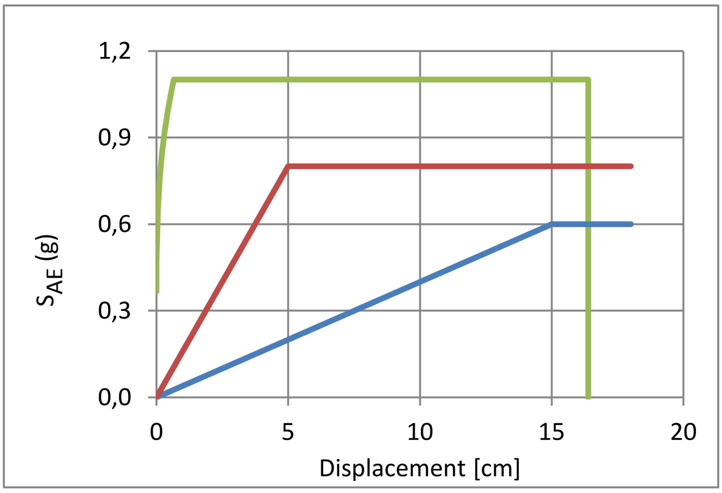

Fig. 7.5 Difference in fulfilment of the displacement demand for two different fictive capacity curves.

High-rise buildings, assuming the mass is linear increased with the additional displacement, are more ductile. This is beneficial for the ductility demand since the value *T** is lower, if *T*<Tc*.

$$\mu = 1 + \left(q_\mu - 1\right)\frac{T_C}{T^*} \quad T^* < T_C \qquad \text{(eq. 7.2)}$$

Besides this the high-rise building has potentially a larger total deformation. Therefore it is capable of reaching the maximum demanded displacement. This also concludes that the building is fulfilling the force based design requirements since the needed q_μ-factor is always reach with the ductility.

7.2 Elastic – plastic idealisation

Besides het influence of the PGA on the demand curve the elastic-plastic idealisation influences capacity curve. The EC8 describes the point of the yield force (F_y) equal at the formation of the first plastic hinge. Since all the deformation is in the connection for the CLT construction it is difficult to identify the point of yielding. In fig. 7.6 two different yielding points are applied for the same push-over results. Graph A belongs to a yielding point (F_y) at 80% of the maximum force (F_{max}) while for line B the yielding point is equal to the maximum force. Both graphs are constructed with the principle of equal energy.

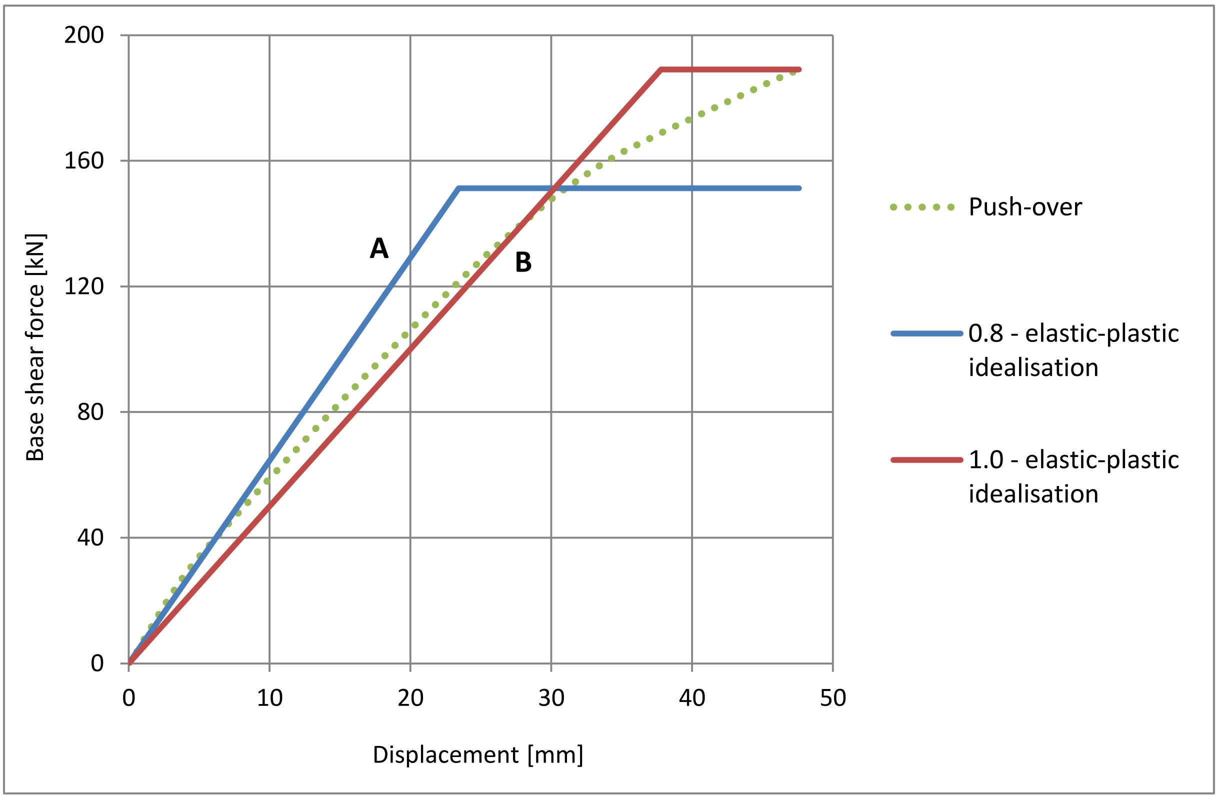

Fig. 7.6 Two different elastic-plastic idealisations.

The first difference between the two graphs is that they lead to a different natural period of the building due difference in initial stiffness. As can be seen (eq. 7.2) this leads to an increase of the ductility demand for graph A compared to graph B. Besides this also the needed q_{μ}-factor for fulfilment of the force based requirements increases for graph A. On the other hand the ductility in the elastic-plastic idealisation increases and therefore a higher ductility demand can be obtained. Concluding that it is dependable on the slope of the push-over result if its beneficial or not. On one hand it increases the ductility on the other hand it decrease the natural period and increased needed q-factor.

Besides the differences between the graphs, the addition or input of brackets also influences the capacity curve and its form. If the input of the brackets has a larger horizontal plastic branch this will lead to a larger horizontal branch in the push-over results. Also when adding additional brackets the outcome changes. Now the push-over is aborted when one of the brackets has reached its final displacement. If there are more brackets there is more force redistribution. When one of the brackets reached its maximum force, redistribution of the forces would occur. The bracket which reached its maximum force will then have additional displacement from the third branch of the tri-linear backbone is used.

For the case study building the results for the different elastic-plastic idealisation are elaborated in table 7.2 and fig. 7.6.

Table 7.2 Outcome when applying a different yield point.

Property	Symbol	Unit	Graph A	Graph B
Max PGA (g)		m/s^2	0.195	0.165
Natural period	T_n	s	0.45	0.51
Yield force	F_y	kN	151	189
q – factor	q_μ	-	1.65	1.19
Yield displacement	d_y	mm	23.44	37.79
Ultimate displacement	d_u	mm	47.59	47.59
Ductility demand	μ	-	2.03	1.26

This is visualised in the AD-diagrams.

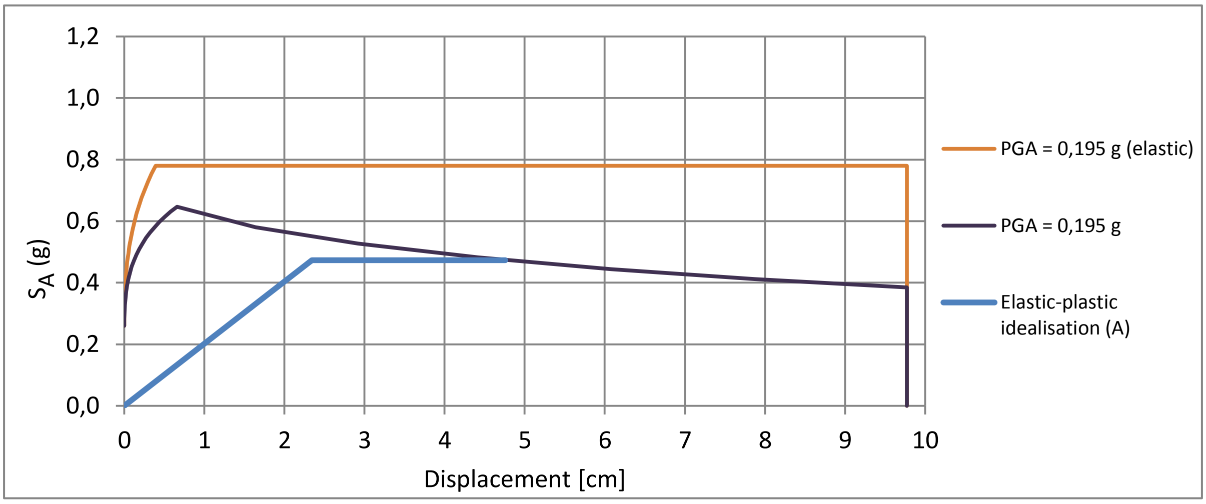

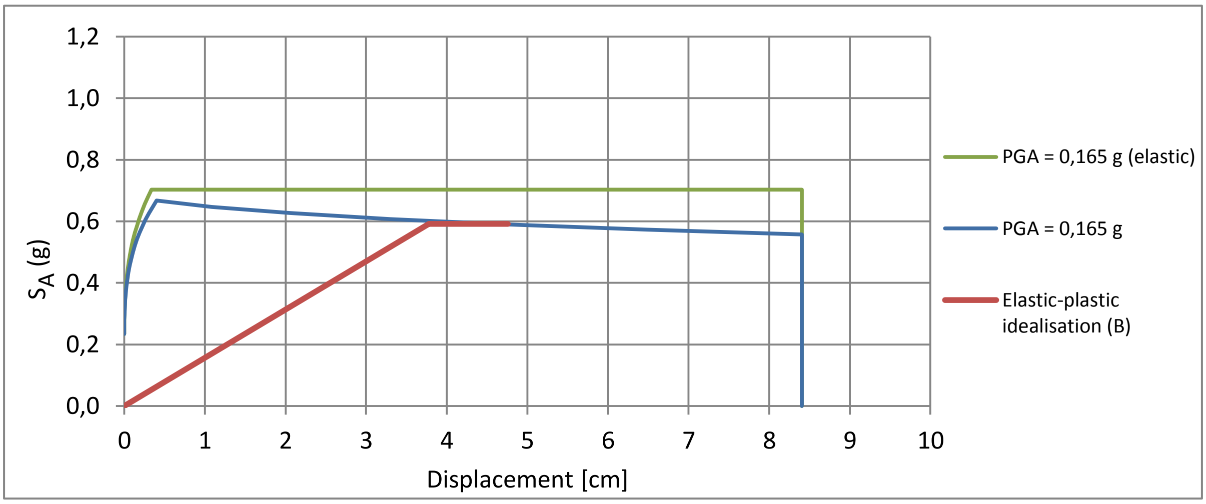

Fig. 7.7 Visualisation of the maximum PGA for the different idealisation.

7.2.1 Discussion

From the differences as descripted in the paragraph the importance of the idealisation is visualised and explained. The method suggested in EC8 is very difficult for timber structures since it is hard to identify the yield. If this is chosen different the maximum PGA which the building can resist is increased or decreased and it also changes the q_μ-factor.

This suggest that it is undesirable to schematise the push-over results into an elastic-plastic idealisation. Because there is not one element which shows a plastic response but it are all tri-linear backbones, resulting in no increase in deformation when the force is slightly increased.

7.3 Force distribution

According to EC8 two different loading situation need to be applied. Namely on according to the mass and one which is displacement based. With these loading situations the fundamental vibration mode of the building is schematised. This is an approximation since the exact force distribution of the fundamental vibration mode of the building is unknown. However it is possible to perform an approximation using the stiffness and the mass of the building. This is what is done in a model response analyses. The modal shapes can be calculated and used as input for the force distribution. Another option is to use the Rayleigh method for calculation of the modal displacements.

Nevertheless the EC 8 prescribes the use of the most unfavourable outcome of the two force distributions. In the case of the investigated building this results in less deformation, because the deformation capability of the second floor is not fully utilized.

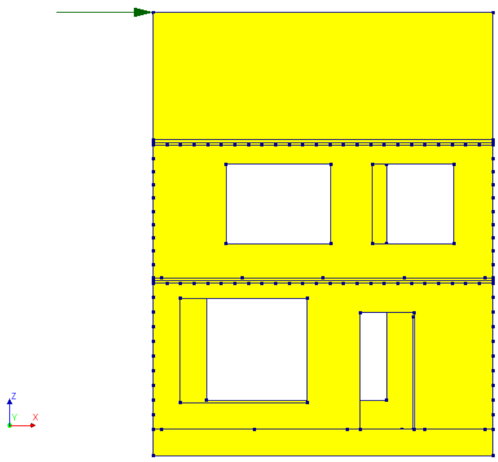

Fig. 7.8 location of the prescribed deformation.

For an overview of the influence of these assumptions the model is also evaluated with a prescribed displacement at the top of the building (fig. 7.8). This leads to the most favourable force distribution for obtaining the largest deformation of the building. Also a displacement based push – over has the benefit of showing the remaining displacement after the maximum force of the building is obtained. However for the case study building this is not the applicable since the third branch of the tri-linear backbone is to short. When the maximum force is reached most of the connections in the model are fully utilised until its maximum force, so there is no redistribution.

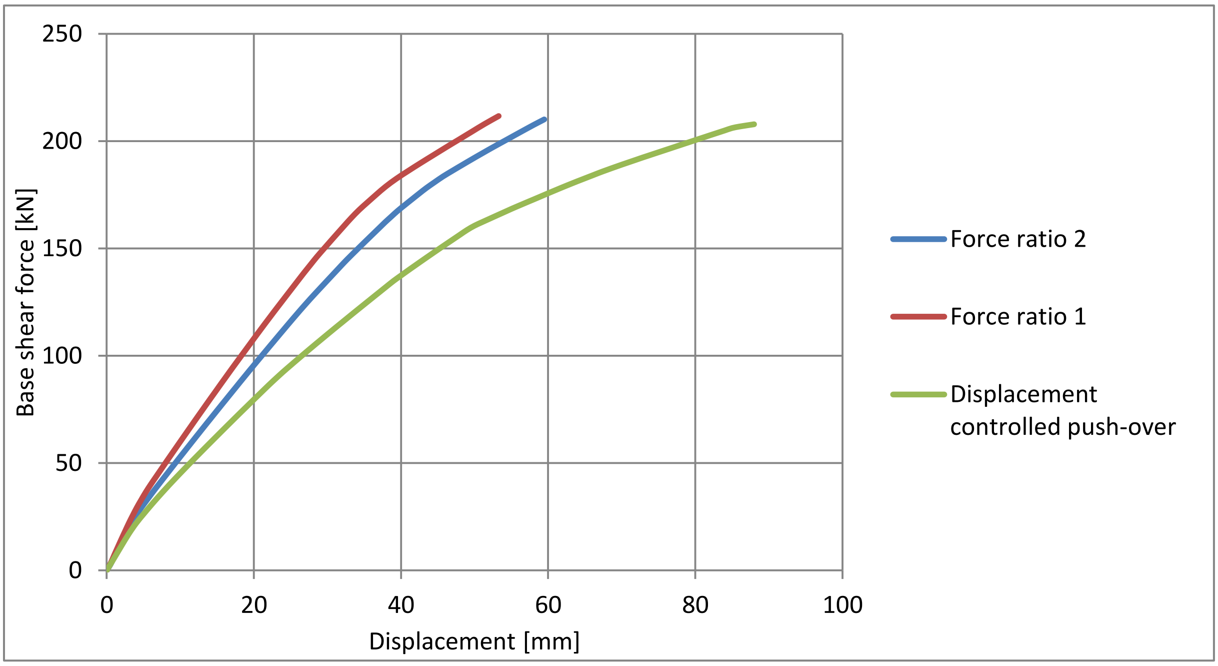

Fig. 7.9 Result of the force and displacement controlled push-overs.

Although the displacement controlled push-over is favourable it does not represent the forces induced by the earthquake. Therefore the code subscribes two different ratios. It is however most likely that it is unfavourable to apply the distribution according to the mass, since this does not involve the stiffness of the building.

7.3.1 Discussion

The combination of the design of the connections in comparison to the force distribution is of importance for obtaining the maximum displacement. This is in particularly applicable to high-rise buildings and due to the fact that the push-over is force controlled. For high-rise buildings special attention should be paid that the strength of the connections is adjusted to the total force. This can be done by adjusting the number of nails. When the number of nails is decreased this leads to a higher force per nail. Resulting in plasticisation and displacement before the maximum displacement of one of the other floors is reached.

Next it is questionable is the most unfavourable result of the push-over should be used. Especially when a modal response analysis is performed and the modal shapes are investigated.

Also the full mass of the building is taken into account instead of the participating mass for a certain modal shape.

7.4 Optimization

This paragraph describes two different solutions which are applied on the case study building in order to fulfil the requirements. The solutions are then discussed together with the solution method and for different building.

7.4.1 Number of connections

From the first push-over curve it is clear that the case-study building is failing at the ground floor. The connection of the wall to the foundation. For the building to resist the maximum PGA of 0.36g either the load bearing capacity has to be increased or the displacement. One of the solutions to this is by adding an additional bracket at the point of failure. The point of failure is discussed in paragraph 6.1.1.

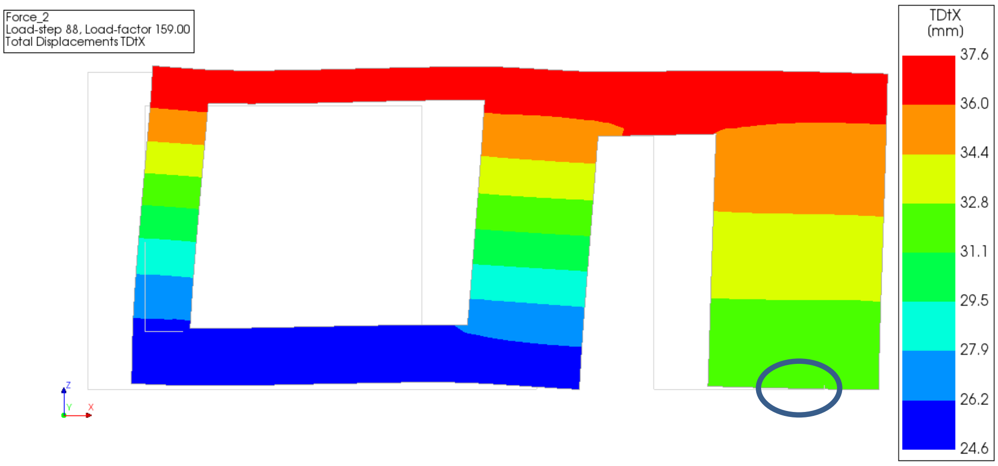

Fig. 7.10 Location of the additional angle bracket. At this location the ultimate displacement is reached.

The new lay-out of connections in the front wall is shown in the figure below.

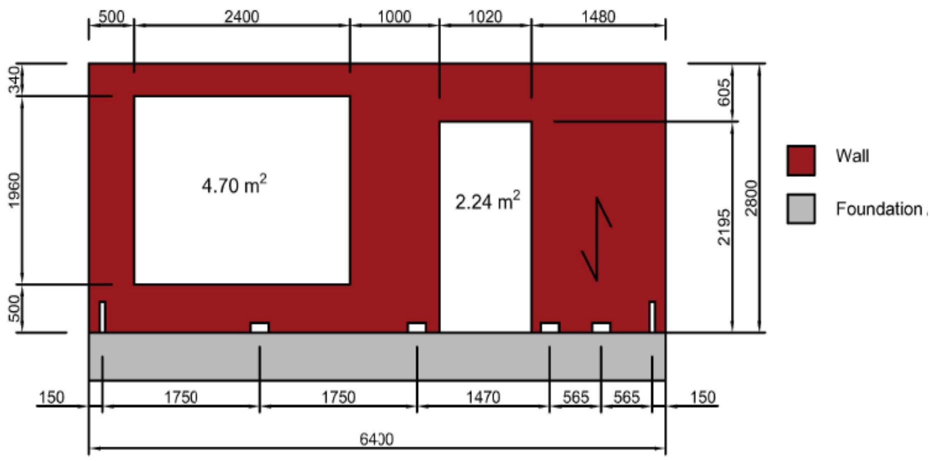

Fig. 7.11 Front wall with additional bracket.

For the push-over the force distribution according to ratio 1 is applied to the building with an additional bracket. First the forces in the connections are shown followed by the push-over curve.

Table 7.3 Overview of the forces and displacement at the brackets at the final step of the analysis. The left part of the table is with the additional bracket and the right one without. The number in the second column corresponds with the connections Fig. 7.10 for the left column and Fig. 5.15 for the right column.

		Step 71 - AB		Step 62	
Location	no.	Force [kN]	Displacement [mm]	Force [kN]	Displacement [mm]
Foundation	1	6.8	25.8	6.6	24.6
	2	22.4	26.4	22.2	25.2
	3	22.2	25.5	22.0	24.2
	4	22.8	28.5	22.5	28.8
	5	22.7	28.6	7.3	29.1
	6	7.3	28.9		
First floor	1	4.1	10.8	3.9	9.3
	2	14.0	11.5	12.0	9.9
	3	13.5	11.2	11.4	9.4
	4	14.0	11.9	11.7	9.7
	5	4.1	11.1	3.9	9.3

From the table it is clear that most of the force is transferred to the stiffer right part of the front wall. First of all this leads to an increase of the total base shear force from 212 kN to 245 kN, due to the additional bracket. This means that also the force acting on the second floor increases. This results in more deformation in the connections at the first floor. The results of the push-over are translated to a SDOF (fig. 7.12) showing increased total base shear and ductility.

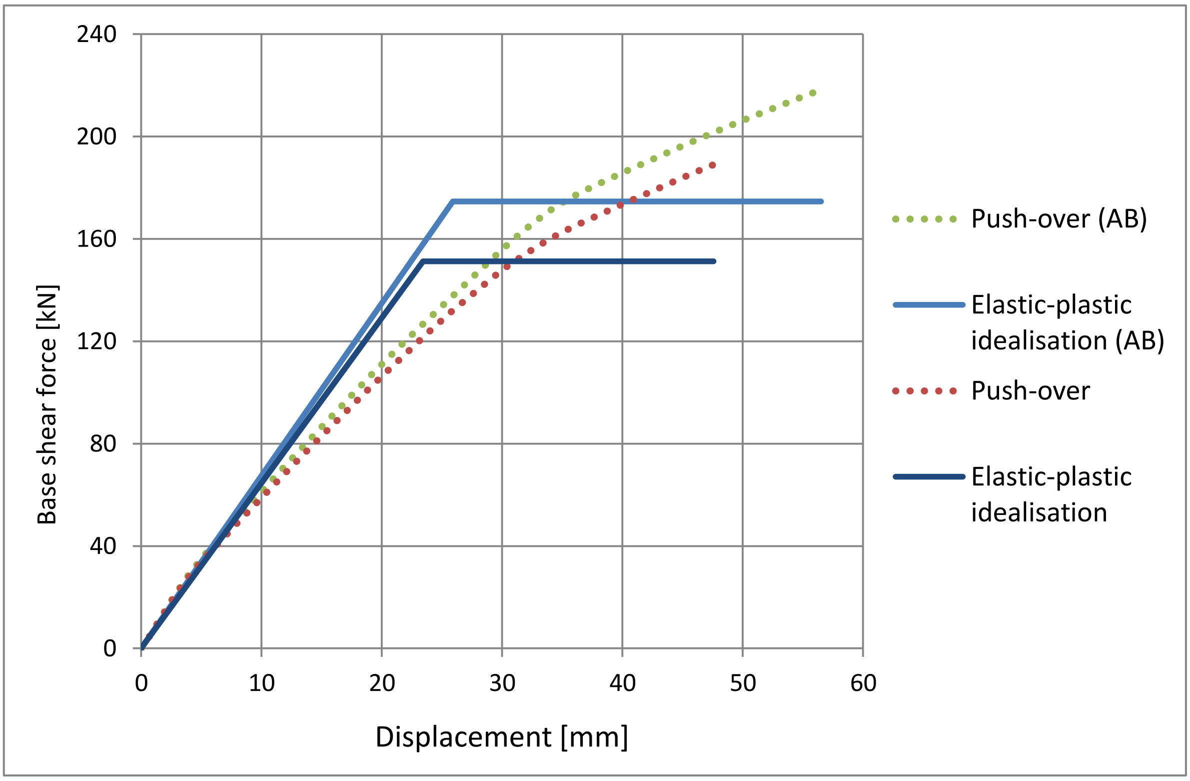

Fig. 7.12 Push-over results with additional bracket, already translated to an equivalent SDOF system.

When analysing the push-over result and visualising it in the AD diagram (fig. 7.13). This results in a maximum PGA of 0.26, a q_μ-factor of 1.70 and a ductility factor of 2.18.

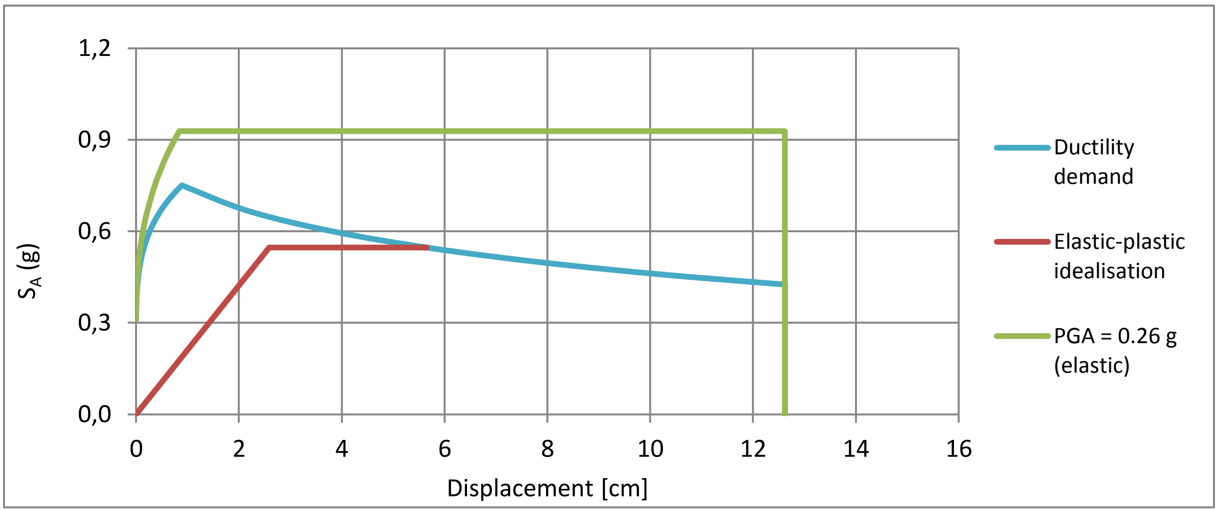

Fig. 7.13 AD visualisation of the push-over analysis with an additional angle bracket.

Still the failure will occur in the stiffest part of the front wall namely right of the door opening. The angle bracket has reached its ultimate capacity in order to deform even more the stiffness of the connector itself will decrease and the construction will fail.

7.4.1.1 Conclusion

The benefit is of the design method is the possibility to adjust the lay-out of the connections. This can lead to a better and optimized design. It is then possible to fully utilise the deformation capacity of the second floor by adjusting the number of connections to the force ratio. This also gives of interest for high-rise buildings with multiple levels.

Table 7.4 Overview of the different outcome of the two models.

Model	Max PGA (g)	q_μ	μ	T_n* [s]
No additional bracket	0.19	1.65	2.03	0.45
Additional bracket	0.26	1.70	2.18	0.44

For the case study building it can be concluded that the additional angle bracket resulted in an increase of the maximum PGA from 0.19g to 0.26g. But also the maximum reduction factor increased from 1.65 to 1.70. This is due to the additional ductility which is utilised from the connections on the first floor.

7.4.2 Additional wall

Besides adding an extra angle bracket in the front wall. another option is adding a wall in x-direction. The location of the wall is shown in the figure below.

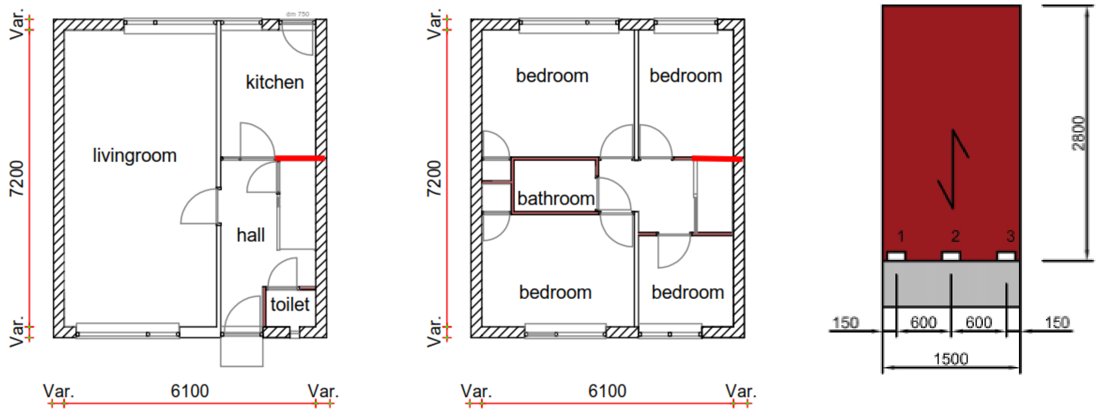

Fig. 7.14 Location indicated with the red line and geometry of the additional wall.

The wall has a width of 1.5 metres and is connected to the foundation and floor by three angle brackets. The wall is added at both floor levels. Next the model is loaded with force ratio 1, resulting in the following capacity curve.

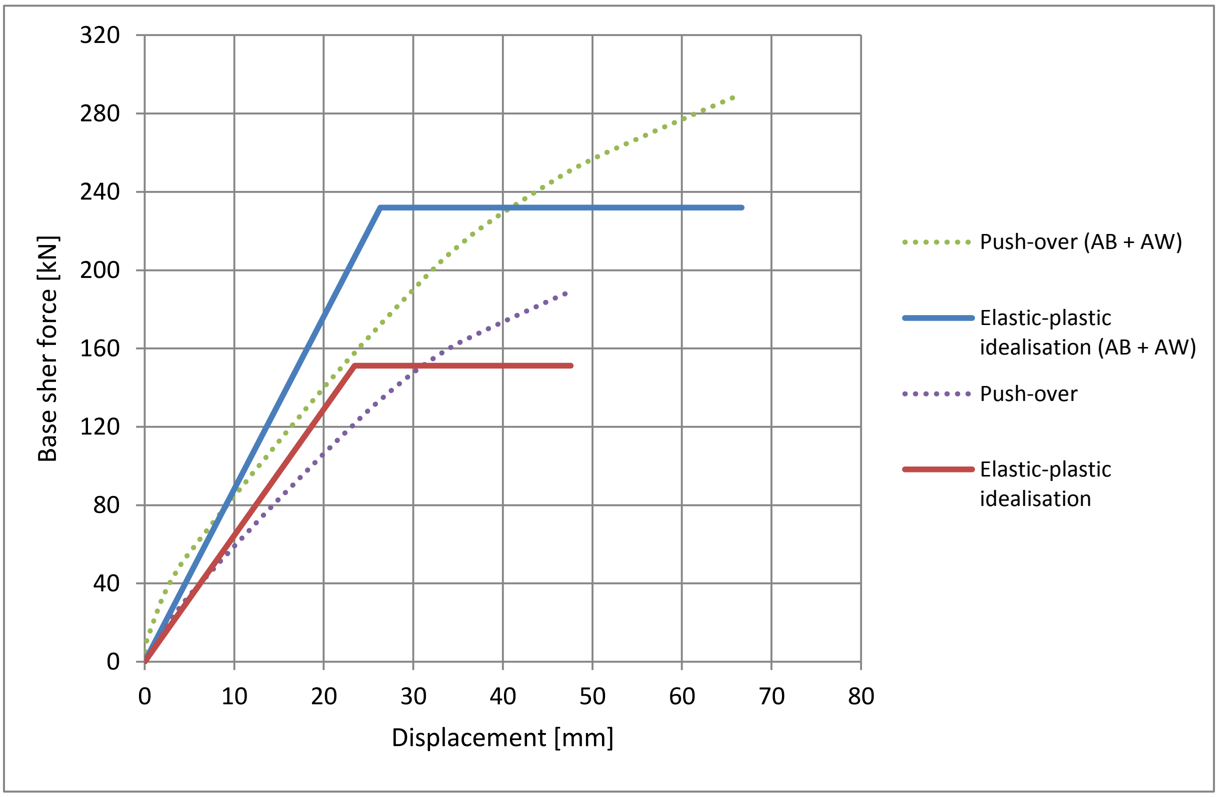

Fig. 7.15 Push-over results and capacity curves of the first design and the building with additional wall and brackets.

The input for the translation of the MDOF to SDOF system is listed in table 7.5. For the location of the yield point F_y is $0.8F_{max.}$

Table 7.5 Output of the push-over analysis. transition factor Γ =1.16.

Description	Symbol	Value	Symbol	Value	Unit
Mass	m	37.40	m*	32.59	Ton
Displacement	$d_{1st.}$	46.7 (0.60)	$d_{1st.}$ *	40.34	mm
	d_{attic}	77.2 (1.00)	d_{attic} *	66.68	mm
Force	F_{max}	336	F_{max}*	290	kN
Natural period			T_n*	0.37	s

The graph shows an increase in stiffness and strength. This is logic because there is a wall with three angle brackets added at the ground floor. The angle brackets have a positive effect on the sliding resistance of the building.

The added wall has no openings and is very stiff and therefore it attracts more forces. Also the height over length ratio of the added wall is higher resulting in more rocking behaviour of the wall. This is also visible in table 7.6.

Table 7.6 Force in the brackets of the added wall at the final step of the push-over

		Step 96			
Location	no.	**Shear**		**Axial**	
		Force [kN]	Displacement [mm]	Force [kN]	Displacement [mm]
Foundation	1	2.5	1.5	19.8	17.9
	2	2.4	1.4	17.0	9.4
	3	1.7	1.0	2.8	1.24
First floor	1	0.0	0.0	0.0	0.0
	2	0.0	0.0	0.0	0.0
	3	0.0	0.0	1.3	0.5

The wall is mostly resisting the force acting on the first floor to the foundation. A reason is the higher horizontal force and the fact that due to the large openings in the walls at the first floor, these walls have a reduced stiffness. Therefore a larger share of the forces will be restraint by the added wall.

The addition of the wall leads to the following capacity and demand curves.

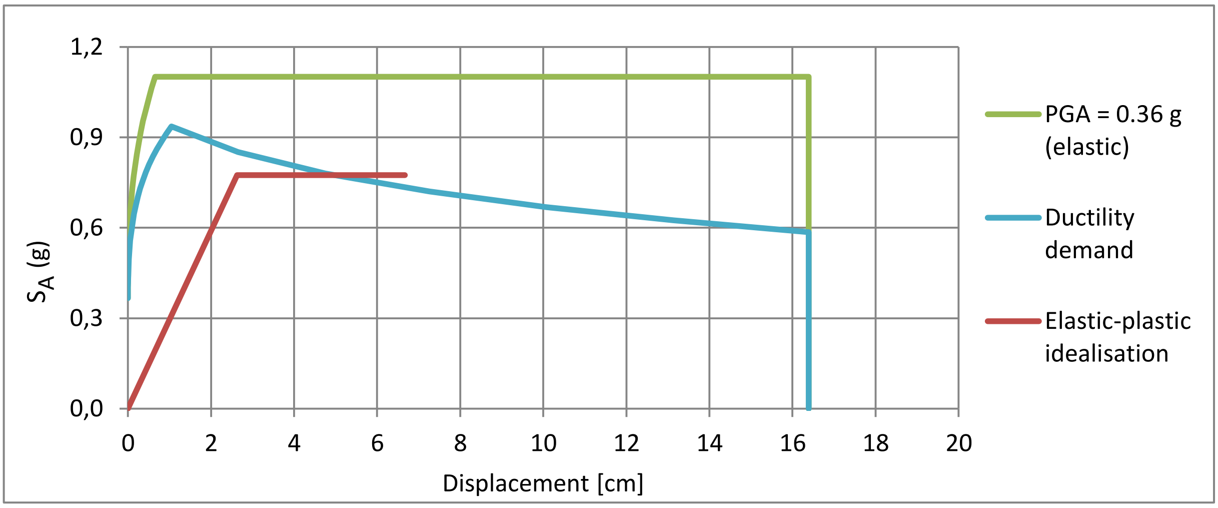

Fig. 7.16 AD - diagram with the visualisation of the push-over with additional brackets and wall.

For the elastic-plastic idealisation the yield force F_y is equal to 80% of the maximum force F_{max} namely 232 kN of the equivalent SDOF system. This leads to a required q_μ-factor of 1.42 and μ-factor of 1.88, resulting in a target displacement of 57 mm for the MDOF system and 49 mm for the equivalent SDOF system.

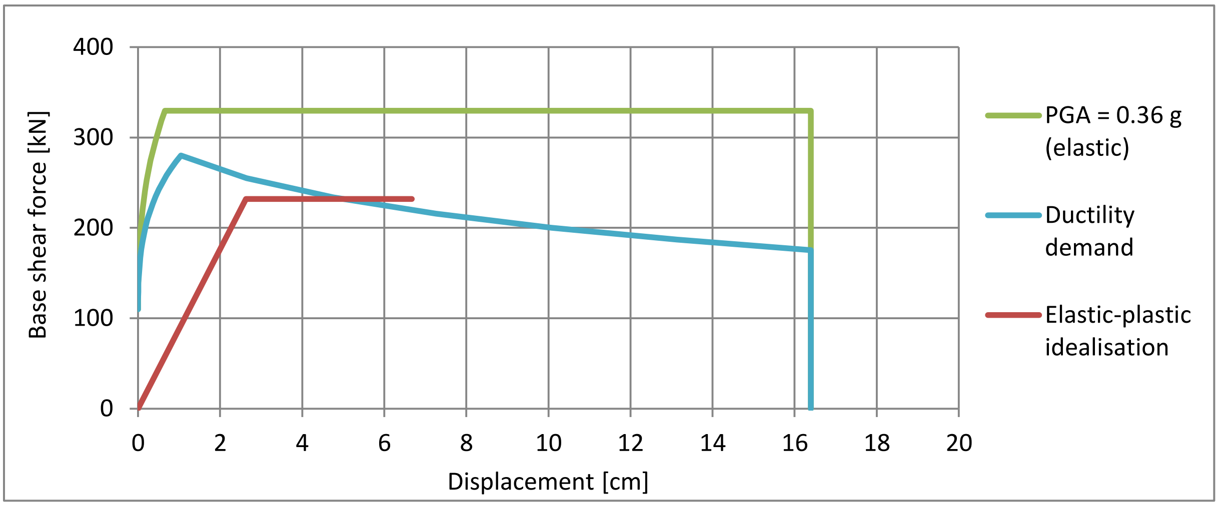

Fig. 7.17 Visualisation in force-displacement diagram.

The natural period T_n* which corresponds with the graphs is equal to 0.37 seconds. Also with this information the needed q_μ-factor and elastic deformation can be determined. From the elastic displacement the target displacement can be calculated analytical (eq. 7.3). The elastic displacement d_{et}^* is the displacement at a natural period of 0.37 seconds in the elastic response spectrum (green line in the figures), which is 57 mm.

$$d_t^* = \frac{d_{et}^*}{q_u}\left(1+\left(q_u-1\right)\frac{T_C}{T^*}\right) = \frac{37.4}{1.42}\left(1+\left(1.42-1\right)\frac{0.77}{0.37}\right) = 49.4 \text{ mm} \qquad \text{(eq. 7.3)}$$

The building is fulfilling the displacement based demands for resisting an earthquake in Groningen with a PGA of 0.36g according to the push-over method. However the EC8 demands that the capacity curve has a ultimate displacement of 1.5 times the target displacement. The target displacement of the MDOF system is equal to 57 millimetre. So the maximum displacement of the building from the push-over must be at least 86 millimetre. But the maximum displacement of the building is 77.2 millimetre. However the building is capable of fulfilling this requirement when a displacement based push-over is performed, this is also shown in paragraph 7.3. Furthermore it is not clear where this requirement is related to and it is not related to the stiffness of the building. If the building reacts stiff and has a large plastic branch this is easily fulfilled. Whereas this is just the other way around it is not possible to fulfil the requirement (fig. 7.5). Therefore the 1.5 times the target displacement is a very harsh requirement, especially since the push-over is a conservative method.

7.4.2.1 Conclusion

Adding the wall increases the total base shear which can be restrained by the building. However this is not only due to an increased total shear resistance of the angle brackets. Since the wall is stiff compared to the front and backs wall with all its openings, it attracts more force. Furthermore the dimensions of the wall are such that is subjected to sliding and rocking deformation. From this three conclusions can be drawn. First the importance of modelling the wall with all the openings. This has a significant influence on the stiffness and therefore the force distribution. Secondly the freedom of the chosen design method which allows one to change for instance the openings in the walls and adjust the stiffness. Finally the importance of modelling the full load bearing wall since this has an influence in the failure mode and the behaviour of the building.

8 CONCLUSIONS

The conclusion will give answers to the research questions mentioned in paragraph 1.3.2 which contributes to the final conclusion regarding the main research question: "What is the influence of the seismic calculation method on a CLT structure ? "

The seismic calculation methods which are taken into account are the lateral force analysis, modal response analysis and the non-linear static push-over. The fourth method which can be applied is a non-linear time history analysis but this is very elaborated and not for designing new structure. It is more suitable for the assesment of exicsting buildings. Since this thesis focussus on new buildings this method is not further discussed.

8.1 Calculation methods

An earthquake introduces lateral forces and vertical forces on a structure. The vertical forces can often be neglected because of the load factors which are applicable for the normal design conditions. For long spanning beams with a high vertical load the vertical force has to be taken into account. Result is that the lateral forces from the earthquake are the main concern. To design a building which fulfils the requirements for resisting the horizontal forces different methods can be applied which are now discussed.

Lateral force method

- The fastest method is the lateral force analysis. It is a quick method to calculate the total base shear force acting on the structure. The method makes use of the response spectrum to account for the dynamical behaviour of the building. The spectrum gives the resonance or damping of the building when it is subjected to the earthquake. This is linked to the natural period of the structure which is difficult to calculate.
- The method only takes the first fundamental vibration mode of the structure into account. Therefore the method is suitable for buildings with certain regularity, so that the fundamental vibration mode is governing.
- To take into account the possible mass participation of other vibration modes. The λ-factor is introduced for buildings with more than two storeys. The -factor reduces the mass of the building by 15%. From the check made with the modal response analysis this was achieved.
- To construct an economical feasible structure the non-linear behaviour of the structure must be incorporated in the design. This is done with the behaviour factor (q-factor). The q-factor is dependable on the structural system and is listed in tables in the Eurocode. However it is dependable on the behaviour of the building which is not regarded in this calculation method.
- For applying the q-factor the capacity design principle is of importance. It ensure that no brittle failure occurs so that the ductility is of the structure is utilised. This is done by

applying over-strength factors for elements with brittle failure. Also the additional over-strength of the structure is incorporated in the q-factor.

- With the lateral force analysis only the forces acting on the building are determined. The method does not give any information about the behaviour of the building and if the needed ductility is reached. This leads to the fact that the method must always be a lower bound estimation of the base shear force. The method is best applicable for simple and regular low-rise buildings for which the behaviour is known.

Modal response

- The modal response analysis takes into account not only the first fundamental vibration mode but also higher vibration modes. This gives a better insight in the mass participation and the dynamics of the schematised building. The forces acting on each storey of the building are calculated from the different modal shapes.
- Furthermore the same holds as for the lateral force analysis namely that the non-linear behaviour and over-strength is taken into account by the q-factor. So the method is purely force based and there is no information about the behaviour of the building. Therefore also for this method the capacity design principle must be applied. With this and a conservative q-factor the method is suitable for structures which have an irregular mass distribution or stiffness. Applying the modal response analyse can lead to a lower total base shear force due to the mass participation and the effect of the higher modes.

The code prescribes a q-factor of two for CLT structures when using force based elastic calculation methods. To analyse the behaviour of the structure and verify the q-factor a non-linear static push-over analysis is executed.

Non-linear static push-over

With the use of a three storey case study building a non-linear static push-over was conducted leading to the following conclusions.

- The push-over analysis results in a reduction factor (q_{μ}-factor) for the elastic force which was lower than the q-factor of two. However the q_{μ} -factor is only based on the displacement and not the over-strength and redundancy of the structure.
- For the first push-over analysis the q_{μ}-factor was equal to 1.65. This means that when also the over-strength of the building is taken into account a q-factor of two for the timber building is achievable.
- Downside of the non-linear static push-over analysis is the elastic – plastic idealisation of the capacity curve of the building. For timber structures it is difficult to indicate the first plastic hinge in the model. This is the yield point for the elastic-plastic idealisation. The location of the yield point is directly related to needed q_{μ}-factor and the ductility factor (μ-factor).
- Another downside of the method is that the force distributions are time independent. This results in a monotonic increasing lateral force distribution which represents only

the first fundamental shape. This makes it conservative since the total mass is applied leading to a higher needed q_μ-factor.

- Also the relation between the μ-factor and the q_μ-factor for structures with a natural period below T_C and a low ductility is conservative, according to research.
- The first model with the number of connections designed according to the lateral force analysis did not fulfil the requirements for the building and its location. This shows the importance of displacement based design compared when only the forces are checked.
- Other benefit of the push-over analysis is the information of the force and displacement by the structure. This also allows optimisation of the strength of the connection and the number of connections. The strength and displacement of the connections can be adjusted by the number nails which are used.
- When broaden the conclusion of the push-over analysis from a low-rise building to a high-rise building the push-over can be a beneficial calculation method. When properly designed it is possible to achieve a higher μ-factor resulting in a higher q_μ-factor. Besides this the spectrum for the Groningen situation has a maximum of demanded displacement of the earthquake which can be reached by a high-rise building.
- Concluding that there are several limitations to the push-over analysis and that it is conservative for low rise buildings. However it is a fast method to get insight in the behaviour and strength of the structure.

The next points of the conclusion are regarding the modelling method applied in this thesis.

- With the modelling method used in this thesis it is easy to adjust the design or add connection. It also incorporates the connection between perpendicular walls. This increases the stiffness and maximum base shear force of the structure due to the 'box' action. With the other two calculation methods only the shear walls in the direction of the lateral force are taken into account, which is conservative. The modelling is done in the FEM DIANA but it can be done in almost any FEM program.
- By further standardising the input for the connection it is also a fast method of modelling and a quick manner to get insight in the behaviour of the structure.
- With optimisation of the building it is capable of resisting the heaviest earthquake which can occur in Groningen.

Concluding that for low-rise buildings applying the elastic force based calculation methods with the prescribed q-factor is a quick and solid method. However it is important that the behaviour of the buildings is known. If not it is preferable to conduct a displacement based calculation to check if the building has sufficient ductility. This is done with a non-linear static push-over. For low-rise buildings the push-over method leads to more conservative results. This due to the fact that the structure is often in the short range period, the full mass is applied and it does not incorporate the over-strength of the building. For high-rise buildings it can be favourable performing a non-linear static push-over and obtain a higher q_μ-factor. For the Groningen spectrum it is even possible to fulfil the maximum displacement demand. The push-over analysis also allows optimisation and information of the behaviour of the structure.

9 RECOMMENDATIONS

In my research I used the push-over method as described in EC8. However there are more methods which have a different way of analysing the demand and capacity curve. For instance a method can be suggested which does not makes use of the elastic-plastic idealisation so no yield point has to be specified. Examples of different methods are the capacity spectrum method (CSM) and displacement coefficient method (DCM).

The CSM also translates the push-over result which is schematised into a bi-linear curve to a capacity curve. Which is then plotted into an AD-diagram . Followed by a performance point. The performance point is often chosen according to the principle of equal displacement. Then the demand spectrum of the earthquake is recalculated taken additional damping due to hysteretic behaviour into account. Finally the check is made if the capacity curve is intersecting the recalculated demand curve close to the performance point. The point of intersection is the target displacement which can be translated to the target displacement of the multi-degree of freedom system.

The DCM uses the push-over result without any translation but translates the elastic displacement to the target displacement. The target displacement of the system is calculated with the use of different coefficients. There are coefficients for the translation of the system from SDOF to MDOF, the inelastic behaviour, effects of the pinched hysteretic behaviour and dynamic behaviour.

Besides the different analysis also a verification of the model is recommended. The model with the backbone is not checked with a model which incorporates the hysteretic behaviour of the connections. When this is done it can be concluded if the modelling method is conservative or an overestimation.

Furthermore it is recommended to have more test results of individual connections. When the connection are designed according to the capacity design principle this gives a better indication of the input for the model. From this the input for the different connections can be standardised.

Besides it would be recommended to have the strength and displacement curves of the connections linked to the number of nails which are used. This allows one to adjust and optimize the design of the connections and obtaining the full displacement.

Insulation can be applied for sound reduction. This is not incorporated in this thesis and therefore not in the model. The sound insulation is a damping material applied below the brackets and underneath the wall. It would be interesting to know the influence of the insulation measurements. Firstly the influences of the insulation on the connection could be investigated. Secondly the combination with the insulation on the connections and below the walls.

10 REFERENCES

Blass, H., & Fellmoser, P. (2004). Design of solid wood panels with cross layers. *Proceedings of the 8th World Conference on Timber Engineering* (pp. 543-548). Lathi, Finland: WCTE 2004.

Blok, R. (2006). *Tabellen voor bouwkunde en waterbouwkunde.* Utrecht/Zutphen: ThiemeMeulenhoff.

Bogensperger, T., Moosbrugger, T., & Silly, G. (2010). Verification of CLT-plates under loads in plane. *World converence on timber engineering.* Nelson, New Zealand: CIB W18.

Brandner, R., Flatscher, G., Ringhofer, A., Schikhofer, G., & Thiel, A. (2015). *Cross laminated timber (CLT): overview and development.* Berlin Heidelberg: Springer-Verlag.

Branz. (2016, Mei 26). *Ground shaking*. Retrieved from Seismic resilience: http://www.seismicresilience.org.nz/topics/seismic-science-and-site-influences/earthquake-hazards/ground-shaking-2/

Ceccotti, A., & Sandhaas, C. (2010). A proposal for a standard procedure to establish the seismic behaviour factor q of timber buildings. *WCTE*.

Chopra, A. k. (2012). *Dynamics of structeres - theory and application to earthquake engineering.* Boston: Prentice Hall.

Collins English Dictionary. (2016, May 12). *Earthquake*. Retrieved from Dictionary.com: http://www.dictionary.com/browse/earhtquake

Dujic, B., Klobcar, S., & Zarnic, R. (2007). *Influence of openings on shear capacity of wooden walls.* -: NZ Timber desing journal.

Elghazouli, A. Y. (2009). *Seismic design of buildings to eurocode 8.* London and New York: Spon Press.

Fajfar, P. (2000). A nonlinear analyses method for performance based seismic design. In *Earthquake spectra* (pp. 573-592).

Follesa, M., Fragiacomo, M., Casagrande, D., Tomasi, R., Piazza, M., Davide, V., & Rossi, S. (2016). *The new version of chapter 8 of eurocode 8.* Vienna: WCTE.

FPinnovations. (2013). *CLT Handbook.* St. Jean: FPinnovations.

Gavric, I., Fragiacomo, M., & Ceccotti, A. (2013). Capacity seismic desing of X-LAM systems based on connection mechanical properties. *CIB-W18*, (pp. 285-298).

Gavric, I., Fragiacomo, M., & Ceccotti, A. (2013). *Cyclic behaviour of typical metal connectors for cross-laminated (CLT) structures.* Rilem.

Gavric, I., Fragiacomo, M., & Ceccotti, A. (2014). *Cyclic behavior of typical screwed connections for cross-laminated (CLT) structures.* Berlin: Springer.

Hedach AG. (2017, Januari 19). Retrieved from Website van Hedach: http://www.hedach.com/nl/systeem

Hummel, J., & Seim, W. (2016). performance-based design as a tool to evaluate behaviour factors for multi-storey timber buildings. *WCTE.* Vienna.

JMconcepten. (2016, December 13). *KLH*. Retrieved from JMconcepten: http://www.jmconcepten.nl/klh/index.html

Khattak, O. (2016, October 18). *Damages from earthquakes*. Retrieved from Learning geology: http://geologylearn.blogspot.nl/2015/11/how-do-earthquakes-causes-damage.html

KNMI. (2016, Mei 26). *KNMI Kennis- & datacentrum*. Retrieved from http://www.knmi.nl/kennis-en-datacentrum

Miranda, E., & Bertero, V. (1994). Evaluation of strength reduction factors for earthquake-resistant design. In *Earthquake spectra, Vol 10, No 2* (pp. 357-379).

NAM. (2016, April 28). Opgehaald van NAM: www.nam.nl

Nederlandse praktijkrichtlijn (NPR 9998). (2015, December).

Nelson, S. A. (2016, October 18). *Deformation of Rock*. Retrieved from Website of Tulane University: http://www.tulane.edu/~sanelson/eens1110/deform.htm

NEN. (2015). *Voorbeeldberekeningen.* NEN.

NIST. (2014). *Seismic design of wood light-frame structural diaphragm systems: A guide for practicing engineers.* Gaithersburg, MD: Nist GCR 14-917-32, prepared by the Applied Technology Council for the National Institute of Standards and Technology.

Piazza, M. (2013). *Seismic performance of multi-storey timber buildings.* SERIES.

ProHolz Austria. (2014). *Cross-laminated timber structural design.* Immenstad: ProHolz Austria.

Rinaldin, G., & Fragiacomo, M. (2016). Non-linear simulation of shaking-table on 3- and 7-storey X-Lam timber buildings. In *Engineering structures* (pp. 133-148). Elsevier.

Rinaldin, G., Amadio, C., & Fragiacomo, M. (n.d.). A Component approach for the hysteretic behaviour of connections in cross-laminated wooden strucutres. In D. 10.1002/eqe.2310 (Ed.), *Earthquake engineering and structural dynamics.* Wiley Online Library.

Rothoblaas. (2016, November 9). *Fastening*. Retrieved from Rothoblaas: http://www.rothoblaas.com/products/fastening

Sto | bewust bouwen. (2016). *StoTherm Wood*. Retrieved from Sto: http://www.sto.nl/nl/producten/gevelisolatie/stotherm-wood.html

Swiss Seismological Service. (2016). *Frequently asked questions*. Retrieved from Schweizerischer Erdbebendienst.

TNO DIANA. (2015). *User's maunals*. Retrieved from dianafea.com/DIANA-manuals: https://dianafea.com/manuals/d100/Diana.html

VBI. (2016, 11 9). Retrieved from VBI: https://www.vbi.nl/

W. u. J. Derix GmbH & Co. | Poppensieker & Derix GmbH & Co. KG. (2016, 12 8). Retrieved from Derix: http://www.derix.de/nl/

Werner, S., Hummel, J., & Vogt, T. (2014). Earthquake design of timber structures - Remarks on force-based design procedures for different wall systems. In *Engineering structures 76* (pp. 124-137). Kassel: Elsevier.

ANNEX A DETERMINATION OF THE RESPONSE SPECTRUM

The response spectrum for the NPR 9998 is used multiple times in the thesis. This annex gives the calculation of the response spectrum.

The following parameters are used as input:

Consequence class	-	CC1B[2]
Design limit state	-	Near Collapse
Maximum reference ground acceleration at ground surface	$a_{g.ref}$	0.36 g
gravity acceleration	g	9.81 m/s^2
Consequence factor	k_{ag}	1.4

Calculation values of the spectral accelerations for short periods (S_S) and long periods (S_1)

$$S_s = 2.2 \cdot a_{g;ref} \cdot k_{ag}$$
$$S_s = 2.2 \cdot 0.36 \cdot 1.4 = 1.09 \text{ g} \qquad \text{(eq. 1.4)}$$

$$S_1 = 0.654 \cdot a_{g;ref} \cdot k_{ag}$$
$$S_1 = 0.654 \cdot 0.36 \cdot 1.4 = 0.330 \text{ g} \qquad \text{(eq. 7.5)}$$

Calculation values of the coefficients for short periods (F_a) and long periods (Fv)

$$F_a = -0.50 \cdot \ln(a_{g;ref} \cdot k_{ag}) + 0.65$$
$$F_a = -0.50 \cdot \ln(0.36 \cdot 1.4) + 0.65 = 0.993 \qquad \text{(eq. 7.6)}$$

$$F_v = -0.87 \cdot a_{g;ref} \cdot k_{ag} + 2.44$$
$$F_v = -0.87 \cdot a_{g;ref} \cdot k_{ag} + 2.44 = 2.002 \qquad \text{(eq. 7.7)}$$

Calculation values of the design values of the spectral accelerations for short periods (S_{MS}) and long periods (S_{M1})

$$S_{MS} = F_a \cdot S_s$$
$$S_{MS} = 0.993 \cdot 1.09 = 1.082 \text{ g} \qquad \text{(eq. 7.8)}$$

$$S_{M1} = F_v \cdot S_1$$
$$S_{M1} = 2.002 \cdot 0.330 = 0.661 \text{ g} \qquad \text{(eq. 7.9)}$$

[2] Building with less than 3 levels which can be repaired within two weeks.

Points T_B and T_C of the elastic response spectrum

$$T_C = \sqrt{\frac{S_{M1}}{S_{Ms}}}$$
$$T_C = \sqrt{\frac{0.661}{1.082}} = 0.781 \text{ s}$$
(eq. 7.10)

$$T_B = 0.2 \cdot T_C$$
$$T_B = 0.2 \cdot 0.781 = 0.156 \text{ s}$$
(eq. 7.11)

Elastic response spectrum ($\eta = 1$ for 5% damping)

***T* = 0**

$$S_e(T) = \frac{S_{MS}}{3}$$
$$S_e(T) = \frac{1.082}{3} = 0.36g$$
(eq. 7.12)

0 < *T* ≤ *T_B*

$$S_e(T) = \frac{S_{MS}}{3} \cdot \left(1 + \frac{T}{T_B} \cdot \left[\eta \cdot 3 - 1\right]\right)$$
$$S_e(T) = \frac{1.082}{3}\left(1 + \frac{2T}{0.156}\right) = \left(0.36 \ + 4.624T\right) g$$
(eq. 7.13)

T_B < *T* ≤ T_C

$$S_e(T) = S_{MS} \cdot \eta$$
$$S_e(T) = 1.082g$$
(eq. 7.14)

T_C ≤ *T*

$$S_e(T) = \frac{S_{M1}}{T^2} \cdot \eta$$
$$S_e(T) = \frac{0.661}{T^2} g$$
(eq. 7.15)

This leads to the following elastic response spectrum. The calculation is made in excel without rounding off to three digits so it is an exact calculation.

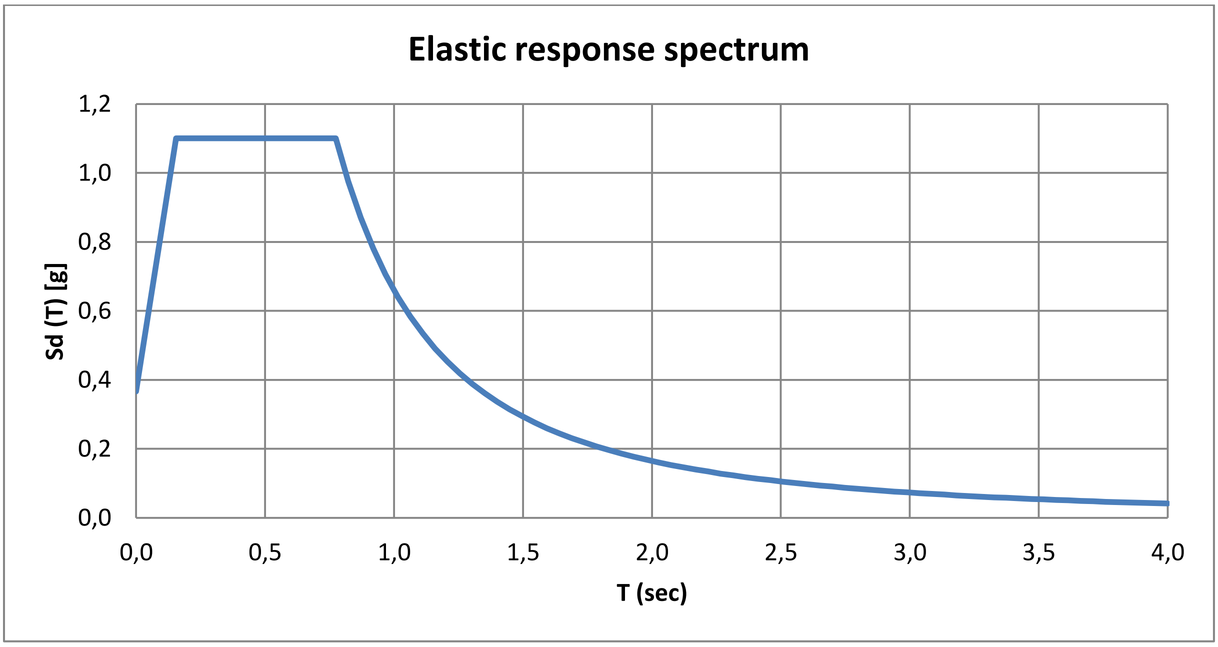
Elastic response spectrum
Sd (T) [g]
1,2
1,0
0,8
0,6
0,4
0,2
0,0
0,0
0,5
1,0
1,5
2,0
2,5
3,0
3,5
4,0
T (sec)

ANNEX B LATERAL FORCE AND MODAL RESPONSE ANALYSIS

Seismic calculation report

Lateral force and modal response

CONTENT

GOAL

The goal of the calculation is to get a feeling of the impact an earthquake has on the design of a timber building. From the results of the calculation variants are proposed and further elaborated. This way it is possible to see the opportunities for seismic engineering and what parameters influences the design.

INTRODUCTION

For the calculation the lay-out of a typical Groningen terraced house is used. Since the goal of the calculation is to get a better understanding of seismic engineering not the whole block is calculated but only one house. Therefor the lay-out is adjusted which will be explained in chapter 3. The lay-out is of an existing brick house and therefor will be recalculated with timber elements. For the calculation the main outlines are treated, this to stick to the goal.

1 GEOMETRY

From a typical block of terraced houses in the province of Groningen, one house is extracted. Originally the houses are constructed with brick work. This is now transformed into timber, by doing so the inner dimensions of the house are kept the same and the width of a single house is adjusted.

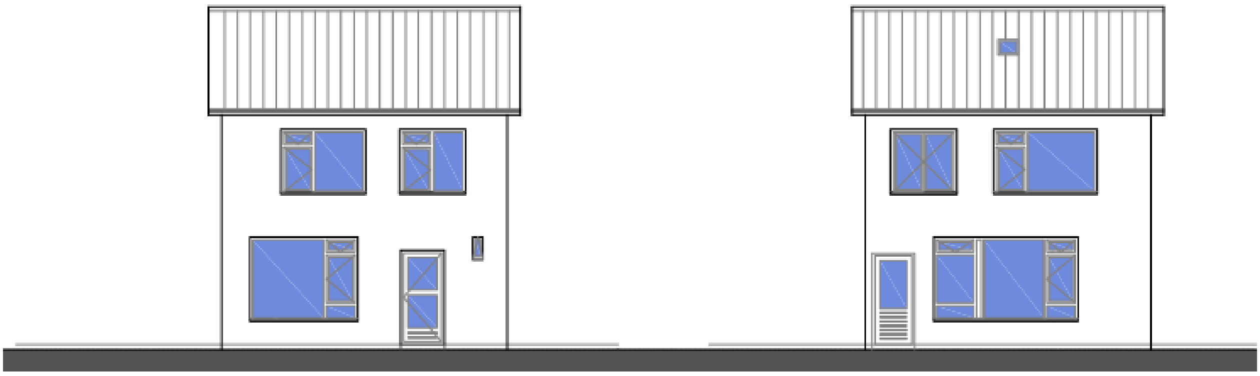

Fig. 1.1 Typical Dutch terraced house.

This is just used for the lay-out. The location of the of windows and doors is not restricted and are adjustable but it is a fact that every room has a window.

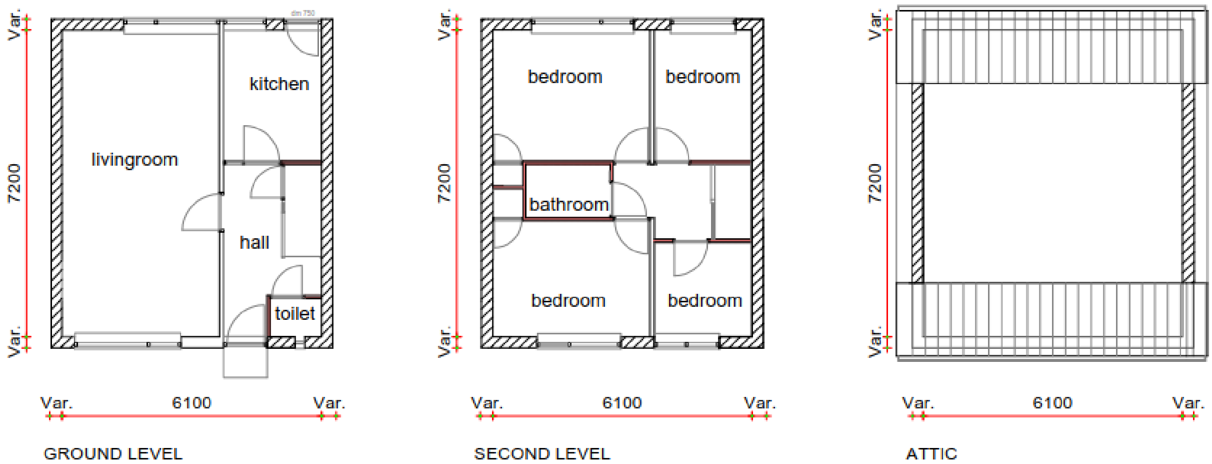

Fig. 1.2 Overview floorplans

2 USED DOCUMENTS

The following codes are used:

- NPR-9998-December: Assessment of buildings in case of erection, reconstruction and disapproval – Basic rules for seismic actions: induced earthquakes

- NEN-EN 1991-1-1 – 2011: Eurocode 1: Actions on structures – part 1- 1: General actions – densities, self-weight, imposed loads for buildings

- NEN-EN 1991-1-5:2011: Design of timber structures – Part 1-1: General – Common rules and rules for buildings

- NEN-EN 1991-1-3:2003: Eurocode 1: Actions on structures - Part 1-3: General actions - Snow loads

3 MATERIALS/ ELEMENTS

The following values are used for the materials and the elements.

OSB elements

Interior wall element		0.30 kN/m^2
Exterior wall element		0.40 kN/m^2

Roof

Roof element	115%	0.21 kN/m^2
Tiles	115%	0.55 kN/m^2
Total		0.76 kN/m^2

Second floor

Top finish		0.25 kN/m^2
40 mm insulation		0.10 kN/m^2
100 mm CLT	$4.50 \cdot 0.10$	0.45 kN/m^2
Partition wall		0.40 kN/m^2
Ceiling		0.10 kN/m^2
Total		1.30 kN/m^2

Ground floor

50 mm cement screed	$20.00 \cdot 0.05$	1.00 kN/m^2
150 mm insulation		0.30 kN/m^2
200 mm concrete hollow core slab		3.00 kN/m^2
Total		4.70 kN/m^2

Finishing

Brick sleeves[1] 0.10 kN/m²

Foundation

Reinforced concrete 25.00 kN/m³

An overview of cross-sections of the element with dimensions is given in figure 3.1. on the next page.

3.1 Material and model factors

The material factor $\gamma_m = 1.0$ but for elements with brittle failure mode $\gamma_m = 1.5$ according to NPR 9998 chapter 8.

The model factor $\gamma_M = 1.0$ according to NPR 9998 table 2.1.

[1] example on page 9.

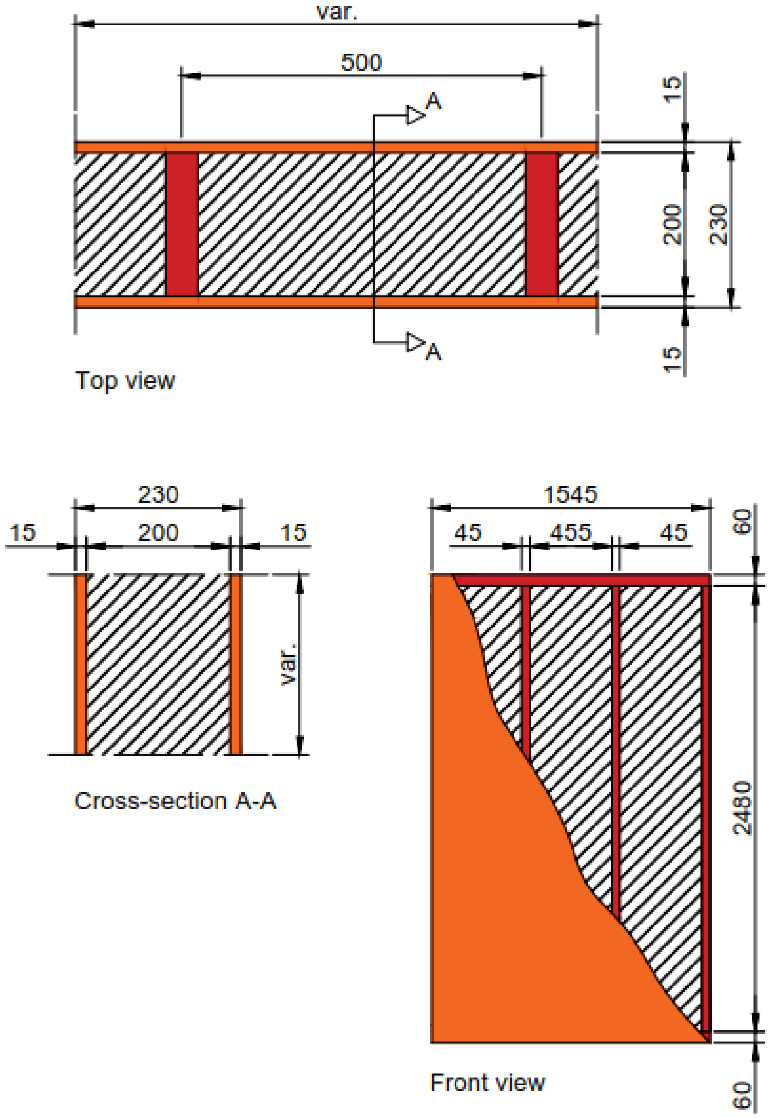

Fig. 3.1 Overview of the TF wall element. With posts and beams of C24 timber and OSB sheeting.

Fig. 3.2Example of brick sleeve

(Hedach AG, 2017)

4 LOADS

The loads taken into account are listed in this chapter, followed by some explanation.

4.1 LC1: Dead weight

The dead weight is calculated with the Excel sheet from annex A, an overview of the results is given in the table below.

Table 4.1 Overview of the self-weight on each vertical load bearing wall shown per floor.

	Living room wall Σ F [kN]	Inner wall Σ F [kN]	Kitchen wall Σ F [kN]	Side wall Σ F [kN]	Total Σ F [kN]
Attic	34	86	18	0	**132**
Second level	30	59	19	17	**125**
Ground level	72	172	38	18	**300**
Foundation	64	42	64	61	**231**
Total	**200**	**353**	**138**	**97**	**787**

Partition walls are taken into account for the dead weight by assuming an additional pressure of 0.4 kN/m^2.

4.2 LC2: Wind load

The total wind load on the building is equal to 125,4 kN resulting in a rotation moment of 450,3 kNm, both are for six houses. If reduced to one building the moment equals 75.1 kNm.

4.3 LC3: Snow load

The snow load is calculated conform Eurocode and the Dutch national annex for determining the characteristic snow load (s_k).

$$S = \mu_i \cdot C_e \cdot C_t \cdot s_k \qquad \text{(eq. 4.1)}$$

With,

$\mu_i = 0.8$ *roof shape factor*

$C_e = 1.0$ *exposure coefficient*

$C_t = 1.0$ *thermal coefficient*

$s_k = 0.7$ *characteristic snow load at ground level*

Therefore the following snow load is applied. The load is applied horizontally over the width of the roof .

$$S = 0.8 \cdot 1.0 \cdot 1.0 \cdot 0.7 = 0.56 \text{ kN/m}^2 \qquad \text{(eq. 4.2)}$$

4.4 LC4: Imposed load

Conform NEN-EN 1991-1-1+C1:2011/NB:2011 the imposed load on floors on a building class A (residential homes) $q_k = 1.75\ \text{kN/m}^2$, following from table NB.1-6.2.

Furthermore the load must be regarded as a variable load and the roof is classified as not accessible.

4.5 LC5: Seismic force

Due to the collaboration on the seismic forces this is treated in chapter 6.

5 COMBINATIONS

Since the calculation is focused on the seismic design and wind force is assumed as not governing, the only combination made is the one where the earthquake is governing. The table below is from the Dutch national annex and gives the load factors for extreme load combinations and for earthquake load combinations.

Load combination: dead weight + snow load + imposed load + seismic force

The table below is from the Dutch national annex and gives the load factors for extreme load combinations and for earthquake load combinations (red square).

Tabel NB.7 – A1.3 — Rekenwaarden van belastingen voor het gebruik in buitengewone en aardbevingsbelastingscombinaties

Ontwerpsituatie	Blijvende belastingen		Overheersende buitengewone of aardbevings-belasting	Veranderlijke belastingen gelijktijdig met de overheersende	
	Ongunstig	Gunstig		Belangrijkste (indien aanwezig)	Andere
Buitengewoon (Vgl. 6.11a/b)	1,0 $G_{k,j,sup}$	1,0 $G_{k,j,inf}$	1,0 A_d	$\psi_{1,1}\, Q_{k,1}$ [a]	$\psi_{2,i}\, Q_{k,i}$ (i >1)
Aardbeving (Vgl. 6.12a/b)	1,0 $G_{k,j,sup}$	1,0 $G_{k,j,inf}$	1,0 A_{ek} of 1,0 A_{Ed}	$\psi_{2,1}\, Q_{k,1}$	$\psi_{2,i}\, Q_{k,i}$ (i >1)

[a] Uitsluitend voor wind in combinatie met brand bij het beoordelen van disproportionele schade volgens NEN-EN 1991-1-7; voor overige gevallen $\psi_{2,1}$.

From the table above the load combination is as following.

$$E_d = 1.0 \cdot G_{k,j,\inf} + 1.0 \cdot A_{Ed} + \psi_{E,i} \cdot Q_{k,j} \qquad \text{(eq. 5.1)}$$

Where,

$\psi_{E,i}$ is $\varphi \cdot \psi_2$

Tabel 4.2 — Waarden voor φ voor de berekening van $\psi_{E;i}$

Klassen van belaste vloeroppervlakken [a]	Bouwlaag	φ
A tot en met C	Dak	1,0
	Overige bouwlagen (vloeren)	0,6
D tot en met F en archieven		1,0

[a] Klasse volgens 6.3.1.2 van NEN-EN 1991-1-1.

From table 4.2 from the NPR9998 $\varphi = 1.0$ for the snow load and $\varphi = 0.6$ for the imposed load.

The next factor to determine is the ψ_2 factor which are given in the table below, coming from the Dutch national annex. The upper red square gives the ψ_2 for the floors of the building. The second red square gives the ψ_2 for the roofs and the snow load, resulting in the fact that now additional forces have to be taken into account on the roof.

Tabel NB.2 – A1.1 — ψ-factoren voor gebouwen

Belasting	ψ_0	ψ_1	ψ_2
Voorgeschreven belastingen in gebouwen, categorie			
Categorie A: woon- en verblijfsruimtes	0,4	0,5	0,3
Categorie B: kantoorruimtes	0,5	0,5	0,3
Categorie C: bijeenkomstruimtes	0,6/0,4 [a]	0,7	0,6
Categorie D: winkelruimtes	0,4	0,7	0,6
Categorie E: opslagruimtes	1,0	0,9	0,8
Categorie F: verkeersruimte, voertuiggewicht ≤ 30 kN	0,7	0,7	0,6
Categorie G: verkeersruimte [b], 30 kN < voertuiggewicht ≤ 160 kN	0,7	0,5	0,3
Categorie H: daken	0	0	0
Sneeuwbelasting	0	0,2	0
Belasting door regenwater	0	0	0
Windbelasting	0	0,2	0
Temperatuur (geen brand)	0	0,5	0

[a] De waarde 0,6 geldt voor delen van het gebouw die in geval van een calamiteit zwaar kunnen worden belast door een mensenmenigte (vluchtroutes, trappen enz.); de waarde 0,4 geldt in overige gevallen.

[b] Met verkeersruimte wordt in dit geval een ruimte bedoeld waar voertuigen kunnen rijden, bijvoorbeeld parkeergarages.

With all the factors known the governing load combination in case of an earthquake is the following.

$$E_d = \mathrm{LC1} + \mathrm{LC5} + 0.18 \cdot \mathrm{LC4} \qquad \text{(eq. 5.2)}$$

Meaning the dead weight of the building plus the seismic force and an additional 0.18 times the characteristic imposed load.

For verification of seismic situation the following equation needs to be fulfilled:

$$E_d \leq R_d \qquad \text{(eq. 5.3)}$$

With,

$$R_d = R\{f_k/\gamma_m\}/\gamma_M \qquad \text{(eq. 5.4)}$$

For γ_m and γ_M see chapter 3.1.

6 SEISMIC FORCE

For determining the seismic force the ground peak acceleration is obtained from Fig. 6.1.

Fig. 6.1 Peak ground acceleration map of Groningen (Source: NPR9998. December 2015)

6.1 Mass calculation

The calculation is made using the sheet in annex B, an overview of the results is given in the next table. The calculation of the masses is needed for response of the building to the seismic forces.

Table 6.1 Overview of the masses

Level	Σ m [ton]
Attic	15.6
Second floor	12.9
Ground floor	28.9
Foundation	22.9
Total	**80.3**

For the mass calculation the building is divided into the following sections.

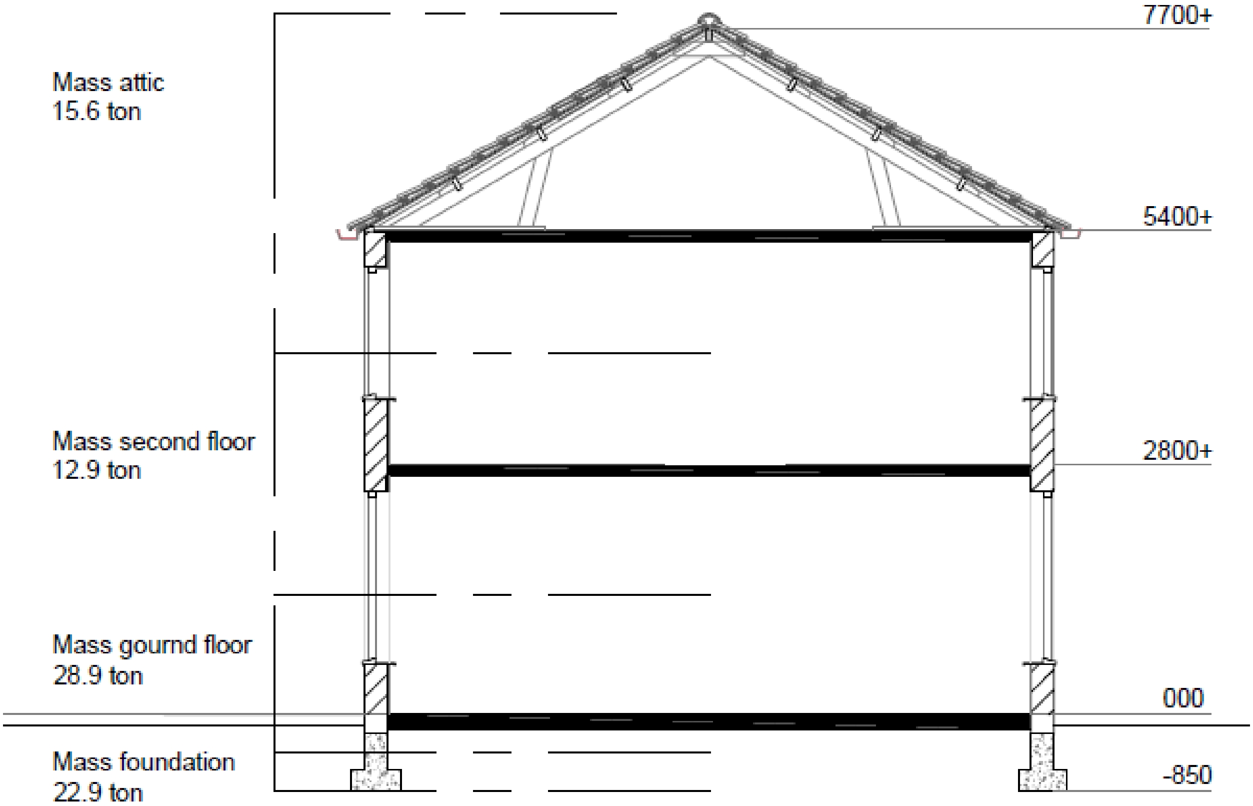

Fig. 6.2 Overview of the calculated masses.

6.2 Stiffness calculation

The stiffness is calculated over the following three walls.

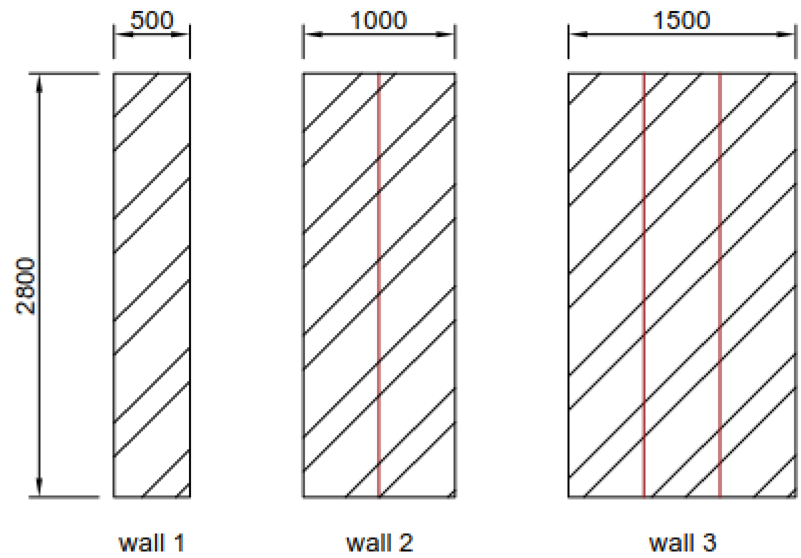

Fig. 6.3Walls used for calculation . It is assumed that these walls are located at both sides of the building.

It is assumed for this calculation the both sides of the building (front and back facade) have the same number of walls and that they are applied over the full length.

6.2.1 Natural period of the building

The natural period of the building can be calculated in different manners.

Table 6.2 Overview calculation method for the natural period.

Method	symbol	unit	natural period
EC8 (1)	T	s	0,25
EC8 (2)	T	s	0,66
Pauley and Priestley	T	s	0,28
Rayleigh method	T	s	0,60

The first method of the Eurocode is an lower bound empirical approach, which means it is conservative. Therefore this is not very representative for the situation and the methods using the stiffness are giving a better likeliness of the natural period. As specially the Rayleigh method gives a precise indication of the first natural period of the system. The third method uses the geometry of the building which is not logical since seismic forces are related to the stiffness and not to the geometry.

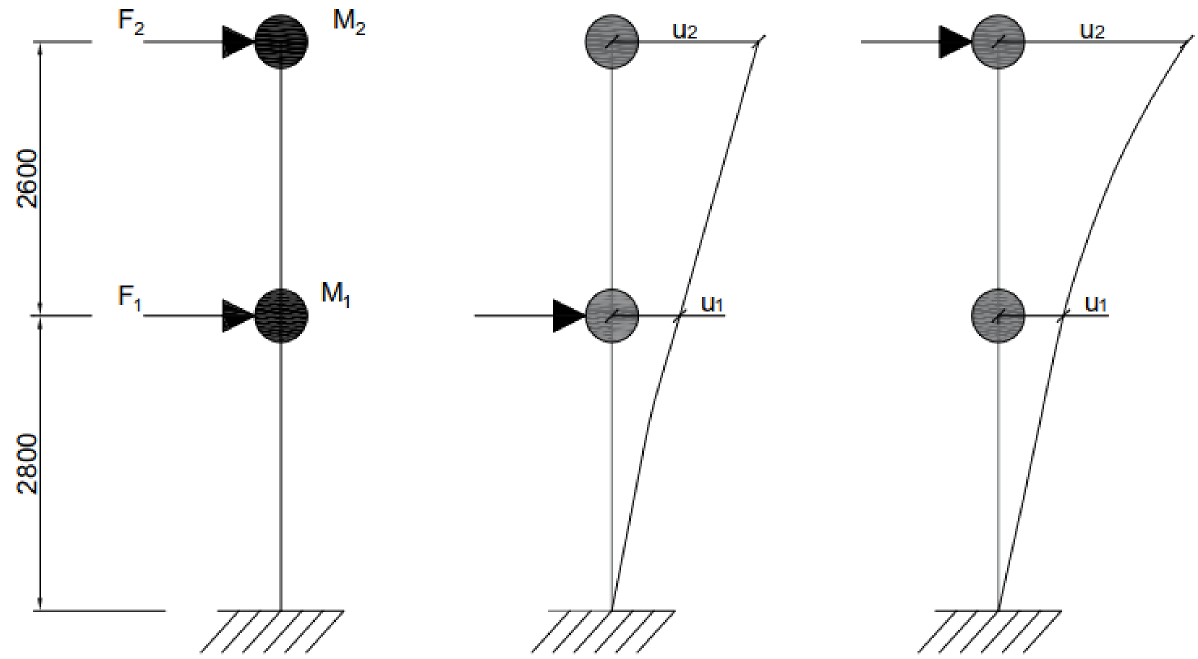

Fig. 6.4 Overview of schematization used for calcution of the natural period.

6.3 Response spectrum

The following parameters are used as input:

Consequence class	-	CC1B[2]
Design limit state	-	Near Collapse
Maximum reference ground acceleration at ground surface	$a_{g,ref}$	0.36 g
gravity acceleration	g	9.81 m/s²
Consequence factor	k_{ag}	1.4

From this and with the use of the NPR9998 the response spectrum diagram is created.

[2] Building with less than 3 levels which can be repaired within two weeks.

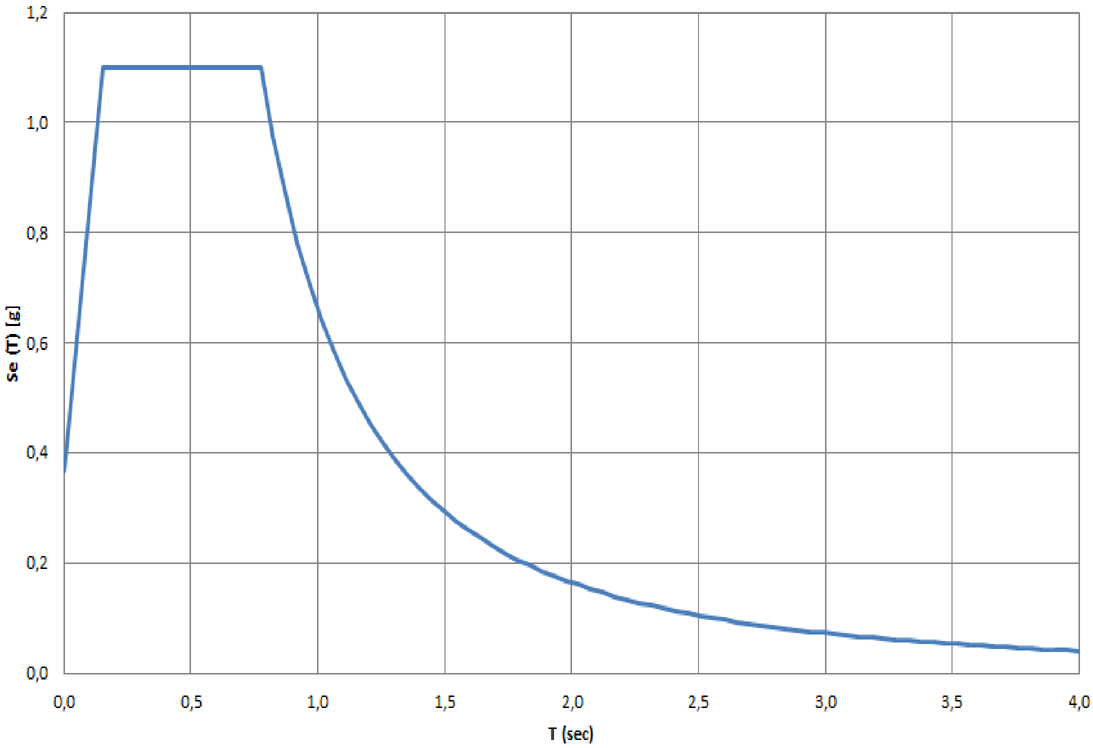

Fig. 6.5 Response spectrum

6.4 Lateral force method

The lateral force method (eq. 6.1)is used for calculation the horizontal force generated by the earthquake.

$$F_b = S_{d(T_1)} \cdot g \cdot m \cdot \lambda \qquad \text{(eq. 6.1)}$$

With,

F_b base shear force

$S_{a(T)}$ design acceleration

m mass above first floor, the two lumped masses are the most oscillated masses.

λ correction factor $\lambda = 0.85$ ($T_1 < 2\ T_c$ *and building levels* > 2)

The calculation is first made assuming an elastic response and later on different values for the behaviour factor are added. The elastic calculation leads to the following elastic response spectrum, using the Rayleigh method for calculation of the normal period.

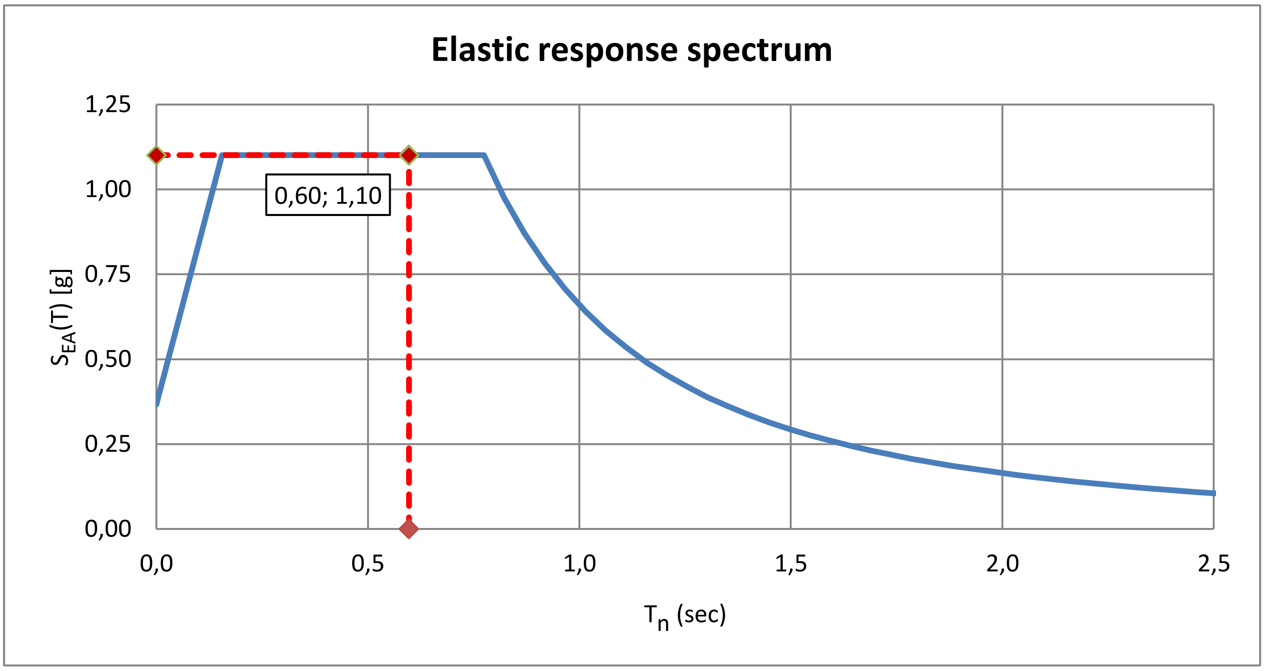

Fig. 6.6 Elastic response spectrum with the acceleration factor belonging to the fundamental natural period calculated with the Rayleigh method.

As indicated the natural period is such that it corresponds with the amplification factor at the plateau.

This leads to the following base shear force.

$$F_b = 1.1 \cdot 9.81 \cdot (15.6 + 12.9) \cdot 0.85 = 261 \text{ kN} \qquad \text{(eq. 6.2)}$$

For the force distribution the building is schematized as a system with two masses, namely at the height of the attic floor (5.4 meter) and second floor (2.8 meter). The distances given are from the top of the foundation. The ground level is floor is not taken into account.

6.5 Force distributions

There are two options for the force distribution, namely based on height or displacement (eq. 6.3)and (eq. 6.4). Both methods are implemented in the excel sheet from annex A.

The force distribution according to the ratio of the mass (m_i) and height(z_i);

$$F_i = F_b \cdot \frac{z_i \cdot m_i}{\sum_{j=1}^{n} z_j \cdot m_j} \qquad \text{(eq. 6.3)}$$

Option two is force distribution according to the ratio of the mass and displacement (s_i);

$$F_i = F_b \cdot \frac{s_i \cdot m_i}{\sum_{j=1}^{n} s_j \cdot m_j} \qquad \text{(eq. 6.4)}$$

The force distribution leads to the following shear and moment lines;

Forces distribution according to equation 6.3:

$$F_{attic} = 183 \text{ kN}$$
$$F_{2^{nd}\ floor} = 78 \text{ kN}$$

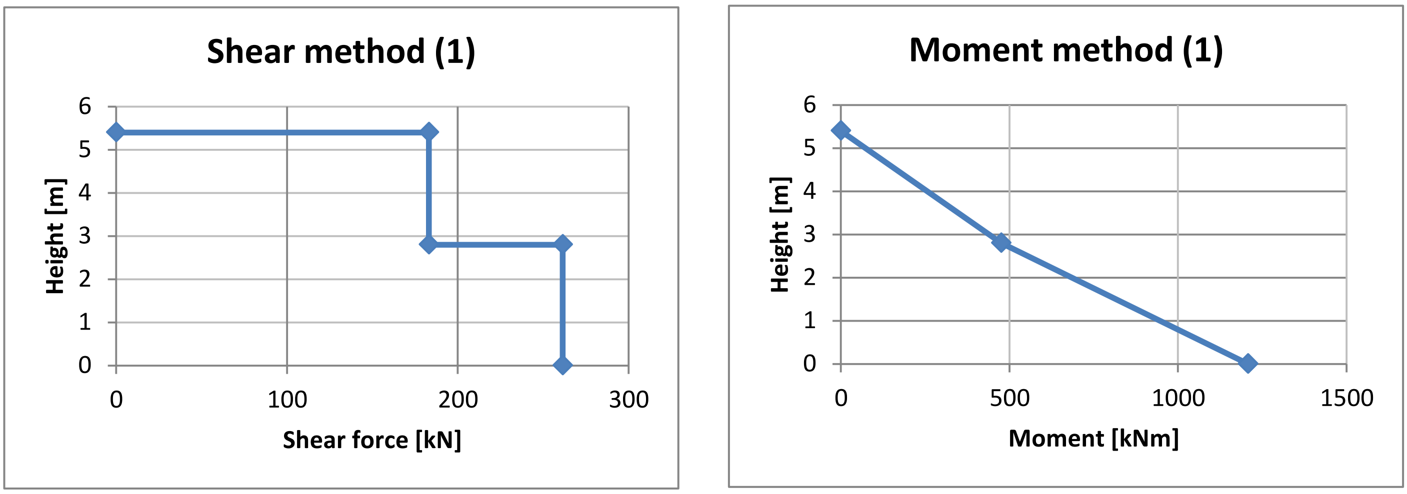

Fig. 6.7 Shear and moment distribution according to equation 6.3.

Forces distribution according to equation 6.4:

$$F_{attic} = 204 \text{ kN}$$
$$F_{2^{nd}\ floor} = 57 \text{ kN}$$

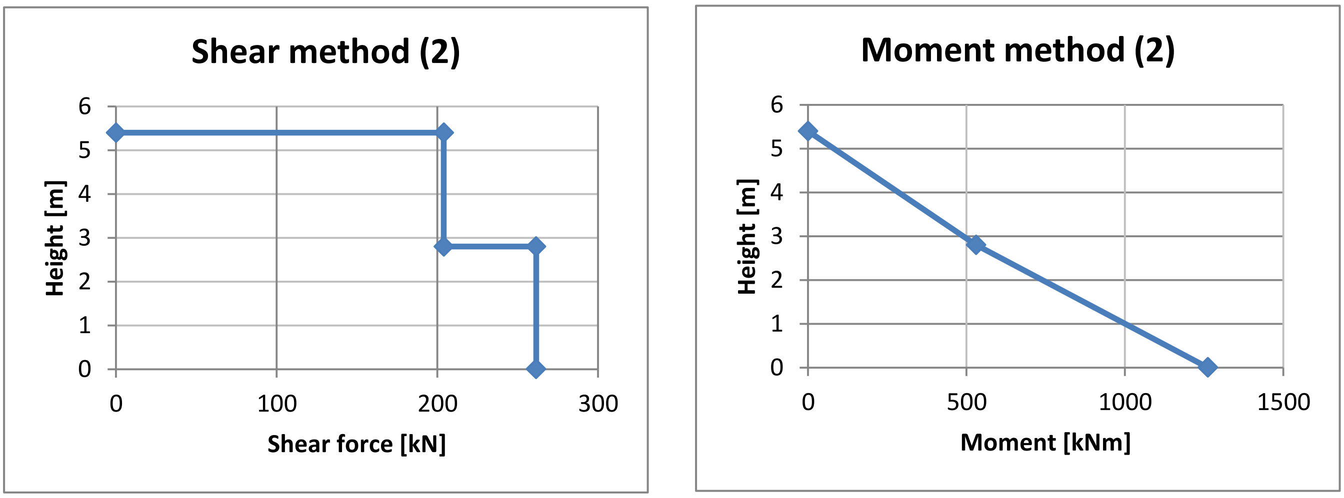

Fig. 6.8 Shear and moment distribution according to equation 6.4.

From the distriubtion graphs above it is clear that the governing distribution is the distribution from the horizontal displacement of the masses. Due to the slightly higher moments and force at the second floor.

6.6 Modal response analysis

The modal response is done with use of an excel sheet which uses the principle described by Chopra, A.K in *Dynamics of structures – theory and applications to earthquake engineering 4th edition*.

For the model response analysis the Excel sheet from annex B is used. An overview of the outcome is given in the table below.

Table 6.3 Natural period, mass participation and base shear force of the modes.

Mode	Natural period (Ti)	Mass participation [ton]	Base shear force [kN]
1	0.60	23.4	252.5
2	0.08	5.1	38.1

The 4th column of table 6.4 uses the SRSS (Squared Root of the Sums of the Squares) which in mathematical terms is:

$$E_E = \sqrt{\Sigma\, E_{E;i}{}^2} \qquad \text{(eq. 6.5)}$$

Table 6.4 Forces acting on each floor

Level	Mode 1 [kN]	Mode 2 [kN]	Total [kN] (SRSS)
Attic	197.1	-18.8	198.0
Second floor	55.4	56.9	79.4
Total	**252.5**	**38.1**	

By knowing forces per level for every mode the shear force can be determined.

Level	Mode 1 [kN]	Mode 2 [kN]	Total [kN] (SRSS)
Attic	197.1	-18.8	198.0
Second floor	252.5	38.1	255.4

7 VERIFICATION

In this chapter the strength of the walls will be verified. This is done according to the elastic response spectrum, in this way the behaviour factor (q-factor) which is needed can be determined.

Connection

The connection between the OSB and the frame is made with steel nails.

Diameter:	*d*	=	Ø3.1mm
Yielding stress:	*fu*	=	600 N/mm²
Centre to centre	*s*	=	60 mm

7.1 Wall Capacity

Calculation shear wall is made conform the simplified method A (EC5 9.2.4.2).

$$F_{i,v,Rd} = \frac{F_{f,v,Rd} \cdot b \cdot c_i}{s} \quad \text{(eq. 7.1)}$$

Where $F_{f,Rd}$ is the strength of a single connector, this is calculated for the timber-timber connections according to EC5 (8.6).

Calculation of embedment strength of the OSB sheet connection (EC5 8.22).

$$f_{h,k,1} = 65 \cdot d^{-0.7} \cdot t^{0.1} = 38.6 \text{ N/mm}^2 \quad \text{(eq. 7.2)}$$

Calculation of embedment strength of the solid timber connection (EC5 8.15).

$$f_{h,k,2} = 0.082 \cdot \rho_k \cdot d^{-0.3} = 20.4 \text{ N/mm}^2 \quad \text{(eq. 7.3)}$$

Next the β and the $M_{y,Rk}$ is determined.

$$\beta = \frac{f_{h,1,k}}{f_{h,2,k}} = 0.53 \quad \text{(eq. 7.4)}$$

$$M_{y,Rk} = 0.3 \cdot f_u \cdot d^{2.6} = 3410 \text{ Nmm} \quad \text{(eq. 7.5)}$$

Finally the formula's given in (EC5 8.6) are calculated and an overview is given in the table below, the 'koordeffect 'is not taken into account.

Table 7.1 Overview of connector strength

Mode	Force	Unit
(a)	1795	N
(b)	2851	N
(c)	1065	N
(d)	735	N
(e)	1587	N
(f)	865	N

From Table 7.1 it is clear that the governing connector strength is 735 N, corresponding to mode d (Fig. 7.1).

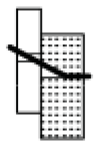

Fig. 7.1 Faillure mode d

$$F_{f,v,Rd} = 2 \cdot 735 \cdot 10^{-3} = 1.47 \text{ kN} \quad \text{(eq. 7.6)}$$

$$F_{1,v,Rd} = \frac{1.47 \cdot 1000 \cdot 0.36}{60} = 8.82 \text{ kN}$$
$$F_{2,v,Rd} = \frac{1.47 \cdot 1000 \cdot 0.71}{60} = 17.40 \text{ kN} \quad \text{(eq. 7.7)}$$
$$F_{3,v,Rd} = \frac{1.47 \cdot 1500 \cdot 1.00}{60} = 36.75 \text{ kN}$$

The total resistance is the summation of the walls.

$$F_{v,Rd} = \sum F_{i,v,Rd} = 62.97 \text{ kN} \quad \text{(eq. 7.8)}$$

The total base shear (eq. 6.2) is 261 kN, to resist the shear force behaviour factor for reducing the base shear force needs to be

$$q_{needed} = \frac{0.5 \cdot 261}{62.97} = 2.07 \quad \text{(eq. 7.9)}$$

However according to NPR9998 in case of NC the q-factor may be multiplied with 1.33 (p 40), the q-factor needed is.

$$q_{NC,needed} = \left(\frac{0.5 \cdot 261}{62.97} \right) \Big/ 1.33 = 1.56 \quad \text{(eq. 7.10)}$$

For the factor of 1.33 a reference is made to EC1998-3 which states the following at chapter 2.2.2 Limit state Near Collapse (NC):

(3) The q-factor approach (see **2.2.1(4)**P, **4.2(3)**P) is generally not suitable for checking this Limit State.

NOTE The values of q = 1,5 and 2,0 quoted in **4.2(3)**P for reinforced concrete and steel structures, respectively, as well as the higher values of q possibly justified with reference to the local and global available ductility in accordance with the relevant provisions of EN 1998-1: 2004, correspond to fulfilment of the Significant Damage Limit State. If it is chosen to use this approach to check the Near Collapse Limit State, then **2.2.3(3)**P may be applied, with a value of the q-factor exceeding those in **4.2(3)**P by about one-third.

The above states that it is not suitable for timber constructions there for the q-factor needs to be 2.07, which is the case conform NPR9998 (table 8.3), timber framed constructions are in the category DCH resulting in a q-factor of q=3.

7.1.1 Distance of studs

Local instability of the plate is restricted according to 9.2.4.2(11) of EC5 when the following condition is met.

$$\frac{b_{net}}{t} \leq 100 \rightarrow b_{net} \leq 1500 \text{ mm} \tag{eq. 7.11}$$

This condition is met for all the walls.

7.1.2 Compression perpendicular to grain and buckling

The vertical studs are pressing onto the horizontal beams at the bottom. Therefor these need to be checked on compression perpendicular to the grain.

The horizontal forces acting on the walls are:

$$F_1 = 0.03 \cdot 130.5 = 3.92 \text{ kN}$$
$$F_2 = 0.22 \cdot 130.5 = 28.71 \text{ kN}$$
$$F_3 = 0.75 \cdot 130.5 = 97.88 \text{ kN}$$

This is translated into the following vertical forces.

$$F_{3,c,Ed} = \frac{F_{3,v,Ed}h}{b_i} = 182.70 \text{ kN} \tag{eq. 7.12}$$

For all walls the forces are the same due to the fact that the force distribution is related to the stiffness of the walls and so is the vertical compression. The total vertical force on ground level is 17 kN in total, this is then distributed over all the walls as described on the previous page. Wall 3 consist of three studs evenly loaded by the vertical pressure therefor the total vertical force in the outer stud is.

$$F_{3,c,Ed} = 182.70 + \frac{(17/2)}{3} = 186 \text{ kN} \tag{eq. 7.13}$$

EC5 6.1.5 Compression perpendicular to the grain

(EC5 – equation 6.3) $\sigma_{c,90,d} \le k_{c,90} f_{c,90,d}$ (eq. 7.14)

$k_{c,90} = 1.25$ according to EC5 6.1.5(3)

Acting compressive stress perpendicular to grain.

$$\sigma_{c,90,d} = \frac{F_{c,90,d}}{A_{ef}} = \frac{186 \cdot 10^3}{200 \cdot 45} = 20.67 \text{ N/mm}^2 \quad \text{(eq. 7.15)}$$

The design material strength.

$$f_{c,90,d} = \frac{k_{\text{mod}} \cdot f_{c,90,k}}{\gamma_m} = 1.1 \cdot 2.5 = 2.75 \text{ N/mm}^2 \quad \text{(eq. 7.16)}$$

$\gamma_m = 1.0$
$k_{\text{mod}} = 1.1$

Verification of the compression perpendicular to the grain.

$$\frac{20.67}{1.25 \cdot 2.75} \le 1.0 \quad \text{not fulfilled} \quad \text{(eq. 7.17)}$$

Calculating with a behaviour factor of q=3.

$$\frac{(20.67/3)}{1.25 \cdot 2.75} \le 1.0 \quad \rightarrow \quad 2.0 \le 1.0 \quad \text{not fulfilled} \quad \text{(eq. 7.18)}$$

Adjust the lower beams to 200 by 90 millimeter.

$$\sigma_{c,90,d} = \frac{F_{c,90,d}}{A_{ef}} = \frac{186 \cdot 10^3}{200 \cdot 90} = 10.33 \text{ N/mm}^2 \quad \text{(eq. 7.19)}$$

Verification of the new dimensions, with q=3.

$$\frac{(10.33/q)}{1.25 \cdot 2.75} \le 1 \rightarrow 1.00 \le 1 \text{ OK!} \quad \text{(eq. 7.20)}$$

EC5 6.1.5 Buckling

Buckling of the stud is checked conform EC 6.1.5 the post is buckling around its y-y axis. The other axis is restrained by the sheathing.

$$I = \frac{1}{12} bh^3 = \frac{1}{12} \cdot 45 \cdot 200^3 = 3.00 \cdot 10^7 \text{ mm}^4 \quad \text{(eq. 7.21)}$$

$$i = \sqrt{\frac{I}{A}} = \sqrt{\frac{3.00 \cdot 10^7}{200 \cdot 45}} = 57.74 \text{ mm} \quad \text{(eq. 7.22)}$$

$$l_{buc} = h_{stud} = 2800 - 2 \cdot 90 = 2620 \text{ mm} \quad \text{(eq. 7.23)}$$

$$\lambda_y = \frac{L_{buc}}{i} = \frac{2620}{57.74} = 45.38 \quad \text{(eq. 7.24)}$$

$$\lambda_{rel,y} = \frac{\lambda_y}{\pi} \sqrt{\frac{f_{c,0,k}}{E_{0.05}}} = \frac{45.38}{\pi} \sqrt{\frac{24 \cdot 1.1}{9400}} = 0.77 \quad \text{(eq. 7.25)}$$

$$k_y = 0.5\left(1 + \beta_c \left(\lambda_{rel,y} - 0.3\right) + \lambda_{rel,y}^2\right) = 0.5\left(1 + 0.2\left(0.77 - 0.3\right) + 0.77^2\right) = 0.84 \quad \text{(eq. 7.26)}$$

$$k_{c,y} = \frac{1}{k_y + \sqrt{k_y^2 - \lambda_{rel,y}^2}} = \frac{1}{0.84 + \sqrt{0.84^2 - 0.77^2}} = 0.85 \quad \text{(eq. 7.27)}$$

Buckling check (EC5 – 6.23)

$$\begin{gathered} \frac{\sigma_{c,0,d}}{k_{c,y} f_{c,0,d}} \leq 1 \\ \frac{20.67}{0.85 \cdot \left(24 \cdot 1.1\right)} = 0.92 \leq 1 \end{gathered} \quad \text{(eq. 7.28)}$$

Even when calculating elastic this requirement is fulfilled.

8 CONCLUSION

The conclusion is split in to the following parts to address the influence of each parameter for the decisive façade - direction.

1. Stiffness and relation to the natural period
2. Number of shear walls
3. Verification
4. Behaviour factor

At all calculation the floors are assumed rigid which means the ratio between the walls and the floors are as following.

$$\frac{EI_{floors}}{EI_{walls}} = \infty \qquad \text{(eq. 8.1)}$$

1. Stiffness and relation to the natural period

In this calculation report the stiffness is simplified to the assumed that the stiffness of the sheeting can be used. From the calculation with the stiffness is becomes clear that for the two-storey building the natural period will be in the ranch of the plateau of the response diagram. For a two storey building the is not possible to reduce the natural period to a more favourable value.

Comparison between the calculation of the natural period between the more extensive modal response analyses and the calculation methods for the lateral force method shows the following; The methods related to the geometry of the building are always lower bound solutions, whereas the Rayleigh method and the EC8 (2) method are more accurate in relation to the modal response calculation.

2. Number of shear walls

For the calculation three shear walls are applied, where the smallest shear wall is 500 millimetre. In contrast to the other two walls which are larger (1000 and 1500 mm) and therefor stiffer, the contribution of the small wall is negligible.

3. Verification

From the verification it became clear that the lower beam of the timber frame had to be adjusted to account for the compression perpendicular to the grain. The lay-out of the frame is something that can be adjusted until certain limits. Interesting is also the fact that the NPR9998 - 8.1.3 states that the no deformation of the plate has to be taken into account if the following condition is met.

$$\frac{l}{t} \leq 70 \qquad \text{(eq. 8.2)}$$

Where t is the plate thickness and l is the smallest centre to centre distance between posts or beams. If this condition is met all the horizontal deformation is due to slip of the connections. Therefor the calculation of the transferred shear forces is of importance because due to spacing requirements of the connectors the adjustments are limit at a certain point.

4. Behaviour factor (q-factor)

The behaviour factor is crucial for designing an economically feasible structure. The q-factor takes the structural capacity of energy dissipation into account, regarding ductility, over-strength etc. Therefor the q-factor is related to the structural details as descripted in the codes. This results in a certain q-factor which reduces the forces which has to be taken into account.

For the verification a q-factor of three has been taken into account according to table 8.3 of the NPR9998 and the additional multiplication of the q-factor with 1.33 has not been taken into account.

ANNEX A: EXCEL CALCULATION

I

Algemeen		
Project	Master thesis	
Plaats	-	
Aantal woningen		1

Dimensions		*l[m]*				
Width living room				*b_living*	3,695	3,985
Width kitchen				*b_kitch*	2,305	2,595
				b_facade		6,580
Length building				*l_woon*	7,20	7,68
Roof slope			30,00			
Ridge height	*p_nok*	7,70				
attic	*p_attic*	5,40		*h_attic*	2,30	
Second floor	*p_sec_floor*	2,80		*h_verd*	2,60	
Ground floor	*p_ground_fl.*	0,00		*h_ground*	2,80	
Bottom foundation	*p_found.*	-0,85		*h_found.*	0,85	
				gutter-found.	6,25	
				pier 1 front facade	1,50	
				pier 2 front facade	1,00	
				pier 1 back facade	1,50	
				pier 2 back facade	1,00	
				Load bearing part side wall	70%	

Walls	*d[mm]*	*Material*
Exterior wall	230	*Timber*
Brick sleeves	10	
Interior wall	100	*Timber*

Floors (withour finishing)	*d[mm]*	*Material*
Attic	200	*CLT*
verdieping	200	*CLT*
ground floor	200	*Concrete hollow core slab*

Roof	*d[mm]*
Timber framed (prefab)	230

Foundation

	Width rib	Height top rib	Height top foundation plate	Extending part	Width foundation plate	thickness foundation plate	Material	Unit weight
Outer wall	310	-340	-740	650	1610	120	C20/25	25
Inner wall	100	-340	-740	650	1400	120	C20/25	25
Side wall	260	-370	-770	140	540	120	C20/25	25

found_outer_wall	7,93	kN/m
found_inner_wall	5,2	kN/m
found_side_wall	4,22	kN/m

Dynamic modulus of subgrade	K_{vert}	8,50	MN/m^3
Horizontal springstiffness perp. To foundation	khor_perp_ros	4,50	MN/m^3
Horizontal springstiffness parralel to foundation	khor_par_ros	6,40	MN/m^3

Annex B

Algemeen								
Project	Master thesis							
Plaats	-							
Aantal woningen	1							
Tekening								

P-lasten

Deel	P [kN/m²]	[kg/m³]	h [mm]	%	naam	P_{perm} [kN/m²]	P_{var} [kN/m²]	ΨE,i
Floors and roofs								
Roof								
Roof element	0,18			115%		0,21		
Roof tiles	0,48			115%		0,55		
ΣP					*Roof*	**0,76**	**0,56**	0,00
Attic								
Top finish	0,25					0,25		
CLT		450	100			0,45		
Insulation	0,1					0,10		
Partition wall	0,4					0,40		
Ceiling	0,1					0,10		
ΣP					*Attic*	**1,30**	**1,75**	0,18
verdieping								
Top finish	0,25					0,25		
CLT		450	100			0,45		
Insulation	0,1					0,10		
Partition wall	0,4					0,40		
Ceiling	0,1					0,10		
ΣP					*second level*	**1,30**	**1,75**	0,18
Ground floor								
Screed/top layer		2000	50			1,00		
Insulation	0,3					0,30		
Concrete slab	3,0					3,00		
Partition wall	0,4					0,40		
ΣP					*ground level*	**4,70**	**1,75**	0,18
Facades and walls								
Living wall								
Mopac element	0,30					0,30		
Insulation	0,10					0,10		
Brike sleeve	0,10					0,10		
ΣP					*Living wall*	**0,50**	**0**	0,00
kitchen wall								
Mopac element	0,30					0,30		
Insulation	0,10					0,10		
Brike sleeve	0,10					0,10		
ΣP					*kitchen wall*	**0,50**	**0**	0,00
Inner wall								
Mopac element	0,30					0,30		
ΣP					*inner wall*	**0,30**	**0**	0,00
Side wall								
Mopac element	0,30			70%		0,21		
Insulation	0,10			70%		0,07		
Brike sleeve	0,10			70%		0,07		
Windows	0,50			30%		0,15		
ΣP					*side wall*	**0,50**	**0**	0,00

Annex B

Algemeen

Project	Master thesis
Plaats	-
Aantal woningen	1
Tekening	

Q-loads

deel	P_{perm} [kN/m^2]	P_{var} [kN/m^2]	$_{ei}$	maat-voering	breedte	naam	Q_{perm} [kN/m]	Q_{var}*Ψ_{ei} [kN/m]	ΣQ [kN/m]	ΣF [kN]	Σm [kg]		$Q_{bd;s}$ [kN/m]	$Q_{md;s}$ [kN/m]	$Q_{od;s}$ [kN/m]

Reactions

Floor fields

Field length living	b_living	4,0
Field length kitchen	b_kitch	2,6
Support reactions	See drawing on the right	

Overview

	Living room wall	Inner wall	Kitchen wall	Side wall	
	Σ F	Σ F	Σ F	Σ F	Σ F
Attic	34	81	17	0	132
Second level	30	59	19	17	125
Ground level	72	172	38	18	300
Foundation	64	42	64	61	231
	200	353	138	97	787

deel	P_{perm}	P_{var}	$_{ei}$	maat-voering	breedte	naam	Q_{perm}	Q_{var}*Ψ_{ei}	ΣQ	ΣF	Σm		$Q_{bd;s}$	$Q_{md;s}$	$Q_{od;s}$
Living room wall				l_building	7,7										
Roof	0,76	0,56	0,00	b_living	4,0	40%	1,21	0	1,21	9,330	933				
Living wall	0,50	0,00	0,00	h_attic	2,3	50%	0,58	0	0,58	4,416	442				
Attic	1,30	1,75	0,18	b_living	4,0	40%	2,07	0,5	2,57	19,8	1977				
				Σ AtticLiving room wall			3,86	0,50	4,36	33,5	3352				
												wandlast verdieping	4,36	5,0	5,7
Living wall	0,50	0,00	0,00	h_verd	2,6	100%	1,30	0	1,30	9,984	998				
second level	1,30	1,75	0,18	b_living	4,0	40%	2,07	0,5	2,57	19,8	1977				
				Σ second levelLiving room wall			3,4	0,5	3,9	29,8	2975				
				Σ subtotal second levelLiving room wall			7,2	1,0	8,2	63,3	6327				
												wandlast begane grond	8,2	8,9	9,6
Living wall	0,50	0,00	0,00	h_ground	2,8	100%	1,40	0	1,40	10,752	1075				
ground level	4,70	1,75	0,18	b_living	4,0	40%	7,49	0,5	7,99	61,4	6139				
				Σ ground levelLiving room wall			8,9	0,5	9,4	72,1	7215				
				Σ subtotal ground levelLiving room wall			16,1	1,5	17,6	135,4	13542				
												wandlast fundering	17,6	17,8	18,1
Living wall	0,50	0,00	0,00	h_found.	0,9	100%	0,4	0	0,4	3,264	326				
foundation				found_outer_wall			7,9		7,9	60,9	6090				
				Σ foundationLiving room wall			8,4	0,0	8,4	64,2	6417				
				Σ subtotal foundationLiving room wall			24,5	1,5	26,0	199,6	19958				
Kitchen wall				l_building	7,7										
Roof	0,76	0,56	0,00	b_kitch	2,6	27%	0,53	0	0,53	4,101	410				
kitchen wall	0,50	0,00	0,00	h_attic	2,3	50%	0,58	0	0,58	4,4	442				
Attic	1,30	1,75	0,18	b_kitch	2,6	27%	0,91	0,2	1,13	8,7	869				
				Σ AtticKitchen wall			2,02	0,22	2,24	17,2	1721				
												wandlast verdieping	2,24	2,9	3,5
kitchen wall	0,50	0,00	0,00	h_verd	2,6	100%	1,30	0	1,30	10,0	998				
second level	1,30	1,75	0,18	b_kitch	2,6	27%	0,91	0,2	1,13	8,7	869				
				Σ second levelKitchen wall			2,2	0,2	2,4	18,7	1867				
				Σ subtotal second levelKitchen wall			4,2	0,4	4,7	35,9	3588				
												wandlast begane grond	4,7	5,4	6,1
kitchen wall	0,50	0,00	0,00	h_ground	2,8	100%	1,40	0	1,40	10,8	1075				
ground level	4,70	1,75	0,18	b_kitch	2,6	27%	3,29	0,2	3,51	27,0	2699				
				Σ ground levelKitchen wall			4,7	0,2	4,9	37,7	3774				
				Σ subtotal ground levelKitchen wall			8,9	0,7	9,6	73,6	7362				
												wandlast fundering	9,6	9,8	10,0
kitchen wall	0,50	0,00	0,00	h_found.	0,9	100%	0,4	0	0,4	3,3	326				
foundation				found_outer_wall			7,9		7,9	60,9	6090				
				Σ foundationKitchen wall			8,4	0,0	8,4	64,2	6417				
				Σ subtotal foundationKitchen wall			17,3	0,7	17,9	137,8	13779				
Inner wall				l_building	7,7										
Roof	0,76	0,56	0,00	b_living	4,0	60%	1,82	0,0	1,82	13,994	1399				
Roof	0,76	0,56	0,00	b_kitch	2,6	73%	1,44	0,0	1,44	11,088	1109				
inner wall	0,30	0,00	0,00	h_attic	2,3	50%	0,35	0,0	0,35	2,6	265				
Attic	1,30	1,75	0,18	b_living	4,0	60%	3,11	0,8	3,86	29,7	2966				
Attic	1,30	1,75	0,18	b_kitch	2,6	73%	2,46	0,6	3,06	23,5	2350				
				Σ AtticInner wall			9,2	1,35	10,5	80,9	8088				
												wandlast verdieping	10,53	10,9	11,3
inner wall	0,30	0,00	0,00	h_verd	2,6	100%	0,78	0	0,78	6,0	599				
second level	1,30	1,75	0,18	b_living	4,0	60%	3,11	0,8	3,86	29,7	2966				
second level	1,30	1,75	0,18	b_kitch	2,6	73%	2,46	0,6	3,06	23,5	2350				
				Σ second levelInner wall			6,4	1,3	7,7	59,1	5914				
				Σ subtotal second levelInner wall			15,5	2,7	18,2	140,0	14003				
												wandlast begane grond	18,2	18,7	19,1
Inner wall	0,30	0,00	0,00	h_ground	2,8	100%	0,84	0	0,84	6,5	645				
ground level	4,70	1,75	0,18	b_living	4,0	60%	11,24	0,8	11,99	92,1	9209				
ground level	4,70	1,75	0,18	b_kitch	2,6	73%	8,90	0,6	9,50	73,0	7296				
				Σ ground levelInner wall			21,0	1,3	22,3	171,5	17150				
				Σ subtotal ground level			36,5	4,0	40,6	312	31153				
												wandlast fundatie grond	40,6	43,2	45,8
Inner wall	0,30	0,00	0,00	h_found.	0,9	100%	0,26	0	0,26	2,0	196				
foundation				found_inner_wall			5,2		5,2	39,9	3994				
				Σ foundationInner wall			5,5	0,0	5,5	41,9	4189				
				Σ subtotal foundationInner wall			42,0	4,0	46,0	353,4	35342				
Side wall **200% betekent voor en achtergevel**				b_gevel	6,58										
Attic	1,30	1,75	0,18	h_attic	6,6	0%	0,0	0,0	0,0	0,0	0				
				Σ AtticSide wall			0,0	0,0	0,0	0,0	0				
												wandlast verdieping	0,00	1,3	2,6
Side wall	0,50	0,00	0,00	h_verd	2,6	200%	2,6	0,0	2,6	17,1	1711				
second level	1,30	1,75	0,18	b_living	6,6	0%	0,0	0,0	0,0	0,0	0				
				Σ second levelSide wall			2,6	0,0	2,6	17,1	1711				
				Σ subtotal second levelSide wall			2,6	0,0	2,6	17,1	1711				
												wandlast begane grond	2,6	4,0	5,4
Side wall	0,50	0,00	0,00	h_ground	2,8	200%	2,8	0,0	2,8	18,4	1842				
ground level	4,70	1,75	0,18	b_living	0,0	0%	0,0	0,0	0,0	0,0	0				
				Σ ground levelSide wall			2,8	0,0	2,8	18,4	1842				
				Σ subtotal ground levelSide wall			5,4	0,0	5,4	35,5	3553				
												wandlast fundering	5,4	5,8	6,3
Side wall	0,50	0,00	0,00	h_found.	0,9	200%	0,9	0,0	0,9	5,6	559				
Foundation				found_side_wall		200%	8,4		8,4	55,5	5554				
				Σ FoundationSide wall			9,3	0,0	9,3	61,1	6113				
				Σ subtotal FoundationSide wall			14,7	0,0	14,7	96,7	9666				

Annex B

Algemeen

Project	Master thesis
Plaats	-
Aantal woningen	1
Tekening	Tekening 1
	Tekening 2

Mass calculation

deel		P_{perm} [kN/m^2]	P_{var} [kN/m^2]	Ψ_{ei}	q_{perm} [kN/m]		lengte [m]		breedte [m]		hoogte [m]	naam	oppervlak [m^2]	m_{perm} [ton]	$m_{var}*\Psi_{ei}$ [ton]	Σm [ton]

Overview

	Σm [ton]	
attic	15,6	
second floor	12,9	
ground floor	28,9	
foundation	22,9	+
total	80,3	

Attic

deel		P_{perm}	P_{var}	Ψ_{ei}	q_{perm}		lengte		breedte		hoogte	naam	oppervlak	m_{perm}	$m_{var}*\Psi_{ei}$	Σm
Roof		0,76	0,56	0,00		*b_facade*	6,58	*l_woon*	7,68			100%	51	3,9	0,0	3,926
Living wall		0,50	0,00	0,00				*l_woon*	7,68	h_attic	2,30	50%	9	0,5	0,0	0,450
kitchen wall		0,50	0,00	0,00				*l_woon*	7,68	h_attic	2,30	50%	9	0,5	0,0	0,5
inner wall		0,30	0,00	0,00				*l_woon*	7,68	h_attic	2,30	50%	9	0,3	0,0	0,3
Attic		1,30	1,75	0,18		*b_facade*	6,58	*l_woon*	7,68			100%	51	6,7	1,6	8,3
Living wall		0,50	0,00	0,00				*l_woon*	7,68	h_verd	2,60	50%	10	0,5	0,0	0,51
kitchen wall		0,50	0,00	0,00				*l_woon*	7,68	h_verd	2,60	50%	10	0,5	0,0	0,5
inner wall		0,30	0,00	0,00				*l_woon*	7,68	h_verd	2,60	50%	10	0,3	0,0	0,3
side wall	f+b	0,50	0,00	0,00		*b_facade*	6,58			h_verd	2,60	100%	17	0,9	0,0	0,9
												Σ attic		14,0	1,6	15,6
												Σ subtotal attic		14,0	1,6	15,6

Second floor

deel		P_{perm}	P_{var}	Ψ_{ei}	q_{perm}		lengte		breedte		hoogte	naam	oppervlak	m_{perm}	$m_{var}*\Psi_{ei}$	Σm
Living wall		0,50	0,00	0,00				*l_woon*	7,68	h_verd	2,60	50%	10	0,5	0,0	0,51
kitchen wall		0,50	0,00	0,00				*l_woon*	7,68	h_verd	2,60	50%	10	0,5	0,0	0,51
inner wall		0,30	0,00	0,00				*l_woon*	7,68	h_verd	2,60	50%	10	0,3	0,0	0,31
side wall	f+b	0,50	0,00	0,00		*b_facade*	6,58			h_verd	2,60	100%	17	0,9	0,0	0,87
second level		1,30	1,75	0,18		*b_facade*	6,58	*l_woon*	7,68			100%	51	6,7	1,6	8,32
Living wall		0,50	0,00	0,00				*l_woon*	7,68	h_ground	2,80	50%	11	0,5	0,0	0,55
kitchen wall		0,50	0,00	0,00				*l_woon*	7,68	h_ground	2,80	50%	11	0,5	0,0	0,55
inner wall		0,30	0,00	0,00				*l_woon*	7,68	h_ground	2,80	50%	11	0,3	0,0	0,33
side wall	f+b	0,50	0,00	0,00		*b_facade*	6,58			h_ground	2,80	100%	18	0,9	0,0	0,94
												Σ second floor		11,3	1,6	12,88
												Σ subtotal second floor		25,2	3,2	28,49

Ground floor

deel		P_{perm}	P_{var}	Ψ_{ei}	q_{perm}		lengte		breedte		hoogte	naam	oppervlak	m_{perm}	$m_{var}*\Psi_{ei}$	Σm
Living wall		0,50	0,00	0,00				*l_woon*	7,68	h_ground	2,80	50%	11	0,5	0,0	0,55
kitchen wall		0,50	0,00	0,00				*l_woon*	7,68	h_ground	2,80	50%	11	0,5	0,0	0,55
inner wall		0,30	0,00	0,00				*l_woon*	7,68	h_ground	2,80	50%	11	0,3	0,0	0,33
side wall	f+b	0,50	0,00	0,00		*b_facade*	6,58			h_ground	2,80	100%	18	0,9	0,0	0,94
ground level		4,70	1,75	0,18		*b_facade*	6,58	*l_woon*	7,68			100%	51	24,2	1,6	25,83
Living wall		0,50	0,00	0,00				*l_woon*	7,68	h_found.	0,85	50%	3	0,2	0,0	0,17
kitchen wall		0,50	0,00	0,00				*l_woon*	7,68	h_found.	0,85	50%	3	0,2	0,0	0,17
inner wall		0,30	0,00	0,00				*l_woon*	7,68	h_found.	0,85	50%	3	0,1	0,0	0,10
side wall	f+b	0,50	0,00	0,00		*b_facade*	6,58			h_found.	0,85	100%	6	0,3	0,0	0,29
												Σ ground floor		27,3	1,6	28,9
												Σ subtotal ground floor		52,5	4,9	57,4

Foundation

deel		P_{perm}	P_{var}	Ψ_{ei}	q_{perm}		lengte		breedte		hoogte	naam	oppervlak	m_{perm}	$m_{var}*\Psi_{ei}$	Σm
Living wall		0,50	0,00	0,00				*l_woon*	7,68	h_found.	0,85	50%	3,3	0,2	0,0	0,17
kitchen wall		0,50	0,00	0,00				*l_woon*	7,68	h_found.	0,85	50%	3,3	0,2	0,0	0,17
inner wall		0,30	0,00	0,00				*l_woon*	7,68	h_found.	0,85	50%	3,3	0,1	0,0	0,10
side wall	f+b	0,50	0,00	0,00		*b_facade*	6,58			h_found.	0,85	100%	5,6	0,3	0,0	0,29
found_outer_wall	L+K				7,93			*l_woon*	7,68			200%		12,42		12,42
found_inner_wall					5,2			*l_woon*	7,68			100%		4,07		4,07
found_side_wall					4,22	*b_facade*	6,58					200%		5,66		5,7
												Σ foundation		22,9	0,0	22,9
												Σ subtotal foundation		75,4	4,9	80,3

Algemeen

Project	Master thesis
Plaats	-
Aantal woningen	1
Tekening	Tekening 1
	Tekening 2

Frequency calculation

Overview	Symbel	unit	natural period
EC8 (1)	T	s	0,25
EC8 (2)	T	s	0,64
Pauley and Priestley	T	s	0,28
Rayleigh method	T	s	0,60

Input

Ridge height	*p_nok*	7,7	m
Bottom foundation	*p_found.*	-0,85	m
Height building	*H*	8,55	m
Length building	*l_woon*	7,68	m
Frame type	Other/timber	C_T	0,05

EC8 (1) *If h < 40 m*	art.	form. Nr.	from.	symbel.	unit		
Dimensionless factor	EN1998-1	4.3.3.2.1		C_T	-	0,05	
EC8 (1) natural period	EN1998-1	4.3.3.2.1	C_T*H^3/4	T	s	0,250	Not accurate

EC8 (2)	art.	form. Nr.	from.	symbel.	unit	
EC8 (2)	EN1998-1	4.3.3.2.1	2*d^0,5	T	s	0,64

Pauley and Priestley	art.	form. Nr.	from.	symbel.	unit		
Natural period			0,09*H/(L^0.5)	T	s	0,278	Not accurate

Rayleigh method	art.	form. Nr.	from.	symbel.	unit	
Rayleigh method			2π(sum(m*u^2)/sum(F*U))^0,5	T	s	0,60

Annex B

Algemeen

Project	Master thesis		code: NPR9998 dec. 15
Plaats	-		
Aantal woningen	1	demping 5% altijd	
Tekening	[Tekening 1]()		
	[Tekening 2]()		

Seismic calculation

	art.	form. Nr.	table	figure	symbel.	unit	
Consequence class	2.1		2.1.2				CC1B
Maximum reference ground acceleration at ground surface	3.2.1			3.1	$a_{g;ref\text{-}v}$	[g]	0,36
gravity acceleration					g	[m/s^2]	9,81
Design limit state							NC
Behaviour factor	-				q		1,0

Seismic data	art.	form. Nr.	table	figure	symbel.	unit	DL	SD	NC
Consequence factor	3.2.1		2.2		k_{ag}		0,3	0,7	1,4
Partial element factor	4.4.2.2		2.2		γ_M		1,0	1,0	1,1

Spectra	art.	form. Nr.	from.	figure	symbel.	unit	
Consequence factor					k_{ag}		1,4
Partial element factor	4.4.2.2		2.2		γ_M		1,1
rekenwaarde van de spectrale versnelling voor korte periode	3.2.2.2.1	(3.4)	$2{,}2 * a_{g;ref} * k_{ag}$		S_S	[g]	1,109
rekenwaarde van de spectrale versnelling voor lange periode	3.2.2.2.1	(3.5)	$0{,}654 * a_{g;ref} * k_{ag}$		S_1	[g]	0,330
coëfficient voor korte trillingsperiode	3.2.2.2	(3.6)	$-0{,}5 * \ln(a_{g;ref} * k_{ag}) + 0{,}65$		F_a		0,993
coëfficient voor lange trillingsperiode	3.2.2.2	(3.7)	$-0{,}87 * a_{g;ref} * k_{ag} + 2{,}44$		F_v		2,002
rekenwaarde ontwerpwaarde versnelling korte trillingsperiode	3.2.2.2	(3.8)	$F_a * S_S$		S_{MS}	[g]	1,101
rekenwaarde ontwerpwaarde versnelling lange trillingsperiode	3.2.2.2	(3.9)	$F_v * S_1$		S_{M1}	[g]	0,660
rekenwaarde van de piekgrondversnelling	3.2.1	(3.3)	$S_e(0) = S_{MS}/3$		$a_{g;d}$	[g]	0,367
plateau	3.2.2.2					T_A	0,00
	3.2.2.2	(3.10)	$0{,}2 * T_C$	3.2		T_B	0,15
	3.2.2.2	(3.11)	$\sqrt{(S_{M1}/S_{MS})}$	3.2		T_C	0,77

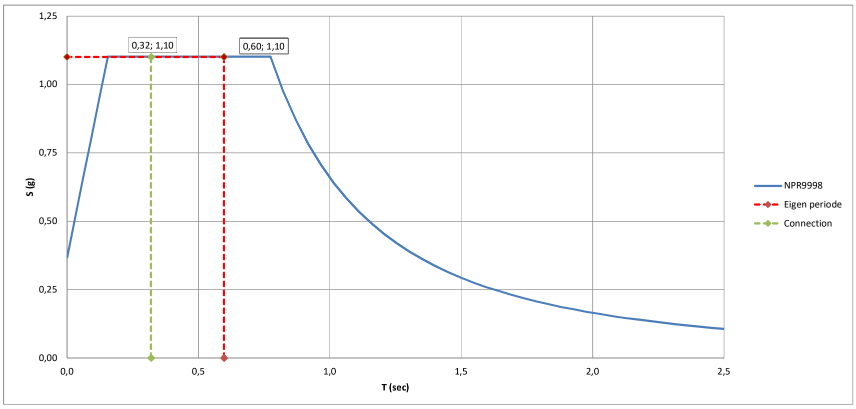

Algemeen

Project	Master thesis
Plaats	-
Aantal woningen	1
Tekening	Tekening 1
	Tekening 2

Lateral force method

Input		norm	art.	formula nr	formula	table	figure	symble	unit	
Fundamental eigen period	Rayleigh method							T_1	s	0,60
Behaviour factor		NPR 9998	8.1.1			8.1		q	-	1,00

Seismic	norm	art.	formula nr	formula	table	figure	symble	unit	
	NPR 9998	3.2.2.2					T_A	[s]	0,00
	NPR 9999	3.2.2.2	(3.10)				T_B	[s]	0,15
	NPR 9999	3.2.2.2	(3.11)				T_C	[s]	0,77
Magnification factor	NPR 9998	3.2.2.4					$S_d(T_1)$	[g]	1,10

Lateral force - distribution (1)	norm	art.	formula nr	formula	table	figure	symble	unit		foundation	ground floor	second floor	attic
mass floor	NPR 9999	4.3.3.2.3					m_i	[ton]	80	23	29	13	16
mass building	NPR 9998	4.3.3.2.2	(4.5)				m	[ton]	28				
Correctionfactor	NPR 9998	4.3.3.2.2	(4.5)	0,85 or 1,0			λ		0,85				
Shear force at foundation/ground floor?	NPR 9998	4.3.3.2.2	(4.5)	$Sd(T_1) * m * \lambda$			F_b	[kN]	261				
							h_i			-0,85	0,00	2,80	5,40
height in comparison to foundation	NPR 9998	4.3.3.2.3					z_i	[m]		0,00	0,00	2,80	5,40
mass floor	NPR 9999	4.3.3.2.3					m_i	[ton]	80	23	29	13	16
	NPR 9998	4.3.3.2.3					$\Sigma z_j * m_j$	[tonm]	120	0	0	36	84
	NPR 9998	4.3.3.2.3	(4.11)	$F_b*z_i*m_i / \Sigma(z_j*m_j)$			F_i	[kN]		0	0	78	183
							V_i	[kN]		261	261	261	183
							M_{total}	[kNm]	1208				

Lateral force - distribution (2)	norm	art.	formula nr	formula	table	figure	symble	unit		foundation	ground floor	second floor	attic
mass building	NPR 9998	4.3.3.2.2	(4.5)				m	[ton]	28				
Correctionfactor	NPR 9998	4.3.3.2.2	(4.5)	0,85 or 1,0			λ		0,85				
Shear force at foundation/ground floor?	NPR 9998	4.3.3.2.2	(4.5)	$Sd(T_1) * m * \lambda$			F_b	[kN]	261				
Displacement/ eigenvector ratio							s_i	[m]				2,54	7,46
height in comparison to foundation	NPR 9998	4.3.3.2.3					z_i	[m]		0,00	0,00	2,54	7,46
mass floor	NPR 9999	4.3.3.2.3					m_i	[ton]	80	23	29	13	16
	NPR 9998	4.3.3.2.3					$\Sigma s_j * m_j$	[tonm]	149	0	0	33	116
	NPR 9998	4.3.3.2.3	(4.11)	$F_b*z_i*m_i / \Sigma(z_j*m_j)$			F_i	[kN]		0	0	57	204
							V_i	[kN]		261	261	261	204
							M_{total}	[kNm]	1667				

Algemeen

Project	Master thesis
Plaats	-
Aantal woningen	1
Tekening	

Shear and moment diagrams

Input	symble	unit	foundation	ground floor	second floor	attic
height in comparison to foundation	z_i	[m]	0	0	2,8	5,4
force method (1)	F_i	[kN]	0	0	78	183
force method (2)	F_i	[kN]	0	0	57	204
Shear method (1)	V_i	[kN]	261	261	261	183
Shear method (2)	V_i	[kN]	261	261	261	204
Moment method (1)	M_i	[kNm]	1208	1208	1208	476
Moment method (2)	M_i	[kNm]	1263	1263	1263	531

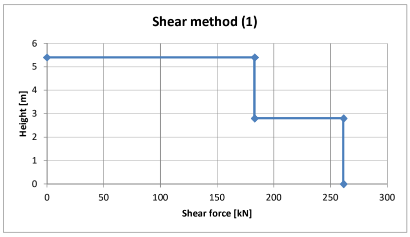

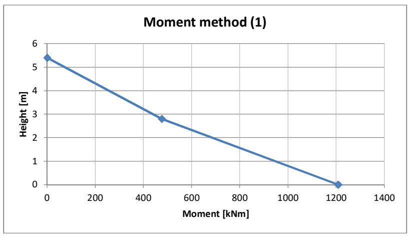

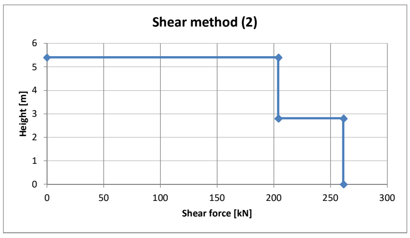

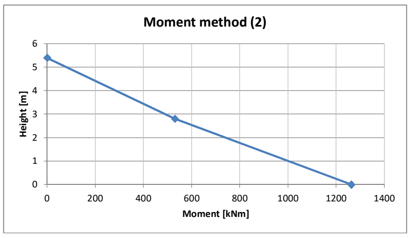

Algemeen

Project	Master thesis	
Plaats	-	
Aantal woningen	1	
Tekening		

Stiffness - multiple walls see below

Input	from.	symble	unit				
height		h	[mm]	2800	h_2	[mm]	2600
thickness		t	[mm]	15			
width		b	[mm]	1500			
number of plates		n	[st.]	2			
number of walls		n_w	[st.]	2			
Modulus of elasticity		E	[N/mm^2]	4000	OSB		
vermeningvuldigingsfactor E-moduli NPR9998			-	1,1	Door korte duur reageert het materiaal stijver		
Output	**from.**	**symble**	**unit**				
Moment of inertia	n*(1/12*t*b^3)	I	[mm^4]	2,25E+10			

Displacement estimation EC(2)

estimation with forget me nots - clamped beam

	from.	symbol	unit	value			
Force (1) second floor		F	[N]	126336	calculating from mass		
Force (2) attic		F	[N]	153140	calculating from mass		
formula (1) -second floor	$F_1L^3/3EI$		[mm]	9,3			
formula (2) -attic	$F_1L^2/2EI$		[theta]	0,0050		[mm]	22,3
formula (1) - attic	$F_2L^3/3EI$		[mm]	81,2			
formula (3) - second floor	$5F_2L^3/48EI$		[mm]	25,4			
Displacement attic			[mm]	103,5			
Displacement second floor			[mm]	34,7			

Displacement estimation RAYLEIGH

Estimation with forget me nots - clamped beam

	from.	symbol	unit	value			
Force (1) second floor		F	[N]	2800			
Force (2) attic		F	[N]	5400			
formula (1) -second floor	$F_1L^3/3EI$		[mm]	0,2070			
formula (2) -attic	$F_1L^2/2EI$		[theta]	0,0001		[mm]	0,5
formula (1) - attic	$F_2L^3/3EI$		[mm]	2,9			
formula (3) - second floor	$5F_2L^3/48EI$		[mm]	0,9			
Displacement attic			[mm]	3,4	[m]	0,003358	
Displacement second floor			[mm]	1,1	[m]	0,001102	
Mass (1) second floor		M	[ton]	12878			
Mass (2) attic		M	[ton]	15611			
Fundamental period				0,60			

Walls

	symbol	unit	value	Stiffness ratio
wall 1 - cladded on both sides				
No. Of plates	n	[-]	2	
height	h	[mm]	2800	
thickness	t	[mm]	15	
width	b	[mm]	500	
Moment of inertia	I	[mm^4]	312500000	0,03 %
wall 2 - cladded on both sides				
No. Of plates	n	[-]	2	
height	h	[mm]	2800	
thickness	t	[mm]	15	
width	b	[mm]	1000	
Moment of inertia	I	[mm^4]	2500000000	0,22 %
wall 3 - cladded on both sides				
No. Of plates	n	[-]	2	
height	h	[mm]	2800	
thickness	t	[mm]	15	
width	b	[mm]	1500	
Moment of inertia	I	[mm^4]	8437500000	0,75 %
Total				
Total one side of building	I	[mm^4]	1,125E+10	
Total both sides of building	I	[mm^4]	2,25E+10	

Algemeen		
	Project	Master thesis
	Plaats	-
	Aantal woningen	1
	Tekening	

Modal repsonse

Mode shape	natural frequency	natural period	mode mass	%	Σ %	Sd(T)	Base shear
1	1,67	0,60	23,4	82,4%	82,4%	1,10	252,5
2	12,01	0,08	5,1	17,6%	100,0%	0,76	38,1

Mode shape	level	height	shape	%	Force	Mass	Force
1	second floor	2,80	-0,00254	25%	***64,2***	12878,27278	55,42
1	attic	5,40	-0,00746	75%	***188,3***	15610,62602	197,05
			-0,01000	100%			252,5

Mode shape	level	height	shape	%	Force	Mass	Force
2	second floor	2,80	0,00835	79%	***30,0***	12878,27278	56,9
2	attic	5,40	-0,00227	-21%	***-8,2***	15610,62602	-18,8
			0,01062	100%			38,1

Total	forces	shear force
second floor	79,4	200,7
attic	197,9	197,9
	277,4	

Algemeen			
Project	Master thesis		Note: Overview of the outcome of the lateral force method and the modal response
Plaats	-		
Aantal woningen	1		
Tekening			

Overview

Method	Method	unit	Natural period	unit	Base shear	sd [m/s^2]	se [m/s^2]	s_{DE}[mm]
LF	EC(2)	[s]	0,64	[kN]	261	10,80	10,80	113,3
LF	Rayleigh	[s]	0,60	[kN]	261	10,80	10,80	97,5
MR	mode 1	[s]	0,60	[kN]	277	10,80	10,80	97,8
	mode 2	[s]	0,08			7,47	7,47	1,3

	second floor	attic	total
LF Rayleigh z	78	183	261
LF Rayleigh s	57	204	261
LF EC (2) z	78	183	261
LF EC (2) s	57	204	261
MR	79	198	277

ANNEX B: MODEL RESPONSE

Berekening eigenfrequenties & aardbevingsresponse **1.7a**

Betreft:	CLT woning					
CC:	CC1b		**importance class:**	IV	<== vervallen	
q	1,000	Type	1	P-Δ case	SRSS	keuze van de te gebruiken situatie voor 2de orde
PGA	0,36	Norm	NPR 2015 Nieuwbouw		Grond conditie	Normaal grond
ka;ref;cc	1,40		**Demping**	**5%**		
γm	1,00	(opgenomen in de response sprectrum en niet in de ag)				
a;g;ref*ka	4,94	m/s²	v	**0,4**		
Invoer						

2de orde effect	
n/(n-1)	1,019
n	54,9
ϴmax	0,023
2de orde	1,000

Massa				**Stijfheid**		
				L[m]	**E[N/mm²]**	**I [mm4]**
m10	15,6	**ton**	10	0,52	4400	2,25E+10
m9	0	**ton**	9	0,52	4400	2,25E+10
m8	0	**ton**	8	0,52	4400	2,25E+10
m7	0	**ton**	7	0,52	4400	2,25E+10
m6		**ton**	6	0,52	4400	2,25E+10
m5	13	**ton**	5	0,56	4400	2,25E+10
m4	0	**ton**	4	0,56	4400	2,25E+10
m3	0	**ton**	3	0,56	4400	2,25E+10
m2	0	**ton**	2	0,56	4400	2,25E+10
m1	0	**ton**	1	0,56	4400	2,25E+10
m0	0	**ton**	H	1,00E+10	kNm/m1	
∑	28	**ton**	C	106070194	kNm/rad	

[redacted]

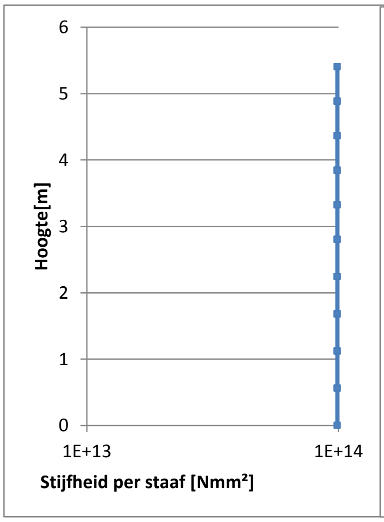

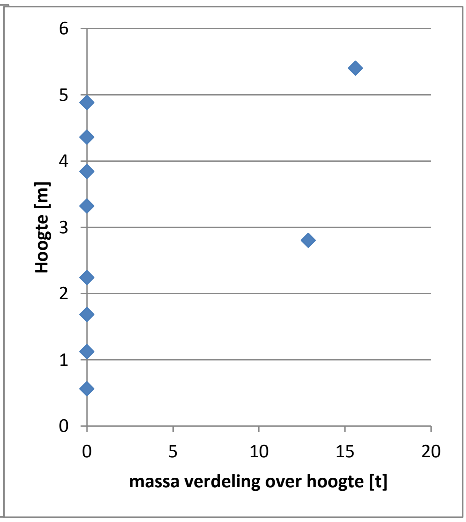

Resultaten:

M. Shape	T(s)	fe [hz]	M*	%	Cum %	Sd [m/s²]	Se [m/s²]	Sde [mm]
1	0,60	1,67	23384	82,1%	82,1%	10,80	10,80	97,8
2	0,08	12,01	5105	17,9%	***100,0%***	6,92	6,92	1,2
3	#DEEL/0!	#DEEL/0!	0	0,0%	***100,0%***	#DEEL/0!	#DEEL/0!	#DEEL/0!
4	#DEEL/0!	#DEEL/0!	0	0,0%	***100,0%***	#DEEL/0!	#DEEL/0!	#DEEL/0!
5	#DEEL/0!	#DEEL/0!	0	0,0%	***100,0%***	#DEEL/0!	#DEEL/0!	#DEEL/0!
6	#DEEL/0!	#DEEL/0!	0	0,0%	***100,0%***	#DEEL/0!	#DEEL/0!	#DEEL/0!
7	#DEEL/0!	#DEEL/0!	0	0,0%	***100,0%***	#DEEL/0!	#DEEL/0!	#DEEL/0!
8	#DEEL/0!	#DEEL/0!	0	0,0%	***100,0%***	#DEEL/0!	#DEEL/0!	#DEEL/0!
9	#DEEL/0!	#DEEL/0!	0	0,0%	***100,0%***	#DEEL/0!	#DEEL/0!	#DEEL/0!
10	#DEEL/0!	#DEEL/0!	0	0,0%	***100,0%***	#DEEL/0!	#DEEL/0!	#DEEL/0!
11	#DEEL/0!	#DEEL/0!	0	0,0%	***100,0%***	#DEEL/0!	#DEEL/0!	#DEEL/0!
		Aantal	2					

Response spectrum

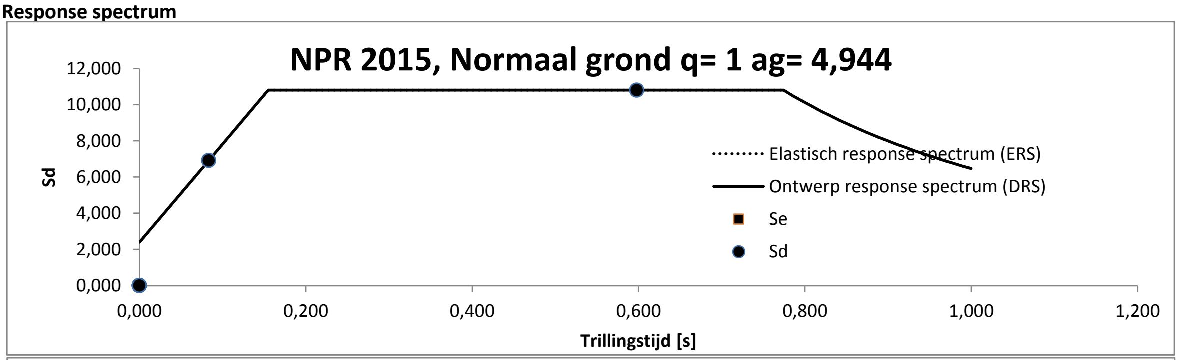

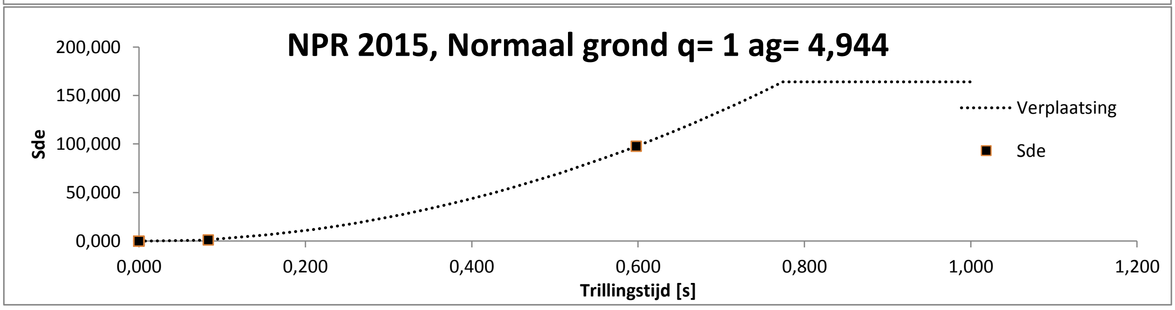

M. Shape

	1	**2**	**3**	**4**	**5**	**6**	**7**	**8**	**9**	**10**	**Massa [kg]**
1	-1,7E-09	4,067E-08									**0**
2	-0,00012	0,0008202									**0**
3	-0,00048	0,0027933									**0**
4	-0,00103	0,0051982									**0**
5	-0,00175	0,0073135									**0**
6	-0,00261	0,0084176									**12878,27278**
7	-0,0035	0,0080531									**0**
8	-0,00447	0,0064936									**0**
9	-0,0055	0,0040378									**0**
10	-0,00656	0,0009846									**0**
11	-0,00765	-0,0023674									**15610,62602**

Base shear

Sd	10,80	6,92
M [t]	23,4	5,1
V [kN]* n/(	252,5	35,3
Gamma	1,17	0,60

Krachten op knopen

H	ϕ1	ϕ2	ϕ3	ϕ4	ϕ5	ϕ6	ϕ7	ϕ8	ϕ9	ϕ10	SRSS
0,0	0,0	0,0									0,0
0,6	0,0	0,0									0,0
1,1	0,0	0,0									0,0
1,7	0,0	0,0									0,0
2,2	0,0	0,0									0,0
2,8	55,4	53,6									77,1
3,3	0,0	0,0									0,0
3,8	0,0	0,0									0,0
4,4	0,0	0,0									0,0
4,9	0,0	0,0									0,0
5,4	197,1	-18,3									197,9

Dwarskrachtenlijn

H	ϕ1	ϕ2	ϕ3	ϕ4	ϕ5	ϕ6	ϕ7	ϕ8	ϕ9	ϕ10	SRSS
-0,1	252	35									255
0,0	252	35									255
0,6	252	35									255
0,6	252	35									255
1,1	252	35									255
1,1	252	35									255
1,7	252	35									255
1,7	252	35									255
2,2	252	35									255
2,2	252	35									255
2,8	252	35									255
2,8	197	-18									198
3,3	197	-18									198
3,3	197	-18									198
3,8	197	-18									198
3,8	197	-18									198
4,4	197	-18									198
4,4	197	-18									198
4,9	197	-18									198
4,9	197	-18									198
5,4	197	-18									198

Momentenlijn

H	ϕ1	ϕ2	ϕ3	ϕ4	ϕ5	ϕ6	ϕ7	ϕ8	ϕ9	ϕ10	SRSS
0	1219	51									1220
0,56	1078	32									1078
1,12	936	12									937
1,68	795	-8									795
2,24	654	-28									654
2,8	512	-47									515
3,32	410	-38									412
3,84	307	-28									309
4,36	205	-19									206
4,88	102	-9									103
5,4	0	0									0

Sd	10,8	6,9
M [t]	23	5
Vd	252	35

Krachten op knopen t.b.v. Vervorming

H	ϕ1	ϕ2	ϕ3	ϕ4	ϕ5	ϕ6	ϕ7	ϕ8	ϕ9	ϕ10	SRSS
0,0	0,0	0,0									0
0,6	0,0	0,0									0
1,1	0,0	0,0									0
1,7	0,0	0,0									0
2,2	0,0	0,0									0
2,8	55,4	53,6									77
3,3	0,0	0,0									0
3,8	0,0	0,0									0
4,4	0,0	0,0									0
4,9	0,0	0,0									0
5,4	197,1	-18,3									198

ANNEX C: CALCULATION NATURAL PERIOD

Two methods are applied namely the Rayleigh method and the method according to the Eurocode 8, where the vertical force is regarded as het horizontal force of the building.

Rayleigh method

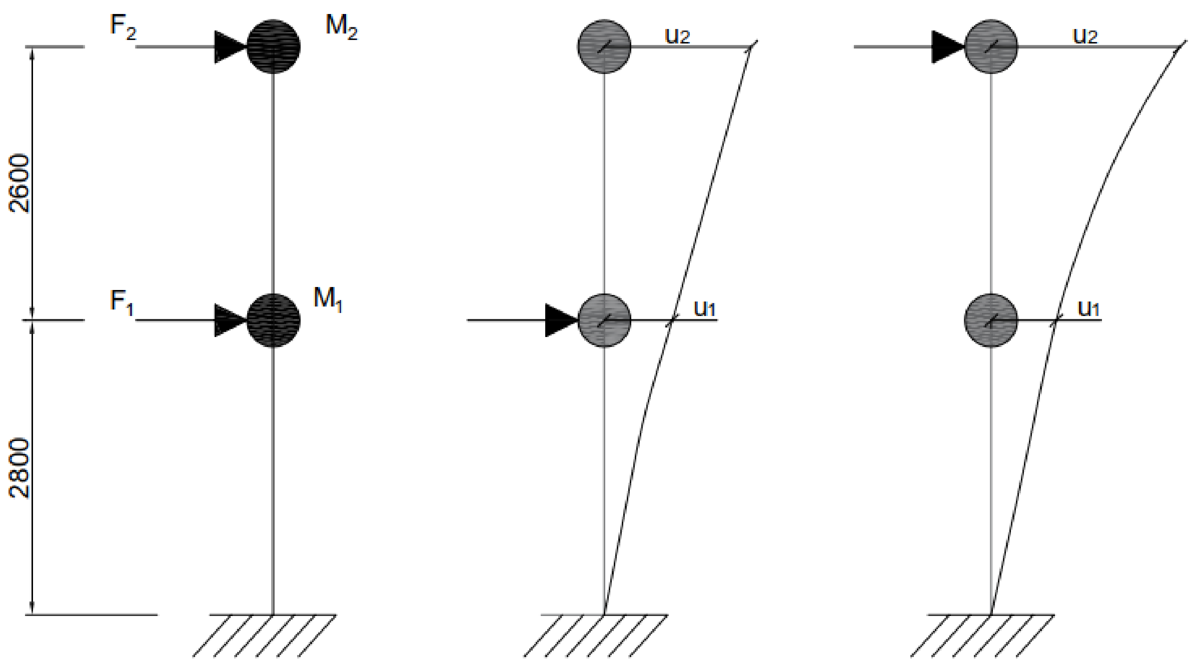

Fig. 1. Overview of schematization for calculating the natural period.

Input

$F_1 = 2800$ N, $F_2 = 5400$ N
$L_1 = 2800$ mm, $L_2 = 2600$ mm
$m_1 = 12.9$ ton, $m_2 = 15.6$ ton
$E = 4400$ N/mm^2
$I = 2.25 \cdot 10^{10}$ mm^4

Calculation of displacement with use of mechanical formula's.

$$u_1 = \frac{F_1 L_1^3}{3EI} = \frac{2800 \cdot 2800^3}{3 \cdot 4400 \cdot 2.25 \cdot 10^{10}} = 0.207 \text{ mm} \tag{1}$$

$$u_2 = u_1 + \frac{F_1 L_1^2}{2EI} \cdot L_2 = 0.207 + \frac{2800 \cdot 2800^2}{2 \cdot 4400 \cdot 2.25 \cdot 10^{10}} \cdot 2600 = 0.495 \text{ mm} \tag{2}$$

The second part of (2) is due to the tail wagging effect.

Now the force is applied at the second nodal mass.

$$u_1 = \frac{5 \cdot F_2 (L_1 + L_2)^3}{48EI} = \frac{5 \cdot 5400(2600 + 2800)^3}{48 \cdot 4400 \cdot 2.25 \cdot 10^{10}} = 0.89 \text{ mm} \tag{3}$$

$$u_1 = \frac{F_2 (L_1 + L_2)^3}{3EI} = \frac{5400(2600 + 2800)^3}{3 \cdot 4400 \cdot 2.25 \cdot 10^{10}} = 2.86 \text{ mm} \tag{4}$$

The total displacement in is as following.

$$u_{1,tot} = 1.10 \text{ mm}$$
$$u_{2,tot} = 3.36 \text{ mm}$$

The Rayleigh formula (5);

$$T_n = 2\pi \sqrt{\frac{m_1 u_1^2 + m_2 u_2^2}{F_1 u_1 + F_2 u_2}} = 2\pi \sqrt{\frac{12.9 \cdot 10^3 \cdot \left(1.1 \cdot 10^{-3}\right)^2 + 15.6 \cdot 10^3 \cdot \left(3.36 \cdot 10^{-3}\right)^2}{2800 \cdot 1.1 \cdot 10^{-3} + 5400 \cdot 1.1 \cdot 10^{-3}}} = 0.60 \text{ s} \tag{5}$$

The Rayleigh method assumes a linear forces distribution over the height therefor it is extremely suitable for calculating the natural period of buildings vibration in the first (linear) mode.

<u>EC8 method 2</u>

The same input holds as for the Rayleigh method only the forces is changed.

Input

$$F_1 = 126.3 \text{ kN}, \quad F_2 = 153.1 \text{ kN}$$
$$L_1 = 2800 \text{ mm}, \quad L_2 = 2600 \text{ mm}$$
$$m_1 = 12.9 \text{ ton}, \quad m_2 = 15.6 \text{ ton}$$
$$E = 4400 \text{ N/mm}^2$$
$$I = 2.25 \cdot 10^{10} \text{ mm}^4$$

Calculation of displacement with use of mechanical formula's.

$$u_1 = \frac{F_1 L_1^3}{3EI} = \frac{126.3 \cdot 10^3 \cdot 2800^3}{3 \cdot 4400 \cdot 2.25 \cdot 10^{10}} = 9.34 \text{ mm} \tag{6}$$

$$u_2 = u_1 + \frac{F_1 L_1^2}{2EI} \cdot L_2 = 9.34 + \frac{126.3 \cdot 10^3 \cdot 2800^2}{2 \cdot 4400 \cdot 2.25 \cdot 10^{10}} \cdot 2600 = 22.34 \text{ mm} \tag{7}$$

The second part of (7) is due to the tail wagging effect.

Now the force is applied at the second nodal mass.

$$u_1 = \frac{5 \cdot F_2 (L_1 + L_2)^3}{48EI} = \frac{5 \cdot 153.1 \cdot 10^3 (2600 + 2800)^3}{48 \cdot 4400 \cdot 2.25 \cdot 10^{10}} = 25.37 \text{ mm} \tag{8}$$

$$u_1 = \frac{F_2(L_1+L_2)^3}{3EI} = \frac{153.1\cdot 10^3(2600+2800)^3}{3\cdot 4400\cdot 2.25\cdot 10^{10}} = 81.17\text{ mm} \tag{9}$$

The total displacement in is as following.

$u_{1,tot} = 34.71\text{ mm}$

$u_{2,tot} = 103.51\text{ mm}$

The Eurocode 8 formula (10);

$$T_n = 2\sqrt{u_2} = 2\sqrt{103.51\cdot 10^{-3}} = 0.64\text{ s} \tag{10}$$

This method shows good similarity with the Rayleigh method, although this method assumes force distribution related to the distribution of the modal masses. Both methods are better than the conservative geometrical based calculations. However the result is that the response of the building still coincides with the plateau of the response spectrum.

ANNEX D: CALCULATION WIND LOAD

Wind calculation

	1st and 2nd floor		Attic floor		Total		
Side facade							
Width	7,5	[m]	7,5	[m]			
Height	5,4	[m]	2,3	[m]			
Area	40,5	[m^2]	8,6	[m^2]	49,1	[m^2]	
Front/back facade + roof	1st and 2nd floor		Attic floor				
Number of houses	6	[st.]	6	[st.]			
Length	6,5	[m]	3,75	[m]			
Heigth	5,4	[m]	2,3	[m]			
Area per house (both sides)	70,2	[m^2]	57,2	[m^2]			
Total area	421,2	[m^2]	343,1	[m^2]	764,3	[m^2]	
	81	[m^2]	66,0	[m^2]			
A_{ref}	340,2	[m^2]	277,1	[m^2]	617,3	[m^2]	
Wind pressure	0,85	[kN/m^2]					
Factor - D	0,8	[-]					
Factor - E	0,7	[-]					
Friction	0,04	[-]					
Windforce	83,62	[kN]					
Gamma factor	1,5	[-]					
Design value	125,4	[kN]					
Moment							
Side facade							
Side *D*	111,5	[kNm]	54,3	[kNm]	165,8	[kNm]	
Side *E*	97,6	[kNm]	47,5	[kNm]	145,1	[kNm]	+
Total	209,1	[kNm]	101,7	[kNm]	310,9	[kNm]	
Front/back facade							
Friction	46,8	[kNm]	92,6	[kNm]	139,4	[kNm]	
Total moment					450,3	[kNm]	

ANNEX C OVERVIEW INPUT FEM MODEL

Model description

This document contains the elements which are used in the DIANA 10.1 model in order to perform a non-linear static push-over. The CLT elements are modelled as shells and the connections as point interface. For the elements the locations are given as well as the material input and assumptions. The input is descripted from the foundation and upwards until the roof.

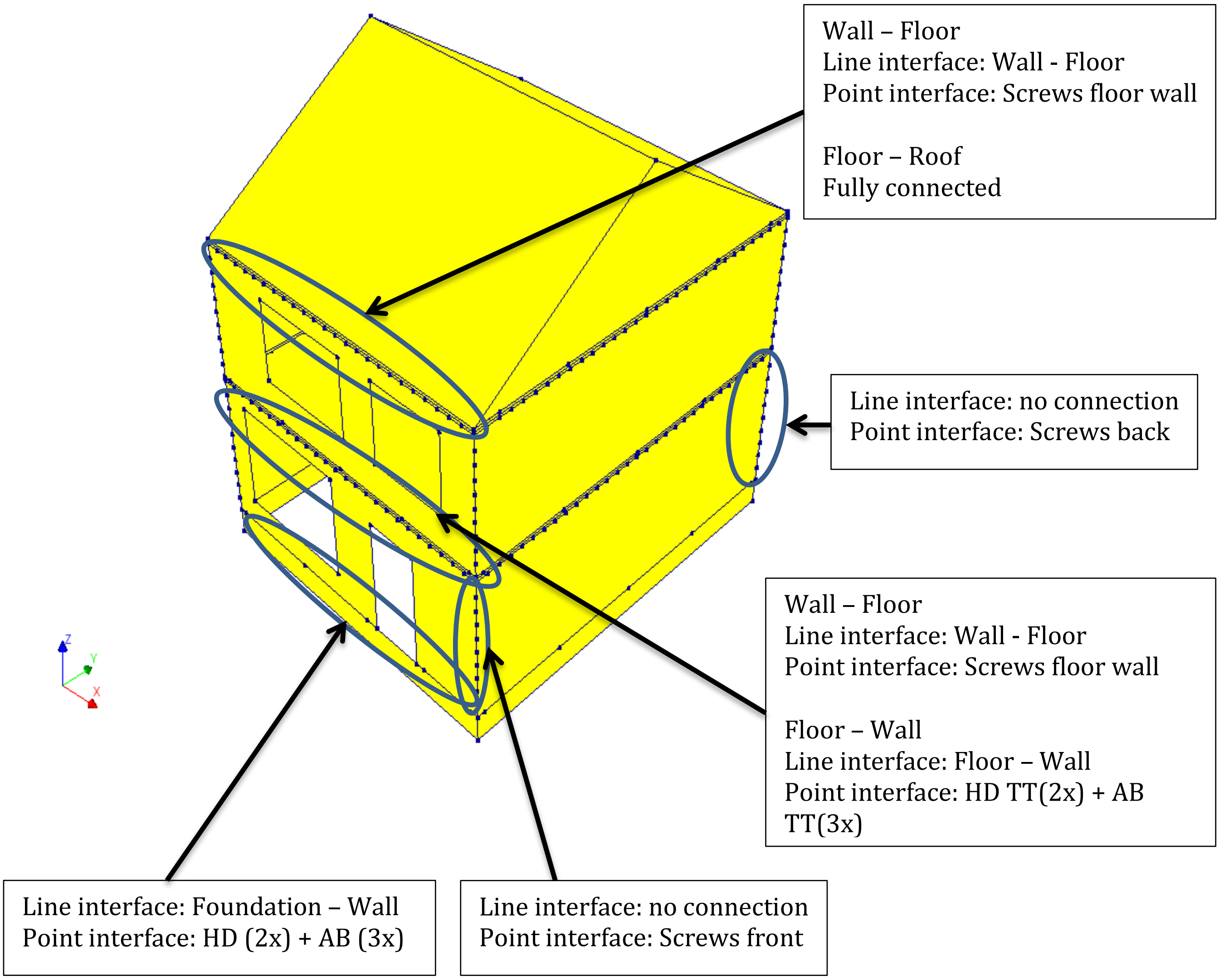

Foundation

The foundation is not really part of the model. Its purpose in this case is that the walls are connected to it. Therefor the stiffness of the elements is increased into a very stiff element to restrict deformation. The line interface between the foundation and the walls restricts deformation by compression and allows uplift due to tension.

The walls are connected to the foundation by means of angle brackets and hold-downs these are descripted at the wall input.

Element	Type	Description (input)
Foundation	Regular curved shell element	Isotropic $E = 3.0 \cdot 10^5$ MPa $\nu = 0.35$
Connection Foundation-wall	Line interface	The interface acts stiff under compression and allows no displacement due to compression and no restriction in tension. K_z = 0.1 kN/mm K_z = -100 kN/mm An elastic friction line interface is modelled with a very low friction coefficient so there is no shear resistance this is modelled in the connection. Next the cohesion of the interface is set to zero so no tension is taken up by the foundation. In the out of plane direction the walls are restrained by the foundation by the input of a high stiffness.
Support	Foundation	The foundation is fully supported at the bottom

Wall 1st floor

The input for the envelope curves for the connection is from the following sources:

- (Gavric, Fragiacomo, & Ceccotti, Cyclic behavior of typical screwed connections for cross-laminated (CLT) structures, 2014)
- (Gavric, Fragiacomo, & Ceccotti, Cyclic behaviour of typical metal connectors for cross-laminated (CLT) structures, 2013)

And can be found on page 17 and 18.

For the hold-down and angle bracket the strength is reduced by 15% due to the biaxial interaction (Hummel & Seim, 2016).

Element	Type	Description (input)
CLT Wall	Regular curved shell element	Orthotropic $d = 100$ mm Build-up : 20|20|20|20|20 $E_{m,0} = 6748$ MPa , calculated on page 10. $E_{m,90} = 4622$ MPa $G_m = 563$ MPa $\nu = 0.30$ $\rho = 970$ kg/m^3, calculated on page 14.
Connection	Point interface	Hold-down (HD), bi-axial

wall-foundation		- See Graph 1
	Point interface	Angle bracket (AB), bi-axial - See Graph 2
Connection wall-wall	Point interface	Screws - See Graph 3 (tri-axial)
CLT Floor	Regular curved shell element	Orthotropic $d = 130$ mm Build-up |30|20|30|20|30| $E_{m,0,eff} = 9471$ MPa $E_{m,90,eff} = 1899$ MPa $G_m = 505$ MPa $\nu = 0.30$ $\rho = 1200$ kg/m³
Connection wall-floor	Point interface	Self-taping screws are used HBS Ø10-260 mm - See Graph 4

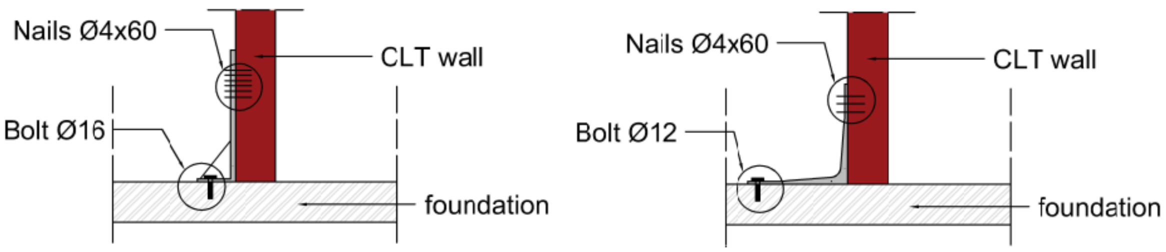

Figure 1 schematization of the connections: Left the connection of the hold-down to the foundations; right the angle brackets connected to the foundation. The number of nails drawn is just for schematization.

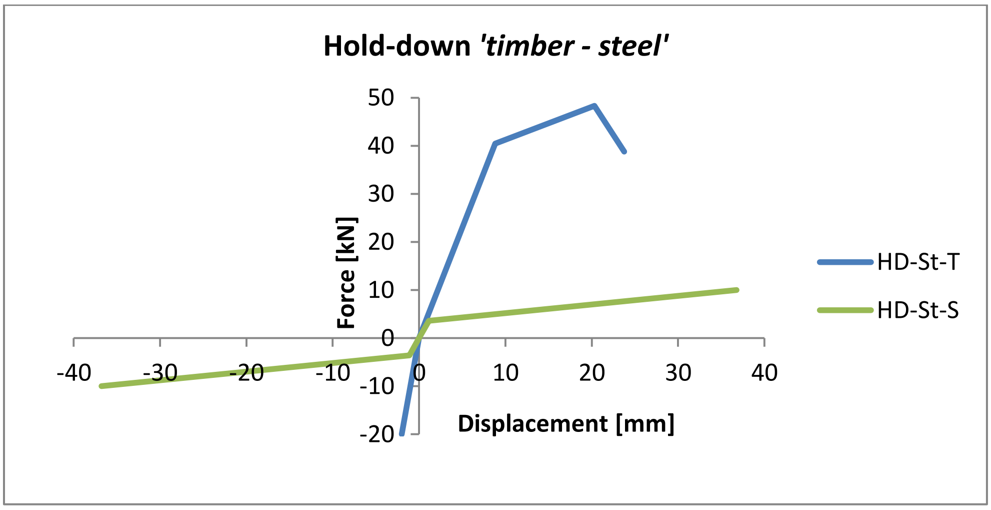

Graph 1 Hold-down: Vertical direction in compression stiff and tension conform experiments (HD-St-T). In shear direction the hold-down will fail brittle due to buckling, therefor the stiffness reduces (HD-St-S).

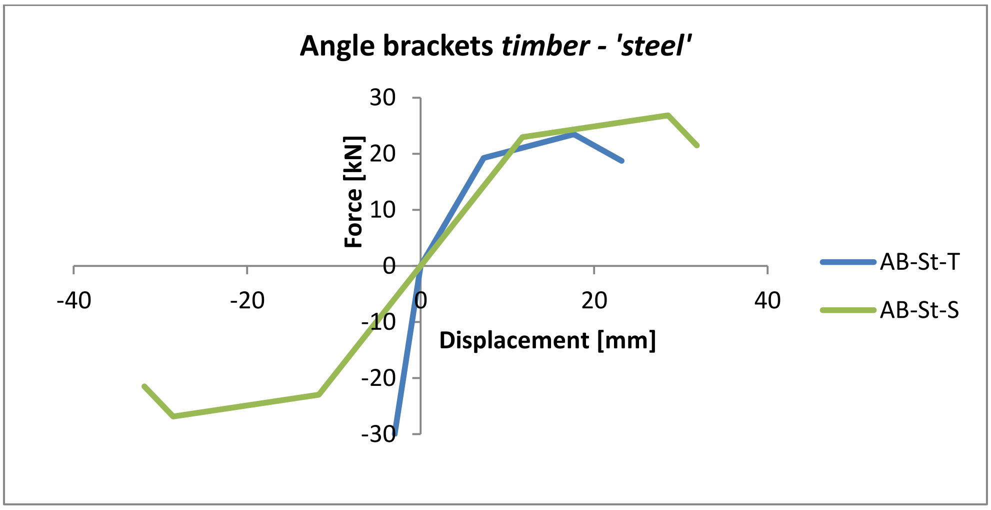

Graph 2 Angle brackets: Vertical same hold as for the hold-downs. In shear direction the input from the experiments is used.

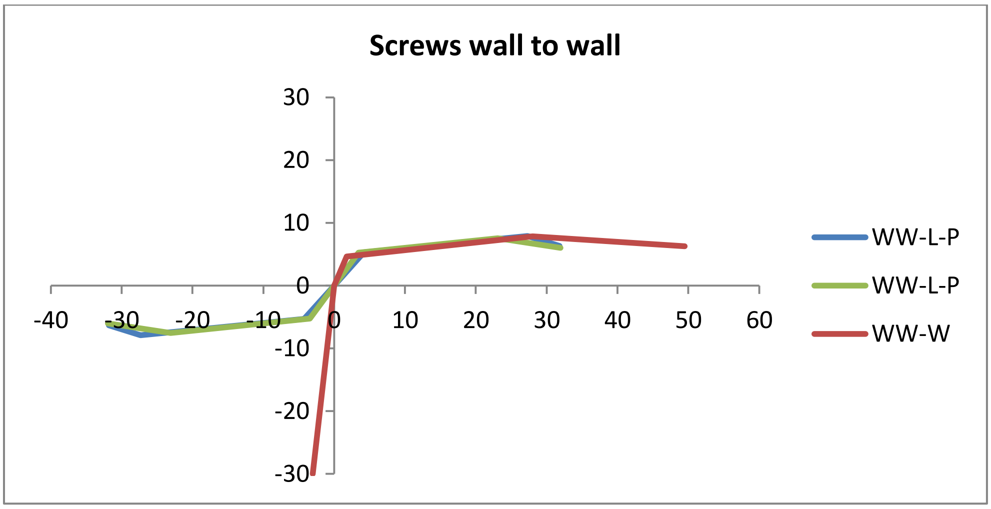

Graph 3 Self-taping screws wall to wall these are for connecting the perpendicular walls to each other. The withdrawal strength is indicated with WW-W, the other are the lateral directions. The difference in the lateral directions is due to the build-up of the CLT. When loaded in compression the connection will act stiff, the elements are pressed to each other.

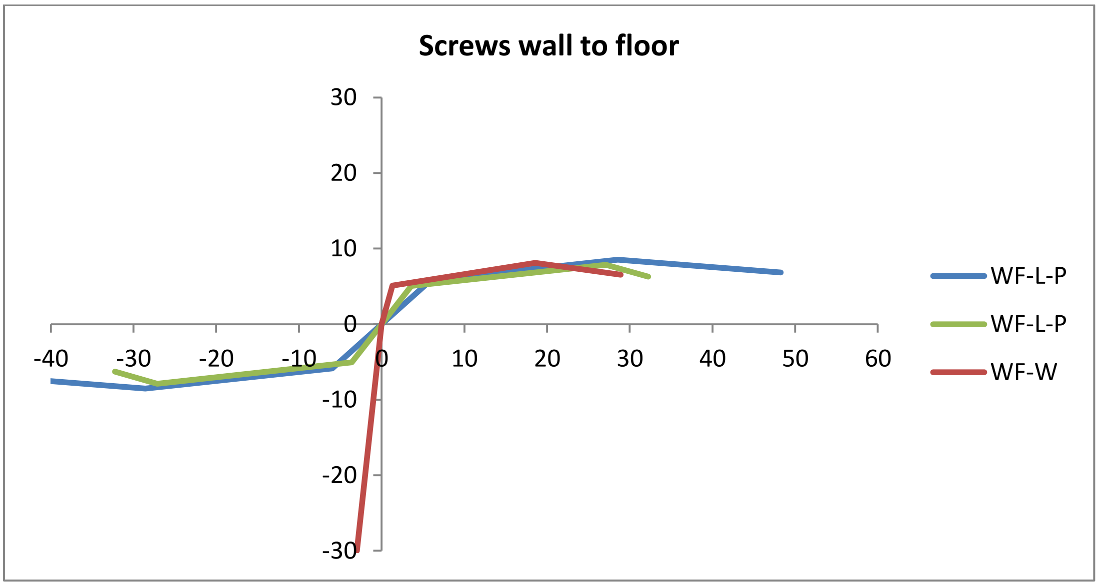

Graph 4 Wall - floor connections. The floor is placed on top of the CLT wall and attached with self-taping screws. Same holds as for graph 3.

Wall 2nd floor

Element	Type	Description (input)
CLT Wall	Regular curved shell element	Orthotropic $d = 100$ mm Build-up : 20|20|20|20|20 $E_{m,0} = 6748$ MPa , calculated on page 10. $E_{m,90} = 4622$ MPa $G_m = 563$ MPa $\nu = 0.30$ $\rho = 970$ kg/m³, calculated on page 14.
Connection wall-floor	Point interface	Hold-down (bi-axial) - See Graph 5
	Point interface	Angle bracket (bi-axial) - See Graph 6
Connection wall-wall	Point interface	Self-taping screws are used HBS Ø10-180 mm - See Graph 3 (tri-axial)
	Line interface	No tension but compression is very stiff
CLT Floor	Regular curved shell element	Orthotropic $d = 130$ mm Build-up : |30|20|30|20|30| $E_{m,0,eff} = 9994$ MPa $E_{m,90,eff} = 1376$ MPa $G_m = 505$ MPa $\nu = 0.30$ $\rho = 1200$ kg/m³
Connection wall-floor	Point interface	Self-taping screws are used HBS Ø10-260 mm - See Graph 4

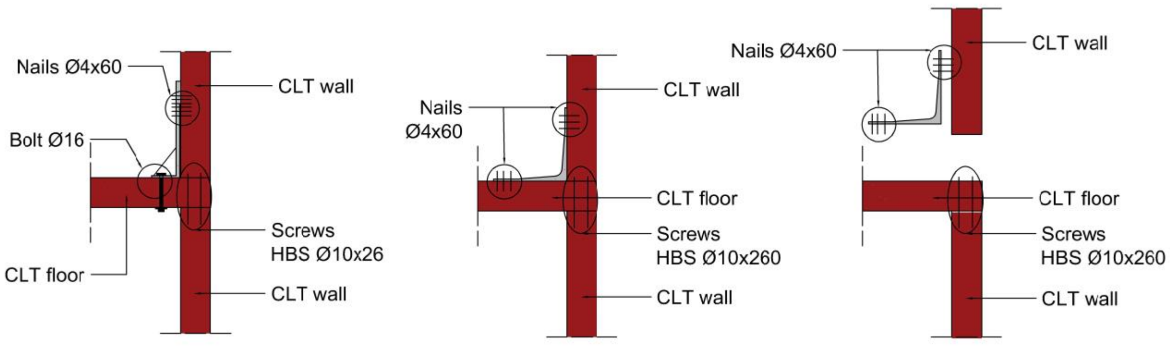

Figure 2 Floor to floor connections: Left the hold-down connection and on the right the connection of the angle brackets.

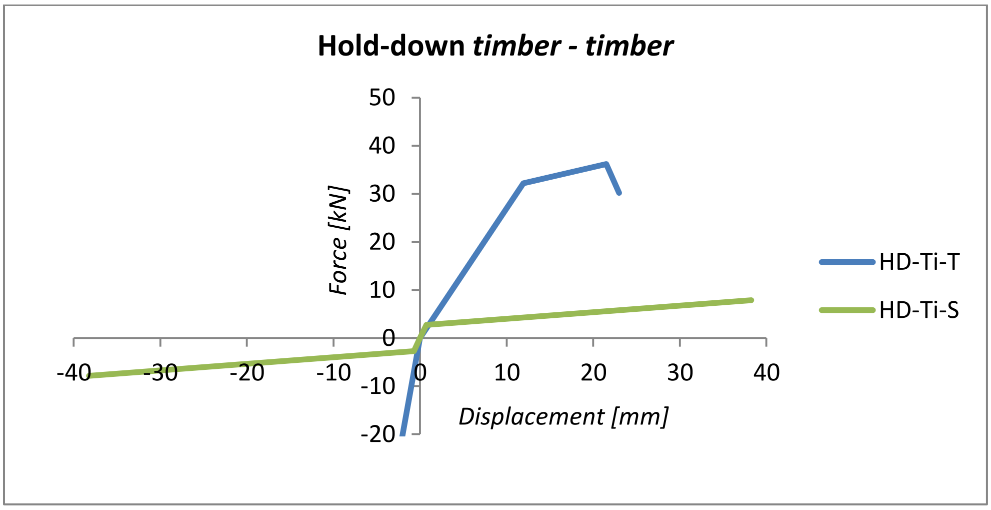

Graph 5 Wall-floor diagram for the hold-down assumption same as for previous hold-down. The reaction is more ductile due to the fact that it is timber connected to timber instead of to a rigid foundation. Also in compression the stiffness will be adopted to 70kN/mm which is still quit stiff, this was found in research (Hummel & Seim, 2016).

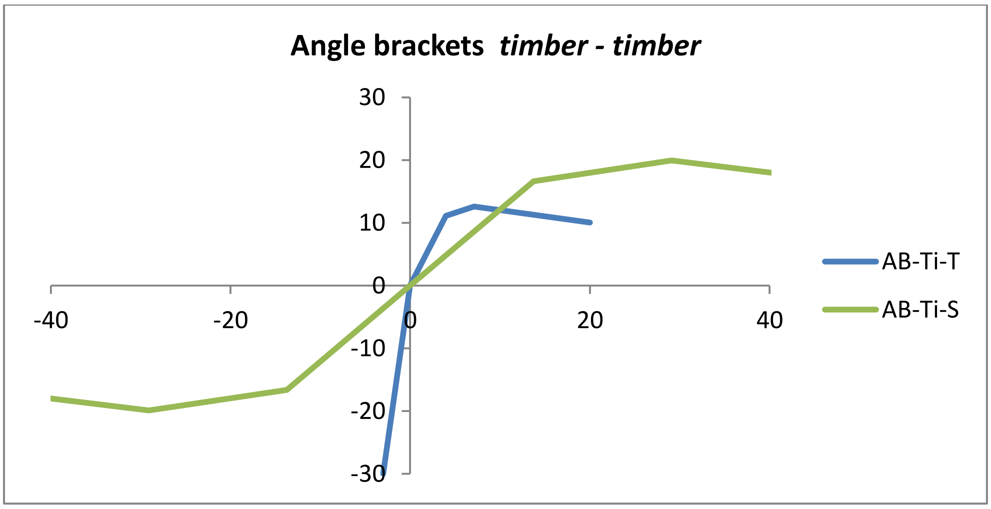

Graph 6 AB diagram for the angle bracket assumption same as for previous angle bracket. For the compression branch the same holds as for graph 5.

Roof structure

Element	Type	Description (input)
CLT plate	Regular curved shell	Orthotropic $d = 130$ mm Build-up : |30|20|30|20|30| $E_{m,0,eff} = 9994$ MPa $E_{m,90,eff} = 1376$ MPa $G_m = 505$ MPa $\nu = 0.30$ $\rho = 690$ kg/m³

The roof structure is simply modelled as a CLT slab with the same dimensions and values as for the CLT floor. The weight used for the plate however is different due to fact that the cross-section of the entire roof is different than the floor.

REFERENCES

Blass, H., & Fellmoser, P. (2004). Design of solid wood panels with cross layers. *Proceedings of the 8th World Conference on Timber Engineering* (pp. 543-548). Lathi, Finland: WCTE 2004.

Blok, R. (2006). *Tabellen voor bouwkunde en waterbouwkunde.* Utrecht/Zutphen: ThiemeMeulenhoff.

Bogensperger, T., Moosbrugger, T., & Silly, G. (2010). Verification of CLT-plates under loads in plane. *World converence on timber engineering.* Nelson, New Zealand: CIB W18.

Brandner, R., Flatscher, G., Ringhofer, A., Schikhofer, G., & Thiel, A. (2015). *Cross laminated timber (CLT): overview and development.* Berlin Heidelberg: Springer-Verlag.

Dujic, B., Klobcar, S., & Zarnic, R. (2007). *Influence of openings on shear capacity of wooden walls.* -: NZ Timber desing journal.

Gavric, I., Fragiacomo, M., & Ceccotti, A. (2013). *Cyclic behaviour of typical metal connectors for cross-laminated (CLT) structures.* Rilem.

Gavric, I., Fragiacomo, M., & Ceccotti, A. (2014). *Cyclic behavior of typical screwed connections for cross-laminated (CLT) structures.* Berlin: Springer.

Hummel, J., & Seim, W. (2016). Performance-based design as a tool to evaluate behaviour factors for multi-storey timber buildings. *WCTE.* Vienna.

Piazza, M. (2013). *Seismic performance of multi-storey timber buildings - TUGraz building.* Series.

ProHolz Austria. (2014). *Cross-laminated timber structural design.* Immenstad: ProHolz Austria.

Rinaldin, G., & Fragiacomo, M. (2016). Non-linear simulation of shaking-table on 3- and 7-storey X-Lam timber buildings. In *Engineering structures* (pp. 133-148). Elsevier.

TNO DIANA. (2015). *User's maunals*. Retrieved from dianafea.com: https://dianafea.com/manuals/d100/Diana.html

SPECIFICATION

Young's modulus

The average modulus of elasticity is calculated according to the Blass-Fellmoser composite theory (Rinaldin & Fragiacomo, 2016).

$$E_m = \frac{n_0 t_0 E_0 + n_{90} t_{90} E_{90}}{t_{tot}} \tag{1}$$

The assumption is made that the CLT consists of five layers with each having a thickness of 20 mm. With the a modulus of elasticity parallel to the grain of 11 GPa and perpendicular 0,37 GPa.

Input

$n_0 = 3$
$t_0 = 20 \text{ mm}$
$E_0 = 11 \text{ GPa}$
$n_{90} = 2$
$t_{90} = 20 \text{ mm}$
$E_{90} = 0.37 \text{ GPa} \approx E_0/30$

Calculation

When using isotropic elements, for orthotropic input which are used in the model see page 10.

$$E_m = \frac{3 \cdot 17 \cdot 11 + 2 \cdot 17 \cdot 0.37}{85} = 6748 \text{ MPa} \tag{2}$$

Floor

Two different methods are applied for the stiffness of the panel when loaded out of plane namely the k-method (Blass & Fellmoser, 2004) and by assuming that the perpendicular layer does not contribute to the stiffness.

Parallel to grain of outer layer , with K-method

The lay-out and input of the CLT floor is as following:

$n_0 = 3$
$t_0 = 30 \text{ mm}$
$E_0 = 11 \text{ GPa}$
$n_{90} = 2$
$t_{90} = 20 \text{ mm}$
$E_{90} = 0.37 \text{ GPa} \approx E_0/30$

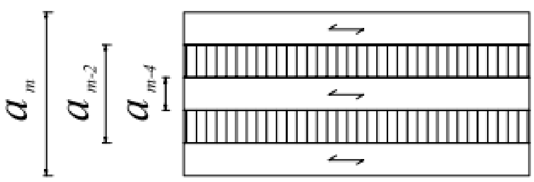

$$E_{m,0,ef} = E_0 \cdot k_1 = 11000 \cdot 0{,}86 = 9471 \text{ MPa} \tag{3}$$

$$k_1 = 1 - \left(1 - \frac{E_{90}}{E_0}\right) \cdot \frac{a_{m-2}^3 - a_{m-4}^3}{a_m^3} = 0{,}86 \tag{4}$$

Perpendicular to grain of outer layer , with K-method

$$E_{m,90,ef} = E_0 \cdot k_2 = 11000 \cdot 0{,}17 = 1889 \text{ MPa} \tag{5}$$

$$k_2 = \left(\frac{E_{90}}{E_0}\right) + \left(1 - \frac{E_{90}}{E_0}\right) \cdot \frac{a_{m-2}^3 - a_{m-4}^3}{a_m^3} = 0{,}17 \tag{6}$$

Parallel to grain of outer layer , with stiffness-method

$$E_{m,0,ef} = E_0 \cdot \frac{I_0}{I} = 9156 \text{ MPa} \tag{7}$$

$$\begin{aligned} I &= \frac{130^3}{12} \cdot 1 = 183083 \text{ mm}^4 \\ I_0 &= \left(\frac{30^3}{12} + 2\left(\frac{30^3}{12} + 30 \cdot 50^2\right)\right) \cdot 1 = 152400 \text{ mm}^4 \end{aligned} \tag{8}$$

Perpendicular to grain of outer layer , with stiffness-method

$$E_{m,90,ef} = E_0 \cdot \frac{I_0}{I} = 1582 \text{ MPa} \tag{9}$$

$$\begin{aligned} I &= \frac{130^3}{12} = 183083 \text{ mm}^4 \\ I_0 &= 2\left(\frac{20^3}{12} + 20 \cdot 25^2\right) = 26333 \text{ mm}^4 \end{aligned} \tag{10}$$

There is not much different between the two methods for input the second is chosen.

Walls

For the walls the k-method is applied, with the following geometry input. The material properties are the same as for the floor.

$n_0 = 3$
$t_0 = 20 \text{ mm}$
$n_{90} = 2$
$t_{90} = 20 \text{ mm}$

Parallel to grain of outer layer:

$$E_{m,0,ef} = E_0 \cdot k_3 = 11000 \cdot 0,61 = 6748 \text{ MPa} \tag{11}$$

$$k_3 = 1 - \left(1 - \frac{E_{90}}{E_0}\right) \cdot \frac{a_{m-2} - a_{m-4}}{a_m} = 0,61 \tag{12}$$

Perpendicular to grain of outer layer:

$$E_{m,90,ef} = E_0 \cdot k_4 = 11000 \cdot 0,42 = 4622 \text{ MPa} \tag{13}$$

$$k_4 = \frac{E_{90}}{E_0} + \left(1 - \frac{E_{90}}{E_0}\right) \cdot \frac{a_{m-2} - a_{m-4}}{a_m} = 0,42 \tag{14}$$

Shear stiffness

For the shear stiffness there are two failure mechanisms, descripted in research (Bogensperger, Moosbrugger, & Silly, 2010).

1. Mechanism I – shear + shear deformation γ_I
2. Mechanism II – torsion + shear deformation γ_{II}

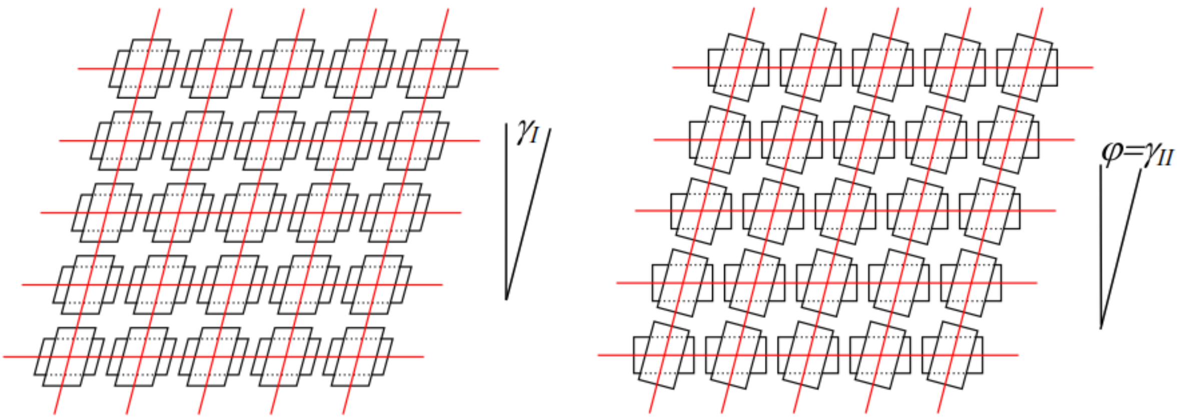

Figure 3 Shear failure mechanisms (Bogensperger, Moosbrugger, & Silly, 2010)

The total deformation is the sum of both failure modes: $\gamma = \gamma_I + \gamma_{II}$.

The first mechanism is defined as.

$$\gamma_I = \frac{\tau_0}{G_{0,mean}} \tag{15}$$

And the second deformation.

$$\gamma_{II} \cong \frac{6 \cdot \tau_0}{G_{0,mean}} \cdot \left(\frac{t}{a}\right)^2 \tag{16}$$

Where a is the board width and t is the board thickness.

Next it is stated that γ_I / γ gives the ratio $G^* / G_{0,mean}$ where $G_{0,mean}$ is the shear stiffness of a single board and G^* is the effective shear modulus of the element.

$$\frac{\gamma_I}{\gamma} = \frac{\gamma_I}{\gamma_I + \gamma_{II}} = \frac{G^*}{G_{0,mean}} = \frac{1}{1 + 6\left(\frac{t}{a}\right)^2} \tag{17}$$

Equation 13 is the general formula for determining the shear stiffness of a CLT element. For a better match with performed results a factor is introduced (α_{FE-FIT}).

$$\frac{G^*}{G_{0,mean}} = \frac{1}{1 + 6 \cdot \alpha_{FE-FIT}\left(\frac{t}{a}\right)^2} \tag{18}$$

α_{FE-FIT} is different for 3 and 5 layered CLT.

$$\alpha_{FE-FIT,orhto,3} = 0.5345\left(\frac{t}{a}\right)^{-0.7947} \tag{19}$$

$$\alpha_{FE-FIT,orhto,3} = 0.4253\left(\frac{t}{a}\right)^{-0.7941} \tag{20}$$

Now the shear stiffness for the CLT element can be calculated according to equation 17.

$$G^* = \frac{G_0}{1 + 6 \cdot \alpha_{FE-FIT}\left(\frac{t}{a}\right)^2} \tag{21}$$

The following shear stiffness is used for the in plane loaded CLT elements.

Wall: $G^* = 563$ N/mm^2

Floor: $G^* = 505$ N/mm^2

The board width (a) is 150 mm which is a common width used for calculation (Bogensperger, Moosbrugger, & Silly, 2010), the thickness of the layers for the wall is 20 mm and for the floors it is 30 mm.

Density

Walls

The density used for the CLT is the mean bulk density 450 kg/m³ (ProHolz Austria, 2014) and the build-up of the elements are discussed in the thesis report. An overview of the input is given below.

Table 1 Input of the wall elements.

Element	P [kN/m²]	ρ [kg/m³]	h [mm]	P_{perm} [kN/m²]
CLT		450	100	0,45
Gypsum plate/ OSB	0,30			0,30
Insulation	0,10			0,10
Brick sleeve	0,10			0,10
Total				**0,95**

This is then recalculated back to the input, in the form of the density.

$$\rho_{walls} = \frac{(0{,}95/g)}{0{,}10} \cdot 1000 = 968 \text{ kg/m}^3.$$

Where g is the gravity constant equal to 9,81 m/s².

Floor

The same principle is applied for the floors.

Table 2 Input of the floor elements.

Element	P [kN/m²]	ρ [kg/m³]	h [mm]	P_{perm} [kN/m²]
Top finish	0,25			0,25
CLT		450	130	0,59
Insulation	0,1			0,10
Partition wall	0,5			0,50
Ceiling	0,1			0,10
Total				**1,54**

This is then recalculated back to the input, in the form of the density.

$$\rho_{walls} = \frac{(1{,}54/g)}{0{,}13} \cdot 1000 = 1208 \text{ kg/m}^3.$$

Roof

For the roof a permanent load is assumed of 0,88 kN/m², with a thickness of 130 mm this results in a density as input of :

$$\rho_{roof\,;\,plate} = \frac{\left(0{,}88/g\right)}{0{,}13} \cdot 1000 = 688 \text{ kg/m}^3$$

DIANA ELEMENTS

The following elements are used:

For the CLT quadratic curved shell elements (CQ40S) so that the bending of the wall is incorporated.

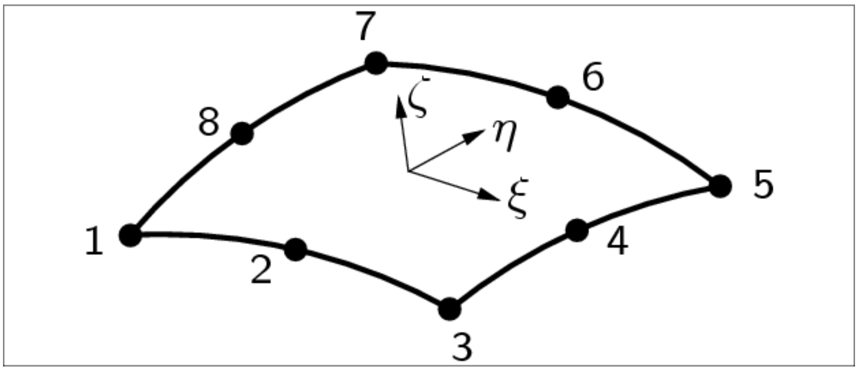

The following interface elements are used (CL24I).

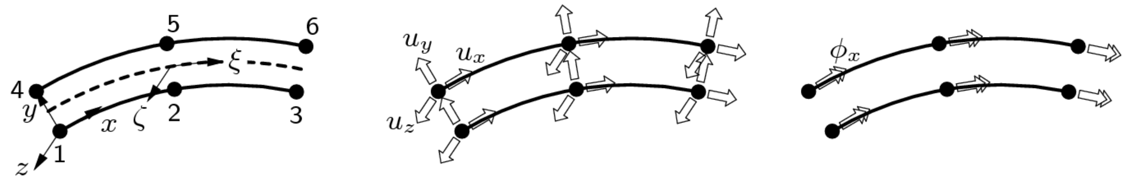

(a) topology (b) displacements

And point interfaces are used (N6IF – 1+1 nodes, 3-D).

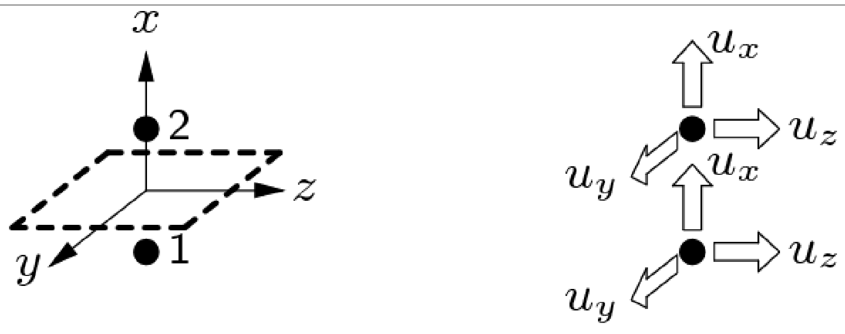

(a) topology (b) displacements

Input backbones

The following test results are used as input for the backbone curves.

(Gavric, Fragiacomo, & Ceccotti, Cyclic behaviour of typical metal connectors for cross-laminated (CLT) structures, 2013)

(Gavric, Fragiacomo, & Ceccotti, Cyclic behavior of typical screwed connections for cross-laminated (CLT) structures, 2014)

Table 1 Metal connectors test configurations and test information

Conf. no.	Metal connector	Nails no.	Connection type	Loading direction	Cyclic test no.	No. of cycles	F_{max} (kN)	$F_{max(3rd)}$ (kN)
1	Hold-down WHT540	12	CLT–foundation	Tension	6	3	48.33	41.33
2	Hold-down WHT440	9	CLT–CLT	Tension	6	3	36.21	31.27
3	Hold-down WHT540	12	CLT–foundation	Shear	6	3	9.98	9.17
4	Hold-down WHT440	9	CLT–CLT	Shear	6	3	7.88	6.85
5	Angle bracket BMF 90 × 116 × 48 × 3	11	CLT–foundation	Tension	6	3	23.47	18.59
6	Angle bracket BMF 100 × 100 × 90 × 3	8	CLT–CLT	Tension	6	3	12.57	10.96
7	Angle bracket BMF 90 × 116 × 48 × 3	11	CLT–foundation	Shear	6	3	26.85	18.80
8	Angle bracket BMF 100 × 100 × 90 × 3	8	CLT–CLT	Shear	6	3	19.91	14.26

Hold-down

Test were performed by (Garvic et al, 2013) with the following outcome for the hold-downs in CLT.

Mechanical property	Test configuration no.							
	1		2		3		4	
	x_{mean}	COV	x_{mean}	COV	x_{mean}	COV	x_{mean}	COV
k_{el} (kN/mm)	4.51	14.31	2.65	19.27	3.40	33.25	1.56	16.20
k_{pl} (kN/mm)	0.75	14.24	0.44	19.13	0.28	7.27	0.21	5.43
F_y (kN)	40.46	8.11	32.21	4.52	3.61	35.59	2.72	28.13
v_y (mm)	8.81	21.76	11.91	19.83	1.13	42.30	1.71	17.23
F_{max} (kN)	48.33	5.37	36.21	5.45	–	–	–	–
$F_{max(3rd)}$ (kN)	41.33	7.53	31.27	7.68	–	–	–	–
v_{max} (mm)	20.30	14.17	21.52	11.00	–	–	–	–
F_u (kN)	38.79	5.31	30.22	12.80	–	–	–	–
v_u (mm)	23.75	13.82	22.99	9.51	–	–	–	–
D [–]	2.76	16.21	1.97	13.75	–	–	–	–
F_{30} (kN)	–	–	–	–	9.98	7.03	7.88	4.78
D_{30} (–)	–	–	–	–	31.26	43.50	18.73	20.00
ΔF_{1-3} (%)	15.90	34.59	66.30	9.05	12.45	25.48	10.98	20.18
$v_{eq(1st)}$ (%)	8.50	5.70	8.11	9.98	19.84	13.91	21.38	6.93
$v_{eq(3rd)}$ (%)	2.78	17.29	3.60	24.40	14.63	17.79	16.09	14.86
$F_{0.05}$ (kN)	42.40		31.59		8.48		7.04	
$F_{0.95}$ (kN)	54.95		41.40		11.70		8.80	
γ_{Rd} (–)	**1.30**		**1.31**		**1.38**		**1.25**	

1. hold-down loaded in tension (wall – foundation) WHT 540 12 ring nails 4 x 60 mm.

2. hold-down loaded in tension (wall –floor) type WHT 440 9 ring nails 4 x 60 mm.

3. hold-down loaded in shear (wall – foundation) WHT 540 12 ring nails 4 x 60 mm.

4. hold-down loaded in shear (wall –floor) type WHT 440 9 ring nails 4 x 60 mm.

Angle bracket

Mechanical property	Test configuration no.							
	5		6		7		8	
	x_{mean}	COV	x_{mean}	COV	x_{mean}	COV	x_{mean}	COV
k_{el} (kN/mm)	2.53	9.72	2.98	22.05	2.09	16.41	1.10	12.34
k_{pl} (kN/mm)	0.42	10.11	0.50	22.01	0.35	16.56	0.18	11.95
F_y (kN)	19.22	2.73	11.12	9.69	22.98	5.19	16.61	7.46
v_y (mm)	7.26	9.04	3.97	28.12	11.74	5.87	13.73	7.27
F_{max} (kN)	23.47	4.32	12.57	7.71	26.85	3.15	19.91	6.95
$F_{max(3rd)}$ (kN)	18.59	9.72	10.96	7.80	18.80	10.25	14.26	9.75
v_{max} (mm)	17.69	9.62	7.10	10.62	28.51	14.75	29.09	7.01
F_u (kN)	18.74	4.32	10.06	7.68	21.48	3.15	15.86	7.59
v_u (mm)	23.19	6.14	20.01	46.39	31.86	0.33	52.26	2.21
D (–)	3.21	6.86	5.40	54.20	2.63	6.03	3.97	10.81
$\Delta F_{1\text{–}3}$ (%)	22.85	32.43	9.26	9.32	32.59	9.31	28.20	6.79
$v_{eq(1st)}$ (%)	12.33	5.43	7.40	11.71	22.75	5.93	17.49	5.59
$v_{eq(3rd)}$ (%)	7.07	19.17	1.74	10.90	14.01	6.84	11.17	14.15
$F_{0.05}$ (kN)	21.16		10.45		24.89		16.80	
$F_{0.95}$ (kN)	26.00		15.05		28.93		23.49	
γ_{Rd} (–)	**1.23**		**1.44**		**1.16**		**1.40**	

5. angle bracket loaded in tension (wall – foundation) BMF 90 x 116 x 48 x 3 with 11 ring nails 4 x 60 mm.

6. angle bracket loaded in tension (wall –floor) BMF 100 x 100 x 90 x 3 with 8 ring nails 4 x 60 mm to the wall and 6 ring nails 4 x 60 + 2 HBS screws 4 x 60 mm.

7. angle bracket loaded in shear (wall – foundation) BMF 90 x 116 x 3 with 11 ring nails 4 x 60 mm.

8. angle bracket loaded in shear (wall –floor) BMF 100 x 100 x 90 x 3 with 8 ring nails 4 x 60 mm to the wall and 6 ring nails 4 x 60 + 2 HBS screws 4 x 60 mm.

Screws

Mechanical property	Test configuration											
	5		6		7		8		9		10	
	x_{mean}	COV	x_{mean}	COV	x_{mean}	COV	x_{mean}	COV	x_{mean}	COV	x_{mean}	COV
k_{el} (kN/mm)	1.49	21.11	1.30	21.36	2.90	6.21	1.45	22.44	0.97	13.60	4.08	11.76
k_{pl} (kN/mm)	0.25	21.11	0.22	21.36	0.19	14.13	0.24	22.44	0.16	13.60	0.23	15.30
F_y (kN)	5.25	6.96	5.29	22.23	4.66	13.03	5.04	16.96	5.84	8.97	5.08	18.63
v_y (mm)	3.44	13.36	4.22	23.45	1.75	15.75	3.59	26.83	5.95	18.86	1.30	23.51
F_{max} (kN)	7.54	6.82	7.92	16.47	7.83	7.27	7.87	13.89	8.53	7.13	8.10	7.78
$F_{max(3rd)}$ (kN)	5.95	9.12	6.14	19.02	6.55	8.27	6.22	17.25	6.93	9.84	6.41	5.39
v_{max} (mm)	23.10	22.64	27.31	13.79	28.04	15.20	27.14	16.76	28.57	10.48	18.56	10.30
F_u (kN)	6.03	6.81	6.34	16.45	6.27	7.27	6.30	13.89	6.82	7.11	6.52	7.40
v_u (mm)	31.94	3.27	31.82	0.61	49.50	14.38	32.25	2.72	48.27	18.55	28.92	17.16
D (–)	9.65	16.77	10.81	25.01	28.77	16.85	10.05	33.95	8.90	23.66	23.80	35.53
D_{mon} (–)	17.27	–	16.35	–	21.85	–	30.61	–	21.57	–	27.74	–
F_{30} (kN)	6.67	3.18	7.46	15.40	7.66	8.32	7.26	13.68	8.17	7.12	–	–
D_{30} (–)	9.04	15.43	10.34	24.02	17.52	14.17	8.92	37.47	5.57	17.93	–	–
$\Delta F_{1\text{-}3}$ (%)	19.53	28.52	20.22	27.76	10.54	24.56	20.86	23.81	18.70	20.50	14.94	20.33
$v_{eq(1st)}$ (%)	17.31	4.38	18.20	9.51	8.25	10.06	17.75	6.44	15.05	9.09	9.17	6.74
$v_{eq(3rd)}$ (%)	13.29	4.68	12.41	21.66	1.32	7.62	13.87	8.18	11.00	14.46	2.15	8.49
$F_{0.05}$ (kN)	6.41		5.27		6.59		5.59		7.16		6.75	
$F_{0.95}$ (kN)	8.83		11.63		9.27		10.91		10.11		9.67	
γ_{Rd} (–)	1.38		2.21		1.41		1.95		1.41		1.43	

5. wall-wall connection lateral test. The result is for one HBS Ø10x180 mm screw.

6. wall-wall connection lateral test. The result is for one HBS Ø10x180 mm screw, differs from test 5 in the direction of the load. Therefore the orientation of the layers compared to the screw is different.

7. wall-wall connection withdrawal test. The result is for one HBS Ø10x180 mm screw.

8. wall-floor connection lateral test. The result is for one HBS Ø10x260 mm screw.

9. wall-floor connection lateral test. The result is for one HBS Ø10x260 mm screw. The difference between test 8 and 9 is the same as for test 5 and 6.

10. wall-floor connection withdrawal test. The result is for one HBS Ø10x260 mm screw.